Synthesis, Characterisation and Charge Transport Properties of a Series of Osmium Containing Polymers.

Robert J. Forster B.Sc.(Hons.)

A Thesis presented at Dublin City University
for the degree of Doctor in Philosophy.

School of Chemical Sciences,
Dublin City University.

June 1990

This thesis is dedicated to my parents.

Acknowledgements.

I would like to express my gratitude to my supervisor Dr. J. G. Vos for his continuous support, encouragement and attention to detail throughout the course of this work.

I wish to thank my fellow post graduate students for their interest and encouragement during the experimental stage of this thesis. In particular, I would like to thank Barbara Buchanan and Andrew Kelly for helpful advice.

I wish to express my gratitude to the technical staff of the school of chemical sciences at Dublin City University.

I would like to acknowledge Professor A. Pratt and the other members of staff in the school of chemical sciences for their useful advice and the use of the facilities of the school of chemical sciences.

I would like to acknowledge Dr. J. F. Cassidy and L. Breen as well as, Dr. M. E. G. Lyons for lively and informative discussion on charge transport through metallopolymers.

Finally, I wish to thank Annette Kearns for her unending support and understanding and for help in the preparation of this thesis.

This thesis is submitted in fulfilment of the requirements for Doctor in Philosophy by research and thesis. It has not been submitted as an exercise for a degree at this or any other university. Except where otherwise indicated, this work has been carried out by the author alone, at Dublin City University.

Robert Forster

Robert J. Forster.

Synthesis, Characterisation and Charge Transport Properties of a Series of Osmium Containing Polymers.

A series of metallopolymers, based on poly(4-vinylpyridine) (PVP) and poly(N-vinylimidazole) (PVI), has been prepared containing both osmium- and ruthenium-bis(2,2'-bipyridyl) centres. The polymers have been characterised using uv/vis and emission spectroscopy as well as, thermal and electrochemical methods. The results obtained are compared with those obtained for the metallopolymers containing only osmium or ruthenium centres as well as, model monomeric complexes. The results for mixed metal polymers suggest that there is little interaction between the metal centres when in solution, either in the ground or excited state.

The rate of homogeneous charge transport through $[Os(bipy)_2(PVP)_nCl]Cl$ films (n = 5, 10, 15, 20 and 25), has been examined using potential step methods and cyclic voltammetry. The effect of redox site loading, electrolyte type and concentration and temperature on D_{CT}, the charge transport diffusion coefficient for homogeneous charge transfer within the immobilised film for the Os(II/III) oxidation, has been investigated. The relevant activation parameters, enthalpy, entropy and free energy changes and activation energy for diffusional charge transport are presented. The results obtained suggest that at short times mass and charge transport can be decoupled, while at longer times the mass transport required to maintain electroneutrality occurs. The standard rate constant k^0 and transfer coefficient characterising the heterogeneous electron transfer reaction from the underlying electrode into the modifying film have also been evaluated. The effect of variations in osmium content within the film, electrolyte type and concentration and temperature on these parameters is examined. The relevant enthalpies for the heterogeneous electron transfer reaction have been evaluated. The reaction entropy is similar for all redox site loading/electrolyte concentration combinations examined suggesting that the local microenvironment of the redox centre remains largely unaltered by changes in the nature of the supporting electrolyte or the active site loading.

The charge transport properties of $[Os(bipy)_2(PVI)_nCl]Cl$ where PVI is poly(n-vinylimidazole) and n = 5, 10, 15, 20 and 25 has been explored in a range of electrolytes based on chloride, sulphate, tosylate and perchlorate anions. The effect of electrolyte and redox site loading and temperature on the homogeneous charge transport process reveals that for low redox site loading/high electrolyte concentration segmental polymer chain motion limits D_{CT}. In contrast, for high active site/low electrolyte concentration combinations the rate of charge transport is controlled by ion transport within the film. The effect of electrolyte and active site loading on k^0 is also explored.

Homogeneous and heterogeneous charge transfer through poly(N-vinylimidazole) containing $[Os(N)_6]^{2+/3+}$ moieties has been examined as a function of the nature of the contacting electrolyte solution and of temperature. The charge transport parameters are sensitive to the nature of the electrolyte anion. In sulphuric acid charge transport is rapid and is consistent with a swollen porous film. In perchloric acid the films appear compact.

The ability of the $[Os(bipy)_2(PVP)_{10}Cl]Cl$ polymer to catalyse the reduction of Fe(III) to Fe(II) in both 0.1 M H_2SO_4 and 1.0 M $HClO_4$ electrolytes is demonstrated. Catalysis occurs at a large portion of the active sites within the polymer in sulphuric acid leading to three dimensional catalysis. In perchloric acid catalysis only occurs within a region of molecular dimensions at the film/electrolyte interface.

Table of Contents.

CHAPTER 1

Introduction, Review and

Theory of Charge Transport

Through Polymer Modified Electrodes.

Section 1.1 Electrochemical Properties of Polymer Modified Electrodes

The structure of the electrode/electrolyte interface is of decisive importance to electrochemical reactions. The ability to control the physical and chemical properties of this interface offers considerable advantage in fields such as analytical applications, electrochemical synthesis, corrosion inhibition etc. The modification of traditional electrode materials with surface deposits using methods such as covalent bonding, adsorption and polymer films, to give rise to a modified electrode gives the opportunity to directly influence the structure of the electrode/film interface. The investigation of modified electrodes has received considerable attention during the last ten to fifteen years [1-4]. Polymer modified electrodes have become recognised as having properties which are desirable for practical applications, including chemical and mechanical stability, rapid charge transport rates and synthetic flexibility. Polymer modified electrodes have some properties in common with traditional metallic or glassy carbon electrodes in that they seek to be highly conductive. However, the interior of a modified electrode is a dynamic matrix whose composition can change e.g charge compensating counterions can move into or out of the film as a function of the electrode potential. Similarly, other species such as solvent or other solutes may have significant long range mobility within the film. It has become realised that the electrochemical behaviour of redox, ion exchange and conducting polymers depends to a large extent on these physicochemical properties of the polymer phase.

This thesis describes;

i) The synthesis of a series of single and multi centre, redox active metallopolymers in which the active site loading, the nature of the redox centre, and the polymer backbone can be varied.

ii) The characterisation of the physical and chemical properties of these materials.

iii) The investigation of the effect of electrolyte type and concentration, redox site loading, pH, temperature and polymer backbone on the electrochemical properties of electrodes modified with these materials.

The principal area of interest in this work has been the examination of the redox processes occurring within these films. Many experimental observations e.g the variation of charge transport rates, cyclic voltammetry peak shapes, non Nernstian electron transfer thermodynamics, activation parameters and ion exchange properties of polymer modified electrodes have been explained in terms of polymer-electrolyte models.

The underlying assumptions of these models are :

1) The modifying film is multilayer in nature and is swollen when in contact with electrolyte solutions. The film is a polyelectrolyte or is transformed into a polyelectrolyte as the potential is changed.

2) The immobilised films are permeable to solvent and ion movement into and out of the coatings. The requirement of electroneutrality is maintained by movement of charge compensating counterions, provided there is no chemical reaction after electron transfer e.g deprotonation.

3) Due to solvent or ion movement into or out of the film, the polymer matrix can swell or become more compact during the redox reaction. Depending on the mechanism of this process, reversible elastic deformation or irreversible transformations can occur. The energy required for the electrochemical transformation will be the sum of that needed for the redox reaction and any additional energy input required. Additional input can arise because of forced swelling of the film due to charge compensating counterion influx or movement of the polymer chain to which the redox sites are bound.

4) Polyelectrolyte layers are sensitive to structure and environment. The effect of interactions between the redox sites and other species within the film is significant due to the high fixed site concentration (typically greater than 1 mol dm^{-3}). Selective binding of counterions, ion pair formation, dimerisation and protonation, affect the rate of charge transport through the film and other properties of the modified electrodes.

5) The distribution of ions between the bulk electrolyte and the film obeys the appropriate Donnan relation at equilibrium. This is frequently termed membrane behaviour.

6) The mechanism of charge propagation through redox polymer films is generally accepted to occur via successive electron hops between oxidised/reduced sites within the film. This rate of charge transport can be limited by one of three processes. i) The intrinsic barrier to electron self exchange. ii) The movement of charge compensating counterion into/out of the film. iii) The segmental motion of the polymer strands to which the redox site

is bound, or where the redox centre is electrostatically bound within the polymer, the diffusive motion of the redox site through the film.

It is to be noted that the structural requirements for rapid electron transport and fast counterion transport required for electroneutrality are opposite i.e rapid electron self exchange is favoured by close redox sites at a high concentration within the film, while an open porous structure will favour facile permeation of counterion and segmental chain motion. The interplay of these three rate limiting processes and the influence of film swelling is of central importance in the work presented here and will be discussed in greater detail later.

Section 1.2 Charge Transport Dynamics Through Polymer Modified Electrodes.

The types of polymeric materials which form modifying films on electrode vary considerably from electronically conducting materials, notably polypyrrole, polyaniline and polythiophene to polymeric materials which possess a bound redox centre. The materials which have been considered in this thesis are of the redox type and it seems pertinent to review the literature with respect to charge transport dynamics through such materials. The aim of this chapter is by no means to present a complete literature survey covering the whole of the polymer modified electrode area, but to survey and present the most interesting and representative examples of the examination of charge transport dynamics through redox polymer modified electrodes. This section is subdivided into parts dealing with polymer modifying films in which; i) the electroactive centre is covalently bound to the polymer backbone e.g the osmium

and ruthenium materials discussed in this dissertation, or have a redox centre comprising part of the polymer backbone e.g poly(vinylferrocene). ii) the electroactive centre is electrostatically bound within the film e.g ferrocyanide within protonated polyvinylpyridine films.

Section 1.2.1 Covalently Bound Redox Centres

The investigation of those systems possessing a functional group which can be polymerised, frequently electrochemically, to give redox polymers with a bound centre will be considered first. Poly(vinylferrocene) (PVF) is one of the earliest such electrode modifiers and its properties have been extensively examined [5-8]. Schroeder and Kaufman have shown that polymer morphology as dictated by supporting electrolyte, electrode potential and doping has a significant influence on the charge transport process [9]. For example, by incorporating a dye, (Sudan III) into the film during casting, and observing the desorption of the dye into solution, a diffusion coefficient of 10^{-9} cm^2s^{-1} was observed for the diffusion of the dye through polyvinylferrocene. The activation energies for the homogeneous charge transport process through PVF have been evaluated as approximately 15.5 kJ/Mol, while the entropy terms are negative (-134 J/(mol deg)) [10]. The charge transport process has been interpreted as being limited by polymer chain motion and counterion transport [11].

Several models for charge transport through polyvinylferrocene have been proposed, notably the porous or pinhole model and the membrane model. These have been investigated by Leddy and Bard and they concluded that PVF films act as a membrane, where material diffuses through the bulk film, rather than through pores [12]. In a series of papers [13-15] non-Nernstian

thermodynamics for PVF films have been interpreted in terms of a mechanical/electrochemical model. This model accounts for the observed behaviour in terms of the forced inclusion of charge compensating counterion and the finite nature of the free volume within the film. The energy required to carry out the electrochemical transformation is, therefore, the sum of the redox reaction and the forced swelling of the polymer film. The effect of structural properties such as crosslinks on this process is discussed. Experimental evidence is reported to support the model and the formation of crosslinks due to the formation of ferrocenium/perchlorate ion pairs. The formation of salts between the oxidised redox sites and the counterions as well as the polyelectrolyte behaviour of poly(vinylferrocene) has been used to explain the differences in the cyclic voltammetry and chronoamperometric response of these films in contact with aqueous and acetonitrile electrolyte solutions [16].

The kinetics of electron transfer through thionine coatings has been extensively studied [17-20]. These studies used conventional potential step and optical measurements to evaluate an apparent charge transport diffusion coefficient, D_{CT}, for homogeneous charge transport through the immobilised films. This gave values which were dependent on the nature of the counterion, ranging from 9.1 x 10^{-13} cm^2s^{-1} in sulphuric acid at pH 1.3 to 0.9 x 10^{-13} cm^2s^{-1} in tosylate solutions. The fact that charge transport depends on the anion size suggests that anion transport limits the rate of charge propagation through the films. The activation energy in sulphuric acid solution was 35 kJ/Mol, which further suggests that ion movement limits the rate of charge propagation. Thionine films have shown considerable catalytic properties, notably with respect to Fe(III) and $[Fe(CN)_6]^{3-}$ reduction [21].

The mediated reaction for Fe(III) occurs at the film/electrolyte interface between the thionine sites in the film and Fe(III) in solution.

An important class of redox active polymers are materials which are electropolymerised from metal complexes containing a pendant vinyl group [22-27]. The thermodynamically unfavourable oxidation of a series of iron, ruthenium and osmium bipyridine and phenanthroline complexes has been examined at poly$[Os(bipy)_2(vpy)_2]^{3+}$ (vpy = 4-vinyl pyridine) modified electrodes [22]. These investigations show simple electron transfer reaction energetics which agree with the Marcus outer sphere cross reaction relation. The permeability of poly cationic (tris(4-methyl-4'-vinyl-2,2'bipyridine)ruthenium) and poly$[Ru(vbpy)_3]^{2+}$ to ferrocene, TCNQ, cationic ferrocenium and anionic $TCNQ^-$ has been examined [28]. The permeation of these species is a function of electrolyte concentration and the charge of the substrate. Permeation rates are typically of the order of 10^{-8} cm^2s^{-1}. The electron transport dynamics through these electropolymerised films can also be investigated using steady state methods where influx of charge compensating counterions into the film is not required [29-30]. This avoids problems such as migration and allows the independent evaluation of electron diffusion coefficients. One of the largest diffusion coefficients measured for a localised electronic state redox polymer, $[Os(bipy)_2(vpy)_2]^{2+/3+}$, sandwiched between platinum and porous gold electrodes in contact with dry N_2, is 1.7 x 10^{-6} cm^2s^{-1} [31]. The dependence of electron diffusion coefficient with electrochemical potential has been explored for these films [32].

The effect of active site loading within the film has been explored for films formed by the electropolymerisation of $[Co(v\text{-}terpy)_2]^{2+}$ (v-terpy is 4'-vinyl-2,2',6',2''-terpyridinyl) [33]. The effect of increasing the redox

site loading on D_{CT} is frequently interpreted in terms of the Dahms-Ruff behaviour which predicts a linear increase in D_{CT} with increasing fixed site concentration. In the above example the rate of charge transport for the $Co^{2+/+}$ redox couple varied linearly with redox site concentration over the range 0.1 to 0.6 M, while D_{CT} for $Co^{3+/2+}$ was independent of the active site concentration. Both charge transport rates are of the order of 10^{-13} cm^2s^{-1}. The effect of intersite separation has been elegantly explored by "diluting" osmium sites with structurally similar ruthenium sites [34]. This avoids problems such as solvent swelling and cross linking changes as the redox centres are separated by dissimilar sites. As the osmium loading within the film is increased D_{CT} initially increases, followed by a region where D_{CT} is relatively insensitive to osmium loading, until at the highest osmium concentrations (1.2 M) D_{CT} increases sharply.

The nature of the supporting electrolyte medium exerts considerable influence over charge transport dynamics for many modified electrodes. The effect of changing the supporting electrolyte system to a molten salt has been explored for poly-$[Ru(bipy)_2(vpy)_2]^{3+/2+}$ in $AlCl_3$/N-(1-butyl)pyridinium chloride and $AlCl_3$/1-methyl(3-ethyl)imidazolium chloride [35]. $D_{CT}{}^{1/2}C$ was 1.7 x 10^{-8} $molcm^{-2}s^{-1/2}$, a decrease of a factor of ~2.6 compared to the value obtained in acetonitrile. This suggests that there is little solvent effect on the rate of charge transport, suggesting that electron self exchange limits the rate of charge transfer.

The tetracyanoquinodimethane (TCNQ) polymer system has been extensively examined [36-38], notably with regard to the effect of electrolyte concentration [39-40]. The peak current maximum for the cyclic voltammetry response is observed for intermediate supporting electrolyte concentrations

(~1.25 M). This behaviour has been interpreted in terms of the formation of ion pairs between reduced redox sites and counterions from the supporting electrolyte. As the supporting electrolyte concentration is increased the film is considered to become more compact since at high counterion concentrations the electrolyte is better able to minimise the electrostatic repulsions between charged centres on the polyelectrolyte [41].

The use of sampled current voltammetry to consider both the rate of homogeneous charge transport through a modifying polymer film, as well as the rate of heterogeneous electron transfer (measured as the standard rate constant k^0), has been considered for poly(styrene-co-chloromethylstyrene) containing pendant viologen groups [42-43]. As the concentration of the fixed redox site within the film is increased from 6.7×10^{-5} to 3.3×10^{-4} mol cm^{-3} D_{CT} increases from 2.5×10^{-11} to 3.9×10^{-10} cm^2s^{-1}. This behaviour follows the Dahms-Ruff relation indicating a significant contribution by electron self exchange to the charge transport rate. k^0 also increases from 3.0 to 8.9×10^{-5} cms^{-1} over this concentration range. The thermodynamic parameters for these homogeneous and heterogeneous charge transport processes have been evaluated by using a non isothermal cell in which the reference electrode is held at constant temperature. This gives activation parameters of approximately 16-30 kJ/Mol with negative entropy terms. The thermodynamic parameters for the heterogeneous charge transfer reactions show negative real entropy terms.

Electrooxidative polymerisation of o-phenylenediamine, N-methylaniline and N-ethylaniline has been used to form modified electrodes and the kinetics of heterogeneous electron transfer examined [44]. The heterogeneous electron transfer obeys the conventional Butler-Volmer equation, while the homogeneous charge transport process can be described via Fick's laws. The rate of

homogeneous charge transport for this material lies between 1 and 4 x 10^{-8} cm^2s^{-1} with k^o between 4 and 6 x 10^{-4} cms^{-1}.

Electrooxidation of a series of $[M(5\text{-}NH_2phenanthroline)_3]^{2+}$, (M=Co, Fe) gives stable modified surfaces [45-46]. Electrodes modified with poly-tris[5-amino-1,10-phenanthroline]iron(II) show charge transport rates of 3 x 10^{-8} cm^2s^{-1} [45]. The activation energy for homogeneous charge transport is 32 kJ/Mol with negative entropy terms. Since substrate permeation is much more rapid than the charge transport rate, electron mobility is considered to limit the charge transport process.

The investigation of charge transport dynamics through materials such as those considered in this thesis, where a redox active centre is coordinatively bound within a preformed polymeric matrix, has been investigated. The effect of the nature of the electrolyte anion on the structure and charge transport rates through partially quaternised poly(4-vinylpyridine) films has been considered recently by coordinating $[Re(CO_3)(phen)]$ and $[Ru(bipy)_2Cl]^{2+/3+}$ [47]. These metal complexes allow the film structure to be probed by both electrochemical and luminescent techniques. The rate of charge transport was typically of the order of 10^{-9} cm^2s^{-1} and was independent of redox site loading but strongly dependent on the nature of the electrolyte anion. The films are strongly hydrated in nitrate solutions while in perchlorate solutions they are dry and compact. The ruthenium analogues of the poly(4-vinylpyridine) metallopolymers presented in this thesis have been reported previously [48-52]. The effect of redox site loading in perchloric acid has been examined [53]. This study showed that the activation energy decreased as the redox site loading was increased. The charge transport parameter $D_{CT}{}^{1/2}C$ decreased with increasing site loading

at high temperatures (318 K), at lower temperatures (288 K) $D_{CT}^{1/2}C$ increased as the redox site loading was increased [53]. The temperature dependence of charge transport processes through $[Ru(bipy)_2(PVP)Cl]Cl$ and $[Ru(bipy)_2(PVP)(MMA)Cl]Cl$ has been investigated [54] (PVP = poly(4-vinylpyridine, MMA = poly(methyl methacrylate). The poly(4-vinylpyridine) system gives activation energies between 32 and 43 kJ/Mol depending on the electrolyte. The co-polymer system exhibits dual slope behaviour in which two activation energies are obtained. For temperatures above 285 K the activation energy is 140 kJ/Mol which decreases to 40 kJ/Mol at lower temperatures. The catalytic properties of $[Ru(bipy)_2PVP_5Cl]Cl$ films in 1.0 M HCl with respect to $[Fe(H_2O)_6]^{2+}$ oxidation have been explored [55]. The charge transport rate has been evaluated as 3×10^{-9} cm^2s^{-1}. The linear range for $[Fe(H_2O)_6]^{2+}$ determination extends to 5×10^{-6} M suggesting their use as analytical sensors [56]. The mediation of $[Fe(CN)_6]^{4-}$ by such films has also been examined as a function of pH, electrolyte and substrate concentration [57]. For surface coverages less than 10^{-8} $molcm^{-2}$ the mediated oxidation of ferrocyanide by the ruthenium containing film is controlled by diffusion of the substrate to the electrode surface.

The effect of factors such as the molecular weight of the polymer, its morphology, the temperature of the supporting electrolyte, the electrochemical solvent and the electrolyte ion on the reduction of Ru(III)EDTA covalently bound to poly(4-vinylpyridine) has been examined [58]. It is proposed that the quantity of anion resident within the film is relatively insensitive to the ionic strength, but highly sensitive to pH. This arises since a low pH electrolyte will protonate the uncoordinated pyridine units causing film

expansion and hence a more porous film. Activation energies are of the order of 20 kJ/Mol suggesting facile ion movement through the film as the rate determining step.

Section 1.2.2 Electrostatically Bound Redox Centres

The incorporation of anionic transition metal complexes, notably hexacyanoferrates and hexachloroiridates into protonated or quaternised polyvinylpyridine films has received considerable attention [59-62]. The rate of charge transport as measured by impedance methods was shown to be dependent on the loading of $[Ir(Cl)_6]^{2-/3-}$ within poly(4-vinylpyridine), decreasing from 11 x 10^{-8} cm^2s^{-1} where the $[Ir(Cl)_6]^{2-/3-}$ concentration is 0.034 M, to 4.6 x 10^{-8} cm^2s^{-1} when the iridium concentration is increased to 0.081 M [63]. These values of D_{CT} were approximately 10 times higher than those observed using chronocoulometry. The consideration of temperature effects on charge transport rates through polymer films has received little attention, despite its ability to aid diagnosis of the rate determining step in the charge transport mechanism. Recently Oh and Faulkner reported on variable temperature chronocoulometry results for ferri/ferro cyanide within partially quaternised poly(4-vinylpyridine) films [64]. E_a increased with increasing ferri/ferrocyanide loading over the range 24-80 kJ/Mol. It is suggested that an increased redox site loading causes increased crosslinking. D_{CT} was also shown to be sensitive to the anion in the electrolyte solution. Infrared spectroscopy has been used to show that perchlorate produces nearly dehydrated, rather impermeable films [64]. The incorporation of dioctyl phthalate as plasticiser into quaternised poly(vinylpyridine) films containing ferrocyanide,

alizarin red S or alizarin complexone has been shown to increase D_{CT} [65]. Without added plasticiser the rate of charge transport for a ferrocyanide containing film was 8 x 10^{-10} cm^2s^{-1}, with a 1:1 mole ratio of dioctyl phthalate to pyridine units D_{CT} increased to 3.8 x 10^{-9} cm^2s^{-1}. Glow discharge polymerisation of 4-vinylpyridine in the presence of $[Fe(CO)_5]$ onto electrodes gives modified surfaces which are permeable to acidic electrolytes [66]. Extensive crosslinking of the polymer chains gave enhanced stability over linear systems. The rate of charge transport varied from 5 x 10^{-12} to 7 x 10^{-11} cm^2s^{-1} depending on the iron concentration. Using $HClO_4$ as background electrolyte resulted in almost complete loss of the cyclic voltammetry signal due to hindered ion permeation / $Fe^{2+/3+}$ diffusion. An in depth study of the role of ion transfer has been presented by Doblhofer for $[Fe(CN)_6]^{3-}$ electrostatically bound within poly(vinylpyridinium) films [67]. This paper highlights the importance of migrational effects in the charge transport process. This leads to a migrational enhancement when the background electrolyte concentration is low. Further examination of this system [68] has lead to evaluation of the diffusion and migration parameters and the conclusion that the contribution to charge transport rates by electron hopping is insignificant. Other models have shown the importance of the supporting electrolyte concentration on the evaluation of D_{CT} [69]. These migrational effects can in some circumstances lead to potential step methods underestimating D_{CT} by as much as a factor of 100 [70]. Whether such migrational effects are observed depends on the system under investigation, for example, investigations using rotating disk voltammetry and chronocoulometry gave identical results for poly(4-vinylpyridine) films in which $[Ir(Cl)_6]^{2-}$ ions were electrostatically confined [71].

Potential step measurements such as chronoamperometry, -coulometry or -potentiometry performed under conditions of finite diffusion have been used to investigate charge transport through a series of hexacyano and octacyano metal complexes within protonated poly(4-vinylpyridine) [72]. In common with many of these electrostatically bound systems which induce crosslinking of polymer chains, D_{CT} decreased as the incorporated anion concentration increased, until a steady state was reached at a concentration of ~1M.

The exploration of heterogeneous charge transfer reactions by sampled current voltammetry of anionic redox couples ($[W(CN)_8]^{4-/3-}$, $[Ir(Cl)_6]^{3-/2-}$) incorporated electrostatically within a protonated poly(vinylpyridine) has been carried out by Oyama and co-workers [73-74]. Cyano complexes of similar structure and charge have shown different dependencies of D_{CT} on the redox site loading. The rate of charge transport is independent of the $[W(CN)_8]^{4-/3-}$ loading, while for $[Mo(CN)_8]^{4-}$ D_{CT} decreases with increasing redox loading. Charge transfer reactions for $[Fe(CN)_6]^{4-/3-}$ confined within protonated poly(vinylpyridine) have been examined via alternating current impedance [75]. This technique gave values of the heterogeneous rate constant, k^o, which were the same as those obtained by sampled current voltammetry, while the homogeneous charge transport rates are reduced by 1 to 2 orders of magnitude. It has been suggested that this behaviour is related to the time scale of the two experiments, the time window of the ac impedance experiment being approximately an order of magnitude shorter than the sampled current observations. Other authors have examined this system using the same technique [76], the heterogeneous electron transfer rate was approximately 10 times less than that observed in [75]. Additional cross linking causing increased repolarisation energy associated with the

electron transfer process has been postulated as a possible explanation of these differing results. Both D_{CT} and k^o typically decrease as the ferrocyanide content of the film is increased. On increasing the ferrocyanide to pyridine ratio from 1:200 to 1:5, D_{CT} decreased from 4.2×10^{-7} to ~1 x 10^{-9} cm^2s^{-1}, while k^o decreased from 1.5×10^{-3} to 1.5×10^{-4} cms^{-1}, with the transfer coefficient remaining approximately constant at a value of 0.52 [77].

The perfluorinated ion-exchange polymer Nafion has been extensively used to immobilise cationic metal complexes [78-79]. This polymer is physically robust and the redox site loading can be easily changed. This has lead to extensive investigations of the effect of increased metal complex content on D_{CT} [80]. Frequently increased redox site loading does not produce a corresponding increase in D_{CT} in accordance with the Dahms-Ruff equation [81]. The nature of the dependence of charge transport on the redox site loading within Nafion films has been explored for a series of structurally similar cationic metal complexes [82]. Despite their structural similarity the rate of charge transport was different, this behaviour was interpreted in terms of hydrophobic and hydrophilic phases within the immobilised films. The heterogeneous electron transfer kinetics and homogeneous charge transport rate for a Nafion-$[Ru(bipy)_3]^{2+}$ system have been explored via convolution voltammetry [83]. This gave the homogeneous charge transport rate as 4×10^{-10} cm^2s^{-1} and k^o as 10^{-4} cms^{-1}.

The electrode kinetics of metal complexes within a series of perfluoro, polycarboxylate and polysulphonate coatings have been explored using normal pulse and current impedance methods [84]. The effect of increased metal content within the film is typically to decrease D_{CT}. By varying the

temperature of the contacting electrolyte, thermodynamic parameters for the homogeneous charge transport process, as well as entropy and enthalpic parameters for the heterogeneous electron transfer were evaluated. Activation energies ranged from 30 to 80 kJ/Mol depending on the nature of the coating. The effect of the Donnan potential on the formal potential of $[Os(bipy)_3]^{2+/3+}$ and other cationic metal complexes immobilised within Nafion films has been explored [85]. The temperature dependence of the formal potentials has been used to calculate entropy terms which include an entropy of transfer as well as an entropy of reaction. These observations have been used to help explain properties of Nafion coatings.

Redox active materials containing two active centres have been investigated [86-87]. Alizarin red S contains two redox sites, namely the 1,2 dihydroxy and 9,10-dione groups and the rate of charge transport through Nafion films containing this material has been measured [87]. These investigations show that charge transport for the conversion of alizarin red S to 1,2-dihydroxyanthracene-9,10-diol-3-sulphonate is significantly larger (D_{CT} = 1.5 x 10^{-10} cm^2s^{-1}) than the conversion to 1,2-dioxoanthracene-9,10-dione-3-sulphonate (D_{CT} = 6.1 x 10^{-11} cm^2s^{-1}) despite both reactions being $2e^-$, $2H^+$ processes. These observations are correlated with different contributions of electron self exchange to the overall charge transport rates. As well as the isolation of cationic materials, electronically conducting polymers such as polypyrrole have been deposited within Nafion [88]. The properties of this composite material differs from the polypyrrole polymer which is normally responsive to the anion type. Charge transport rates through the composite is similar to that obtained for the homopolymer polypyrrole, with a D_{CT}/L^2 value of 3.96 s^{-1}.

The charge transport properties of poly(methylviologen) has been examined within a Nafion film [89]. The nature and concentration of the supporting electrolyte affected both the homogeneous and heterogeneous charge transport kinetics.

Poly(styrenesulphonate) has also been used for the electrostatic confinement of positively charged metal complexes. The electrochemical properties of $[Ru(bipy)_3]^{2+/3+}$ electrostatically bound within this matrix has been explored [90]. D_{CT} was not significantly affected by the concentration of $[Ru(bipy)_3]^{2+}$ within the film over the range 0.38 to 0.08 M, maintaining a value of approximately 1.3×10^{-9} cm^2s^{-1}. D_{CT} decreased with increasing anion size D_{CT} $BF_4^- \simeq ClO_4^- > PF_6^- > CH_3C_6H_4SO_3^-$. This suggested that the transport of charge compensating counterion plays a significant role in the charge propagation rate [91]. Other complexes which have been confined include $[Co(bipy)_3]^{2+}$, $[Co(phen)_3]^{2+}$ and $[Ru(NH_3)_6]^{3+}$ [92], $[Ru(bipy)_2(OH_2)_2]^{2+}$, $[Ru(bipy)_2(OH_2)_2]_2^{4+}O$ [93] and Cu^{2+} [94].

Another important anion exchange material is polylysine. By exchanging $[Co(C_2O_4)_3]^{3-}$ into protonated polylysine coatings two independent pathways for physical diffusion have been diagnosed [95]. There are regions within the film which are filled with electrolyte solution, and species located here behave as for bulk solution, and regions typical of a polymer phase. Species located within "Donnan domains" are confined by electrostatic forces, and give diffusion coefficients of the order of 10^{-7} cm^2s^{-1}. The kinetics of the cross exchange reaction between $[Co(tpy)_2]^{2+}$ (tpy=2,2',2''-terpyridine) and $[Mo(CN)_8]^{3-}$ or

$[W(CN)_8]^{3-}$ confined within protonated poly-L-lysine have also been investigated in terms of the Andrieux-Saveant theory [96].

Poly(N,N-dimethylaniline) can be electropolymerised to form an ionene polymer with quaternary ammonium sites [97]. These sites can be used to bind negatively charged species such as ferrocyanide electrostatically. The rate of charge transport through a 2.75 um film, containing 5 x 10^{-4} $molcm^{-2}$ ferrocyanide with 0.2 M CF_3COONa as supporting electrolyte, was 1.8 x 10^{-9} cm^2s^{-1}. The heterogeneous electron transfer rate for this system was measured as 1.4 x 10^{-4} cms^{-1}. Tris(bathophenanthroline disulphanato)iron(II) has also been immobilised within these films by electropolymerisation [98]. In this system the homogeneous charge transport rate is dependent on the concentration of iron complex within the film. For low fixed site concentrations the homogeneous charge transport rate is 2-3 x 10^{-9} cm^2s^{-1}, while at higher concentrations (0.23 M) D_{CT} is reduced to 2 x 10^{-10} cm^2s^{-1}. The heterogeneous electron transfer rate is between 2.4 and 6.7 x 10^{-5} cms^{-1}, with the transfer coefficient remaining constant at 0.23 ± 0.02.

Section 1.3 Evaluation of Charge Transport Rates for Modified Electrodes.

The importance of the modified electrode lies both in its ability to provide widespread applications, as well as model systems for examining electron transfer reactions. The success of any attempt to exploit modified electrodes in either of these fields lies in a detailed understanding of both charge transport rate and mechanism. This is particularly so for practical applications since ideally, charge should be transported such that it does not

limit the electrode performance. In this section methods of evaluating charge transport rates using cyclic voltammetry, chronoamperometry and sampled current voltammetry are discussed.

Section 1.3.1 Theory of Cyclic Voltammetry.

Cyclic voltammetry has been widely exploited for the elucidation of electrochemical reaction mechanisms, and for the evaluation of diffusion coefficients for solution species. The investigation and characterisation of modified electrodes is also facilitated by this technique. It gives a wide variety of information over a potential range without the need for specialised experimental conditions. The surface coverage of electroactive species and peak position of the active centre are readily accessible.

Cyclic voltammetry can be used to evaluate charge transport rates for modified electrodes, notably by examining the current response of the modified electrode at high sweep rate [4]. This leads to semi-infinite diffusion conditions where the depletion layer produced in the redox reaction does not extend to the film/electrolyte interface. These conditions lead to solution type behaviour and so established theory can be used. The consideration of the modifying layer as a finite diffusion space in order to evaluate both kinetic and charge transport parameters is less widely exploited, despite the well developed theory [1].

Firstly, the theory of semi-infinite linear diffusion for linear sweep voltammetry as applied to modified electrodes is considered [99]. The peak current of a cyclic voltammogram for a modified electrode in the case of a reversible electrode reaction, where a semi-infinite diffusion regime is maintained, is given by the Randles-Sevcik equation (Equation 1) [100]:

$$i_p = 0.4463 \frac{n^{3/2} F^{3/2} A (D_{CT} \nu)^{1/2} C}{(RT)^{1/2}} \quad (1)$$

Other features of the voltammograms are :

$$E_P = E_{pa} - E_{pc} = 0.0592/n \text{ V at } 25\ ^{o}C \quad (2)$$

and

$$i_{pa} / i_{pc} = 1 \quad (3)$$

where i_p is the peak current, n the number of electrons passed (unity for all reactions considered here), F the Faraday constant, R the gas constant, T the temperature, A the electrode area, D_{CT} and C are the charge transport diffusion coefficients and concentration of electroactive species within the film respectively, ν the sweep rate, E_{pa} and E_{pc}, i_{pa} and i_{pc} the anodic and cathodic peak potentials and currents respectively. This analysis will be obeyed for all modified electrodes which show reversible electrochemistry at a sufficiently rapid sweep rate, since the only requirement is that the depletion layer remain sufficiently far inside the modifying film. The Randles-Sevčik equation has been used to evaluate charge transport rates for a monoquaternised bipyridine film [101] and for $[Ru(bipy)_3]^{2+}$ within polybipyrazine [102], as well as, for the materials examined in this thesis

[103]. It is evident that the sweep rate at which semi-infinite diffusion behaviour is observed is a function of the charge transport rate. This observation has been exploited by Andrieux to evaluate D_{CT} for poly(p-nitrostyrene) [104].

Under these semi-infinite diffusion conditions only a proportion of the modifying film is oxidised or reduced. By controlling the timescale of the experiment the situation arises where all electroactive material, which is not kinetically isolated undergoes a redox reaction. This gives rise to the surface or thin-layer situation which is described by equation 4 [105] :

$$i_p = \frac{n^2F^2A\,\nu}{4RT} \qquad (4)$$

$$E_{pa} = E_{pc} \qquad (5)$$

$$\text{FWHH} = 90.6 / n \text{ mV at } 25\ ^{o}C \qquad (6)$$

where Γ is the total amount of electroactive material confined on the electrode surface, (this can be readily obtained from cyclic voltammetry via the relation $\Gamma = Q/nFA$ where Q is the charge passed after background correction in the slow sweep rate voltammogram (typically 1 or 2 mV/s)), further $\Gamma = CL$ where L is the film thickness, FWHH is the full width at half height.

The problem presented by modified electrodes where the surface coverage is greater than a monolayer, is that a cyclic voltammogram representative of pure diffusion or pure surface behaviour may be difficult to attain. This is frequently ascribed to interactions between the adsorbed molecules due to the high concentration [106] or the applied electric field [107]. Other problems arise, such as uncompensated resistance associated with the film or the electrolyte solution which manifests itself in a similar manner to kinetic limitations, causing for example peak to peak separation [108]. Thus one must exercise considerable care as to the manner in which data are obtained and interpreted. The rate of the heterogeneous electron transfer from the underlying electrode material to the modifying layer can sometimes play a role, posing a kinetic limitation at high sweep rates [109]. It is to be noted however that in the majority of cases this does not represent a rate limiting step [110].

The diffusion equation for linear sweep voltammetry with finite diffusion space has been examined by Aoki et al [111] for reversible kinetics with the following assumptions.

1) Mass transfer of both the oxidised (Ox) and reduced (Red) forms of the redox couple is subject only to diffusion described by Fick's second law.

2) The thin film initially contains R with concentration C^0.

3) Both oxidised and reduced forms of the redox couple share a common diffusion coefficient D.

4) Electroactive species cannot pass through the interface between the film and the solution i.e the redox centres are confined within the film.

5) The electrode reaction is sufficiently rapid to ensure a Nernstian equilibrium.

The boundary conditions which describes this situation are given in equation 7:

$$C_0(O, t) / C_R(O,t) = \exp [nF (E_i + \nu t - E^0) / RT]$$

$$i / nF = D(\delta C_R/\delta x)_{x=0} = - D(\delta C_0/\delta x)_{x=0} \qquad (7)$$

$$-(\delta C_0/\delta x)_{x=d} = (\delta C_R/\delta x)_{x=d} = 0$$

The i-E curve is evaluated as the ratio of the thickness of the diffusion space to the diffusion layer goes from a semi-infinite to finite diffusion condition. This leads to a single approximate equation describing the peak current response as a function of the nature of the diffusion space (Equation 8).

$$i_p = 0.4463\ nFA\ \{D_{CT}C/L\}\ \omega^{1/2}\ \tanh\ (0.56\,\omega^{1/2} + 0.05\,\omega) \qquad (8)$$

where $$\omega = nFL^2\,\nu\ /D_{CT}RT$$

This analysis has been extended to cover irreversible and quasi-reversible cases and a kinetic zone diagram (Figure 1.3.1) has been

constructed to describe the effects of differing charge transport and interfacial electron transfer kinetics [109]. Equation 8 allows calculation of charge transport diffusion coefficients over a large range of sweep rates, from a knowledge of surface coverage and peak current at a given sweep rate. The theory also predicts an upper limit for the peak width, at half height of 200/n mV, on transition from surface behaviour to semi-infinite diffusion, the surface case being given by a FWHH of 90.6/n mV. Classical "solution" type behaviour is accounted for in equation 8 since when ω is large (thick layers and/or slow charge transport) it reduces to the Randles-Sevčik equation.

The dependence of the peak potential on sweep rate is given by equation 9 :

$$E_p = E^0 + 0.555\,(RT / nF)\,[1 + \tanh\{2.41\,(\omega^{0.46} - 1.20) + 1.20(\omega^{0.46} - 1.20)^3\}] \qquad (9)$$

The peak width at half height (FWHH) is given by equation 10 :

$$E_{p/2} = [5.72 + 2.20 \tanh\{1.38(\omega^{0.30} - 1.96) + 0.4(\omega^{0.30} - 1.96)^3\}](RT / nF) \qquad (10)$$

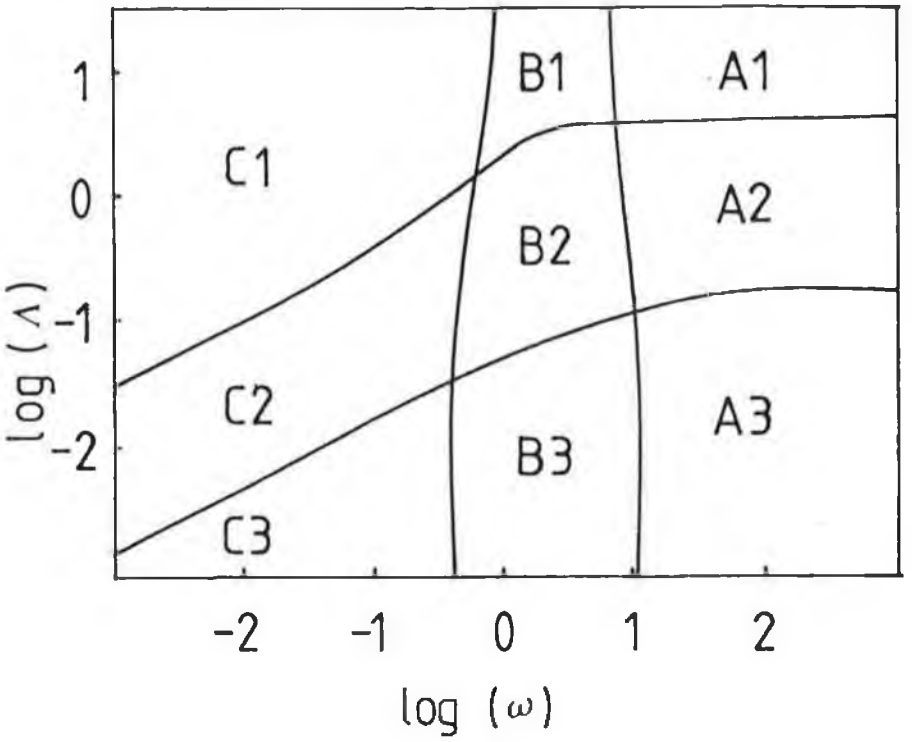

Figure 1.3.1 Domains of Λ (= $k^0(RT/nFD_{CT}\nu)^{1/2}$) and ω for the degrees of reversibility and finite nature of the diffusion space. 1, 2 and 3 denote the reversible, quasi-reversible and irreversible regions respectively. A, B and C are the regions corresponding to the cases of infinite diffusion, finite diffusion and surface wave respectively.

Section 1.3.2 Theory of Potential Step Chronoamperometry.

Chronoamperometry and chronocoulometry can also be performed under semi-infinite or bounded diffusion conditions [112]. Figure 1.3.2 shows the concentration profiles for times $t = t_o = 0$, t_1, t_2 after applying a potential step.

The electroactive species occupies only a thin film of solution (or the modifying layer) and no reactant exists at distances beyond the film thickness L. The equation describing the response obtained after a potential step on a solution is given by equation 11 [112]:

$$i(t) = \frac{nFAD_{CT}^{1/2}C}{\pi^{1/2}t^{1/2}} \sum_{k=0}^{\infty} (-1)^k \exp\left[\frac{-k^2d^2}{D_{CT}t}\right] - \exp\left[\frac{-(k+1)^2d^2}{D_{CT}t}\right] \quad (11)$$

The use of this finite diffusion space equation can yield information at longer times, where different equilibria to those observed at the short timescale can affect the observed response. By recording the current response to a perturbing potential step at sufficiently short times, where the depletion layer does not extend to the film/electrolyte interface, then equation 11 reduces to the classical Cottrell equation [113] describing diffusion in solution (12).

$$i(t) = \frac{nFAD_{CT}^{1/2}C}{\pi^{1/2}t^{1/2}} \quad (12)$$

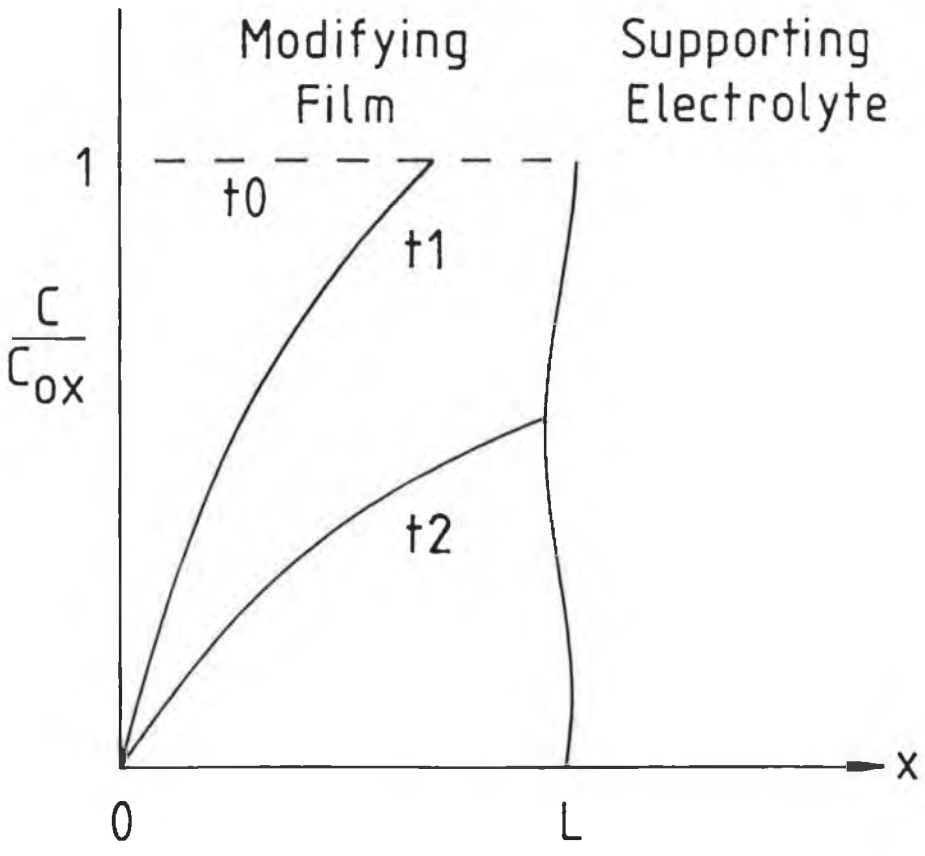

Figure 1.3.2 Concentration profiles for electroactive species within a polymer film after application of an oxidising potential step.

The effect of uncompensated resistance on large amplitude chronoamperometric experiments has been considered by several authors [114-116]. The presence of large Faradaic currents in the presence of uncompensated resistance, R_u, can produce an ohmic drop, causing the actual electrode potential to be less than the intended value. This can lead to significant errors in the estimation of kinetic parameters [117]. The Nernst equation [118] is assumed to govern the surface concentration for reversible electrode processes. Since iR_u drop prevents the actual electrode potential from attaining the desired value, i.e. that required for the redox reaction to proceed independently of the electrode potential, uncompensated resistance means that the Nernst equation does not apply. The effect of uncompensated resistance on the potential step measurements for the osmium containing metallopolymers examined in this thesis is considered in chapter 3 (vide infra).

Section 1.3.3 Theory of Sampled Current Voltammetry.

The rate of charge percolation can also be examined using sampled current voltammetry. The waveform involves applying a series of potential steps of increasing amplitude, encompassing a potential range, where there is initially no redox reaction, to a point where the response is diffusion controlled. The current decay from the exciting pulses is then recorded instantaneously at several different times, unlike conventional normal pulse polarography where signal averaging toward the end of the pulse is employed [119]. Thus the values of the apparent charge transport diffusion parameter $D_{CT}{}^{1/2}C$ for the process of charge transport within the coatings can be obtained from the slopes of i_{lim} vs $t^{-1/2}$ plots via the Cottrell equation

(equation 12).

The current-potential relationship for the sampled current voltammograms for the simple electrode process Red = Ox + ne^-, has been derived [120] and is given for the oxidation process by :

$$E = E^* \pm RT/\alpha nF \ln\left[x\left[\frac{1.75 + x^2(1 + \exp(\pm\xi))^2}{1 - x(1 + \exp(\pm\xi))} \right] \right] \qquad (13)$$

$$E^* = E^o \pm RT/\alpha nF \left[\frac{\ln\ 4\ \ k^o\ \tau^{1/2}}{3^{1/2}\ \ D_{CT}{}^{1/2}} \right]$$

where E is the electrode potential, E^o is the reversible half-wave potential, α is the anodic transfer coefficient, k^o is the standard rate constant, τ is the sampling time, R is the gas constant, T is the absolute temperature, $\xi = (nF/RT)(E-E^o)$, D_{CT} is the charge transport diffusion coefficient, and x is the ratio of the current i at potential E, to the limiting diffusion controlled current.

From equation 13 it can be seen using the value of E^o obtained from cyclic voltammetry, that when the logarithm of the third term on the right hand side is plotted against E for the oxidation process a straight line is obtained. The slope of these lines and their intersection with the zero line are equal to $\alpha nF/RT$ and $E^o-(RT/\alpha nF)\ln\{(4/3^{1/2})(k^o(\tau/D_{CT})^{1/2})\}$ respectively. These values can then be used to evaluate the transfer coefficient and standard rate constant.

Section 1.4 Evaluation of Thermodynamic Parameters for Modified Electrodes.

Section 1.4.1 Homogeneous Charge Transport

The dependence of D_{CT} on the temperature of the supporting electrolyte can be used to calculate the thermodynamic parameters for homogeneous charge transport, namely E_a, $\Delta H^{\ddagger}$, $\Delta S^{\ddagger}$ and $\Delta G^{\ddagger}$. The Arrhenius equation [9] (Equation 14) describes the response for activated charge transport through polymer films :

$$D_{CT} = D_{CT}^{o} \exp(-E_a / RT) \qquad (14)$$

where D_{CT} is the rate of homogeneous charge transport evaluated either by cyclic voltammetry or chronoamperometry, D_{CT}^{o} is the preexponential factor, E_a is the activation energy, R the gas constant and T the absolute temperature. The activation enthalpy $\Delta H^{\ddagger}$ is then given by E_a - RT. The entropy of charge transport can be derived from the Eyring equation [121] (Equation 15):

$$D_{CT}^{o} = e\delta^{2}(k_B T/h)\exp(\Delta S^{\ddagger}/R) \qquad (15)$$

where e is the base of the natural log, K_B is the Boltzmann constant, h Planck's constant and δ is the equilibrium separation of vicinal redox sites.

Section 1.4.2 Heterogeneous Electron Transfer

Temperature effects on k^o have been examined to evaluate enthalpic and entropic parameters for the heterogeneous electron transfer reaction. The effect of temperature on the standard heterogeneous rate constant is considered to obey the following relation [122-124]:

$$\log (k^o) = \log\{Z_{el} k p \exp[(\Delta S_{\ddagger}^{o})_{real}/R]\} \qquad (16)$$

$$-(\Delta H_{\ddagger}^{o})_{real}/2.303RT$$

where Z_{el} is the heterogeneous collision frequency (assumed to have negligible temperature dependence), k and p are constants (assumed equal to unity), $(\Delta S_{\ddagger}^{o})_{real}$ and $(\Delta H_{\ddagger}^{o})_{real}$ represent the entropic and enthalpic barriers at the standard potential after correction for the entropic and enthalpic driving forces, $\Delta H_{rc}^{o}(=T\Delta S_{rc}^{o})$ and ΔS_{rc}^{o} respectively. ΔS_{rc}^{o} can be calculated from the temperature dependence of the formal potential of the redox couple [125,126]:

$$\Delta S_{rc}^{o} \simeq F(\delta E^{o}/\delta T) \qquad (17)$$

This reaction entropy difference between the reduced and oxidised forms of the redox couple can also be evaluated using an electrostatic model [127]:

$$(\Delta S_{rc}^{o})_{Born} = 47.88(Z_{Ox}^{2}/a_{Ox} - Z_{Red}^{2}/a_{Red}) \quad (18)$$

where Z_{Ox} and Z_{Red} are the net charges and a_{Ox} and a_{Red} are the equivalent radii in angstroms of the oxidised and reduced species respectively.

The temperature dependence of k^{o} can also be used to calculate $(\Delta H^{o})_{ideal}$ and $(\Delta S^{o})_{ideal}$ which give the enthalpic and entropic barriers to electron transfer at a particular potential where they are evaluated from Equation 19 and 20 [122-124]

$$(\Delta H^{o})_{ideal} = (\Delta H^{o})_{real} + \alpha T \Delta S_{rc}^{o} \quad (19)$$

$$(\Delta S^{o})_{ideal} = (\Delta S^{o})_{real} + \alpha \Delta S_{rc}^{o} \quad (20)$$

Section 1.5 Concluding Remarks.

From this review, it is evident, that charge transport through polymer films on electrode surfaces in which redox active groups have been immobilised either coordinatively or electrostatically has been extensively examined. The subject is now approaching a mature state, and more recent publications have centred upon quantitative measurements of charge transport rates through polymer films and the more subtle features of electron transfer dynamics.

The range of materials which has been examined is large, including electropolymerised redox active systems, as well as materials in which the redox active centre is immobilised, either by electrostatic or covalent binding after the initial synthesis of a polymeric backbone. Redox active polymers can give rise to films which are smooth, monolithic, pore free overlayers or granular films which contain pores and/or different phases e.g. hydrophobic and hydrophilic regions in Nafion films or Donnan domains in polylysine. The concentration of active sites within the films varies considerably. Those systems in which the redox centres are electrostatically bound, generally have relatively lower concentrations as dictated by the partition coefficient, while electropolymerised / preformed polymers can have redox site concentrations as high as 10 M.

The rate of charge transport through polymer films is strongly dependent on the chemical and physical composition of the film as well as on temperature and electrolyte. Charge transport rates of between 10^{-12} and 10^{-6} cm^2s^{-1} are observed with the most rapid charge transport rates being observed via steady state techniques such as interdigitative arrays and the "closed-face sandwich" method of Pickup and Murray, where ion transport/migration effects are avoided. However, conventional electrochemical

techniques such as cyclic voltammetry chronoamperometry and chronocoulometry find the most widespread application in the diagnosis of charge transport processes. Under certain experimental conditions charge propagation through polymer modified electrodes is typically diffusional and obeys Fick's laws of diffusion. In general, the electron transfer kinetics both from the underlying electrode into the film and within the film obey the conventional models describing electron transfer such as Butler-Volmer kinetics. The slow rate of homogeneous charge transport through polymer films is due to a combination of slow diffusion of the electroactive species through the viscous polymer medium, restricted segmental polymer chain motion, inter/intra chain interactions and ion transport limitations. The identification of the rate determining step for the charge transport process by altering the redox site loading, electrolyte type and concentration has been examined for electrostatically bound redox centres but less so for active sites which are coordinatively bound to polymer chains. The evaluation of thermodynamic parameters has not been widely exploited, presumably because a large number of systems are incompatible with a wide variation of temperature.

It is becoming apparent, that the application of modified electrodes will be dependent on the production of stable electrodes which are highly permeable for ions but at the same time possess highly oriented redox centres at a high concentration for fast electron transfer. However, these requirements are to some extent mutually exclusive. Optimum conditions can be found by varying both the structure and chemical composition of the modifying film and external parameters such as electrolyte type and concentration of the electrolyte.

Section 1.6 References.

1. R. W. Murray, Ann. Rev. Mater. Sci., 1984, 13, 191
2. R. W. Murray, Acc. Chem. Res., 1980, 13, 135
3. W. J. Albery and A. R. Hillman, Roy. Soc. Chem., Ann. Rep. C, 1981, 78, 377
4. A. R. Hillman in Electrochemical Science and Technology of Polymers, vol. 1, ed. R. G. Linford, Elsevier Applied Science, Amsterdam, 1987, p. 103
5. M. Umana, P. Denisevich, D. R. Rolison, S. Nakahama and R. W. Murray, Anal. Chem., 1981, 53, 1170
6. B. R. Shaw, G. P. Haight and L. R. Faulkner, J. Electroanal. Chem., 1982, 140, 147
7. P. J. Peerce and A. J. Bard, J. Electroanal. Chem., 1980, 114, 89
8. R. J. Nowak, F. A. Schultz, M. Umana, R. Lam and R. W. Murray, Anal. Chem., 1980, 52, 315
9. A. H. Schroeder and F. B. Kaufman, J. Electroanal. Chem., 1980, 113, 209
10. P. Daum, J. R. Lenhard, D. Rolison and R. W. Murray, J. Am. Chem. Soc., 1980, 102, 4649
11. P. Daum and R. W. Murray, J. Phys. Chem., 1981, 85, 389
12. J. Leddy and A. J. Bard, J. Electroanal. Chem., 1983, 153, 223
13. E. F. Bowden, M. F. Dautartas and J. F. Evans, J. Electroanal. Chem., 1987, 219, 49
14. M. F. Dautartas, E. F. Bowden and J. F. Evans, J. Electroanal. Chem., 1987, 219, 71

15. E. F. Bowden, M. F. Dautartas and J. F. Evans, J. Electroanal. Chem., 1987, 219, 91

16. G. Inzelt and L. Szabo, Electrochim. Acta, 1986, 31, 1381

17. W. J. Albery, M. G. Boutelle, P. J. Colby and A. R. Hillman, J. Electroanal. Chem., 1982, 133, 135

18. W. J. Albery, W. R. Bowen, F. S. Fisher, A. W. Foulds, K. J. Hall, A. R. Hillman, R. G. Egdell and A. R. Orchard, J. Electroanal. Chem., 1980, 107, 37

19. W. J. Albery, A. W. Foulds, K. J. Hall and A. R. Hillman, J. Electrochem. Soc., 1980, 127, 654

20. W. J. Albery, A. W. Foulds, K. J. Hall, A. R. Hillman, R. G. Egdell and A. F. Orchard, Nature, 1979, 282, 793

21. W. J. Albery, M. G. Boutelle and A. R. Hillman, J. Electroanal. Chem., 1985, 182, 99

22. C. R. Leidner and R. W. Murray, J. Am. Chem. Soc., 1984, 106, 1606

23. T. Ikeda, R. Schmehl, P. Denisevich, K. Willman and R. W. Murray, J. Am. Chem. Soc., 1982, 104, 2683

24. K. W. Willman and R. W. Murray, J. Electroanal. Chem., 1982, 133, 211

25. R. H. Schmehl and R. W. Murray, J. Electroanal. Chem., 1983, 152, 97

26. L. D. Margerum, T. J. Meyer and R. W. Murray, J. Electroanal. Chem., 1983, 149, 279

27. H. D. Abruna and A. J. Bard, J. Am. Chem. Soc., 1982, 104, 2641

28. A. G. Ewing, B. J. Feldman and R. W. Murray, J. Phys. Chem., 1985, 89, 1263

29. P. G. Pickup and R. W. Murray, J. Am. Chem. Soc., 1983, 105, 4510

30. P. G. Pickup, W. Kutner, C. R. Leidner and R. W. Murray, J. Am. Chem. Soc., 1984, 106, 1991

31. J. C. Jernigan and R. W. Murray, J. Am. Chem. Soc., 1987, 109, 1738

32. C. E. D. Chidsey and R. W. Murray, J. Phys. Chem., 1986, 90, 1479

33. A. R. Guadalupe, D. A. Usifer, K. T. Potts, H. C. Hurrell, A. E. Mogstad and H. D. Abruna, J. Am. Chem. Soc., 1988, 110, 3462

34. J. S. Facci, R. H. Schmehl and R. W. Murray, J. Am. Chem. Soc., 1982, 104, 4959

35. P. G. Pickup and R. A. Osteryoung, J. Electroanal. Chem., 1985, 186, 99

36. G. Inzelt, R. W. Day, J. F. Kinstle and J. Q. Chambers, J. Phys. Chem., 1983, 87, 4592

37. G. Inzelt, R. W. Day, J. F. Kinstle and J. Q. Chambers, J. Electroanal. Chem., 1984, 161, 147

38. G. Inzelt, J. Q. Chambers, J. F. Kinstle and R. W. Day, J. Am. Chem. Soc., 1984, 106, 3396

39. G. Inzelt, J. Bacskai, J. Q. Chambers and R. W. Day, J. Electroanal. Chem., 1986, 201, 301

40. S. B. Khoo, J. K. Foley and S. Pons, J. Electroanal. Chem., 1986, 215, 273

41. G. Inzelt, Electrochim. Acta, 1989, 34, 83

42. N. Oyama, T. Ohsaka, H. Yamamoto and M. Kaneko, J. Phys. Chem., 1986, 90, 3850

43. T. Osaka, H. Yamamoto and N. Oyama, J. Phys. Chem., 1987, 91, 3775

44. K. Chiba, T. Ohsaka and N. Oyama, J. Electroanal. Chem., 1987, 217, 239

45. F. W. Nyasulu and H. A. Mottola, J. Electroanal. Chem., 1988, 239, 175

46. I. De Gregori, F. Bedioui and J. Devynck, J. Electroanal. Chem., 1987, 238, 197

47. S. M. Oh and L. R. Faulkner, J. Am. Chem. Soc., 1989, 111, 5613

48. J. M. Clear, J. M. Kelly, C. M. O'Connell and J. G. Vos, J. Chem. Res., M, 1981, 3039

49. O. Haas and J. G. Vos, J. Electroanal. Chem., 1980, 113, 139

50. O. Haas, M. Kriens and J. G. Vos, J. Am. Chem. Soc., 1981, 103, 1313

51. O. Haas, N. Muller and H. Gerischer, Electrochim. Acta, 1982, 27, 991

52. O. Haas, H. Zumbrunnen and J. G. Vos, Electrochim. Acta, 1985, 30, 1551

53. C. P. Andrieux in Electrochemistry, Sensors and Analysis, Analytical Symposia Series, Vol. 25, Elsevier, Amsterdam, 1986, 235

54. M. E. G. Lyons, H. G. Fay, J. G. Vos and A. J. Kelly, J. Electroanal. Chem., 1988, 250, 207

55. C. P. Andrieux, O. Haas and J. M. Saveant, J. Am. Chem. Soc., 1986, 108, 8175

56. S. M. Geraty, D. W. M. Arrigan and J. G. Vos in Electrochemistry, Sensors and Analysis, Analytical Symposia Series, Eds. M. R. Smyth and J. G. Vos, Vol. 25, Elsevier, Amsterdam, 1986, 303

57. J. F. Cassidy, A. G. Ross and J. G. Vos in Electrochemistry, Sensors and Analysis, Analytical Symposia Series, Eds. M. R. Smyth and J. G. Vos, Vol. 25, Elsevier, Amsterdam, 1986, 269

58. N. Oyama and F. C. Anson, J. Electrochem. Soc., 1980, 127, 640

59. K. Shigehara, N. Oyama and F. C. Anson, Inorg. Chem., 1981, 20, 518

60. H. R. Zumbrunnen and F. C. Anson, J. Electroanal. Chem., 1983, 152, 111

61. N. Oyama and F. C. Anson, Anal. Chem., 1980, 52, 1192

62. N. Oyama, J. Shimomura, K. Shigehara and F. C. Anson, J. Electroanal. Chem., 1980, 112, 271

63. C. R. Martin, I. Rubenstein and A. J. Bard, J. Am. Chem. Soc., 1982, 104, 4817

64. S. M. Oh and L. R. Faulkner, J. Electroanal. Chem., 1989, 269, 77

65. K. K. Shiu, R. Chemerika and D. J. Harrison, Anal. Chem., 1989, 61, 570

66. K. Dobhlhofer, W. Durr and M. Jauch, Electrochim. Acta., 1982, 27, 677

67. K. Doblhofer, H. Braun and R. Lange, J. Electroanal. Chem., 1986, 206, 93

68. R. Lange and K. Doblhofer, J. Electroanal. Chem., 1987, 216, 241

69. R. Lange and K. Doblhofer, J. Electroanal. Chem., 1987, 237, 13

70. X. Chen, P. He and L. R. Faulkner,J. Electroanal. Chem., 1983, 222, 97

71. B. Lindholm, J. Electroanal. Chem., 1988, 250, 341

72. N. Oyama, S. Yamaguchi, Y. Nishiki, K. Tokuda, H. Matsuda and F. C. Anson, J. Electroanal. Chem., 1982, 139, 371

73. N. Oyama, T. Ohsaka and T. Ushirogouchi, J. Phys. Chem., 1984, 88, 5274

74. T. Ohsaka, T. Okajima and N. Oyama, J. Electroanal. Chem., 1986, 215, 191

75. T. Ohsaka, T. Ushirogouchi and N. Oyama, Bull. Chem. Soc. Jpn., 1985, 58, 3252

76. B. Lindholm, M. Sharp and R. D. Armstrong, J. Electroanal. Chem., 1987, 235, 169

77. N. Oyama, T. Ohsaka, M. Kaneko, K. Sato and H. Matsuda, J. Am. Chem. Soc., 1983, 105, 6003

78. D. A. Buttry and F. C. Anson, J. Electroanal. Chem., 1981, 130, 333

79. M. N. Szentirmay and C. R. Martin, Anal. Chem., 1984, 56, 1898

80. H. S. White, J. Leddy and A. J. Bard, J. Am. Chem. Soc., 1982, 104, 4811

81. C. R. Martin, I. Rubenstein and A. J. Bard, J. Am. Chem. Soc., 1982, 104, 4817

82. D. A. Buttry and F. C. Anson, J. Am. Chem. Soc., 1983, 105, 685

83. J. Leddy and A. J. Bard, J. Electroanal. Chem., 1985, 189, 203

84. N. Oyama, T. Ohsaka, T. Ushirogouchi, S. Sanpei and S. Nakamura, Bull. Chem. Soc. Jpn., 1988, 61, 3103

85. R. Naegeli, J. Redepenning and F. C. Anson, J. Phys. Chem., 1986, 90, 6227

86. Y. M. Tsou and F. C. Anson, J. Phys. Chem., 1985, 89, 3818 and refs therein

87. T. Ohsaka, N. Oyama, Y. Takahira and S. Nakamura, J. Electroanal. Chem., 1988, 247, 339

88. G. Nagasubramanian, S. Di Stefano and J. Moacannin, J. Phys. Chem., 1986, 90, 4447

89. T. Ohsaka, N. Oyama, K. Sato and H. Matsuda, J. Electrochem. Soc., 1985, 132, 1871

90. M. Majda and L. R. Faulkner, J. Electroanal. Chem., 1984, 169, 77

91. M. Majda and L. R. Faulkner, J. Electroanal. Chem., 1982, 137, 149

92. N. Oyama, J. Shimomura, K. Shigehara and F. C. Anson, J. Electroanal. Chem., 1980, 112, 271

93. C. D. Ellis, J. A. Gilbert, W. R. Murphy and T. J. Meyer, J. Am. Chem. Soc., 1983, 105, 4842

94. J. Wang, B. Greene and C. Morgan, Anal. Chim. Acta, 1984, 158, 15

95. F. C. Anson, T. Ohsaka and J. M. Saveant, J. Phys. Chem., 1983, 87, 640

96. F. C. Anson, T. Ohsaka and J. M. Saveant, J. Am. Chem. Soc., 1983, 105, 4883

97. N. Oyama, T. Ohsaka and T. Shimizu, Anal. Chem. 1985, 57, 1526

98. N. Oyama, T. Ohsaka and M. Nakanishi, J. Macromol. Sci., 1987, A24, 375

99. E. Laviron, J. Electroanal. Chem., 1980, 112, 1

100. A. Sevcik, Collect. Czech. Chem. Commum., 1948, 44, 327

101. K. M. O'Connell, E. Waldner, L. Roullier and E. Laviron, J. Electroanal. Chem., 1984, 162, 77

102. P. K. Ghosh and A. J. Bard, J. Electroanal. Chem., 1984, 169, 113

103. R. J. Forster, A. J. Kelly, J. G. Vos and M. E. G. Lyons, J. Electroanal. Chem., 1989, 270, 365

104. C. P. Andrieux and J. M. Saveant, J. Electroanal. Chem., 1980, 111, 377

105. D. M. Mohliner, J. Electroanal. Chem., 1983, 146, 417

106. A. P. Brown and F. C. Anson, Anal. Chem., 1977, 49, 1589

107. H. Gerischer and D. A. Scherson, J. Electroanal. Chem., 1985, 188, 33

108. H. Daifuku, K. Aoki, K. Tokuda and H. Matsuda, J. Electroanal. Chem., 1985, 183, 1

109. K. Aoki, K. Tokuda and H. Matsuda, J. Electroanal. Chem., 1984, 160, 33

110. F. C. Anson, J. Phys. Chem., 1980, 84, 3336

111. K. Aoki, K. Tokuda and H. Matsuda, J. Electroanal. Chem., 1983, 146, 417

112. D. M. Oglesby, S. H. Omang and C. N. Reilley, Anal. Chem., 1965, 37, 1312

113. H. Gerischer and W. Vielstich, Z. Phys. Chem., 1955, 3, 16

114. F. C. Anson, J. H. Christie and R. A. Osteryoung, J. Electroanal. Chem., 1967, 13, 343

115. W. Richtering and K. Doblhofer, Electrochim. Acta, 1989, 34, 1685

116. L. Roullier and E. Laviron, J. Electroanal. Chem., 1983, 157, 193

117. J. Leddy and A. J. Bard, J. Electroanal. Chem., 1985, 189, 203

118. A. J. Bard and L. R. Faulkner, Electrochemical Methods-Fundamentals and Aplications, Wiley, New York (1980)

119. G. C. Barker and A. W. Gardner, Z. Anal. Chem., 1960, 173, 79

120. H. Matsuda, Bull. Chem. Soc. Jpn., 1980, 53, 3439

121. R. C. Bowers and R. W. Murray, Anal. Chem., 1966, 38, 461

122. M. J. Weaver, J. Phys. Chem., 1976, 83, 2645

123. J. T. Hupp and M. J. Weaver, J. Electroanal. Chem., 1983, 145, 43

124. N. Sutin, M. J. Weaver and E. L. Yee, Inorg. Chem., 1980, 19, 1096

125. K. J. Vetter, Electrochemical Kinetics, Academic Press, New York and London 1987 p. 107

126. E. L. Yee, R. J. Cave, K. L. Guyer, P. D. Tyma and M. J. Weaver, J. Am. Chem. Soc., 1979, 101, 1131

127. R. M. Noyes, J. Am. Chem. Soc., 1962, 84, 513

CHAPTER 2

Synthesis, Characterisation and Properties of a Series of Osmium and Ruthenium Containing Metallopolymers

Section 2.1 Introduction.

Metallopolymers constitute a class of materials that is attracting increasing attention because of their potentially widespread application [1-5]. In particular, polymers containing covalently bound ruthenium complexes have been investigated in some detail and the application of these materials as redox catalysts, photosensitisers and molecular diodes has been proposed [6-21]. In these studies, the materials are often applied as thin layers on solid electrode surfaces and the properties of the so formed modified electrodes are investigated. Ruthenium containing metallopolymers are of interest due to their long lived excited state and facile electron exchange dynamics, which can be exploited in areas such as photosensitisation. However, photochemically induced ligand exchange reactions are frequently a feature of these materials [20-23]. Investigations of polymers of the type $[Ru(bipy)_2(Pol)_nCl]Cl$ and $[Ru(bipy)_2(Pol)_n]Cl_2$ (where bipy = 2,2'-bipyridyl and Pol = poly-4-vinylpyridine (PVP), poly-N-vinylimidazole (PVI) or a copolymer of 4-vinylpyridine and styrene or methylmethacrylate) have been reported [15-16]. In these investigations detailed information about the charge transport processes within the polymer layers was obtained and it was shown that the nature of the polymer backbone and the metal to polymer ratio (n) are important factors, which determine the electrochemical process, and hence influence the utility of these materials. However, little is known about the relationship between the physical properties of the metallopolymer and its electrochemical response. For example, the effect of chain mobility or interactions between the polymer bound metal centres has not been addressed in any detail [24]. This chapter describes the synthesis and characterisation of

a series of novel metallopolymers of the type $[Os(bipy)_2polCl]^+$ or $[Os(bipy)_2pol_2]^{2+}$ (pol= poly-4-vinylpyridine (PVP) or poly-N-vinylimidazole(PVI)) as well as metallopolymers containing two different redox centres based on ruthenium and osmium bis(2,2'-bipyridyl) moieties. The aim of these studies is to systematically investigate series of polymers containing different redox active groups, with different metal to polymer ratios, and with different polymer backbones. The metallopolymers described offer considerable synthetic flexibility in that, unlike other systems, many of the parameters which influence the response can be independently and easily varied. The effect of the presence of two redox centres in the same polymer on ground and excited state properties has been explored using electrochemical and spectroscopic techniques. It is anticipated that such investigations should allow a better understanding of the correlation between the electrochemical and mechanical properties of thin layers of these materials. Finally the investigation of possible interactions between the polymer bound metal centres is of interest.

Section 2.2 Experimental Section

Section 2.2.1 Equipment and Methods.

Uv-visible spectra were recorded on Hewlett-Packard 342A diode array and Shimadzu UV 240 spectrophotometers. Emission spectra were recorded using a Perkin-Elmer LS-5 luminescence spectrometer equipped with a red-sensitive Hamamatsu R928 detector. Spectra were recorded using an emission slit width of 10 nm at room temperature and 2.5 nm at 77 K and are not corrected for photomultiplier response. Electrochemical measurements were performed using an

E. G. & G. PAR 273 potentiostat/galvanostat. A visible 100 W light source was used for the photochemical experiments. Glassy carbon electrodes of 7 mm diameter were modified by pipetting the required quantity of a methanolic 1% (w/v) solution of the metallopolymer directly onto their surface. The solvent was then allowed to evaporate slowly in a solvent saturated chamber followed by air drying. All potentials are quoted versus a potassium saturated calomel electrode (SCE) without regard for liquid junction potentials. Peak positions for the redox couples of the metallopolymer coatings were obtained at slow sweep rates where the anodic and cathodic peaks typically converge. Potential step chronoamperometry was used to determine Os(II/III) charge transport rates by stepping from -0.4 V to 200 mV past the formal potential of the redox couple. Charge transport rates for Ru(II/III) oxidation were calculated by stepping from -0.4 V to 1.3 V and then subtracting out the current contribution from the Os(II/III) oxidation. Alternatively by initially holding the potential past the formal potential of the osmium couple, until the osmium oxidation is complete, and then stepping to 1.3 V, the charge transport rate could be assessed without an osmium contribution. These transient current/charge measurements were made over the time range 0 to 20 ms by means of a Philips 3311 digital storage oscilloscope interfaced to a BBC microcomputer for data interrogation and allowing signal averaged results to be obtained [25]. Differential scanning calorimetry (D.S.C.) was performed using 2 mg samples of vacuum dried materials using a Stanton Redcroft CPC 706 Temperature Programmer, a DSC lineariser and a DC amplifier. Experiments were carried out in static air with a heating rate of 10 ^{o}C per minute up to temperatures of 350 ^{o}C.

Section 2.2.2 Synthesis of Monomeric and Polymeric Materials.

$[Ru(bipy)_2Cl_2]$ [26], $[Ru(bipy)_2(H_2O)_2](PF_6)_2$ [27], $[Ru(bipy)_2(PVP)_{10}Cl]Cl$, (1), [17] $[Ru(bipy)_2(PVP)_{10}](Cl)_2$, (2), [17] $[Ru(bipy)_2(PVI)_{10}Cl]Cl$ (3), [20] and $[Ru(bipy)_2(PVI)_{10}]Cl_2$, (4), [20] were prepared as described previously. $[Os(bipy)_2Cl_2]$ was prepared as described by Buckingham et al. [28].

Poly(4-vinylpyridine) : Poly(4-vinylpyridine) was prepared by bulk polymerisation of freshly distilled 4-vinylpyridine under a nitrogen atmosphere using 2,2'-azoisobutyronitrile as initiator at 70 ^{o}C. The product was purified by repeated precipitation in diethyl ether from methanol. The resulting polymer was fractionated by partial precipitation from methanol solutions by addition of toluene to cloud point, followed by raising the temperature. The molecular weight of the precipitant at 40 ^{o}C was determined by viscometry measurements in ethanol in conjunction with the Mark-Houwink equation $[n] = 2.5 \times 10^{-4} M_v^{0.68}$, to be approximately 430,000 g/Mol [29].

Poly(N-vinylimidazole) : Poly(N-vinylimidazole) was prepared from freshly distilled monomer as described above for PVP and similarly fractionated. The molecular weight, as determined by viscometry in ethanol in conjunction with the Mark-Houwink equation; $[n] = 9.83 \times 10^{-4} M_v^{0.54}$, was 110,000 g/Mol. [30]

$[Os(bipy)_2(Pol)_nCl]Cl$ pol=poly-4-vinylpyridine or poly-N-vinylimidazole; n = 5, 10, 15, 25. PVP polymers labelled as compounds 5 - 8, PVI polymers as compounds 9 - 12 respectively. The metallopolymers were prepared as the analogous ruthenium polymers [17,20] except that longer reflux times were required. $[Os(bipy)_2Cl_2]$ and the appropriate amount of the polymer were heated at reflux in ethanol for periods of up to 3 days. The reaction was monitored by uv-visible spectroscopy and cyclic voltammetry. Although no photochemical reactions were observed the reactions were routinely carried out in the dark. The metallopolymers were isolated by precipitation into diethyl ether and purified by repeated precipitation (3x) in diethyl ether from methanol. In a typical synthesis of $[Os(bipy)_2(PVP_5)Cl]Cl$ 40 mg (0.07 mM) of $[Os(bipy)_2Cl_2]$ was dissolved in 30 cm^3 of ethanol and refluxed for 30 minutes. 73 mg (0.7 mM) of PVP in 10 cm^3 of ethanol were then added and refluxing continued for 72 hours. The metallopolymer was recovered by precipitation into diethyl ether and vacuum dried. Yield 104 mg, 92%. The perchlorate salts of these polymers were prepared by addition of a two molar excess of lithium perchlorate to the ethanol solution of the metallopolymer. The precipitant polymer was recovered by filtration and purified as for the materials where chloride was the anion. These materials are labelled as 5a - 8a for the PVP polymers and 9a - 12a for the PVI polymers.

$[Os(bipy)_2(PVP)_{10}]Cl_2$, Compound 13:

$[Os(bipy)_2Cl_2]$ (57 mg, 0.1 mmol) and PVP (104 mg, 1 mmol) were heated at reflux in 75 cm^3 ethanol-water (50:50) in the dark for 8 days. The metallopolymer was recovered by solvent stripping and subsequent dissolution in methanol followed by precipitation into diethylether and vacuum dried. The reaction could also be carried out in ethylene glycol/water mixtures with some reduction in the reflux time. Yield 146 mg, 91%.

$[Os(bipy)_2(PVI)_{10}]Cl_2$, Compound 14:

This polymer was prepared as reported above for the analogous PVP polymer. Yield 87%.

Metallopolymers of the type $[Os(bipy)_2polCl]Cl$ / $[Os(bipy)_2pol_2]Cl_2$ (pol=poly(4-vinylpyridine) or poly(N-vinylimidazole)) could be isolated during the preparation of 13 and 14 respectively. The reactions appear to be stepwise in nature with the $[Os(bipy)_2polCl]Cl$ species being initially formed before the second chloride anion is displaced to give the $[Os(bipy)_2pol_2]Cl_2$ species. Thus by isolating the products during the reaction any desired ratio of mono to bis substituted products could be obtained. The properties of these materials are similar to a combination of those associated with their respective constituents.

$[Os(bipy)_2(PVP)_{10}Cl]Cl/[Ru(bipy)_2(PVP)_{10}Cl]Cl$, Compound 15 :

To 57 mg (0.035 mmol) of $[Os(bipy)_2(PVP)_{10}Cl]Cl$ (6) in 75 cm^3 methanol, $[Ru(bipy)_2Cl_2]$ (17 mg, 0.035 mmol) was added and the solution refluxed in the dark for three days. The resulting metallopolymer was

recovered by precipitation into diethyl ether (3x) and vacuum dried. Yield 68 mg, 92%.

$[Os(bipy)_2(PVI)_{10}Cl]Cl/[Ru(bipy)_2(PVI)_{10}Cl]Cl$, Compound 16:

To 53 mg (0.035 mmol) of $[Os(bipy)_2(PVI)_{10}Cl]Cl$ (10) in 75 cm^3 methanol $[Ru(bipy)_2Cl_2]$ (17 mg, 0.035 mmol) was added and the solution refluxed in the dark for 24 hours. The resulting metallopolymer was recovered by precipitation into diethyl ether (3x) and vacuum dried. Yield 62 mg, 88%.

$[Ru(bipy)_2(PVP)_{10}](Cl)_2/[Os(bipy)_2(PVP)_{10}Cl]Cl$, Compound 17.

To 62 mg (0.04 mmol) of $[Ru(bipy)_2(PVP)_{10}](Cl)_2$ (2) dissolved in 75 cm^3 methanol 23 mg (0.04 mmol) of $[Os(bipy)_2Cl_2]$ were added. The resulting solution was refluxed in the dark for 3 days. The product was recovered as described above and purified by precipitating three times in diethyl ether from methanol. Yield 67 mg, 80%.

$[Ru(bipy)_2(PVI)_{10}](Cl)_2/[Os(bipy)_2(PVI)_{10}Cl]Cl$, Compound 18.

This mixed ruthenium/osmium metallopolymer was prepared from compound 4 and purified as given above for compound 17. Yield 85%.

$[Os(bipy)_2(PVP)_{10}](Cl)_2/[Ru(bipy)_2(PVP)_{10}](Cl)_2$, Compound 19.

To $[Os(bipy)_2(PVP)_{10}](Cl)_2$ (13) (50 mg, 0.03 mmol) in 75 cm^3 methanol $[Ru(bipy)_2(H_2O)_2](ClO_4)_2$ (19 mg, 0.03 mmol) was added. The resulting solution was refluxed in the dark for 3 days. The product was recovered by precipitation in diethyl ether and vacuum dried. Yield 60 mg, 86%.

$[Os(bipy)_2(PVI)_{10}](Cl)_2/[Ru(bipy)_2(PVI)_{10}](Cl)_2$, Compound 20.

This metallopolymer was prepared as given above for compound 19 using $[Os(bipy)_2(PVI)_{10}](Cl)_2$ (14) as starting material. Yield 82%.

The following compounds were synthesised using literature methods [14,17,31] from $Os(bipy)_2Cl_2$ pic = 4-methylpyridine, mim = N-methylimidazole. $[Os(bipy)_2(pic)Cl](PF_6)$, (21). Calculated for $C_{26}ClF_6H_{23}N_5OsP$ C:40.22; H:2.96 and N:9.02. Found C:40.57; H:3.02 and N:9.07. $[Os(bipy)_2(pic)_2](PF_6)_2$, (22). Calculated for $C_{32}F_{12}H_{30}N_6OsP_2$ C:39.26; H:3.06 and N:8.58. Found C:39.32; H:3.10 and N:8.59. $[Os(bipy)_2(mim)Cl](PF_6)$, (23). Calculated for $C_{24}ClF_6H_{22}N_6OsP$ C:37.66; H:2.87 and N:10.98. Found C:37.32; H:2.74 and N:10.51. $[Os(bipy)_2(mim)_2](PF_6)_2$, (24). Calculated for $C_{28}F_{12}H_{28}N_8OsP_2$ C:35.14; H:2.92 and N:11.71. Found C:35.16; H:2.87 and N:11.79.

Section 2.3 Results and Discussion.

Section 2.3.1 General:

In the literature some reports of osmium polypyridyl containing polymeric materials have appeared, however in these cases heavily crosslinked materials were formed by electropolymerisation at electrode surfaces [32-34]. This procedure typically gives rise to insoluble products in which the ratio of metal centres : polymer units is difficult to control or determine.

This report is the first attempt to systematically investigate a series of metallopolymers in which multiple metal centres are bound to a

preformed polymer backbone. The synthetic approach used is to react the appropriate metal complexes with preformed PVP or PVI, so that crosslinking can be avoided and soluble polymers are obtained. In this manner the materials can be characterised in solution and as thin films on electrode surfaces.

The formation of the different metallopolymers is based on the well documented lability of the chloride ions in the complex $[M(bipy)Cl_2]$, M = Ru, Os. Extensive studies have shown that the first chloride ion is easily removed by refluxing in methanol or ethanol, whereas the removal of the second chloride occurs only in aqueous solutions or in high boiling point organic solvents [17,20,26,27,35]. Therefore, in syntheses which aimed to prepare monosubstituted materials such as $[Os(bipy)_2(PVP)_{10}Cl]Cl$ ethanol was used as a solvent (see reactions 1 and 2), whereas for the synthesis of species such as $[Os(bipy)_2(PVP)_{10}]Cl_2$ water was added to the reaction mixture (see reactions 1-4, S = solvent)

$$[M(bipy)_2Cl_2] + S \longrightarrow [M(bipy)_2(S)Cl]^+ + Cl^- \quad (1)$$

$$[M(bipy)_2(S)Cl]^+ + Pol \longrightarrow [M(bipy)_2(Pol)Cl]^+ + S \quad (2)$$

$$[M(bipy)_2(Pol)Cl]^+ + H_2O \longrightarrow [M(bipy)_2(Pol)H_2O]^{2+} + Cl^- \quad (3)$$

$$[M(bipy)_2(Pol)H_2O]^{2+} + Pol \longrightarrow [M(bipy)_2(Pol)_2]^{2+} + H_2O \quad (4)$$

M=Ru or Os.

The osmium polymers are prepared in a similar way to the corresponding ruthenium polymers, but because of the inertness of osmium complexes longer reflux times are needed. The synthetic flexibility of the procedure is evident since materials with different metal to polymer ratios can be prepared easily by adding the appropriate amounts of reactants. The polymer backbone can be changed provided it has a pendant coordinating group and the nature of the metal centre can also be varied. The metal loading of the materials reported here is based on the quantity of starting material employed, assuming complete reaction. This assumption is supported by the continuous monitoring of the reactions using spectroscopic and electrochemical techniques. The coordination around the metal ions was examined by comparison of the spectroscopic and electrochemical properties of the polymers with those of appropriate model compounds (vide infra). Approximate extinction coefficients have also been evaluated, this is however, complicated by problems as to the degree of hydration of the homopolymers and the subsequent metallopolymers. The extinction coefficients however, remain useful for examining the ratio of metal centres to polymer units.

Section 2.3.2 Glass Transition Temperature.

The effect of metal loading and the nature of the counterion in the $[Os(bipy)_2(PVP)_nCl]X$ and $[Os(bipy)_2(PVI)_nCl]X$ metallopolymers, where the counterion X is chloride or perchlorate, on T_g, has been examined. The thermal stability of the metal centres in these materials means that it is possible to examine T_g as a function of redox site loading. $[Ru(bipy)_2Cl]Cl$ units have been used previously as probes of structure and

dynamics in quaternised poly(4-vinylpyridine) [24]. Table 2.3.2.1 shows that the glass transition temperature is sensitive to the metal loading, with T_g increasing considerably over the homopolymer values with increasing metal loading. Thoroughly dried poly-4-vinylpyridine has a glass transition temperature of approximately 142^{o}C which is largely independent of molecular weight [37]. The higher glass transition temperature with increasing metal content most likely reflects a greater difficulty in obtaining fluid like motion within the metallopolymers, as the molecular weight is increased by addition of metal centres. We have attempted to correlate these observations with thermodynamic parameters observed for charge transport through films of these materials immobilised on electrode surfaces, when in contact with aqueous electrolyte [Chapters 4-6], [19]. Under certain circumstances two activation energies for homogeneous charge transport are observed. This behaviour will be considered more extensively in Chapters 4 and 5 but it appears to be connected with the internal polymer organisation. However the temperature at which the change in activation energy occurs, typically 285 K for the poly(4-vinylpyridine) metallopolymers, is significantly different from the glass transition temperatures reported here and cannot therefore, be directly connected. Given that the electrochemical measurements are made on thin films in contact with an aqueous electrolyte this is not entirely unexpected.

PVP is thermally stable in a nitrogen atmosphere up to 300 - 350 ^{o}C. On conversion to the acid salt or 1-alkylpyridinium salt the thermal stability decreases, the decrease being a function of the extent of quaternisation. For the materials described here however no loss of thermal stability via D.S.C measurements is observed and both spectroscopic and electrochemical measurements suggest that the metallopolymers do not decompose

Table 2.3.2.1. Glass transition Temperatures for $[Os(bipy)_2(Pol)_nCl]X$ polymers.

Compound		T_g (°C)	Compound	T_g (°C)
	PVP	143	PVI	182
$X=Cl^-$	5	230	9	260
	6	205	10	226
	7	192	11	207
	8	180	12	193
$X=ClO_4^-$				
	5a	252	9a	278
	6a	223	10a	240
	7a	209	11a	217
	8a	189	12a	198

at temperatures of up to 300 ^{o}C. The degradation in the polymeric 1-alkylpyridinium salts is generally accepted as occurring in two stages: loss of the 1-alkyl group and scission of the polymer backbone [38]. That these metal containing polymers remain stable suggests a strong coordination between the metal and polymer nitrogen.

The glass transition temperature of the perchlorate salt of these polymers shows an increase over those values obtained when chloride is the counterion. For quaternised PVP films containing ferrocyanide, in contact with perchlorate containing solutions [39], it has been recently proposed, that a nearly completely dehydrated material results, with consequential loss of internal fluid like motion. It seems likely that such a process is also occuring in these polymers and that this is being reflected in the T_g measurements.

Section 2.3.3 Absorption and Emission Spectroscopy.

Electronic spectroscopy has proved useful in the characterisation of ruthenium containing polymers [16,17]. In particular the position of the lowest absorption maxima and the wavelength of emission are often characteristic for a particular ruthenium moiety, and by comparison with mononuclear model compounds, the coordination sphere of the metal ion bound to the polymer backbone can be established. The data obtained for the absorption and emission spectra of the metallopolymers, together with data obtained for some model compounds, have been given in Table 2.3.3.1. The spectral features observed are typical of osmium and ruthenium compounds respectively. A detailed analysis of the spectroscopic features of osmium and ruthenium compounds has been given elsewhere, [16-20,26-27,31] and will not be considered

Table 2.3.3.1 Spectroscopic and Electrochemical Data for the Metallopolymers and Monomeric Model Compounds.

	λ max, abs nm[a](log ϵ)	λ max,em r.t./nm[a]	λ max,em 77K /nm[a]	$E_{1/2}^{ox}$ V[b]	$E_{1/2}^{red}$ V[b]
1	498 (3.92), 440 (3.87)	704	680	0.75	-1.50
2	455 (4.01), 464 (4.05)	604	594	1.25	-1.36
3	502 (3.75), 347 (3.73)	638	626	0.57	-1.48
4	485 (3.97), 345 (3.86)	626	617	0.86	-1.40
5	364 (4.05), 431 (4.08)	-	-	0.35	-1.47
	486 (4.04), 730 (3.45)				
9	364 (3.72), 431 (3.65)	-	-	0.23	-1.57
	524 (3.67)				
13	354 (4.23), 444 (4.08)	764	750	0.75, 2.15	-1.15
	616 (3.46)				
14	344 (3.67), 404 (3.59)	758	748	0.48	-1.30
	496 (3.88), 666 (3.07)				
15	358 (4.28), 486 (4.18)	716	684	0.35, 0.75	-1.52
16	354 (4.14), 506 (4.13)	700	684	0.25, 0.67	-1.60
17	352 (4.35), 432 (4.21)	650	616	0.33, 1.15	-1.48
	486 (4.20)				
18	346 (3.94), 488 (3.93)	643	626	0.22, 0.88	-1.62
19	352 (4.28), 432 (4.33)	618	600	0.75, 1.15	-1.15
	480 (4.22)	730(sh)	750		
20	344 (4.14), 488 (4.03)	650	632,754	0.48, 0.95	
21	358 (4.07), 428 (4.09)	-	-	0.33, 1.78	-1.46
	506 (4.08), 730 (3.49)				
22	358 (4.24), 390 (4.02)	766	750	0.73, 2.20	-1.32
	442 (4.09), 610 (3.50)				
23	365 (3.92), 430 (4.12)	-	-	0.23	-1.57
24	346 (3.86), 416 (3.80)	754	750	0.95	-1.30
	512 (3.85), 686 (3.37)				

[a] measured in methanol, compounds 21 - 24 measured in acetonitrile.

[b] electrolyte 0.1 M TEAP/acetonitrile

here. The electronic transitions observed in the visible region are attributed to metal-to-ligand charge transfer bands (MLCT), while the emission is thought to occur from a ligand based triplet state. The spectra obtained for the polymers 5 - 12 do agree well with those observed for the model compounds 21 and 23 (see Figures 2.3.3.1 and 2.3.3.2). For these model compounds and metallopolymers no emission was observed. This suggests a coordination of $[OsN_5Cl]Cl$ for these polymers. Due to the spectral complexity however no definite assignment of the coordination sphere around the osmium ion can be made from the absorption data alone. The absorption spectra of the osmium polymers 13 and 14 are very similar to those observed for the model compounds 22 and 24 respectively. A significant feature of the uv-visible data is the similarity of the extinction coefficients between the polymeric and monomeric species. Also for both sets of compounds emission signals at about 750 nm are observed. This strongly suggests the presence of the $[OsN_6]Cl_2$ moiety in these polymers, so that two nitrogen units from the polymer backbone are bound to the osmium centre. These observations are in agreement with the synthetic conditions employed.

The spectra obtained for the mixed metal compounds, show the presence of both metal centres, but the complexity of the spectra prevents a conclusive analysis of the composition of the materials. More specific information can be obtained from the emission spectra. For the mixed polymers 15 and 16 the presence of an emission maximum at about 700 nm can, by comparison with analogous compounds [41], be explained by the presence of a $[RuN_5Cl]Cl$ moiety. As anticipated no evidence for an osmium based emission was observed in these materials. For the polymers 17 and 18 an emission at about 625 nm at 77 K is indicative for the presence of $[RuN_6]Cl_2$ groupings [15-19].

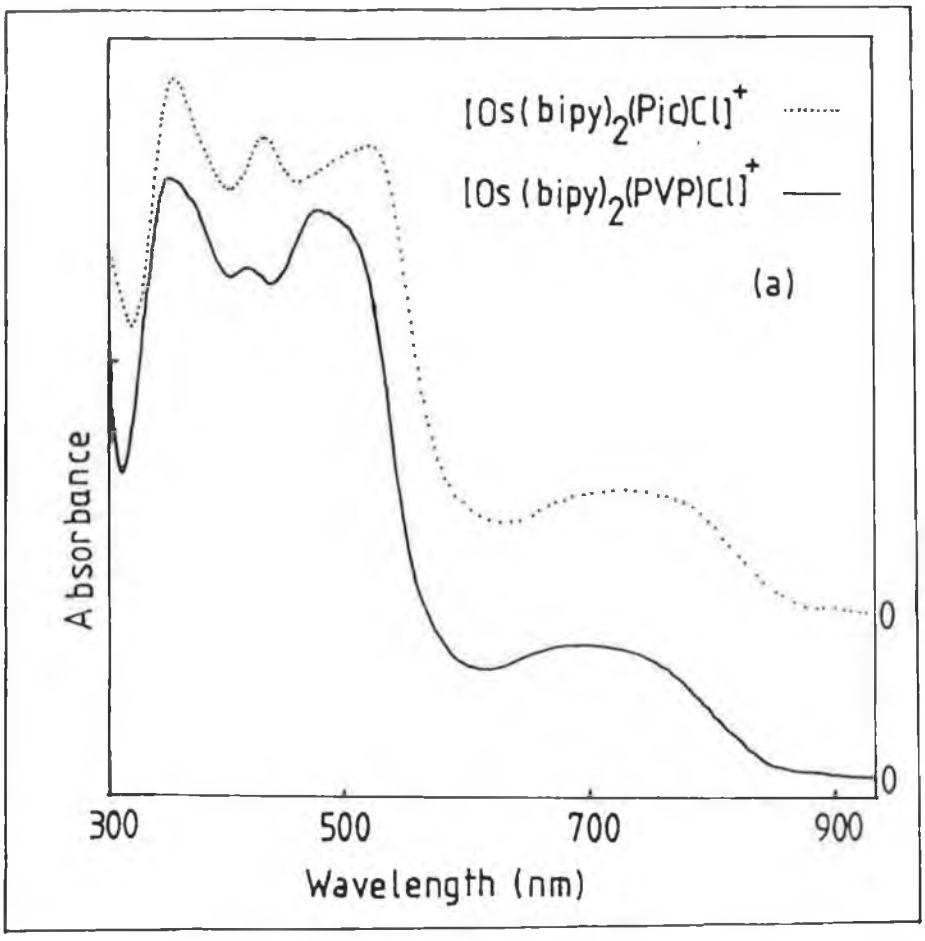

Figure 2.3.3.1. Uv-visible spectrum of metallopolymer 5 and model compound 21. Spectrum of the metallopolymer was recorded in methanol, model compound in acetonitrile. Sample concentration 10^{-4} mol dm^{-3}.

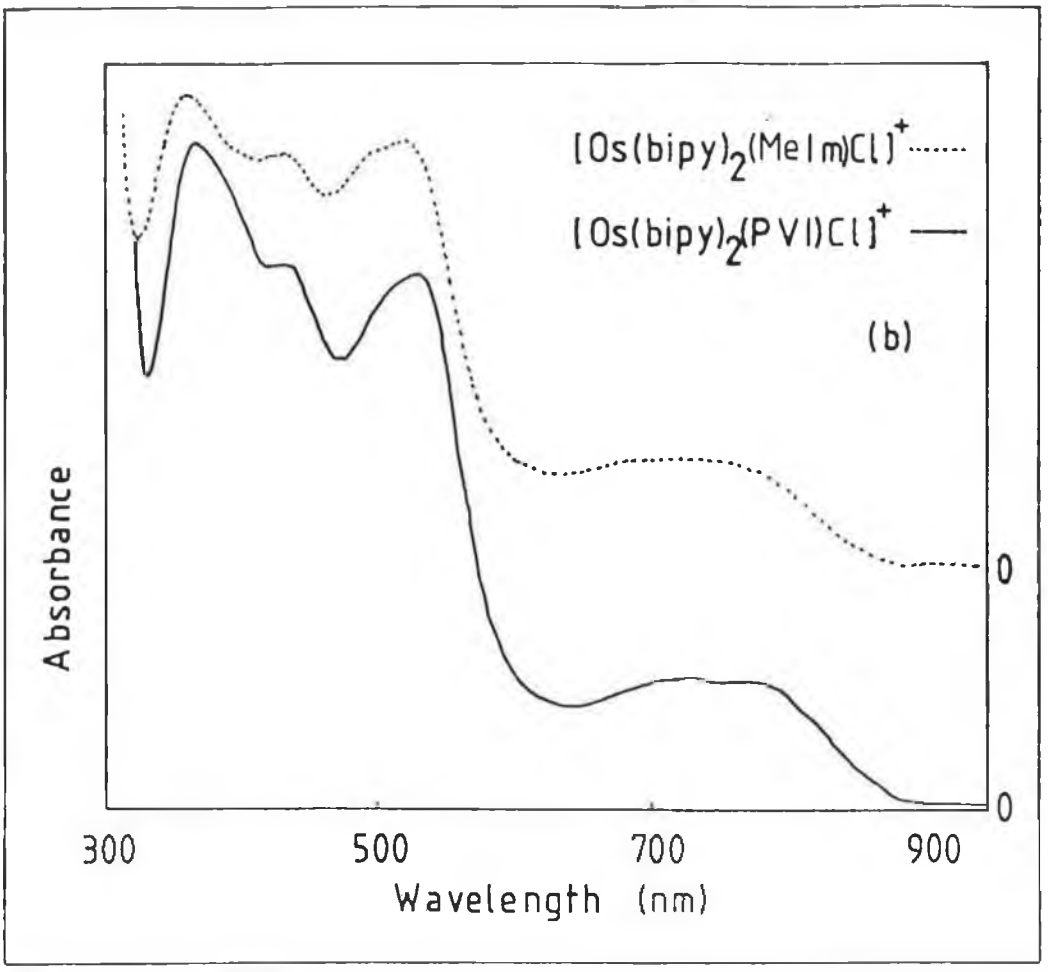

Figure 2.3.3.2. Uv-visible spectrum of metallopolymer 9 and model compound 22. Spectrum of the metallopolymer was recorded in methanol, model compound in acetonitrile. Sample concentration 10^{-4} mol dm^{-3}.

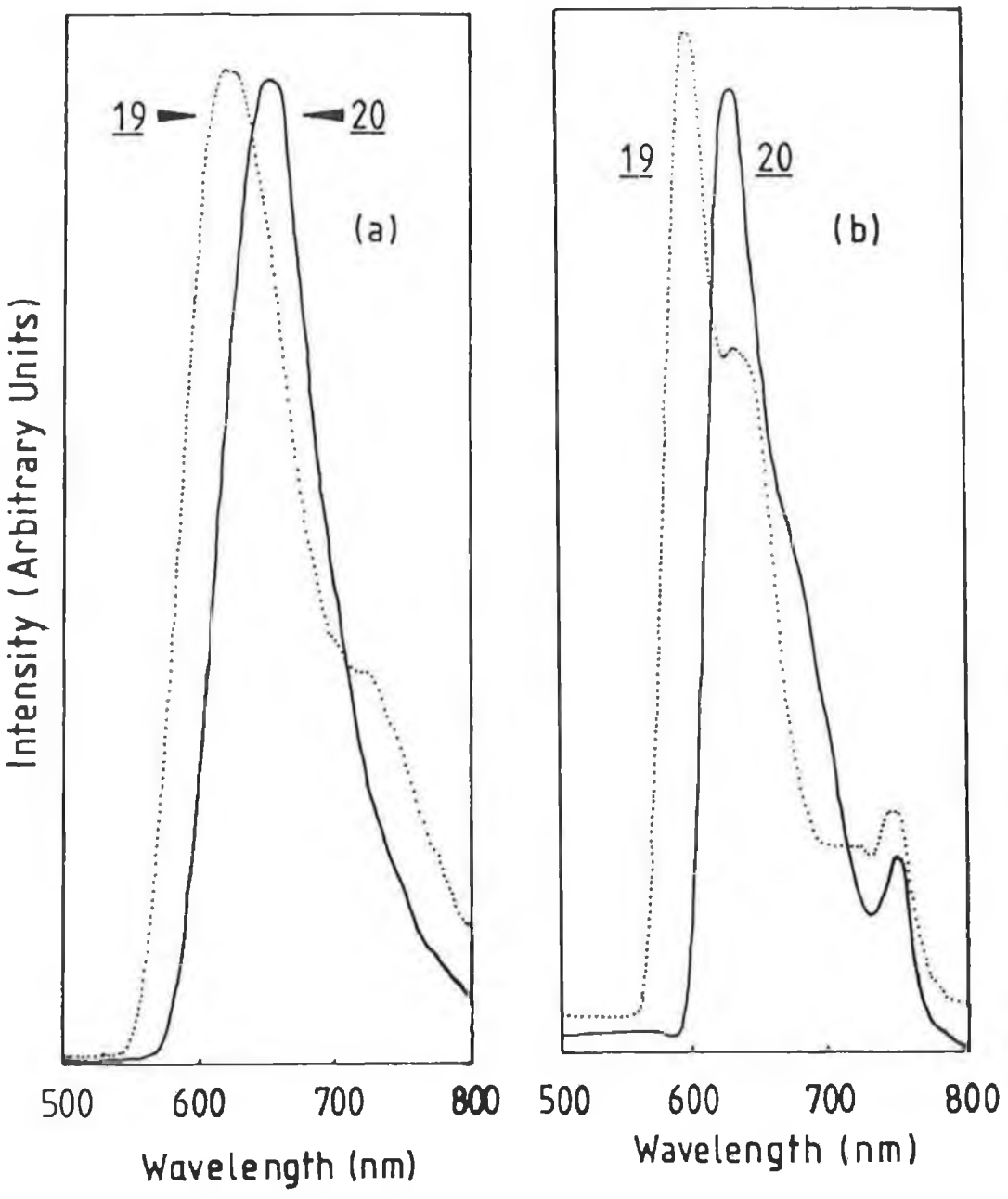

Figure 2.3.3.3. (a) Room temperature and (b) 77-K emmision spectra of metallopolymers 19 and 20 in methanol. Sample concentration 10^{-4} mol dm^{-3}.

For these compounds no osmium based emission was observed. For polymer 19 emission signals at room temperature are observed at 618 nm with a shoulder at 730 nm. At 77 K emission maxima at 600 and 750 nm are observed for these materials. The position of these maxima, and the rather large difference in the high energy band between room temperature and 77 K, suggest that this band is due to emission from the $[RuN_6]Cl_2$ moiety, while the temperature insensitive band at 750 nm most likely represents emission from the $[OsN_6](Cl)_2$ unit. The response observed for $[Os(bipy)_2PVI_2](Cl)_2$/ $[Ru(bipy)_2PVI_2](Cl)_2$ (20) is similar with a ruthenium emission occurring at 643 and 618 nm for room temperature and 77 K respectively. The osmium emission is less sensitive to temperature and occurs at 758 and 748 nm respectively. This behaviour is illustrated in Figure 2.3.3.3. Where significant excited state interaction exists between metal centres e.g in dimeric complexes [42], a single emission is observed from the lowest energy state. The fact that both centres in these materials emit (at least at this loading and in solution) suggests that significant excited state interaction is absent.

Section 2.3.4 Electrochemical Properties.

The materials obtained were further characterised using electrochemical techniques. The formal potentials of the M(II/III) redox couple of the metallopolymers coated as thin films on glassy carbon electrodes have been listed in Table 2.3.3.1. A typical cyclic voltammogram of a mixed metal metallopolymer (15) has been given in Figure 2.3.4.1. As expected the osmium analogues of previously reported ruthenium metallopolymers show

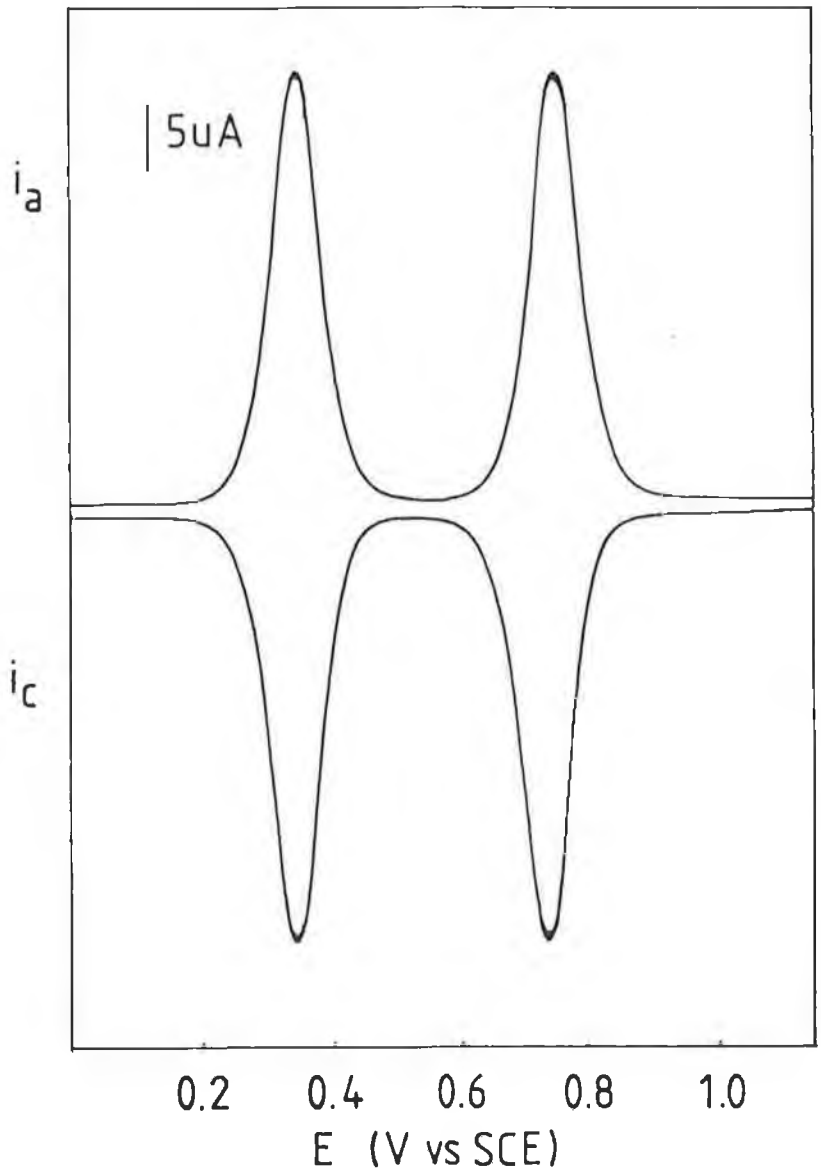

Figure 2.3.4.1 Cyclic voltammogram of metallopolymer 15 deposited as a thin film on a glassy carbon electrode. Electrolyte 0.1 M TEAP/Acetonitrile. Surface coverage 1 x 10^{-8} molcm^{-2}. Electrode area 0.0706 cm^2. Scan rate 5 mV/s.

reversible redox couples at less positive potentials [31,35-36]. The redox potentials obtained for compounds 5 - 12 did not show any variation with the metal loading. When examined as surface deposits these metallopolymers show surface behaviour [43] at slow sweep rates, with peak currents directly proportional to the scan rate. At scan rates higher than 20 mV/s apparent semi-infinite diffusion [43] is observed with the peak current being proportional to the square root of the scan rate. The rate of charge transport for the PVP and PVI metallopolymers has been extensively examined as a function of electrolyte, pH, redox site loading and temperature and will be discussed in Chapters 4, 5 and 6.

Table 2.3.3.1 shows that the position of the Os(II/III) oxidation is sensitive to the nature of the osmium moiety and that the synthetic conditions outlined here result in the formation of only one electroactive product. By comparing the redox potentials obtained for the metallopolymers with those of analogous polymeric [15-19] and mononuclear model compounds, assignments about the nature of the polymer bound moieties can be made. These assignments are in total agreement with those given above based on the absorption and emission results. The redox potentials obtained for the ruthenium groups in the mixed metal polymers are in close agreement with those reported earlier for polymers only containing ruthenium. This coupled to the fact that the waveform remains undistorted suggests that little interaction exists between the metal centres [44-47]. The redox potentials observed for a particular osmium or ruthenium moiety in different metallopolymers are the same within experimental error. For some of the osmium containing polymers an additional irreversible oxidation was observed at around 2 V vs SCE. This oxidation has, by comparison with data reported for analogous compounds, been assigned to the Os(III/IV) redox couple

[31]. Also data for the first reduction potentials were obtained. As in other similar compounds these reductions are thought to be bipyridyl based [48]. No detailed analysis of these reductions was carried out however, as in most cases only a single reduction is observed, it is not possible to definitely assign these reductions to either the osmium or ruthenium moities.

The nature of any ground state interaction can also be investigated by evaluating charge transport rates through thin films of these materials. Chronoamperometry was used to evaluate homogeneous charge transport rates, given as D_{CT}, for both Os(II/III) and Ru(II/III) oxidation for glassy carbon electrodes modified with films of the mixed osmium/ruthenium polymers. The Cottrell behaviour for electrodes modified with $[Os(bipy)_2(PVP)_{10}Cl]Cl/[Ru(bipy)_2(PVP)_{10}Cl]Cl$ (compound 15) in 0.1 M tetraethyl ammonium perchlorate is illustrated in Figure 2.3.4.2. This clearly shows that the rate of charge propogation through the polymer phase via the osmium centres is more rapid than through the ruthenium centres, D_{CT} is 2.1 x 10^{-9} cm^2s^{-1} and 9.8 x $10^{-10}cm^2s^{-1}$ for the osmium and ruthenium centres respectively. The same values were obtained for the corresponding polymers containing only osmium or ruthenium centres, i.e compound 6 and compound 1. This suggests that little interaction exists between the redox centres. The activation energies for these mixed metal polymers are also similar to their single metal analogues. In the above electrolyte the osmium activation energy is 20 kJ/Mol while the ruthenium activation energy is 15 kJ/Mol, these values are the same to within experimental error to those obtained for compounds 6 and 1. Other electrochemical data including the reaction entropy, which has proved itself sensitive to changes in redox centre

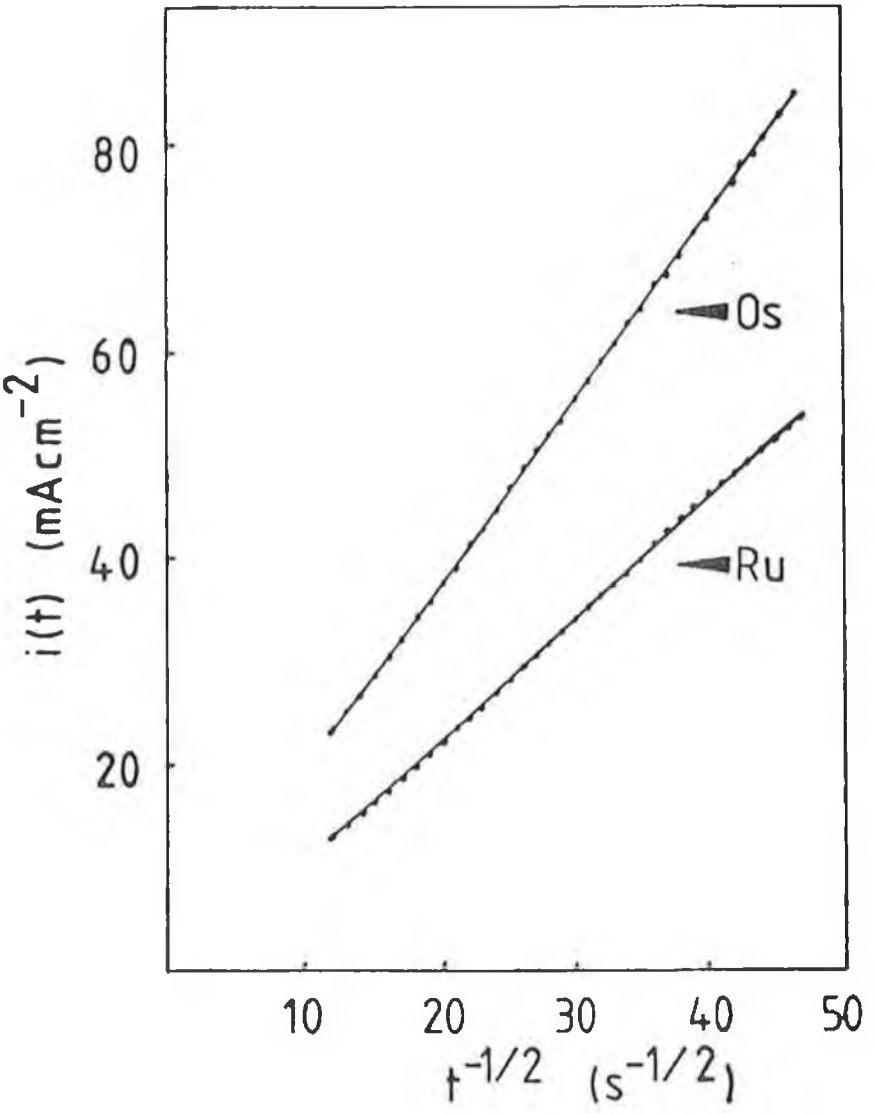

Figure 2.3.4.2 The chronoamperometric response presented as Cottrell plots for the Os(II/III) and Ru(II/III) oxidation, for compound 15. 0.1 M tetraethyl ammonium perchlorate as supporting electrolyte. Surface coverage 2 x 10^{-8} molcm^{-2}.

solvation [32] remain constant at a value of 19.5 J/Mol/K on going from the monometallic to the bimetallic polymers.

Section 2.3.5 Photochemical Properties.

Earlier work on ruthenium based metallopolymers has shown these polymers can be photolabile, and the photochemically induced ligand exchange reactions have been studied in some detail [49]. Because of the presence of two different absorbing species in the mixed metal polymers the use of absorption spectroscopy is of little value for monitoring such ligand exchange reactions. However, cyclic voltammetry can be used to examine the photochemistry of thin films of the polymers reported here. It was found, that metallopolymers containing only osmium centres, are photostable both in methanol solution and as thin films on glassy carbon electrode surfaces in a wide variety of electrolyte salts and solvents. This photostability of osmium compounds with respect to the analogous ruthenium compounds is generally accepted to arise because of the increased energy of the anti-bonding dd-orbitals, responsible for the photochemically induced ligand exchange reactions [50]. Both the $[RuN_5Cl]Cl$ and the $[RuN_6]Cl_2$ moieties showed photochemically induced photosubstitution, with the product in both cases having a redox potential of about 800 mV vs SCE. A typical example of cyclic voltammograms taken during the photolysis of an electrode modified with polymer 15 has been given in Figure 2.3.5.1. It can be seen that the osmium redox couple remains stable but that the signal originally observed for the ruthenium redox couple shifts upon photolysis from 650 to about 800 mV vs SCE. Such a shift has in other ruthenium containing polymers been explained by a ligand exchange reaction as in reaction 5:

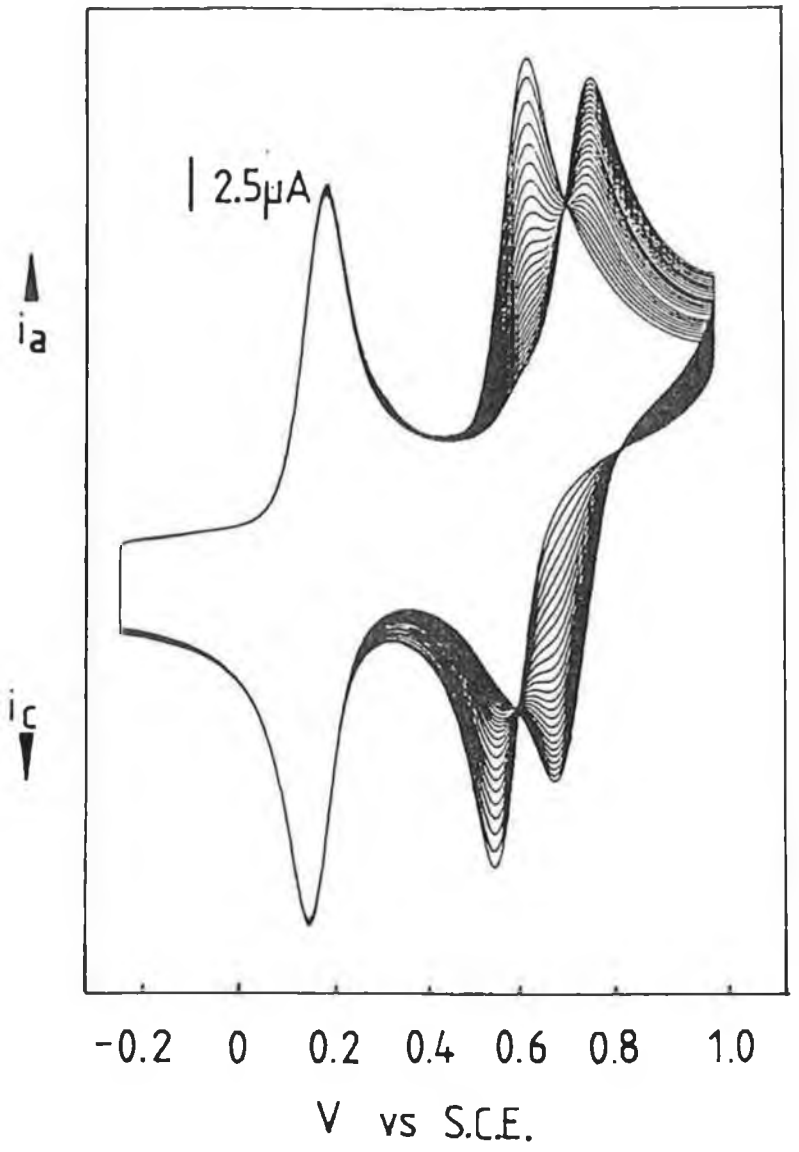

Figure 2.3.5.1 Photochemically induced ligand exchange reactions in a thin, electrode bound film of metallopolymer 15 using 1 M aqueous $HClO_4$ as electrolyte. Scan rate 100 mV/s. Surface coverage 1 x 10^{-8} molcm^{-2}. Interval between scans 30 seconds.

$$[Ru(bipy)_2(PVP)Cl]^+ \xrightarrow{h\nu/H_2O} [Ru(bipy)_2(PVP)H_2O]^{2+} + Cl^- \quad (5)$$

The shift in potential observed here is in agreement with such a ligand exchange [50]. The photochemically induced ligand substitution of the ruthenium metallopolymers provides a convenient means of changing the redox potential of the surface immobilised species. This has potential applications in sensor development and information storage while the photostable osmium centre can act as an internal standard. It is also important to realise that the clear difference in redox potential between the $[Ru(N)_5H_2O]Cl_2$ and other moieties strongly suggests that no significant amounts of this aquo species are present in the polymers prepared. Since the photochemically induced ligand exchange can be complete, it is a convenient way of preparing a pure species that cannot be synthesised by direct methods.

Section 2.3.6 Metallopolymer Diffusion in Solution:

The possibility of labelling, at a low loading, macromolecules with an electroactive centre and then determining their diffusion rate in solution using conventional electrochemical procedures has been investigated using the $[Os(bipy)_2Cl]^+$ redox centre. A low loading of 1:100 Metal centre:monomer units was used. Since this increases the molecular weight by only 5% and eliminates only 5% of the pendant nitrogens the effect of the label on the macromolecules diffusion rate is expected to be minimal. The effect of the molecular weight on this diffusion rate was considered using a series of poly(4-vinylpyridine) polymers of differing molecular weights (as determined

using viscometry) over the range M_v= 16,000 to 360,000 g/Mol. The possibility of establishing a relation between polymer molecular mass and its diffusion coefficient in solution is attractive given the difficulties in determining polymer molecular weights for nitrogen containing polymers by conventional methods such as gel permeation chromatography. The diffusion rate of these metallopolymers in a background electrolyte of 0.1 M tetra-ethyl ammonium perchlorate (TEAP) in acetonitrile was measured using conventional cyclic voltammetry and potential step chronoamperometry. At this level of loading reproducible signals were obtained which followed the conventional models for diffusion in solution. An increase in molecular weight from 6,000 to 180,000 g/Mol initially decreases the solution diffusion rate after which point D_{soln} remains constant with further increase in the polymer molecular weight (see Figure 2.3.6.1). The rate of polymer diffusion in solution is of the order of 10^{-7} cm^2s^{-1} compared to a rate of 10^{-5} - 10^{-6} cm^2s^{-1} which would be expected for monomeric species. These observations suggest that the transition from monomeric to polymeric species significantly retards the molecules movement through solution, but that changes in the mass of the polymeric species have less effect. The fact that at at high molecular weight D_{soln} becomes independent of molecular mass may be related to the ability of the macromolecule to form a helical coil thus presenting a minimum surface area to solution. By suitably constraining the polymer molecular mass range it may be possible to establish a working relationship between the rate of diffusion in solution and the molecular weight.

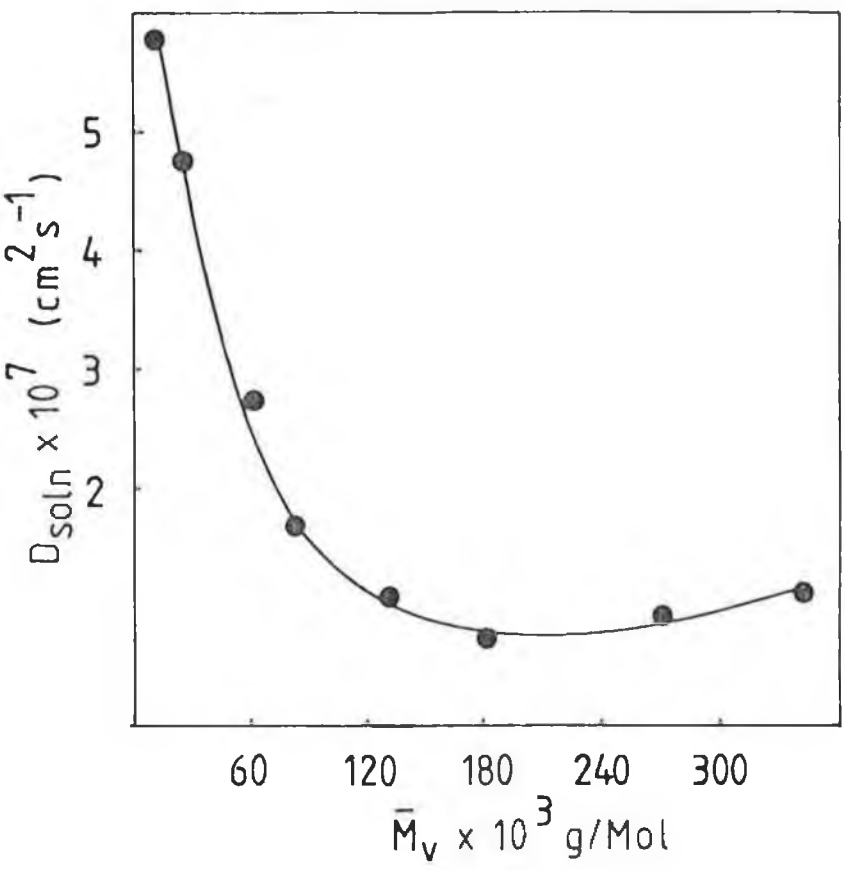

Figure 2.3.6.1 The effect of increasing molecular weight for the diffusion of $[Os(bipy)_2(PVP)_{100}Cl]Cl$ in solution.

Section 2.4 Concluding Remarks.

The synthetic strategy developed here allows the stepwise formation of multifunctional polymers. The metallopolymers can be readily characterised by UV-visible and emission spectroscopy and can be prepared with controlled loadings by varying the stoichiometric ratio of the starting polymer to metal complex. Electrochemical measurements and emission spectroscopy confirm that the excited state and redox properties of the metal centres are maintained upon polymeric attachment. This is significant since one can identify a suitable metal complex for a given application and then synthesise a polymeric analogue with similar properties.

The T_g measurements suggest that the rigidity of the metallopolymers increases with increasing metal loading. Electrochemical and emission data suggest that at best a weak interaction exists between the different redox centres when in solution. This is perhaps somewhat unexpected, especially as with the metal loadings used, the coordination spheres are expected to be in very close contact and the separation between the metal centres will be of the order of 15 Å.

Section 2.5 References.

1. M. Kaneko and E. Tsuchida, J. Macromol. Sci., Rev. Macromol. Chem. 1981, 16, 397.
2. D. Chauvin, D. Commereuc and F. Dawans, Prog. Polym. Sci. 1977, 5, 95.
3. S. L. Davydova and N. A. Plate, Coord. Chem. Rev. 1975, 16, 195.
4. R. W. Murray, A. G. Ewing and R. A. Durst, Anal. Chem. 1987, 59, 379A.
5. J. G. Redepenning, Tr. Anal. Chem. 1987, 6, 18.
6. E. D. Chidsey and R. W. Murray, Science 1986, 231, 25.
7. T. D. Westmoreland, J. M. Calvert, R. W. Murray and T. J. Meyer, J. Chem. Soc., Chem. Commun. 1983, 65
8. H. D. Abruna, M. Denisevich, M. Umana, T. J. Meyer and R. W. Murray, J. Am. Chem. Soc. 1981, 103, 1.
9. M. Kaneko, A. Yamada and Y. Kurimura, Inorg. Chim. Acta 1980, 45, L73.
10. M. Kaneko, A. Yamada, E. Tsuchida and Y. Kurimura, J. Phys. Chem. 1984, 88, 1061.
11. M. Kaneko, T. Okada, S. Teratani and K. Taya, Electrochim Acta 1987, 32, 1405.
12. M. Kaneko, J. Macromol. Sci. Chem. Ed. 1987, 24, 357.
13. M. Kaneko and H. Nakamura, Macromolecules, 1987, 20, 2265.
14. K. Murao and K. Suzuki, J. Chem. Soc., Chem. Commun. 1984, 238.
15. K. T. Potts and D. A. Usifer, Macromolecules 1988, 21, 1985.
16. J. M. Clear, J. M. Kelly and J. G. Vos, Makromol. Chem. 1983, 184, 613.
17. J. M. Clear, J. M. Kelly, C. M. O'Connell and J. G. Vos, J. Chem. Res. 1981, (M), 3039.
18. O. Haas and J. G. Vos, J. Electroanal Chem. 1980, 113, 139.

19. M. E. G. Lyons, H. G. Fay, J. G. Vos and A. J. Kelly, J. Electroanal. Chem. 1988, 250, 207.

20. S. M. Geraty and J. G. Vos, J. Chem. Soc., Dalton Trans. 1987, 3073.

21. R. C. McHatton and F. C. Anson, Inorg. Chem. 1984, 23, 3935

22. O. Haas, M. Kriens and J. G. Vos. J. Am. Chem. Soc. 1981, 103, 1318.

23. O. Haas, H. R. Zumbrunnen and J. G. Vos. Electrochim. Acta, 1985, 30, 1551.

24. S-M. Oh and L. R. Faulkner, J. Am. Chem. Soc. 1989, 111, 5613.

25. R. J. Forster, A. J. Kelly, J. G. Vos and M. E. G. Lyons; J. Electroanal. Chem., 1989, 270, 365.

26. B. P. Sullivan, P. J. Salmon and T. J. Meyer Inorg. Chem. 1978, 17, 3334.

27. E. C. Johnson, B. P. Sullivan, P. J. Salmon, S. A. Adeyemi and T. J. Meyer, Inorg. Chem. 1978, 17, 2211.

28. D. A. Buckingham, F. P. Dwyer, H. A. Goodwin and A. M. Sargeson, Aust. J. Chem. 1964, 17, 325

29. J. B. Berkowitz, M. Yamin and R. M. Fuoss, J. Polym. Sci. 1958, 28, 69.

30. C. H. Bamford and E. Schofield, Polymer 1981, 22, 1227

31. E. M. Kober, J. V. Caspar, B. P. Sullivan and T. J. Meyer, Inorg. Chem., 1988, 27, 4587.

32. J. M. Calvert, R. H. Schmehl, B. P. Sullivan, J. S. Facci, T. J. Meyer and R. W. Murray, Inorg. Chem. 1983, 22, 2151.

33. R. H. Schmehl and R. W. Murray, J. Electroanal. Chem. 1983, 152, 97.

34. J. S. Facci, R. H. Schmehl and R. W. Murray, J. Am. Chem. Soc. 1982, 104, 4959.

35. E. M. Kober, J. L. Marshall, W. L. Dressick, B. P. Sullivan, J. V. Caspar and T. J. Meyer, Inorg. Chem. 1985, 24, 2755.

36. E. M. Kober, J. V. Caspar, R. S. Lumpkin and T. J. Meyer, J. Phys. Chem. 1986, 90, 3722.

37. J. Brandrup and E. H. Immergut, Ed. Polymer Handbook J. Wiley and Sons, Inc., 1975, p. 111.

38. H. C. Haas and R. D. Moreau, J. Polym. Sci. 1977, 15, 1225.

39. S-M. Oh and L. R. Faulkner, J. Electroanal. Chem., 1989, 269, 77.

40. K. Niwa and K. Doblhofer, Electrochim. Acta., 1986, 31, 549.

41. B. A. Moyer and T. J. Meyer, Inorg. Chem., 1981, 20, 444.

42. P. Doppelt and T. J. Meyer, Inorg. Chem., 1987, 26, 2027.

43. A. R. Hillman, Electrochemical Science and Technology of Polymers, R. G. Linford Ed, Elsevier Applied Science, 1987, p.241.

44. H. Daifuku, K. Aoki, K. Tokuda and H. Matsuda, J. Electroanal. Chem. 1985, 183, 1.

45. A. P. Brown and F. C. Anson, Anal. Chem. 1977, 49, 1589.

46. H. Gerischer and D. A. Scherson, J. Electroanal. Chem. 1985, 188, 33.

47. E. Laviron and L. Roullier, J. Electroanal. Chem. 1980, 115, 65.

48. B. P. Sullivan, D. J. Salmon and T. J. Meyer, Inorg. Chem. 1978, 17, 3334.

49. J. M. Calvert and T. J. Meyer, Inorg. Chem. 1982, 21, 3978.

50. J. V. Casper and T. J. Meyer, Inorg. Chem. 1983, 22, 2444.

CHAPTER 3

Electrochemical Methods

Section 3.1 Electrode Preparation and Coating.

The stability of electrodes modified with the osmium containing discussed here is dependent on the preparation of that surface. As well as this, the reproducibility of homogeneous charge transport rates, and more noticably heterogeneous electron transfer rates, is affected by the nature and history of the underlying electrode. In order to produce electrode surfaces, which show reversible kinetic behaviour, in a reproducible manner, the following electrode pretreatment regime was adopted. Firstly, the surface of the glassy carbon electrodes was renewed by mechanical abrasion using silicon carbide paper of successively smaller grit size. This established a new surface and removed any surface defects. During this procedure the abrasive paper must be kept continually wet. This serves two purposes, it removes particulate carbon stripped from the surface which might otherwise cause surface scratching and, it prevents frictional heating of the electrode. Frictional heating causes problems with electrode leakage, but more importantly it irreversibly increases the background charging observed during electrochemical measurements. The electrode surface was then copiously washed with deionised water and methanol before polishing with a 0.5 μm alumina slurry on a felt bed. This was continued until a perfect mirror finish was obtained. The electrode was finally polished on a felt bed with water before washing with deionised water and methanol. The background of the electrode was checked electrochemically prior to modification. This involved cycling the electrode between -0.5 and +1.2 V vs SCE at 5 mV/s. These polished electrodes were further treated by pipetting 250 ul of chlorosulphonic acid directly onto their surfaces and left for 5 minutes, followed by washing with deionised water.

It has been suggested that this process forms highly polar groups on the electrode surface [1]. This process significantly improves surface adhesion of the osmium metallopolymers.

Electrochemical pretreatment was also investigated as a means of electrode surface renewal [2-5]. This involved holding the potential of a polished electrode at 1.5 V for 5 minutes (pre-anodization). The osmium containing polymer was then pipetted directly onto the surface and allowed to dry. Equilibrium was more rapidly established within the films, which were more stable and showed a higher rate of heterogeneous electron transfer. There was however, an increase of approximately 30% in the capacitive current. In an alternative procedure, the electrode was pre-anodised and subsequently pre-cathodised at -1.5 V for 3 minutes. This regime further improved film adhesion but also increased background charging. For this reason electrochemical pretreatment was not used extensively.

The nature of electrode configuration in an electrochemical cell, where the working electrode is modified, is of considerable importance due to the combination of relatively low electrolyte and high redox active concentrations. It is known, that where large currents, such as those produced at a modified electrode, are passed through an electrolyte, it does not act as an equipotential volume [6]. This means that the interfacial potential difference, between the working electrode and the solution, varies across the surface of the working electrode. This gives rise to non uniform current density, with those points on the working electrode surface closest to the auxiliary electrode giving the largest current densities [7]. It is apparent therefore, that the active area of the working electrode is less than its

geometric area. In order to minimise this effect the auxiliary electrode should be placed such that all points on the working electrode are equidistant from the working electrode, whilst maintaining the reference electrode position. In this study a 5 cm^2 platinum gauze, positioned horizontally under the working electrode was used as counter. This positioning, as well as the large surface area are expected to give rise to uniform current densities.

Section 3.2 Cyclic Voltammetry

Electrochemical measurements were performed using an E. G. & G. Model 273 potentiostat / galvanostat. Where necessary iR compensation was achieved via positive feedback circuitry (vide infra). Electrochemical cells were of conventional design and were thermostatted to within $\pm$ 1 ^{o}C. All potentials are referenced with respect to the potassium saturated calomel electrode (SCE) without regard for liquid junction potentials.

The thin layer or finite diffusion characteristics of modified electrodes were discussed previously in section 1.3.1. This theoretical framework clearly defines the properties which a surface wave must have i.e a peak width at half height of 90/n mV and zero peak to peak separation as well as equal peak currents which increase as ν . Linearity of i_p vs ν is frequently accepted as sufficient condition for surface behaviour, this is a necessary but insufficient condition. i_p must be linear with ν but must also have a slope of unity, thus for example, when the sweep rate is increased from 1 mV/s to 2 mV/s i_p must actually double. The other features of zero peak to peak separation and a 90/n mV peak width should also be observed. For some electrolyte/loading combinations these features can be difficult to observe e.g Figure 3.2.1.

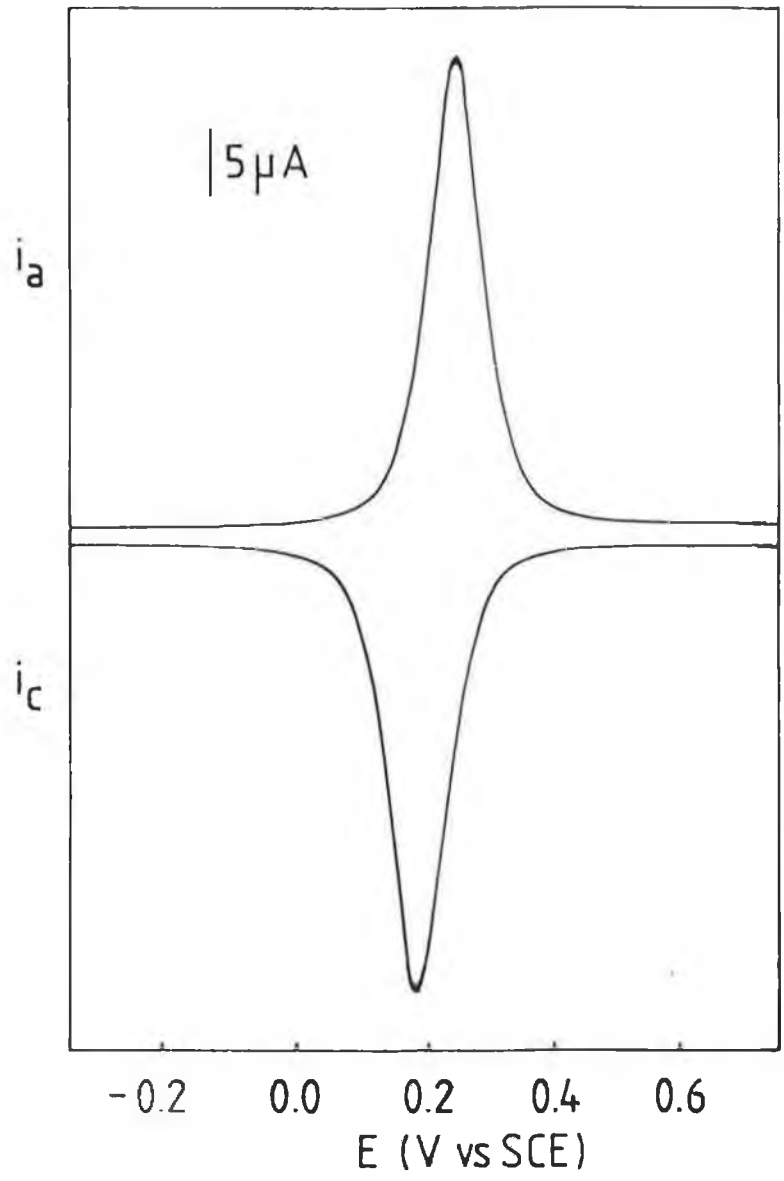

Figure 3.2.1 (a) Cyclic voltammogram for an electrode modified with $[Os(bipy)_2(PVP)_{10}Cl]Cl$. Sweep rate 5 mV/s. Surface coverage 1.7 x 10^{-8} mol cm^{-2}. Electrode area 0.3848 cm^2. Supporting electrolyte 0.1 M $HClO_4$.

This shows a cyclic voltammogram of $[Os(bipy)_2(PVP)_{10}Cl]Cl$ in 0.1 M perchloric acid. The wave is clearly not surface but would be deemed by many to be acceptable to calculate a surface coverage. The fact is however, that the film is exhibiting a slow oxidation rate and is not being exhaustively oxidised. In fact a timescale considerably longer than that provided by the 1 mV/s sweep rate is required. A plot of i_p vs ν is linear but the normalised slope (including the required constants) is less than unity (0.9). Controlled potential coulometry shows that such films can take as long as 30 minutes to be completely oxidised. If such waves are used to calculate surface coverages then a serious underestimate is obtained. Figure 3.2.1b shows the same modified electrode under identical conditions but in 0.1 M sulphuric acid as supporting electrolyte. The total apparent surface coverage has almost doubled, which has important consequences for the accurate determination of D_{CT}. The peak current vs sweep rate plot is linear and has the theoretical normalised slope of unity. In this work, the problem of slow exhaustive oxidation has been solved by either using very slow sweep rates (<1 mV/s), chronocoulometry or measuring the surface coverage in an electrolyte in which the film can be totally oxidised more easily.

Similar problems to these exist for semi-infinite diffusion conditions. The peak current should exhibit a linear dependence on $\nu^{1/2}$ but must also have a normalised slope of unity. A slope larger than this suggests a contribution from finite diffusion, while a lower slope suggests a problem either with iR drop or a problem with electrode kinetics. D_{CT} is most simply evaluated from waves which show semi-infinite diffusion behaviour, as shown in Figure 3.2.2. The features of the cyclic voltammograms include a separation of 58/n mV at 25 ^{o}C, linear i_p vs $\nu^{1/2}$ (with normalised slope = 1) and

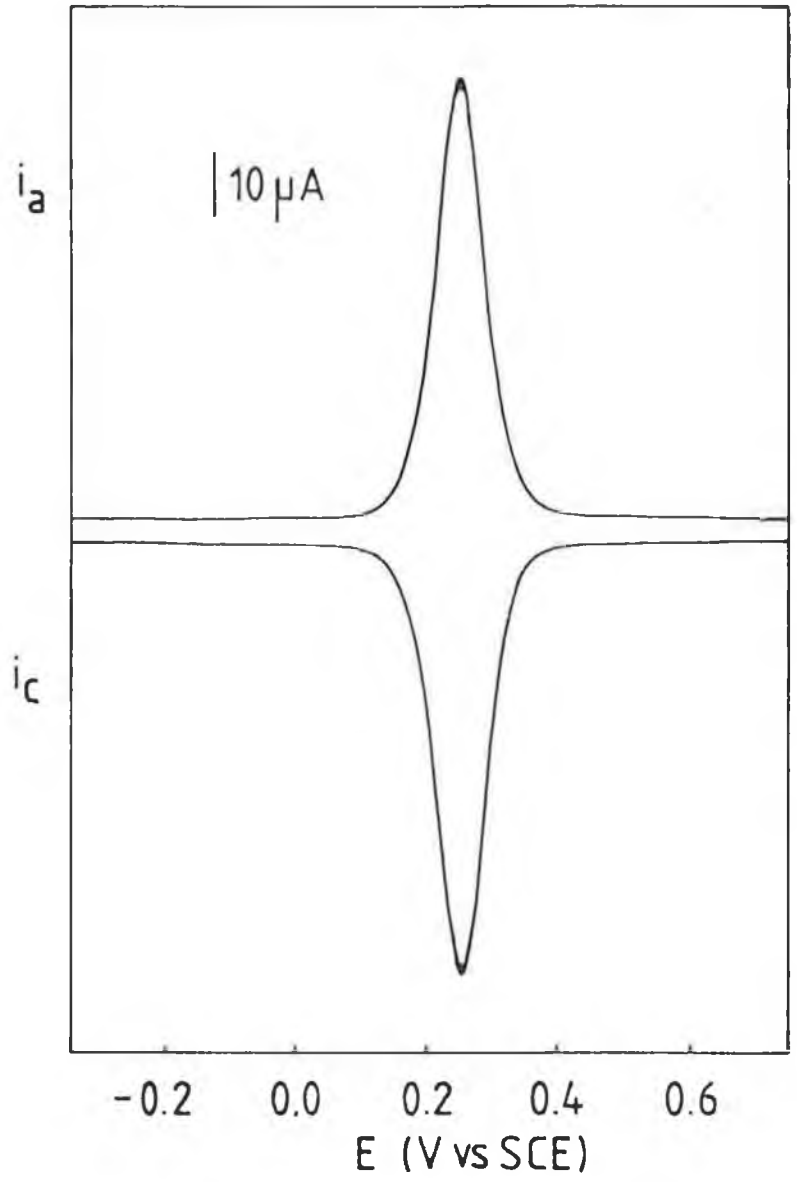

Figure 3.2.1 (b) Same electrode as given in 3.2.1 (a) with 0.1 M H_2SO_4 as supporting electrolyte.

i_{pa}/i_{pc} = 1. This suggests that there are no kinetic or other problems in the electrode process. A contribution from finite diffusion can be corrected for by using the Aoki approach described in chapter 1 which calculates the nature of the diffusion space, it does, however, rely on an accurate determination of surface coverage and layer thickness.

The instrumentation used in this work allowed for iR compensation using positive feedback circuitry. This was implemented as follows. Firstly, a train of small amplitude potential steps (50 - 200 mV) was applied to the modified electrode in a potential region where no redox reaction occurred. The current output was monitored using a digital storage oscilloscope. iR compensation was then applied incrementally until the potentiostat began to oscillate. iR compensation of 85% of the value which initiated oscillation was then applied to compensate for iR drop within the cell.

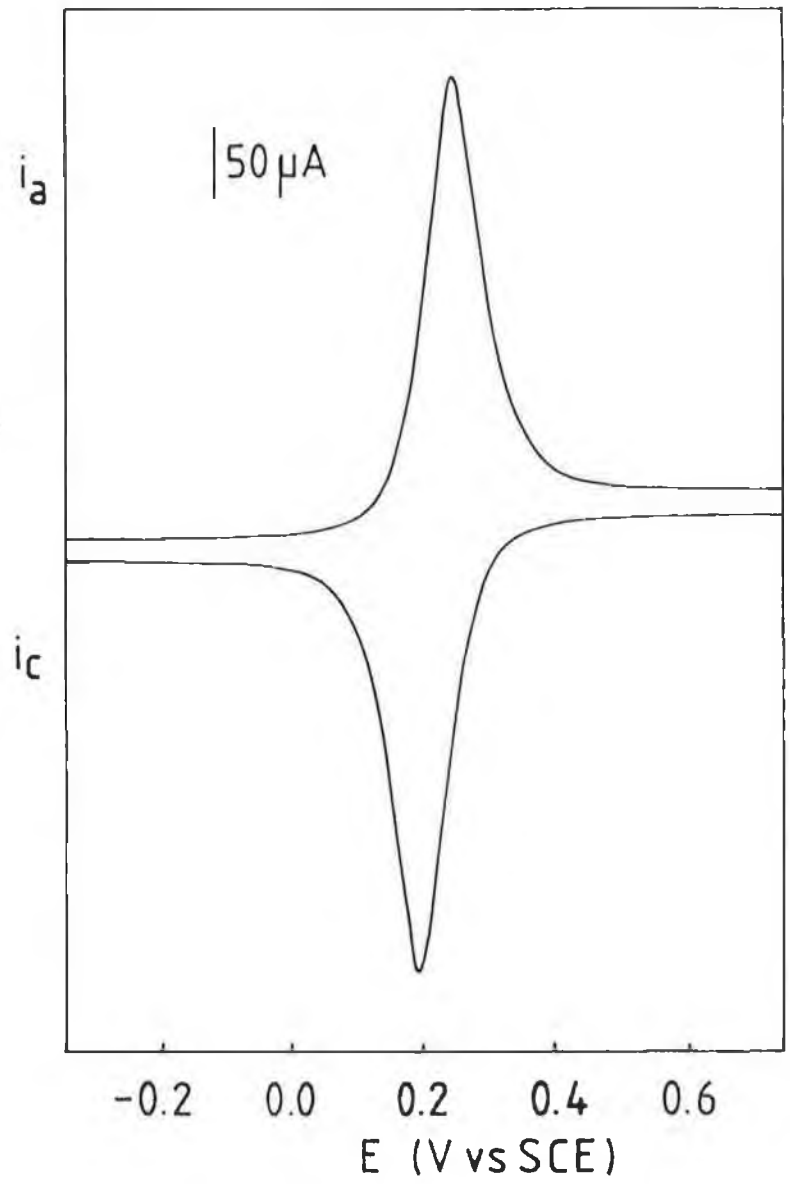

Figure 3.2.2 Cyclic voltammogram of electrodes modified with $[Os(bipy)_2(PVP)_5Cl]Cl$ electrodes. Sweep rate 100 mV/s. 1.0 M $HClO_4$ as supporting electrolyte. Surface coverage 2 x 10^{-8} molcm^{-2}. Electrode area 0.3848 cm^2.

Section 3.3 Potential Step Methods

Chronoamperometry

Short timescale transient amperometric/coulometric measurements were made by means of a Phillips 3311 digital storage oscilloscope interfaced to a BBC microcomputer for data interrogation and allowing signal averaged results to be obtained. For both the redox active potential step and for background correction 5 signals were averaged.

Large amplitude potential step chronoamperometry is a standard technique in the study of electrochemical systems. In this section the experimental implementation of this method to evaluate charge transport rates through osmium containing polymer films is described. The current-time transients are usually considered to be controlled by the potential driven rate of heterogeneous electron transfer and by the rate of homogeneous charge transfer within the film, this process plays the same role as physical diffusion of the redox species in solution. In the case of polymer modified electrodes some features which must be considered include background correction for capacitive currents, uncompensated resistance effects and the experimental timescale.

In the chronoamperometry experiment a potential step across the formal potential of the redox couple, produces not only a Faradaic response, but also generates capacitive currents. These must be corrected for in the accurate determination of charge transport rates. In this work the removal of capacitive currents has been examined using two techniques. Firstly, the current response of an unmodified electrode during a potential step across the potential region of interest is performed in background electrolyte and the response recorded. This is then considered to represent the capacitive

contribution, to the total current observed, for the same electrode after modification, during the same potential step. This capacitive component is then subtracted from the total current response. The remaining current thus represents the Faradaic current from which D_{CT} is calculated. In this work however, this procedure is considered to be unsatisfactory since it assumes that the charging of the double layer is the same before and after modification. An alternative to this approach is to evaluate the capacitive contribution after modification. This involves performing small potential steps at the foot of the redox wave and linearly extrapolating the observed capacitive current. This is in turn subtracted from the total current observed when the potential is stepped across the redox couple, to yield the Faradaic component from which D_{CT} is calculated. The significance of the capacitive component varies according to the electrolyte and redox site concentration, but also depends on the particular morphology which the film adopts in a given electrolyte solution. Thus, for example, the capacitive current may only contribute 1% of the total current observed in sulphuric acid, while in perchlorate the capacitive current can contribute as much as 10% to the total current. In these circumstances background correction is a necessity.

Redox polymer modified electrodes usually possess a high concentration of redox active material within the film e.g for the systems described here this ranges from 0.3 to 1.2 M. These high concentrations give rise to large Faradaic currents, which, in the presence of uncompensated resistance can produce a significant potential drop at the electrode surface [8]. This effect can cause significant errors to be made in the evaluation of kinetic parameters. In potential step experiments designed to obey the Cottrell equation, it is assumed that the actual electrode potential governs the surface

concentration as described by the Nernst equation. Where R_u exists the electrode does not reach the required potential and the reaction does not proceed at a rate which is independent of the electrode potential.

The effect of uncompensated resistance on the Cottrell behaviour is illustrated using data obtained for $[Os(bip)_2(PVP)_{10}Cl]Cl$ films. The effect of H_2SO_4 concentration on the chronoamperometric behaviour without iR compensation, presented as Cottrell plots is presented in Figure 3.3.1. The current response does not follow the Cottrell equation, most notably in low electrolyte concentrations. At short times the observed current falls below that given by the Cottrell equation. This is considered to be a consequence of the potential which is attained at the electrode surface. At short times the electrode fails to attain the potential required for the reaction to proceed at a rate independent of the electrode potential. This leads to less of the metallopolymer being oxidised and hence reduced currents. If this data is used to calculate D_{CT} then a significant underestimation of the charge transport rate occurs. It also leads to a positive intercept on the current axis, for this reason charge transport data with non zero intercepts for Cottrell plots must be considered with caution. At longer times the applied potential is realised, but now the Os(II) concentration is larger than that which is dictated by a Cottrell response, thus leading to larger currents. In low electrolyte concentrations this leads to a distinct current "overshoot" at intermediate times. If this data is used to evaluate D_{CT} an overestimate is obtained together with a negative current intercept.

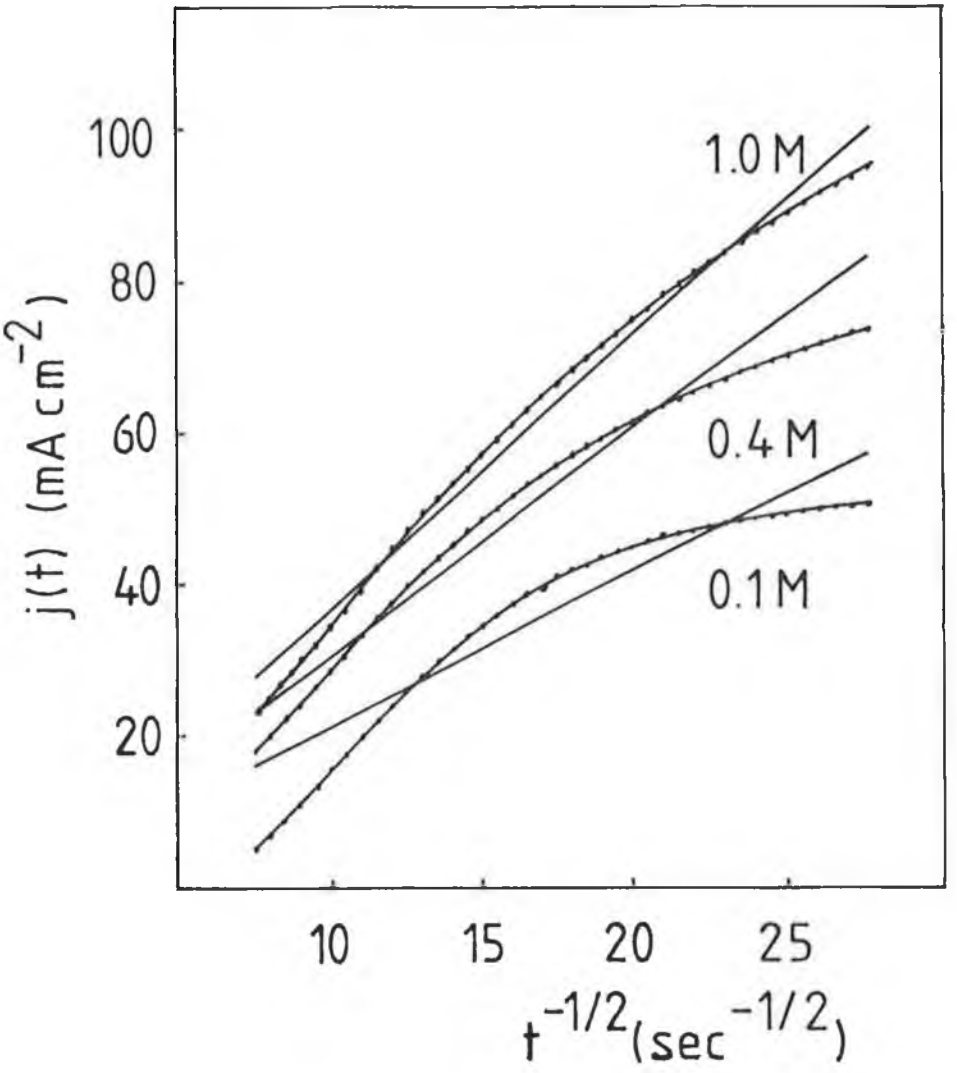

Figure 3.3.1 The effect of H_2SO_4 concentration on the chronoamperometric response of $[Os(bipy)_2(PVP)_{10}Cl]Cl$ modified electrodes. Data points show the response without iR compensation, while the solid lines show the Cottrell response after iR compensation. Potential step from -0.4 to +0.4 V vs SCE.

The deviation of the chronoamperometric response from the Cottrell equation is more apparent for low concentrations of supporting electrolyte. This suggests that the ion population exerts considerable influence over charge transport properties. The solid lines of Figure 3.3.1 shows that the effect of adding iR compensation using positive feedback circuitry to compensate for both film and solution resistance.

An alternative to iR compensation is to step the potential further past the formal potential of the redox couple, this means that despite a potential drop at the working electrode, the potential attained is still sufficient for the oxidation to proceed at a potential independent rate. This is possible only where the formal potential of the metallopolymer is considerably less than the upper potential limit of the electrolyte solution, which is approximately 1.2 - 1.3 V vs SCE for these aqueous electrolyte systems. The Cottrell response for $[Os(bipy)_2(PVP)_{10}Cl]Cl$ films where the potential is stepped to 1.0 V is illustrated for $HClO_4$ electrolyte in Figure 3.3.2.

The behaviour illustrated in Figure 3.3.2 shows that for longer times the current falls below that given by the Cottrell equation. This arises due to the onset of thin layer behaviour. The time at which this behaviour is observed is a function of both D_{CT} and the film thickness. This is illustrated for $[Os(bipy)_2(PVP)_{10}Cl]Cl$ films in Figures 3.3.3 and 3.3.4, where the surface coverage is varied from 10^{-7} to 10^{-10} molcm^{-2}. Since the redox centre is part of the polymer chain for these systems an increase in Γ is expected to increase the layer thickness L. This data illustrates two aspects of charge transport through these films. When the surface coverage is varied significantly $D_{CT}(PS)$ becomes dependent on the surface coverage.

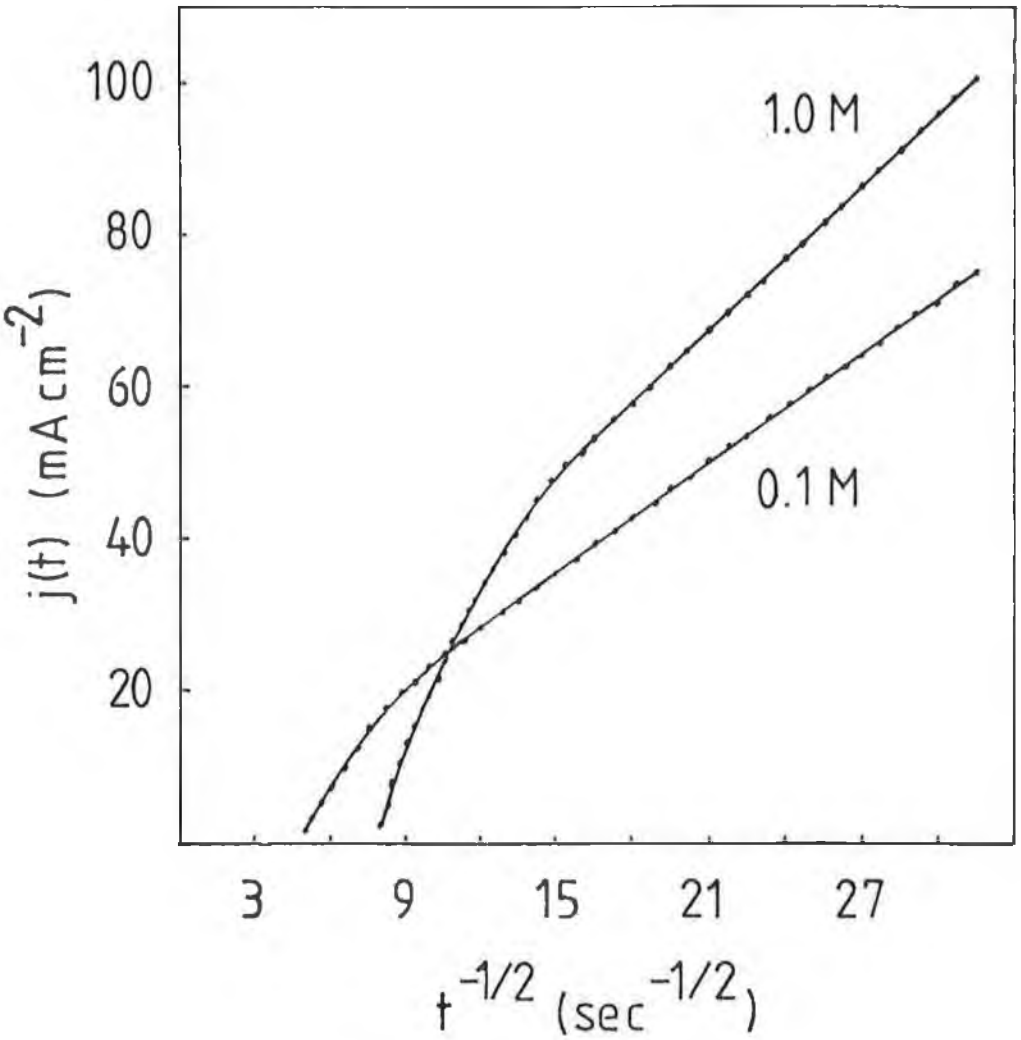

Figure 3.3.2 The effect of $HClO_4$ concentration on the large amplitude potential step chronoamperometric response for $[Os(bipy)_2(PVP)_{10}Cl]Cl$ modified electrodes. Potential step from -0.4 to +1.0 V vs SCE.

This is not entirely unexpected, since where charge propagation is limited by a mass transport process such as ion movement, such a mass transport process will be impeded by an increased film thickness. Also, the time at which the chronoamperometric response deviates from the Cottrell equation is clearly dependent on the film thickness. In table 3.3.1 the ratio of the thickness of the diffusion layer to the film thickness is investigated using the data from Figures 3.3.3 and 3.3.4.

This table shows that the Cottrell equation becomes invalid at times where the diffusion layer thickness is between 50 and 82% of the dry film thickness in sulphuric acid and between 42 and 47% of dry film thickness for perchloric acid. The sulphuric acid data obtained for small surface coverages suggests that the film thicknesses calculated from density measurements are not grossly inaccurate. The difference between the times at which the chronoamperometric response fails to obey the Cottrell equation in sulphuric and perchloric acid, may arise due to variations of film thickness between the two electrolytes for the same surface coverage. The fact that in $HClO_4$ the Cottrell equation is obeyed for diffusion layer thicknesses of only 40% of the dry film thickness, suggests that the film may become more compact in perchloric acid media. Alternatively, the data may suggest, that the processes controlling charge transport remain the same throughout the total film thickness in sulphuric acid, while in perchloric acid, kinetic barriers to mass transport exist at longer times.

Table 3.3.1 The ratio of diffusion layer thickness to total film thickness where the chronoamperometric response fails to obey the Cottrell equation.

Γ (mol cm^{-2})	L (cm)	D_{CT}(PS) (cm^2s^{-1})	δ /L
0.1 M H_2SO_4 as supporting electrolyte.			
$3.60x10^{-7}$	$5.10x10^{-4}$	$1.00x10^{-9}$	0.50
$3.66x10^{-8}$	$5.24x10^{-5}$	$2.95x10^{-9}$	0.55
$4.55x10^{-9}$	$6.50x10^{-6}$	$4.40x10^{-9}$	0.71
$5.05x10^{-10}$	$7.14x10^{-7}$	$6.20x10^{-9}$	0.82
0.1 M $HClO_4$ supporting electrolyte			
$2.56x10^{-7}$	$3.65x10^{-4}$	$7.11x10^{-10}$	0.42
$2.58x10^{-8}$	$3.69x10^{-5}$	$2.03x10^{-9}$	0.44
$2.70x10^{-9}$	$3.85x10^{-6}$	$5.21x10^{-9}$	0.47
$2.55x10^{-10}$	$3.64x10^{-7}$	$7.13x10^{-9}$	0.47

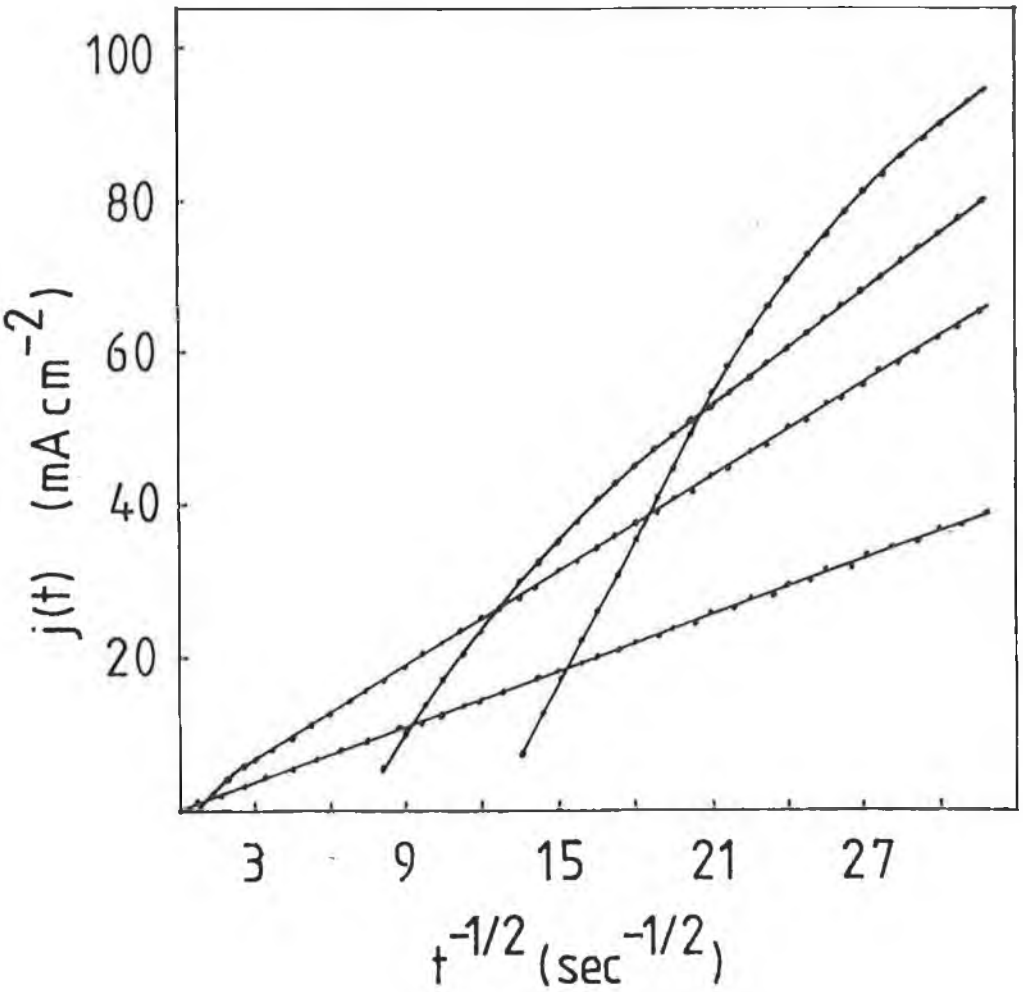

Figure 3.3.3 The effect of surface coverage on the chronoamperometric response of $[Os(bipy)_2(PVP)_{10}Cl]Cl$ modified electrodes. Supporting electrolyte is 0.1 M H_2SO_4. Surface coverages are, from top to bottom, 5 x 10^{-10}, 5 x 10^{-9}, 5 x 10^{-8} and 5 x 10^{-7} molcm^{-2} respectively. Potential step from -0.4 to 1.0 V vs SCE.

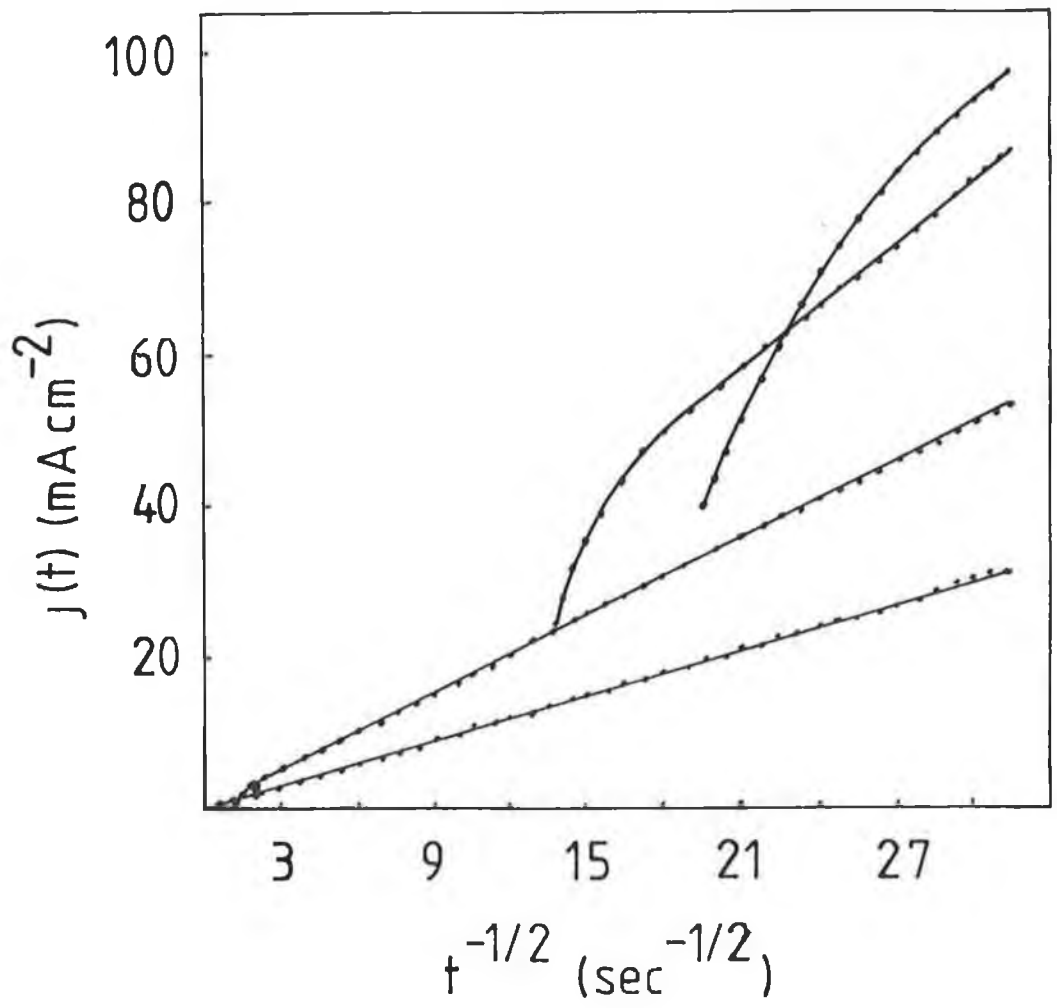

Figure 3.3.4 The effect of surface coverage on the chronoamperometric response of $[Os(bipy)_2(PVP)_{10}Cl]Cl$ modified electrodes. Supporting electrolyte is 0.1 M $HClO_4$. Surface coverages are, from top to bottom, 5 x 10^{-10}, 5 x 10^{-9}, 5 x 10^{-8} and 5 x 10^{-7} molcm^{-2} respectively. Potential step from -0.4 to 1.0 V vs SCE.

Sampled Current Voltammetry

Sampled current voltammetry was performed using an E. G. & G. Model 273 potentiostat interfaced to a B.B.C microcomputer for data acquisition, storage and analysis. A pulse width of 200 ms and an interval of 10 s between successive pulses was employed. The current was sampled before application of the potential step and confirmed to be zero, this ensures that the depletion layer of the oxidised species due to the preceding step has been completely re-reduced. Sampling times of 1, 2, 4 and 10 ms after application of the potential step, where the current response was under semi-infinite diffusion control and obeyed the Cottrell equation, were employed throughout this study.

The data were analysed as described in section 1.3.3 to yield both the rate of homogeneous charge transport and the rate of heterogeneous electron transfer. However, the calculation of D_{CT} from four current samples is considered unreliable and these values were only used to confirm chronoamperometry results.

The limiting current observed in sampled current voltammetry should obey the Cottrell equation as discussed for chronoamperometry in the preceding section. The experimental timescale (1-10 ms) has been chosen in order that Cottrell behaviour be observed for the maximum number of cases. Other important features include a constant background charging and well defined limiting current as illustrated in Figure 3.3.5.

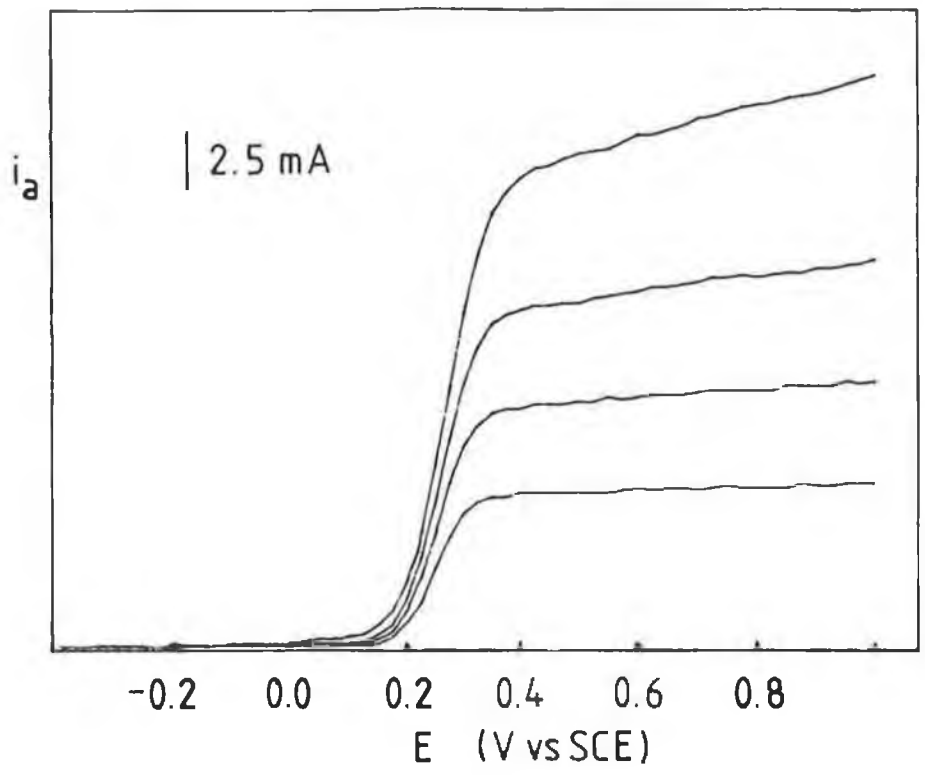

Figure 3.3.5 Sampled current voltammogram of $[Os(bipy)_2(PVP)_{10}Cl]Cl$ films in 0.6 M HCl. Sampling times are 1, 2, 4 and 10 ms after the application of potential steps. Surface coverage 2×10^{-8} molcm^{-2}

Section 3.6 References.

1. E. T. Turner-Jones and L. R. Faulkner, J. Electroanal. Chem., 1987, 222, 201
2. R. C. Engstrom, Anal. Chem., 1982, 54, 2310
3. R. C. Engstrom and V. A. Strasser, Anal. Chem., 1984, 56, 136
4. G. E. Cabaniss, A. A. Diamantis, W. R. Murphy, R. W. Linton and T. J. Meyer, J. Am. Chem. Soc., 1985, 107, 1845
5. I. Hu, D. H. Karweik and T. Kuwana, J. Electroanal. Chem., 1985, 188, 59
6. D. E. Smith, Crit. Rev. Anal. Chem., 1971, 2, 247
7. J. E. Harrar and C. L. Pomernacki, Anal. Chem., 1973, 35, 47
8. K. D. Oldham, J. Electroanal. Chem., 1966, 11, 171

CHAPTER 4

Charge Transport Properties of

$[Os(bipy)_2(PVP)_nCl]Cl$ Modified Electrodes.

Section 4.1 Introduction:

As discussed previously in chapter 1 the potential application of modified electrodes in domains as diverse as sensor design [1-6], energy conversion [7], corrosion protection [8] and catalysis [9], has lead to extensive investigations in this area of electrochemistry. The nature of charge transport through the modifying layer is recognised as being of central importance in these investigations, not only for fundamental reasons but also because the applied utility of these materials will ultimately be dictated by the charge transport properties of the modifying layer. Despite this, the number of reports dealing with the effect of electrolyte, redox site loading and temperature on charge transport dynamics remains meagre for materials with immobile redox centres [10,11].

For the investigation of charge transport mechanisms and kinetics of polymer modified electrodes, steady state (ring-disk and array electrodes) and transient methods (chronoamperometry, chronocoulometry and normal pulse voltammetry) have been explored extensively [12-19]. These short timescale techniques typically give information about the charge transport properties of the modifying film close to the polymer/electrode interface. The results obtained in this manner may not be typical for the whole modifying layer due to different morphologies and/or redox composition.

In this chapter the effect of electrolyte type and concentration, temperature, pH, redox site loading and experimental timescale on both the homogeneous and heterogeneous charge transport properties of $[Os(bipy)_2(PVP)_nCl]Cl$, where n= 5, 10, 15, 20 and 25, modified electrodes is investigated. The rate of homogeneous charge transport has been explored for each redox site loading in 0.1 to 1.0 M supporting electrolyte. The

supporting electrolytes examined are HCl, $HClO_4$ and H_2SO_4. Cyclic voltammetry and short timescale potential step methods give detailed information of the charge transport properties of this type of material at different timescales. Thermodynamic parameters have been evaluated from the temperature dependence of both D_{CT} as measured by potential step and cyclic voltammetry methods. Similarly, the dependence of heterogeneous electron transfer from the underlying electrode into the metallopolymer film on the above variables has been explored using sampled current voltammetry.

Section 4.2 Experimental

Materials. $[Os(bipy)_2(PVP)_nCl]Cl$ n= 5, 10, 15, 20 and 25 were prepared as described previously in chapter 2.

Apparatus and procedures Electrochemical measurements were performed using an E.G.& G. Model 273 potentiostat/ galvanostat as described in chapter 3.

Surface coverages were estimated by graphical integration of the background corrected slow sweep rate cyclic voltammograms (1 mV/s), and were typically 2 - 4 x 10^{-8} molcm^{-2}. The quantity of osmium immobilised on the electrode surface was kept constant as the loading was varied. This means that the layer thickness for the 1:25 loading is approximately 3.5 times greater than the 1:5 loading. However, the same results within experimental error are obtained for homogeneous charge transport when layer thickness is kept constant. Where the layer thickness is varied more extremely D_{CT} typically decreases with increasing film thickness (see chapter 3 for further discussion

of layer thickness effects). The advantage of keeping the quantity of osmium on the electrode constant is that a high Faradaic to capacitive current ratio is maintained where the electrolyte, redox site concentrations and temperature are low. Layer thickness was estimated from the individual densities of the dry metallopolymers as measured by flotation in non swelling solvents, namely petroleum ether and dichloromethane; n = 25, 1.07 g/cm^3; n = 20, 1.08 g/cm^3; n = 15, 1.09 g/cm^3; n = 10, 1.20 g/cm^3 and n = 5 1.40 g/cm^3. These gave a value for the maximum concentration of osmium centres within the film as follows n = 25, 0.33 M; n = 20, 0.38 M; n = 15, 0.46 M; n = 10, 0.70 M and n = 5, 1.17 M. These values have been used to calculate D_{CT} from the experimentally determined $D_{CT}{}^{1/2}C$.

In studies where the electrolyte concentration was varied, all the experiments were carried out with fresh coatings. This avoids possible problems from "memory effects" where the rate of charge transport through a film would be dependent on the electrolytes to which it had previously been exposed. The values for the diffusion coefficients, and activation parameters are reproducible to within ± 2% on a single coating and to ± 10% between coatings.

Section 4.3 Results : The Effect of Electrolyte and Redox Site Concentration on Homogeneous Charge Transport Rates.

Section 4.3.1 General Potential step chronoamperometry, chronocoulometry and sampled current voltammetry were employed in conjunction with the Cottrell equation [20] to estimate the charge transport rates for the Os(II/III) oxidation as apparent diffusion parameters $D_{CT}(PS)^{1/2}C$ and $D_{CT}(PS)$, where

PS indicates potential step in accordance with the methods described in chapter 3 and the Cottrell equation (section 1.3.2).

For the cyclic voltammetry experiments sweep rates in the range 1 to 500 mV/s were used. Charge transport rates were evaluated from the peak current obtained at sweep rates between 50 and 500 mV/s using both the Aoki [21] and Randles-Sevcik [22] approaches described in 1.3.1 and the methodologies described in chapter 3. This rate of homogeneous charge transport derived from cyclic voltammetry data is labelled as $D_{CT}(CV)$.

The rate of charge transport through these osmium containing metallopolymer films has been evaluated as the osmium loading within the film has been changed from 1:25 to 1:5 ($[Os(bipy)_2Cl]^+$: pyridine monomer units).

Section 4.3.2 Hydrochloric Acid

Figure 4.3.2.1 shows the effect of osmium loading on the Cottrell response obtained from chronoamperometric experiments carried out in 1.0 M HCl. This figure clearly shows that the rate of charge transport is dependent on the osmium concentration within the film. The linearity and zero intercept of the Cottrell plot suggests that the response is diffusion controlled. It also shows, that for osmium loadings between 1:25 and 1:10 $D_{CT}(PS)$, as obtained from the slope of the plots, increases as the osmium concentration increases, but that for the 1:5 loading a decrease is observed. The time at which the chronoamperometry response fails to obey the Cottrell equation is dependent on both the redox site loading and the electrolyte concentration. The diffusion layer thickness at this time can be approximated by $\delta = (\pi D_{CT}t)^{1/2}$. The effect of active site loading on the ratio of the diffusion

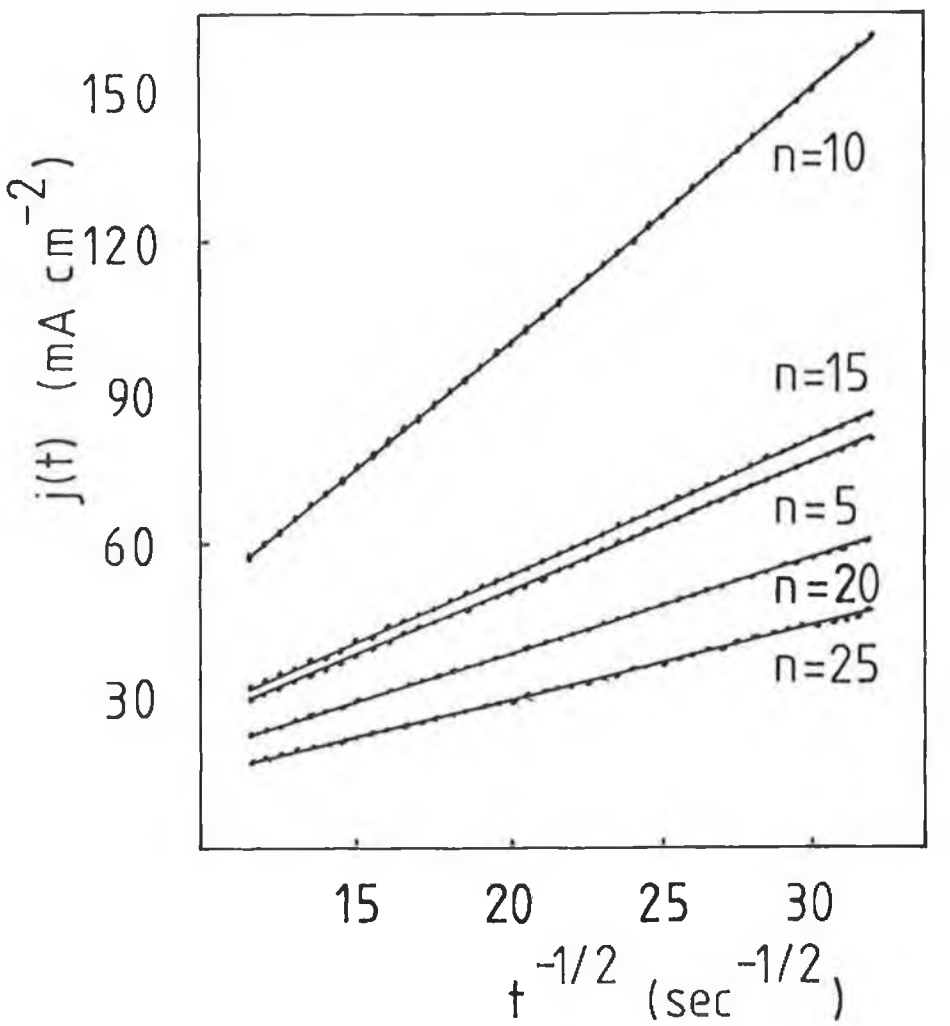

Figure 4.3.2.1 The effect of redox site loading on the chronoamperometric response for $[Os(bipy)_2(PVP)_nCl]Cl$ films on glassy carbon electrodes presented as Cottrell plots. 1.0 M HCl as supporting electrolyte.

layer thickness to the layer thickness in 0.8 M HCl is given in Table 4.3.2.1. This table shows that the Cottrell equation is only obeyed for times considerably less than those required for complete oxidation of the film.

The effect of redox site loading on D_{CT}(PS) has been explored at various concentrations of HCl as supporting electrolyte and the results presented in Figure 4.3.2.2 and Table 4.3.2.2. Table 4.3.2.2 shows that for high electrolyte concentrations, and for osmium loadings less than 1:5, a linear increase of D_{CT}(PS) with osmium loading is observed, while at low electrolyte concentration a decrease is observed for osmium loadings where n<15.

Table 4.3.2.2 shows that D_{CT}(PS) increases with increasing HCl concentration for all of the loadings examined. However, the extent of this increase differs for each osmium loading. For the 1:5 loading D_{CT}(PS) does not increase as significantly compared with the other osmium loadings. For the 1:10 loading a large variation in D_{CT}(PS) is observed, with much of this increase occurring between 0.6 and 0.8 M HCl. For the lower osmium loadings the effect of HCl concentration on D_{CT}(PS) is less than that observed for the 1:10 loading, and the increase of D_{CT}(PS) with HCl concentration is largely monotonic.

The effect of osmium loading on both D_{CT}(CV) and the redox potentials as obtained from cyclic voltammetry in HCl are given in Table 4.3.2.2. As observed using potential step methods, CV also shows an initial linear increase in D_{CT}(CV) with increasing osmium loading. The loading that limits this linear response differs between CV and potential step methods, for the CV experiments linear behaviour is observed for loadings lower than 1:15. The effect of increased HCl concentration is again to increase the charge

Table 4.3.2.1 The effect of redox site loading on the ratio of diffusion layer (δ) to film thickness (L) as measured by potential step methods. Table A shows data where the surface coverage is kept constant and B where film thickness is constant.

	Redox Site Loading	Surface Coverage ($x10^8$ mol cm^{-2})	Layer Thickness ($x\ 10^5$ cm)	Diffusion Layer Thickness ($x\ 10^5$ cm)	δ /L
(A)	1:5	2.54	2.17	0.54	0.25
	1:10	2.32	3.31	1.39	0.42
	1:15	2.10	4.56	1.59	0.35
	1:20	2.29	6.02	1.98	0.33
	1:25	2.40	7.27	2.18	0.30
(B)	1:5	5.91	5.05	1.16	0.23
	1:10	3.71	5.30	2.12	0.40
	1:15	2.35	5.10	1.73	0.34
	1:20	1.86	4.89	1.61	0.33
	1:25	1.72	5.21	1.46	0.28

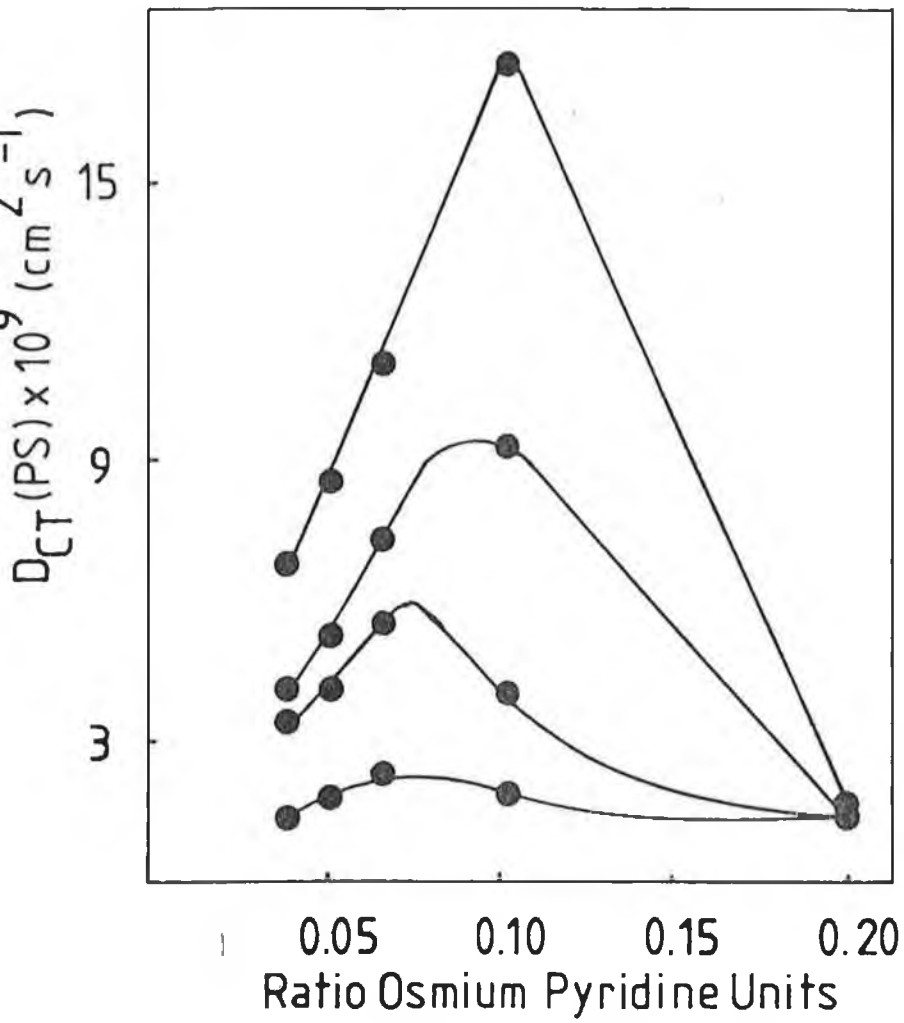

Figure 4.3.2.2 The effect of HCl concentration and redox site loading on $D_{CT}(PS)$ of $[Os(bipy)_2(PVP)_nCl]Cl$ films. The HCl concentrations are from top to bottom 1.0, 0.8, 0.6 and 0.1 M.

Table 4.3.2.2: The effect of concentration of hydrochloric acid supporting electrolyte and redox site loading on charge transport parameters of $[Os(bipy)_2(PVP)_nCl]Cl$ modified electrodes.

Loading	Conc. M	D_{CT}(PS) $*10^9$ cm^2s^{-1}	D_{CT}(CV) $*10^{10}$ cm^2s^{-1}	E^o V
n=5	0.1	1.42	0.88	0.210
	0.2	1.48	1.25	0.225
	0.4	1.49	1.21	0.235
	0.6	1.47	1.22	0.235
	0.8	1.48	1.20	0.230
	1.0	1.60	1.33	0.230
n=10	0.1	1.96	0.012	0.215
	0.2	3.10	0.029	0.205
	0.4	3.43	0.111	0.190
	0.6	3.95	0.395	0.200
	0.8	9.44	0.488	0.188
	1.0	17.27	0.688	0.180
n=15	0.1	2.33	1.75	0.240
	0.2	3.52	1.78	0.240
	0.4	5.37	2.09	0.240
	0.6	5.62	2.31	0.250
	0.8	7.32	4.35	0.250
	1.0	10.85	4.85	0.250
n=20	0.1	1.79	1.03	0.240
	0.2	2.50	1.23	0.240
	0.4	4.12	1.45	0.245
	0.6	4.22	1.73	0.245
	0.8	5.09	3.09	0.245
	1.0	8.47	3.67	0.245
n=25	0.1	1.42	0.83	0.245
	0.2	2.31	0.94	0.245
	0.4	3.23	1.11	0.250
	0.6	3.42	1.38	0.250
	0.8	3.97	2.55	0.250
	1.0	6.89	2.77	0.250

transport rate. The rate of charge transport increases rapidly between 0.6 and 0.8 M HCl for osmium loadings lower than 1:10.

Section 4.3.3 Perchloric Acid.

The timescale over which the Cottrell equation is obeyed for potential step experiments in 0.1 M perchloric acid is shown in Table 4.3.3.1. For low redox site loadings the Cottrell equation is valid only for diffusion layer thicknesses of between 28 and 43% of the total film thickness and is dependent on both active site and electrolyte concentration. From the linear portion of the Cottrell plot, which shows a zero current intercept, $D_{CT}(PS)$ was evaluated. The effect of redox site loading and perchloric acid concentration on $D_{CT}(PS)$ is shown in Figure 4.3.3.1 and in Table 4.3.3.2. For osmium loadings between 1:25 and 1:15 $D_{CT}(PS)$ is relatively insensitive to the redox site loading, for the 1:10 loading a sharp increase is observed, while for the 1:5 loading the rate of charge transport decreases from the 1:10 value to a rate which is comparable to that seen at the lower loadings. The effect of increased perchloric acid concentration as supporting electrolyte is typically to increase the charge transport rate, notably for the 1:10 loading.

The variation of $D_{CT}(CV)$ with redox site loading is given in Table 4.3.3.2 and shows a region where the charge transport rate is relatively insensitive to osmium loading followed by an substantial increase for the 1:5 loading. The effect of electrolyte concentration is distinctly different to that seen in all other electrolytes, with the exception of $[Os(bipy)_2(PVP)_{25}Cl]Cl$ in sulphuric acid. An <u>increasing</u> perchlorate concentration steadily <u>decreases</u> $D_{CT}(CV)$ and also results in a less positive

Table 4.3.3.1 The effect of redox site loading on the ratio of diffusion layer (δ) to film thickness (L) in 0.1 M $HClO_4$ as measured by potential step methods.

Redox Site Loading	Surface Coverage ($x10^8$ $molcm^{-2}$)	Layer Thickness ($x\ 10^5$ cm)	Diffusion Layer Thickness ($x\ 10^5$ cm)	δ/L
1:5	3.22	2.72	2.22	0.81
1:10	2.89	4.12	1.77	0.43
1:15	3.19	6.93	2.49	0.36
1:20	3.01	7.92	2.53	0.32
1:25	2.75	8.33	2.33	0.28

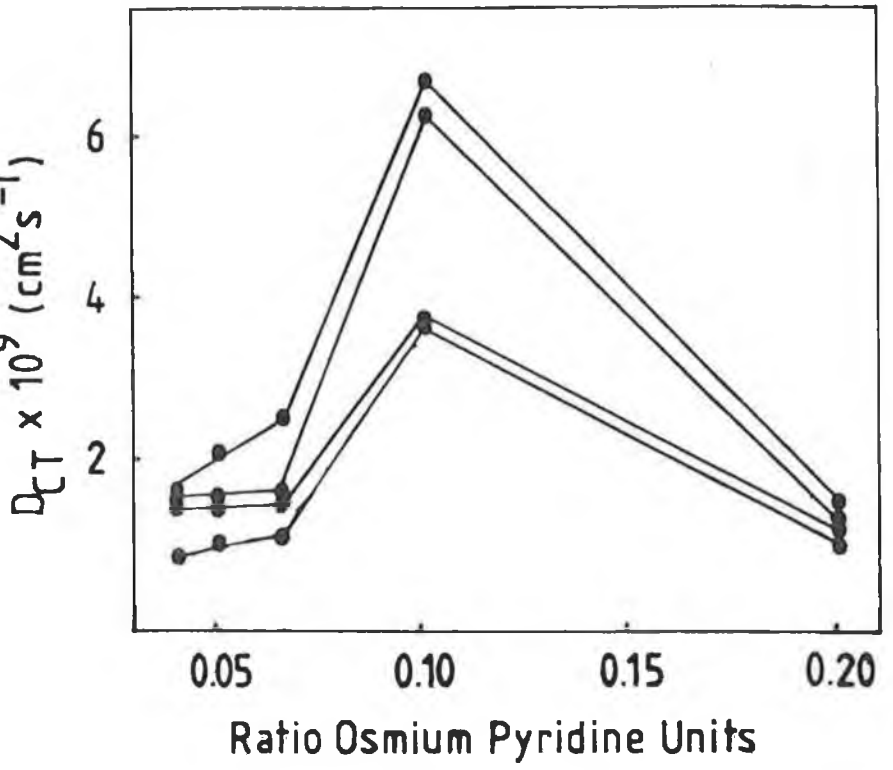

Figure 4.3.3.1 The effect of $HClO_4$ concentration and redox site loading on $D_{CT}(PS)$ of $[Os(bipy)_2(PVP)_nCl]Cl$ films. The electrolyte concentrations are from top to bottom 1.0, 0.6, 0.4 and 0.1 M

Table 4.3.3.2: The effect of concentration of perchloric acid supporting electrolyte and redox site loading on charge transport parameters of $[Os(bipy)_2(PVP)_nCl]Cl$ modified electrodes.

Loading	Conc. M	D_{CT}(PS) $*10^9$ cm^2s^{-1}	D_{CT}(CV) $*10^{10}$ cm^2s^{-1}	E^o V
n=5	0.1	0.95	2.62	0.245
	0.2	1.05	2.29	0.240
	0.4	1.10	2.23	0.225
	0.6	1.25	1.85	0.215
	0.8	1.40	1.33	0.210
	1.0	1.44	0.93	0.215
n=10	0.1	3.69	0.48	0.215
	0.2	3.77	0.41	0.220
	0.4	3.69	0.35	0.215
	0.6	6.35	0.24	0.170
	0.8	6.35	0.12	0.142
	1.0	6.72	0.05	0.125
n=15	0.1	1.02	1.10	0.245
	0.2	1.30	1.02	0.260
	0.4	1.44	0.73	0.250
	0.6	1.54	0.64	0.240
	0.8	1.72	0.52	0.245
	1.0	2.50	0.47	0.215
n=20	0.1	0.99	1.07	0.240
	0.2	1.15	1.04	0.235
	0.4	1.41	0.74	0.240
	0.6	1.53	0.63	0.230
	0.8	1.76	0.51	0.225
	1.0	2.09	0.44	0.225
n=25	0.1	0.83	1.23	0.240
	0.2	0.94	1.10	0.235
	0.4	1.46	0.73	0.225
	0.6	1.62	0.62	0.190
	0.8	1.62	0.51	0.195
	1.0	1.62	0.39	0.180

redox potential. Overall the variations in $D_{CT}(CV)$ are small, with the exception of the 1:10 loading.

Section 4.3.4 Sulphuric Acid.

The timescale over which the Cottrell equation is obeyed has been examined as a function of the active site loading. Table 4.3.4.1 shows the dependency of δ /L on redox site loading in 1.0 M H_2SO_4. Significantly, for loadings where $D_{CT}(PS)$ and $D_{CT}(CV)$ are similar e.g $[Os(bipy)_2(PVP)_5Cl]Cl$ the Cottrell equation is obeyed for nearly 80 % of the total film thickness. Where more significant differences exist between $D_{CT}(CV)$ and $D_{CT}(PS)$ the chronoamperometric response fails to obey the Cottrell equation at earlier times.

The influence of sulphuric acid concentration on $D_{CT}(PS)$ of various osmium loadings is shown in Figure 4.3.4.1 and in Table 4.3.4.2. $D_{CT}(PS)$ increases approximately linearly with increasing osmium loading between 1:25 and 1:15, before decreasing for the 1:10 and 1:5 loadings.

The effect of an increased electrolyte concentration is dependent on the redox site loading. For the 1:25 loading $D_{CT}(PS)$ is relatively less sensitive to sulphuric acid concentration. As the redox site loading is increased $D_{CT}(PS)$ increases more significantly with electrolyte concentration, and for the 1:20, 1:15 and 1:10 loadings it is seen to increase greatly between 0.2 and 0.4 M H_2SO_4. For the 1:5 loading $D_{CT}(PS)$ is again rather insensitive to sulphuric acid concentration.

Table 4.3.4.2 also gives the dependence of D_{CT} with redox site loading and sulphuric acid concentration as measured by cyclic voltammetry. A change in the osmium loading from 1:25 to 1:20 reduces $D_{CT}(CV)$ but after this

Table 4.3.4.1 The effect of redox site loading on the ratio of layer thickness (L) to diffusion layer thickness (δ) in 1.0 M sulphuric acid as measured by potential step methods.

Redox Site Loading	Surface Coverage ($\times 10^8$ mol cm^{-2})	Layer Thickness ($\times 10^5$ cm)	Diffusion Layer Thickness ($\times 10^5$ cm)	δ/L
1:5	2.10	1.79	1.42	0.79
1:10	2.23	3.14	1.88	0.59
1:15	2.01	4.36	1.30	0.30
1:20	2.11	5.55	1.94	0.35
1:25	2.32	7.03	3.86	0.55

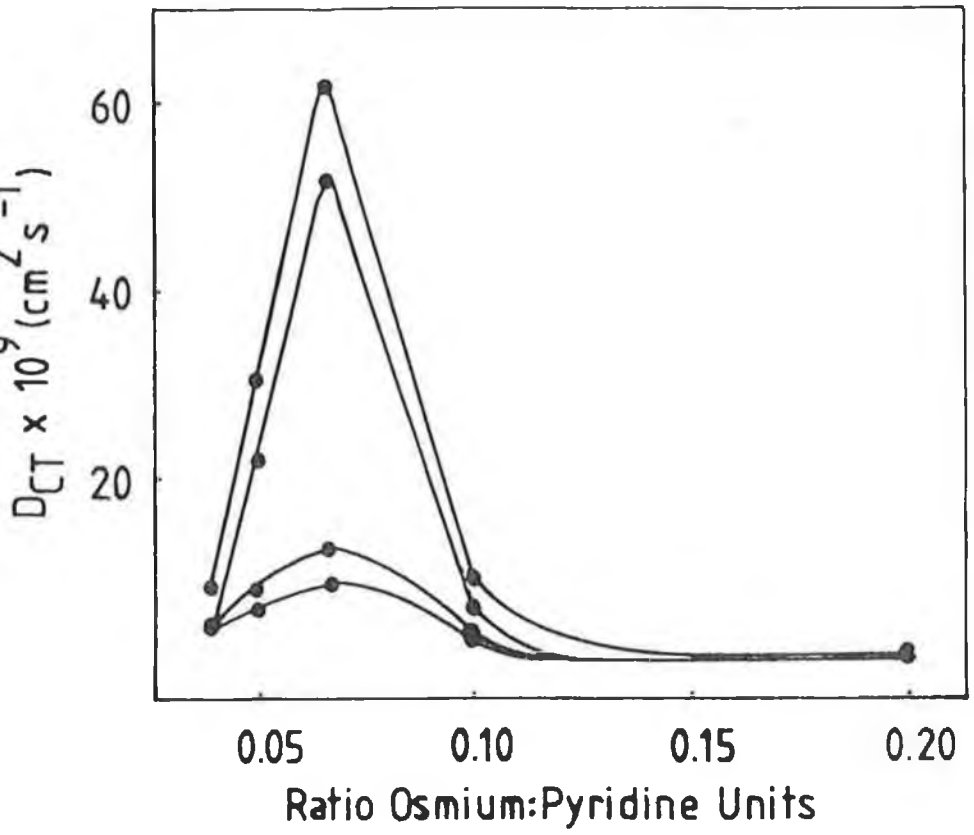

Figure 4.3.4.1 The effect of H_2SO_4 concentration and redox site loading on $D_{CT}(PS)$ of $[Os(bipy)_2(PVP)_nCl]Cl$ films. The electrolyte concentrations are from top to bottom 1.0, 0.4, 0.2 and 0.1 M

Table 4.3.4.2: The effect of concentration of sulphuric acid supporting electrolytes and redox site loading on charge transport parameters of $[Os(bipy)_2(PVP)_nCl]Cl$ modified electrodes.

Loading	Conc. M	D_{CT}(PS) $*10^9$ cm^2s^{-1}	D_{CT}(CV) $*10^{10}$ cm^2s^{-1}	E^o V
n=5	0.1	1.27	3.22	0.270
	0.2	1.16	4.18	0.255
	0.4	1.16	4.77	0.260
	0.6	1.16	6.50	0.255
	0.8	1.16	8.39	0.260
	1.0	1.16	9.12	0.255
n=10	0.1	2.95	2.51	0.260
	0.2	3.77	6.11	0.248
	0.4	6.40	8.75	0.250
	0.6	8.89	12.75	0.250
	0.8	9.01	14.88	0.250
	1.0	9.16	16.70	0.250
n=15	0.1	8.89	1.70	0.237
	0.2	12.85	4.07	0.235
	0.4	52.10	4.54	0.235
	0.6	59.05	5.53	0.220
	0.8	59.97	6.60	0.220
	1.0	62.06	7.80	0.225
n=20	0.1	6.32	2.10	0.235
	0.2	8.01	4.01	0.235
	0.4	22.10	5.22	0.230
	0.6	23.92	5.43	0.220
	0.8	28.63	6.53	0.225
	1.0	30.10	7.52	0.223
n=25	0.1	3.78	21.00	0.240
	0.2	4.20	21.22	0.230
	0.4	4.24	13.95	0.225
	0.6	4.56	11.00	0.210
	0.8	5.92	10.63	0.210
	1.0	8.54	9.65	0.200

an increased osmium loading does not significantly affect the charge transport rate. Where n<20 the effect of increasing sulphuric acid concentration is to increase $D_{CT}(CV)$. The behaviour for the 1:25 loading is however, significantly different with $D_{CT}(CV)$ decreasing as the H_2SO_4 concentration is increased.

Section 4.4.1 Determination of Thermodynamic Parameters for Homogeneous Charge Transport.

The evaluation of thermodynamic parameters can be useful in the identification of the rate determining step of the charge transport process [23]. Activation energies have been evaluated by varying the temperature of the contacting electrolyte over the range 278-303 K, measuring the charge transport rate and evaluating the activation energy, E_a, via the Arrhenius equation (Equation 5) as described in chapter 3.

The activation parameters obtained in this manner for 0.1 and 1.0 M electrolytes from potential step and for CV measurements are given in Tables 4.4.2.1 to 4.4.4.2.

Section 4.4.2 Hydrochloric Acid.

This behaviour of $E_a(PS)$ with changing redox site loading in both 0.1 and 1.0 M HCl is illustrated in Figure 4.4.2.1. With 0.1 M HCl as supporting electrolyte, $E_a(PS)$ remains unchanged with redox site loading at about 25 kJ/Mol, and is coupled to a negative entropy term. In 1.0 M HCl $E_a(PS)$ changes with redox site loading. For the 1:25 to 1:15 loadings the activation energy is 42 ± 2 kJ/Mol, while for the 1:10 and 1:5 loadings it is reduced to less than 10 kJ/Mol. The entropy term is negative for all loadings and becomes less negative with decreasing loading.

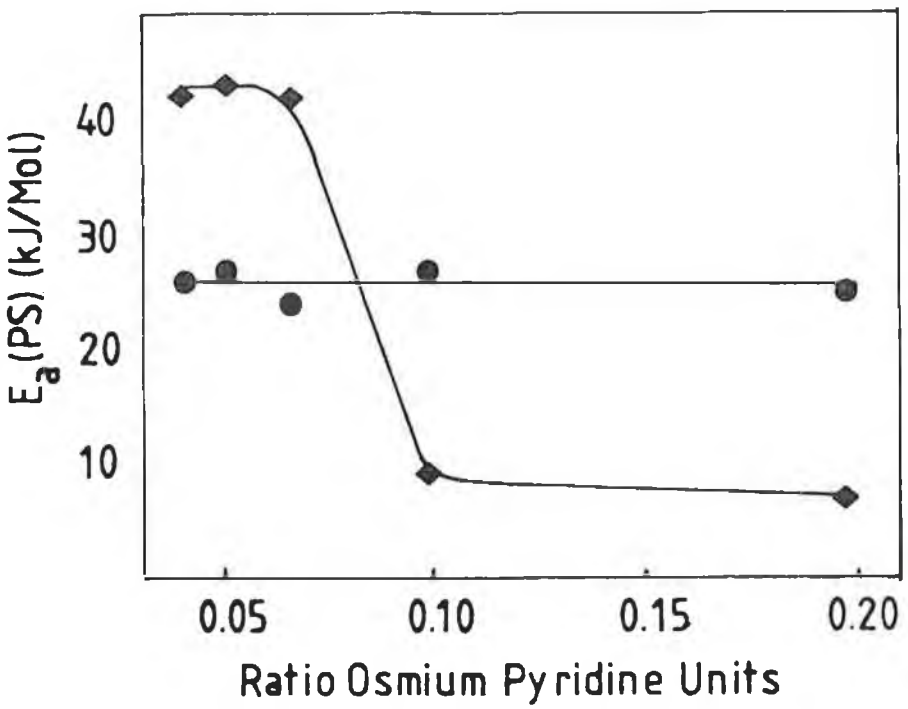

Figure 4.4.2.1 The effect of redox site loading in $[Os(bipy)_2(PVP)_nCl]Cl$ polymer films on E_a(PS) in ◆ 1.0 M HCl and ● 0.1 M HCl.

Table 4.4.2.1 : Activation parameters for charge transport through $[Os(bipy)_2(PVP)_nCl]Cl$ films as obtained by sampled current voltammetry in hydrochloric acid.

Loading		$E_a(PS)$ kJ/Mol	$\Delta H(PS)^{\neq}$ kJ/Mol	$\Delta S(PS)^{\neq}$ $JMol^{-1}K^{-1}$	$\Delta G(PS)^{\neq}$ kJ/Mol
n=5	0.1 M	25.0	22.6	-74.3	44.7
	1.0 M	6.9	4.5	-134.1	44.4
n=10	0.1 M	27.1	24.6	-76.0	47.3
	1.0 M	9.0	6.5	-118.8	41.9
n=15	0.1 M	23.5	21.0	-93.5	48.9
	1.0 M	42.1	29.6	-18.3	45.1
n=20	0.1 M	27.1	24.6	-88.4	50.9
	1.0 M	43.5	41.0	-20.4	47.1
n=25	0.1 M	25.6	23.1	-99.1	52.6
	1.0 M	42.1	39.6	-30.6	48.7

The behaviour observed using cyclic voltammetry is similar in both 0.1 and 1.0 M HCl (see Table 4.4.2.2). For the low redox site loadings <1:10 E_a(CV) is large at 90-130 kJ/Mol and the entropy term is positive, with the higher values being observed for the higher electrolyte concentration. For 1:10 and 1:5 loadings lower activation energies of 20-40 kJ/Mol and negative entropy terms were obtained.

Section 4.4.3 Perchloric Acid

The activation parameters evaluated from potential step data are given in Table 4.4.3.1. For the 1:25, 1:20 and 1:15 loadings E_a(PS) is approximately 40 kJ/Mol in both 0.1 and 1.0 M perchloric acid. This activation energy is reduced to 15.9 and 9.9 kJ/Mol in 0.1 and 1.0 M electrolyte respectively for the 1:5 loading. The 1:10 loading shows a similar value of 14.5 kJ/Mol in 0.1 M electrolyte. In 1.0 M perchloric acid an unusual dual slope behaviour is observed, which is illustrated in figure 4.4.3.1. At temperatures below 285 K E_a(PS) is similar to that observed for the lower loadings with a value of 51 kJ/Mol, however, above that temperature the activation energy is larger (134 kJ/Mol). All of the above activation energies, except the one obtained for the 1:10 system at high temperature, show negative entropy terms.

The E_a(CV) values are considerably larger than those observed using potential step methods (see Table 4.4.3.2). For loadings $\leq$ 1:15 E_a(CV) is of the order of 100-150 kJ/Mol and has a positive entropy term. For the 1:5 loading little variation of the activation energy with electrolyte concentration is observed, and E_a(CV) is coupled to a negative entropy term. The 1:10 loading represents a transition situation that shows dual slope

Table 4.4.2.2 : Activation parameters for charge transport through $[Os(bipy)_2(PVP)_nCl]Cl$ films as obtained by cyclic voltammetry in hydrochloric acid.

Loading		$E_a(CV)$ kJ/Mol	$\Delta H(CV)^{\ddagger}$ kJ/Mol	$\Delta S(CV)^{\ddagger}$ $JMol^{-1}K^{-1}$	$\Delta G(CV)^{\ddagger}$ kJ/Mol
n=5	0.1 M	37.8	35.3	-54.5	51.6
	1.0 M	44.9	42.4	-27.2	50.5
n=10	0.1 M	18.0	15.5	-168.1	65.6
	1.0 M	16.0	13.5	-141.2	55.6
n=15	0.1 M	88.4	85.9	102.8	55.3
	1.0 M	134.5	132.0	265.9	52.7
n=20	0.1 M	87.6	85.1	90.9	58.0
	1.0 M	133.3	130.8	246.4	54.9
n=25	0.1 M	86.1	83.6	80.4	59.7
	1.0 M	132.2	129.8	237.0	56.7

Table 4.4.3.1 : Activation parameters for charge transport through $[Os(bipy)_2(PVP)_nCl]Cl$ films as obtained by sampled current voltammetry in perchloric acid.

Loading		$E_a(PS)$ kJ/Mol	$\Delta H(PS)^{\neq}$ kJ/Mol	$\Delta S(PS)^{\neq}$ $JMol^{-1}K^{-1}$	$\Delta G(PS)^{\neq}$ kJ/Mol
n=5	0.1 M	15.9	13.1	-108.2	45.7
	1.0 M	9.9	7.5	-123.9	44.5
n=10	0.1 M	14.5	12.0	-113.1	45.7
T>285 K	1.0 M	134.0	131.5	292.8	44.3
T<285 K		51.0	48.5	-38.0	60.0
n=15	0.1 M	41.0	38.5	-41.6	50.9
	1.0 M	44.4	41.9	-22.8	48.7
n=20	0.1 M	44.1	41.6	-36.3	52.4
	1.0 M	39.3	36.8	-46.2	50.6
n=25	0.1 M	42.6	40.1	-46.5	53.9
	1.0 M	35.3	32.8	-65.4	52.3

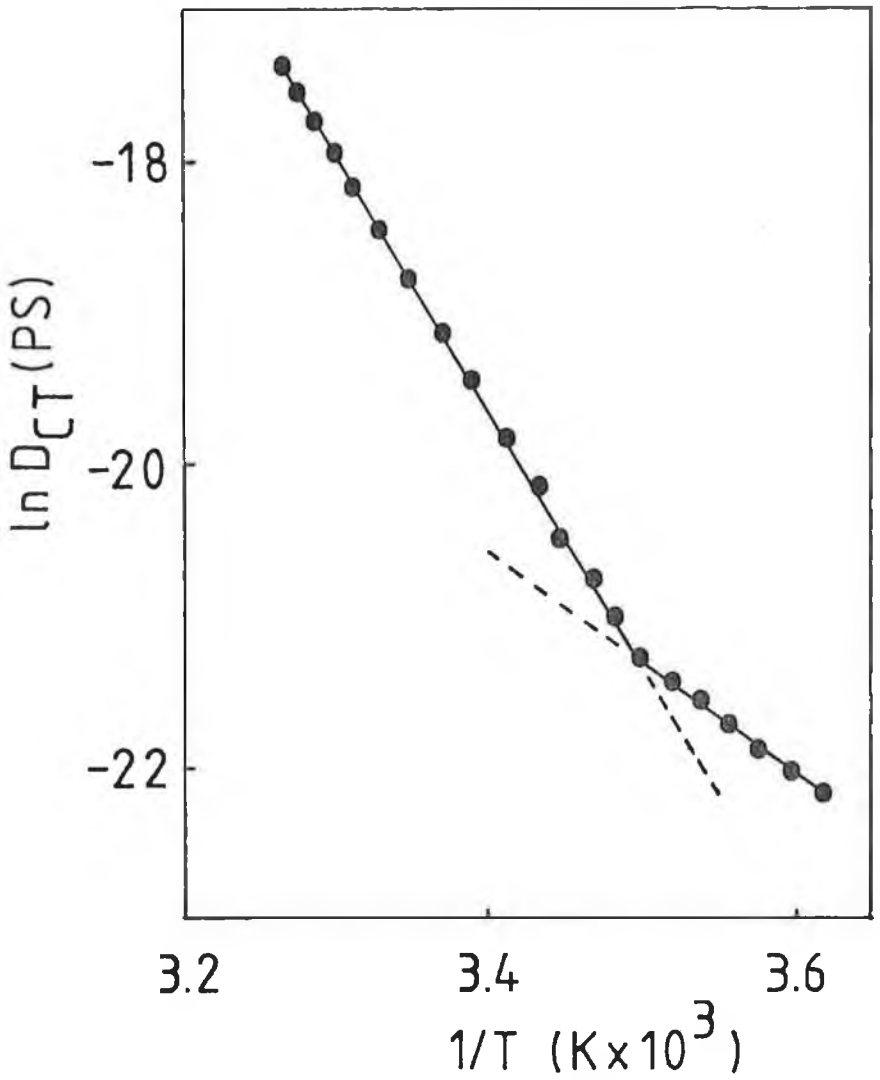

Figure 4.4.3.1 Temperature dependence of D_{CT}(PS) for $[Os(bipy)_2(PVP)_{10}Cl]Cl$ films in 1.0 M $HClO_4$.

Table 4.4.3.2 : Activation parameters for charge transport through $[Os(bipy)_2(PVP)_nCl]Cl$ films as obtained by cyclic voltammetry in perchloric acid.

Loading		$E_a(CV)$ kJ/Mol	$\Delta H(CV)^{\ddagger}$ kJ/Mol	$\Delta S(CV)^{\ddagger}$ $JMol^{-1}K^{-1}$	$\Delta G(CV)^{\ddagger}$ kJ/Mol
n=5	0.1 M	48.6	46.0	-9.2	48.9
	1.0 M	42.2	39.7	-39.3	51.4
n=10 T>285 K	0.1 M	224.0	221.5	548.0	58.2
T<285 K		35.0	32.5	-106.0	64.0
	1.0 M	92.0	89.5	92.0	62.1
n=15	0.1 M	162.7	160.2	332.5	61.1
	1.0 M	151.3	148.8	295.2	60.8
n=20	0.1 M	160.1	157.6	319.8	62.3
	1.0 M	154.2	151.7	290.5	65.1
n=25	0.1 M	158.4	155.9	304.0	65.3
	1.0 M	156.6	154.1	297.6	65.4

behaviour in 0.1 M perchloric acid. Above 285 K E_a(CV) is large and coupled to a positive entropy as observed for the lower redox loadings. Below that temperature a lower E_a(CV) coupled to a negative entropy term is observed. In 1.0 M electrolyte a large activation energy with a large positive entropy value is observed.

Section 4.4.4 Sulphuric Acid

The values obtained for E_a(PS) in 0.1 M sulphuric acid, increase as the redox site loading is increased and are associated with negative entropy terms (see Table 4.4.4.1). The behaviour in 1.0 M sulphuric acid is similar to that observed previously for 1.0 M HCl. At low loadings E_a(PS) is high (35-40 kJ/Mol) and is then reduced at higher redox site loading.

The cyclic voltammetry behaviour in 1.0 M sulphuric acid exhibits a large E_a(CV) associated with a positive entropy term (see Table 4.4.4.2). As the osmium content in the film is increased to 1:5 E_a(CV) is reduced and becomes associated with a negative entropy term. In 0.1 M sulphuric acid the activation energy decreases sharply from the value obtained for the 1:25 loading of 79 kJ/Mol to a value of 10 kJ/Mol for the 1:10 loading, followed by an increase to 45 kJ/Mol for the 1:5 loading.

Table 4.4.4.1 : Activation parameters for charge transport through $[Os(bipy)_2(PVP)_nCl]Cl$ films as obtained by sampled current voltammetry in sulphuric acid.

Loading		$E_a(PS)$ kJ/Mol	$\Delta H(PS)^{\neq}$ kJ/Mol	$\Delta S(PS)^{\neq}$ $JMol^{-1}K^{-1}$	$\Delta G(PS)^{\neq}$ kJ/Mol
n=5	0.1 M	47.6	45.1	0.6	44.9
	1.0 M	2.6	0.1	-151.2	45.2
n=10	0.1 M	24.0	21.5	-83.1	46.3
	1.0 M	6.0	3.5	-134.1	43.5
n=15	0.1 M	14.5	12.0	-131.7	51.3
	1.0 M	39.2	36.7	-13.5	40.8
n=20	0.1 M	6.0	3.5	-148.7	47.8
	1.0 M	34.9	32.4	-38.8	44.0
n=25	0.1 M	14.5	12.0	-128.2	50.2
	1.0 M	34.9	32.4	-52.9	48.2

Table 4.4.4.2 : Activation parameters for charge transport through $[Os(bipy)_2(PVP)_nCl]Cl$ films as obtained by cyclic voltammetry in sulphuric acid.

Loading		$E_a(CV)$ kJ/Mol	$\Delta H(CV)^{\ddagger}$ kJ/Mol	$\Delta S(CV)^{\ddagger}$ $JMol^{-1}K^{-1}$	$\Delta G(CV)^{\ddagger}$ kJ/Mol
n=5	0.1 M	45.2	42.7	-18.9	48.3
	1.0 M	27.9	25.4	-68.3	45.8
n=10	0.1 M	10.5	8.5	-155.6	52.4
	1.0 M	115.5	113.0	220.1	47.1
n=15	0.1 M	21.4	18.9	-130.7	55.4
	1.0 M	90.4	87.7	170.6	51.6
n=20	0.1 M	59.7	57.2	3.0	56.3
	1.0 M	80.1	77.6	67.9	57.4
n=25	0.1 M	79.2	76.7	84.0	51.7
	1.0 M	74.9	72.4	63.2	53.6

Section 4.5 Discussion of Homogeneous Charge Transport.

Charge transport through such modifying films is now widely accepted as occurring through electron self exchange reactions between reduced/oxidised redox couples. The rate determining step for charge propagation can be limited by; i) the rate of segmental polymer chain motion, ii) the transport of charge compensating counterion into/out of the modifying film during redox, iii) the intrinsic barrier to electron self exchange.

The rate of charge transport through the $[Os(bipy)_2(PVP)_nCl]Cl$ films reported here is clearly dependent on the electrolyte type, its concentration and the redox site loading. Significantly, the apparent rate of charge transport also appears to be dependent on the timescale of the method used to evaluate it. Traditionally, the investigation of charge transport through such metallopolymer films has been accomplished using short timescale potential step measurements. The fact that short timescale chronoamperometry gives a charge transport rate, $D_{CT}(PS)$, which is larger than that obtained using cyclic voltammetry, $D_{CT}(CV)$, suggests that for these osmium containing polymers, there are kinetic barriers to the movement of mobile species participating in the overall redox process, over and above those controlling the charge injection rate. Such a multiequilibrium model is supported by the fact that activation energies measured by cyclic voltammetry are larger and frequently reflect processes, notably polymer chain motion, which are expected to occur under more complete equilibrium conditions (vide infra). The timescale over which the Cottrell equation is valid depends on both the active site and supporting electrolyte concentrations. Significantly, in those electrolytes, such as H_2SO_4, where $D_{CT}(PS)$ and $D_{CT}(CV)$ are similar the Cottrell equation is valid for up to 80 % of the total film thickness. This

further suggests that where kinetic barriers to mass transport are absent that charge is propagated through the whole film thickness at a similar rate. The origins of these kinetic barriers to mass transport within the film is discussed later. The observations of this chapter clearly show that electrochemical methods, as well as, radiotracer techniques and the quartz crystal microbalance [25-27] can be used to investigate the time dependence of mass transport.

The difference in charge transfer rates when the electrolyte solution is varied, suggests that the contacting electrolyte directly influences ion availability within the film and/or the coatings morphology. The effect of increased electrolyte concentration is to increase D_{CT}(PS) for all electrolytes and loadings examined. The increase is not linear and frequently shows an electrolyte concentration above which D_{CT}(PS) increases significantly. It is well known that polyelectrolyte films can act to exclude ions where the ion concentration in solution is below the fixed site concentration within the film. This occurs due to the films associated Donnan potential [28]. It seems likely, therefore, that the rate of charge transport is limited by ion availability dictated by Donnan exclusion, where the electrolyte concentration is low, and that only when the electrolyte concentration exceeds the fixed site concentration is it possible to remove the ion transport limitation. Other factors, such as the electrolytes ability to mobilise or solubilise polymer chains or swell the film, will also influence ion availability.

The effect of electrolyte concentration on the cyclic voltammetry experiments has also been explored (see Tables 4.3.2.2 - 4.3.4.2). In HCl an increased electrolyte concentration gives an enhanced D_{CT}(CV), with much of

the increase occurring between 0.6 and 0.8 M electrolyte. This again suggests that Donnan exclusion operates for high redox site loading/low electrolyte combinations and that as the electrolyte concentration is increased, other processes limit $D_{CT}(CV)$. The formal potential data in HCl support the above interpretation (see Table 4.3.2.2). E_0 in HCl is insensitive to electrolyte concentration for the 1:15, 1:20 and 1:25 loadings. At the 1:10 loading E_0 decreases significantly between 0.6 and 0.8 M HCl, the same point at which $D_{CT}(CV)$ increases sharply. At the 1:5 loading E_0 actually increases with increasing HCl concentration supporting the view that for this loading Donnan exclusion operates at all the HCl concentrations examined. The situation in perchloric acid is in stark contrast to the behaviour discussed above, with $D_{CT}(CV)$ <u>decreasing</u> as the perchlorate concentration is <u>increased</u>. Perchlorate salts of these metallopolymers are unusual in that they are insoluble in aqueous media. These observations suggest that as the perchlorate ion concentration is increased, the film becomes more compact, thus hindering ion transport. This agrees with recent reports on partially quaternised poly(4-vinylpyridine) films containing $Re(CO)_3$(phen), phen = 1,10-phenanthroline, which were shown to form nearly dehydrated compact films in perchlorate containing media [29]. In sulphuric acid an increase in electrolyte concentration typically increases $D_{CT}(CV)$, except for the 1:25 loading. This increase is monotonic, which suggests that the film is extensively swollen. This is supported by the data obtained from the 1:25 loading where $D_{CT}(CV)$ <u>decreases</u> as the sulphuric acid concentration is <u>increased</u>. This behaviour is explained by extensive film swelling as the electrolyte is increased. This process increases the intersite separation, requiring that the polymer strands move in order that electron self exchange

occur.

With the exception of sulphuric acid an increased redox site loading initially increases $D_{CT}(CV)$. $D_{CT}(CV)$ does not increase over the whole loading range investigated except in perchloric acid, but for the highest loading examined (1:5) $D_{CT}(CV)$ decreases. This coupled to the observed dependence of $D_{CT}(CV)$ on electrolyte concentration suggests that ion transport plays a significant role in determining $D_{CT}(CV)$. The fact that redox site loading has little effect on the charge transport rate when the electrolyte concentration is low, again suggests ion transport limitations. At the highest redox site loading examined (1:5) the fixed site concentration is approximately 1.17 M. Thus a change in electrolyte concentration from 0.1 to 1.0 M does not dramatically alter $D_{CT}(CV)$, since the charge compensating counterion concentration in solution is always less that the fixed site concentration and so Donnan exclusion will always operate.

Interestingly, the dependence of both $D_{CT}(PS)$ and $D_{CT}(CV)$ on the fixed site concentration is frequently linear for low redox site loadings. This behaviour is generally accepted as being indicative of a Dahms-Ruff relation in which electron self exchange makes a significant contribution to the observed charge transport rate [30-33]. However, both the variation of electrolyte concentration and thermodynamic data (vide infra) clearly suggest that ion or polymer chain movement, not electron self exchange represents the rate determining step. Also, measurements conducted on similar ruthenium containing materials using steady state methods, suggest that the values obtained for electron self exchange are considerably larger than the D_{CT} values observed here [34].

The above interpretation, in which ion movement and availability play a significant role in the charge transport process, a limitation which can only be removed for low redox site/high electrolyte concentration combinations, is supported by the thermodynamic data. The E_a(PS) values obtained are different in 0.1 and 1.0 M electrolytes. However, ΔS(PS) values are always negative except for 1.0 M perchloric acid at high temperatures. These negative entropies suggest that an ordering process, namely ion transport limits the rate of charge propagation at both electrolyte concentrations. These negative entropy terms arise, since electron transport requires an ordering of polymer chains in a localised activation zone around the electroactive centre [24]. Coupled to this, the requirement of charge compensating counterion movement into the polymer film will reduce polymer chain flexibility. Both effects will bring about an increase in the systems order and hence a negative entropy term.

The E_a(PS) values in 0.1 M HCl are constant for all loadings examined. This, in combination with the insensitivity of D_{CT}(PS) to redox site loading, suggests that in 0.1 M HCl that Donnan exclusion controls the ion availability within the film for all redox site loadings. In 1.0 M electrolyte E_a(PS) is large (>40 kJ/Mol) for the 1:25, 1:20 and 1:15 loadings. This is reduced to less than 10 kJ/Mol for the 1:10 and 1:5 loadings. This, combined with the effect on D_{CT}(PS) of redox site concentration changes discussed previously, suggests that in 1.0 M HCl ion transport controls the rate of charge propagation for all loadings. The data suggest that in 1.0 M HCl Donnan exclusion has broken down for the 1:25 to 1:10 loadings. This is supported by the increase of D_{CT}(PS) with increasing redox site concentration up to the 1:10 loading. The large value of E_a(PS) observed for these low loadings,

also suggests large scale ion movement within the film. For the 1:5 loading Donnan exclusion operates even in 1.0 M HCl due to the fixed site concentration of 1.17 M, as evidenced by the suppressed D_{CT}(PS) values. The E_a(PS) values for the 1:10 and 1:5 loading are small. The E_a(PS) value obtained for the 1:10 is thought to reflect facile ion movement in the film. For the 1:5 case Donnan exclusion means that transport of charge compensating counterion across the film/electrolyte interface is the rate determining step, which is reflected in the low activation energy observed.

When the activation energies are evaluated using cyclic voltammetry the same trend is observed in both 0.1 and 1.0 M HCl. For low loadings E_a(CV) is large and coupled to a positive entropy term. This implies that the rate determining step is a disordering one. Thus it appears that segmental polymer chain motion limits D_{CT}(CV) for the 1:25 to 1:15 loadings. Significantly, in 0.1 M HCl the activation energy is less that the 1.0 M case, suggesting that the film is less swollen at lower HCl concentration thus reducing the requirement of chain movement for the electron self exchange to occur. The E_a(CV) and entropy values obtained at high loadings suggest ion transport as the rate limiting step.

In perchloric acid E_a(PS) decreases from 35-50 kJ/Mol for the 1:25 to 1:10 loadings to 10 kJ/Mol at the 1:5 loading. The behaviour in 1.0 M electrolyte was broadly similar except for the 1:10 loading. For the 1:25 to 1:15 loadings both D_{CT}(PS) and E_a(PS) remain relatively constant as the perchlorate concentration is increased from 0.1 to 1.0 M. This, coupled to the negative entropy term, suggests that the films are compact, and that ion transport is impeded, even at electrolyte concentrations where Donnan exclusion is expected to be broken down. At the 1:5 loading E_a(PS) is low and reflects

membrane behaviour similar to that discussed for HCl. The 1:10 loading appears to represent a transition situation. In 0.1 M perchlorate the charge transport rate is limited by ion availability as controlled by Donnan exclusion, while in 1.0 M electrolyte the two rate determining processes are observed. For temperatures above 285 K the large activation energy and positive entropy suggest polymer chain motion as the rate determining step [35,36]. The removal of the ion transport limitation causes the increased D_{CT}(PS) values observed for the 1:10 loading. At lower temperatures ion transport again limits the charge propagation rate. The large E_a(CV) values, coupled to positive entropies, represent polymer chain motion as the rate determining step for the 1:25 to 1:15 loadings in both 0.1 and 1.0 M perchloric acid. Donnan exclusion again controls the processes for the 1:5 loading. In 1.0 M perchloric acid, polymer strand motion controls D_{CT}(CV) for the 1:10 system, while dual slope behaviour is observed in 0.1 M electrolyte. This suggests that polymer chain movement controls the charge transport process at higher temperatures, while ion movement limits D_{CT}(CV) for temperatures below 285 K.

In 0.1 M sulphuric acid E_a(PS) increases steadily as the redox site loading is increased. It is presumed that where the osmium content within the film is low, the electrolytes ability to solubilise the film is at a maximum. As the osmium content is increased, the film becomes less swollen hence impeding ion transport, which in turn results in an increased activation energy. In 1.0 M sulphuric acid the rate determining step remains as ion movement within the film. The observed increase in D_{CT}(PS) is a consequence of an increased ion population within the film. D_{CT}(PS) for the 1:5 loading is again under Donnan exclusion control, this acts to limit ion availability within the film thus reducing D_{CT}(PS). The homogeneous activation energy

which represents the barrier of ion transport within the film remains low however. The large E_a(CV) and positive entropy values for the 1:25 loading in 0.1 and 1.0 M sulphuric acid both imply a polymer chain movement limitation. In 0.1 M electrolyte an increase in osmium content changes the rate determining step to ion movement (low activation energies and negative entropies). The films Donnan potential can be overcome by the 1.0 M electrolyte for all loadings except 1:5. Therefore, ion transport limits D_{CT}(CV) for all sulphuric acid concentrations examined at the 1:5 loading. This is in agreement with the electrolyte concentration effects discussed earlier.

Section 4.6 Electrolyte and Redox Site Loading Effects on Heterogeneous Electron Transfer Reactions

Section 4.6.1 General

A typical sampled current voltammogram for the Os(II/III) oxidation within $[Os(bipy)_2(PVP)_{25}Cl]Cl$ films with 0.1 M sulphuric acid as electrolyte is shown in Figure 4.6.1.1. These sigmoid shaped waves are similar to those observed at unmodified electrodes for solution phase reactants [37]. The anodic currents increase with decreasing sampling time and at the same time the half wave potentials of the voltammograms for the oxidation process shift in a positive direction with decreasing sampling time. This behaviour is accepted as being indicative of Butler-Volmer kinetics [38] and the conventional analysis for sampled current voltammograms is, therefore, expected to be appropriate. The rising portion of the sampled current voltammogram has been analysed using the method of Matsuda [39] (Section 1.3.3) to give the standard rate constant, k^o, and anodic transfer coefficient, α , for the heterogeneous electron transfer.

The values for the heterogeneous rate constants, enthalpies and entropies are reproducible to within $\pm$ 2% on a single coating and to $\pm$ 10% between coatings. Transfer coefficients are accurate to within $\pm$0.05.

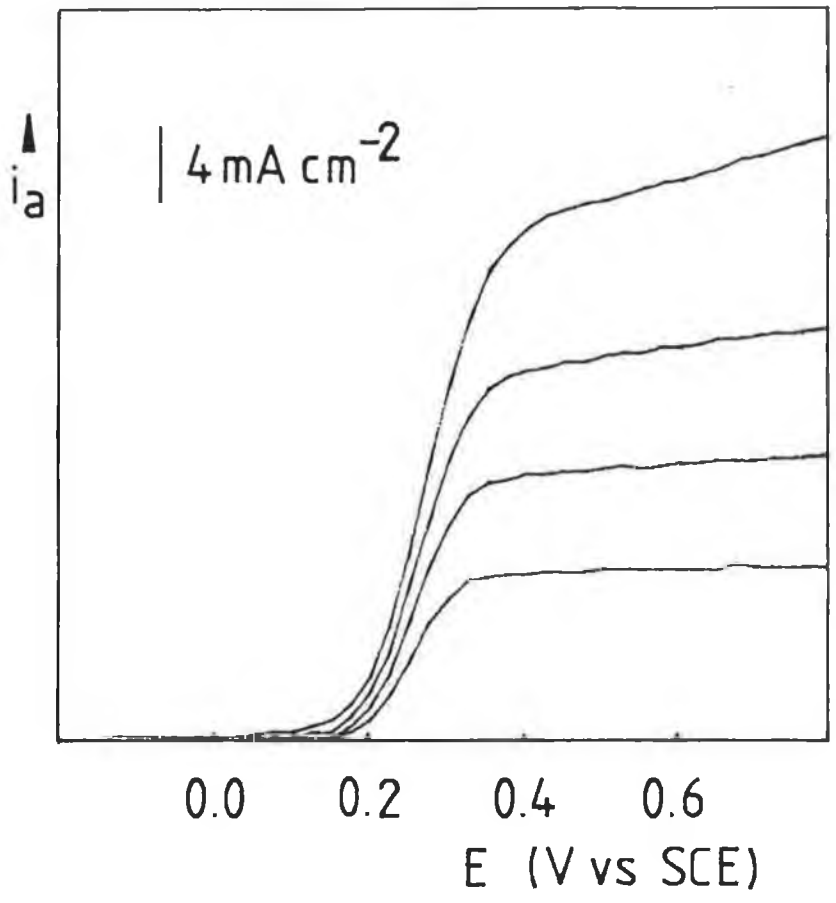

Figure 4.6.1.1 Typical sampled current voltammograms for the Os(II/III) reaction within $[Os(bipy)_2(PVP)_{25}Cl]Cl$ films. Electrolyte 0.1 M H_2SO_4. Sampling times are, from top to bottom, 1, 2, 4, 10 ms. Surface coverage 2 x 10^{-8} molcm^{-2}.

Section 4.6.2 Hydrochloric acid

Figure 4.6.2.1 and Table 4.6.2.1 give the dependence of k^o and transfer coefficient on both HCl concentration and redox site loading. k^o increases with increasing HCl concentration, the nature of this increase being dependent on the redox site loading. For the low loadings a near linear variation of k^o and HCl concentration is observed. For the 1:15 and 1:10 loadings k^o increases significantly between 0.6 and 0.8 M. When the redox site loading is increased to 1:5, k^o becomes largely insensitive to electrolyte concentration. Redox site loading also alters the rate of heterogeneous electron transfer. An increased osmium content initially sharply increases k^o. This increase is not sustained over the complete loading range examined and decreases after the 1:15 loading for low HCl concentrations. In 0.8 and 1.0 M electrolyte k^o decreases after the 1:10 loading.

The transfer coefficient shows considerable sensitivity to electrolyte concentration and redox site loading and reflects the trend observed for k^o, reaching a maximal value for the 1:10 loading. For high osmium loadings α is influenced by electrolyte concentration and increases steadily with increased electrolyte concentration, reaching a value of 0.37 ± 0.05 for 1.0 M HCl. For osmium loadings below 1:10 α is significantly reduced and is relatively less influenced by electrolyte concentration.

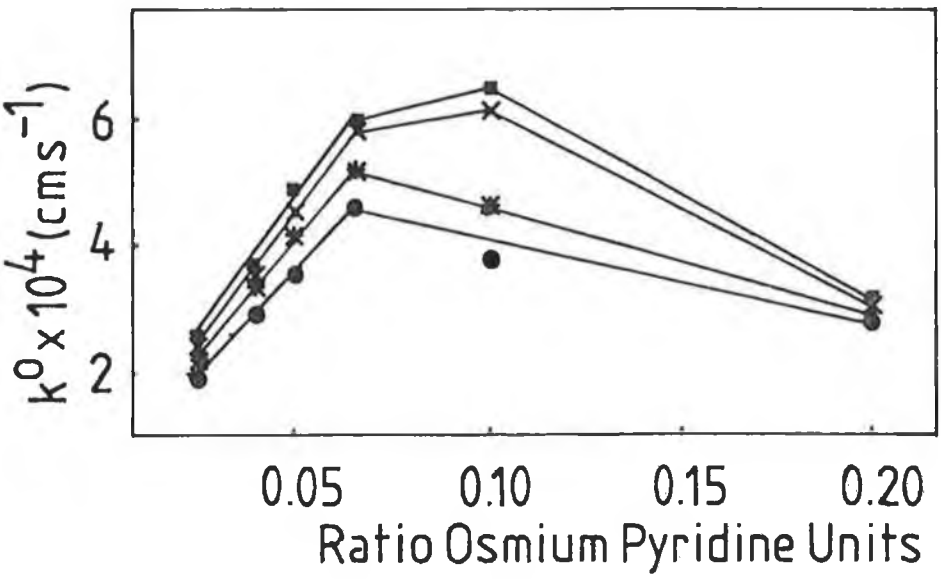

Figure 4.6.2.1 The effect of redox site loading and HCl concentration on k^0 for $[Os(bipy)_2(PVP)_nCl]Cl$ films. Surface coverage 2 x 10^{-8} molcm^{-2}. The electrolyte concentrations are, from top to bottom, 1.0, 0.8, 0.6 and 0.1 M.

Table 4.6.2.1: The effect of concentration of hydrochloric acid supporting electrolyte and redox site loading on heterogeneous electron transfer parameters for $[Os(bipy)_2(PVP)_nCl]Cl$ modified electrodes.

Loading	Conc. M	k^o*10^4 cms^{-1}	α
n=5	0.1	2.89	0.17
	0.2	2.94	0.29
	0.4	2.95	0.34
	0.6	3.00	0.36
	0.8	3.15	0.35
	1.0	3.27	0.37
n=10	0.1	3.81	0.18
	0.2	4.09	0.27
	0.4	4.38	0.31
	0.6	4.66	0.35
	0.8	6.17	0.36
	1.0	6.53	0.38
n=15	0.1	4.65	0.10
	0.2	5.15	0.17
	0.4	5.19	0.20
	0.6	5.19	0.22
	0.8	5.97	0.24
	1.0	6.02	0.24
n=20	0.1	3.60	0.16
	0.2	3.81	0.21
	0.4	4.16	0.22
	0.6	4.49	0.24
	0.8	4.53	0.24
	1.0	4.97	0.25
n=25	0.1	2.95	0.14
	0.2	3.10	0.14
	0.4	3.29	0.16
	0.6	3.38	0.17
	0.8	3.59	0.19
	1.0	3.73	0.24

Section 4.6.3 Perchloric acid

The dependence of k^o on $HClO_4$ concentration and osmium content is given in Table 4.6.3.1. The effect of increased perchloric acid is to increase k^o. This increase is typically monotonic and the total change in k^o on going from 0.1 to 1.0 M perchlorate solutions is similar for all loadings. Initially an increased osmium content increases k^o, this is sustained until the 1:5 loading, where k^o is suppressed.

The transfer coefficient is again significantly lower than the theoretical value of 0.5 for a reversible reaction. α remains approximately constant (0.16 ± 0.04), with increasing electrolyte concentration for the 1:25 to 1:15 loadings. For the 1:10 and more particularly, the 1:5 loading α increases steadily with increasing perchloric acid concentration.

Section 4.6.4 Sulphuric acid

In sulphuric acid the values of k^o are considerably larger than those observed in the other electrolytes (see Tables 4.6.2.1 - 4.6.4.1). For $n<25$ k^o increases as the sulphuric acid concentration in the contacting electrolyte is increased (see Figure 4.6.4.1). This increase is linear for all loadings between 1:20 and 1:5. The 1:25 loading shows a decrease in k^o with increasing electrolyte concentration. As observed in the other electrolytes examined, k^o initially increases as the redox site loading is increased. The increase is significantly larger than that observed in the other electrolytes examined. As the redox site loading is increased to greater than 1:15, k^o decreases for sulphuric acid concentrations above 0.4 M.

Table 4.6.3.1 The effect of concentration of perchloric acid supporting electrolyte and redox site loading on heterogeneous electron transfer parameters of $[Os(bipy)_2(PVP)_nCl]Cl$ modified electrodes.

Loading	Conc. M	k^o*10^4 cms^{-1}	α
n=5	0.1	2.22	0.30
	0.2	2.35	0.31
	0.4	2.75	0.31
	0.6	3.10	0.32
	0.8	3.50	0.32
	1.0	3.93	0.32
n=10	0.1	3.10	0.14
	0.2	3.41	0.18
	0.4	3.85	0.19
	0.6	4.11	0.20
	0.8	4.67	0.20
	1.0	4.95	0.24
n=15	0.1	2.60	0.14
	0.2	3.15	0.18
	0.4	3.26	0.18
	0.6	3.30	0.18
	0.8	3.50	0.18
	1.0	3.84	0.18
n=20	0.1	2.51	0.14
	0.2	2.61	0.14
	0.4	2.73	0.15
	0.6	3.10	0.16
	0.8	3.23	0.18
	1.0	3.51	0.18
n=25	0.1	2.45	0.12
	0.2	2.24	0.13
	0.4	2.50	0.14
	0.6	2.74	0.15
	0.8	2.95	0.15
	1.0	3.22	0.16

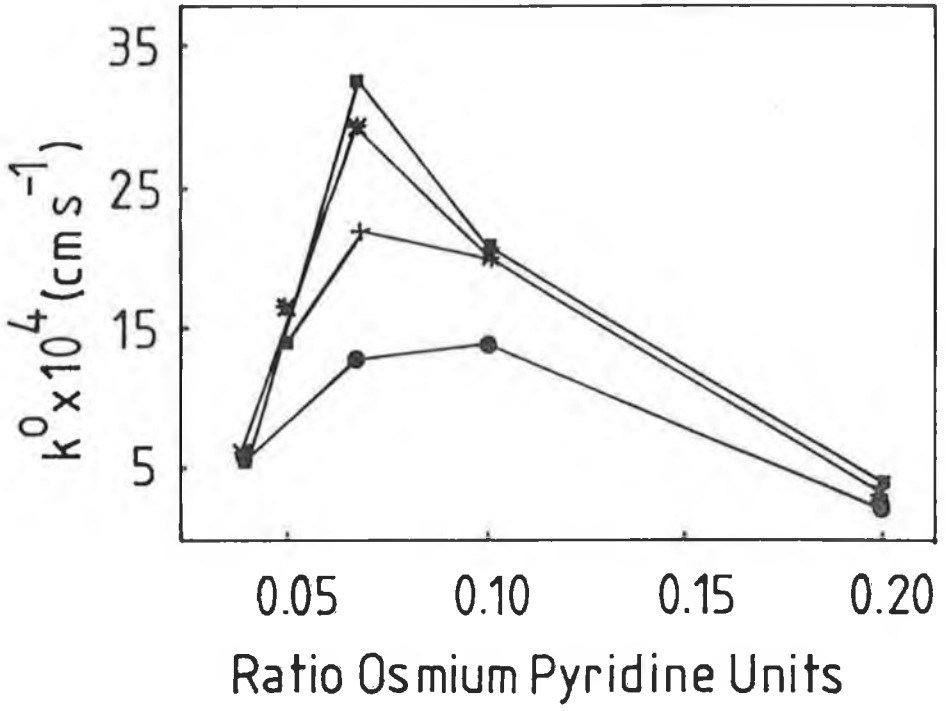

Figure 4.6.4.1 The effect of redox site loading and H_2SO_4 concentration on k^0 for $[Os(bipy)_2(PVP)_nCl]Cl$ films. Surface coverage 2 x 10^{-8} $molcm^{-2}$. The electrolyte concentrations are, from top to bottom, 1.0, 0.6, 0.4 and 0.1 M.

Table 4.6.4.1 The effect of concentration of sulphuric acid supporting electrolytes and redox site loading on heterogeneous electron transfer parameters for $[Os(bipy)_2(PVP)_nCl]Cl$ modified electrodes.

Loading	Conc. M	k^o*10^4 cms^{-1}	α
n=5	0.1	3.00	0.31
	0.2	3.17	0.45
	0.4	3.30	0.47
	0.6	3.25	0.50
	0.8	3.84	0.51
	1.0	4.05	0.48
n=10	0.1	19.80	0.32
	0.2	19.85	0.38
	0.4	19.91	0.41
	0.6	20.10	0.42
	0.8	20.22	0.46
	1.0	20.86	0.46
n=15	0.1	12.9	0.35
	0.2	17.1	0.37
	0.4	21.9	0.37
	0.6	27.6	0.48
	0.8	29.3	0.50
	1.0	32.5	0.49
n=20	0.1	9.10	0.35
	0.2	11.00	0.37
	0.4	13.51	0.38
	0.6	16.32	0.45
	0.8	17.80	0.48
	1.0	19.12	0.48
n=25	0.1	6.27	0.42
	0.2	5.90	0.37
	0.4	5.51	0.38
	0.6	5.33	0.39
	0.8	5.21	0.37
	1.0	5.12	0.38

The transfer coefficient is larger than in other electrolytes and approaches the theoretical value of 0.5 for a reversible reaction for $n \leq 20$ in 1.0 M electrolyte. It shows no variation as n is varied from 5 to 20. For n = 25 the transfer coefficient decreases from 0.42 in 0.1 M electrolyte to 0.38 in 1.0 M electrolyte.

Section 4.7 Temperature Effects on Heterogeneous Electron Transfer Reactions

Section 4.7.1 General

Temperature effects on k^o have been examined to evaluate enthalpic and entropic parameters for the heterogeneous electron transfer reaction. This has been accomplished within the theoretical framework of section 1.4 and the methodology described in section 3.4 [40-43].

Section 4.7.2 Hydrochloric acid.

The effect of increased redox site loading in 0.1 M HCl is to linearly decrease both $(\Delta H_{\neq}^{o})_{real}$ and $(\Delta S_{\neq}^{o})_{real}$ (see Table 4.7.2.1). In 1.0 M HCl the reverse trend is observed with both entropy and enthalpy terms increasing linearly with increasing redox site loading. Except for the 1:5 loading the enthalpy terms are larger, while the absolute value of the entropy terms are smaller in 1.0 M HCl than 0.1 M HCl. The temperature dependence of the formal potential for the Os(II/III) oxidation, is similar in both 0.1 and 1.0 M HCl for all loadings and yields a value of 19 ± 2.4 $JMol^{-1}K^{-1}$ for ΔS_{rc}^{o}. This behaviour is illustrated in Figure 4.7.2.1 and is typical of the response observed in all electrolytes.

Table 4.7.2.1 Thermodynamic Parameters for the Heterogeneous Electron Transfer Reaction of the Os(II/III) Couple in $[Os(bipy)_2(PVP)_nCl]Cl$ polymers in HCl.

Loading	$(\Delta H_{\neq}^{\circ})_{real}$ $kJMol^{-1}$	$(\Delta S_{\neq}^{\circ})_{real}$ $JMol^{-1}K^{-1}$	ΔS_{rc}° $JMol^{-1}K^{-1}$	$(\Delta H_{\neq}^{\circ})_{ideal}$ $kJmol^{-1}$	$(\Delta S_{\neq}^{\circ})_{ideal}$ $JMol^{-1}K^{-1}$
n=5					
0.1M	23	-63.6	18.2	23.8	-60.2
1.0M	21.6	-68.6	18.5	23.6	-62.2
n=10					
0.1M	18.2	-82	19.3	19.2	-78.7
1.0M	32.3	-28.6	20.7	34.6	-20.9
n=15					
0.1M	16.4	-86.0	17.1	16.9	-84.3
1.0M	36.5	-14.2	18.3	37.8	-9.8
n=20					
0.1M	15.7	-88.1	19.6	16.6	-84.9
1.0M	38.2	-8.3	19.3	39.6	-3.5
n=25					
0.1M	15.2	-90.1	17.9	15.9	-87.6
1.0M	40.3	-2.9	21.5	41.8	2.3

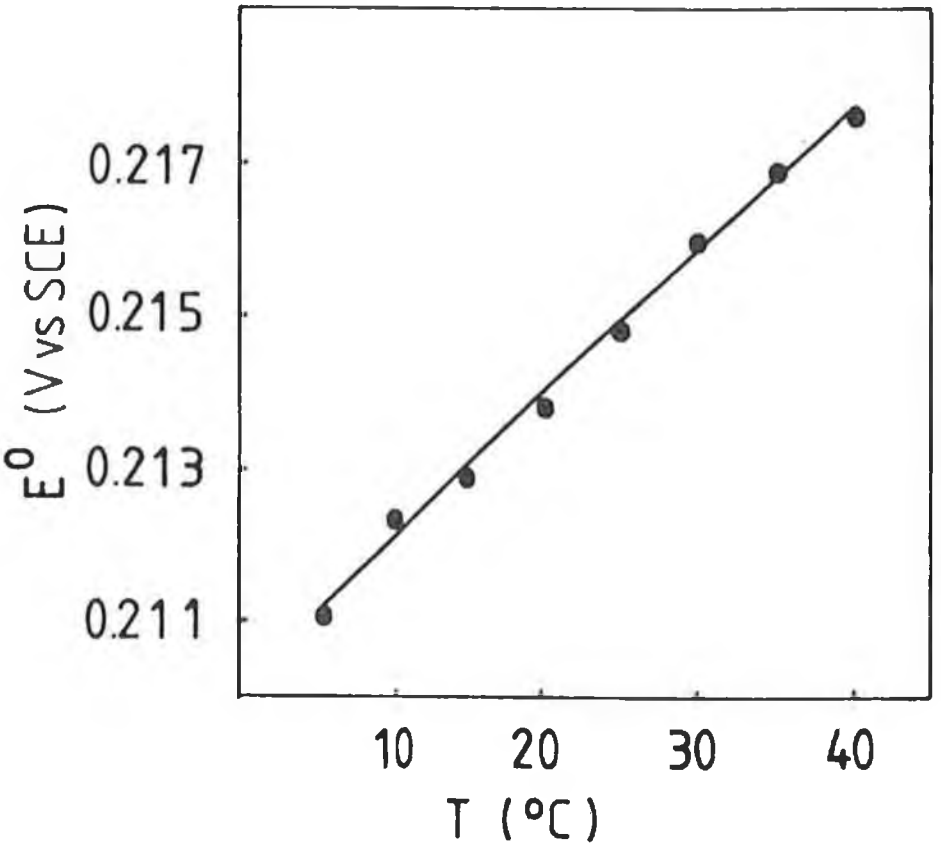

Figure 4.7.2.1 Temperature dependence of the formal potentials of the Os(II/III) oxidation within $[Os(bipy)_2(PVP)_{10}Cl]Cl$ films, as determined by cyclic voltammetry. Supporting electrolyte 0.1 M HCl. Surface coverage 2.3 x 10^{-8} molcm^{-2}.

Section 4.7.3 Perchloric acid.

In perchloric acid, unlike hydrochloric and sulphuric acid (vide infra), the effect of redox site loading on the enthalpy and entropy terms is similar in both 0.1 and 1.0 M electrolyte. As the redox site loading is increased $(\Delta H_{\neq}^{o})_{real}$ increases in a linear manner. An increase in redox site loading also increases $(\Delta S_{\neq}^{o})_{real}$ linearly, changing from negative entropy terms at low redox site loading to positive terms at the high loadings. The 1:15 loading shows dual slope behaviour, which to our best knowledge has not been previously reported. This is considered to be related to the dual slope behaviour observed previously for homogeneous charge transport. The reaction entropy term again shows little variation with either active site loading or electrolyte concentration with a value of 19.2 $\pm$ 2.1 $JMol^{-1}K^{-1}$, except for the 1:10 loading where it is reduced to 16.5 $JMol^{-1}K^{-1}$ for temperatures below 285 K.

Section 4.7.4 Sulphuric acid.

The variation of log k^{o} with T^{-1} in 0.1 M sulphuric acid is illustrated in Figure 4.7.4.1. In this electrolyte concentration the enthalpy and entropy of activation for heterogeneous electron transfer become more positive and less negative respectively with increasing osmium loading. In 1.0 M electrolyte this behaviour is reversed. The reaction entropy is largely unaffected by redox site loading maintaining a value of 19.5$\pm$0.7 $JMol^{-1}K^{-1}$.

Table 4.7.3.1 Thermodynamic Parameters for the Heterogeneous Electron Transfer Reaction of the Os(II/III) Couple in $[Os(bipy)_2(PVP)_nCl]Cl$ polymers in $HClO_4$

Loading		$(\Delta H_{\neq}^{o})_{real}$ $kJMol^{-1}$	$(\Delta S_{\neq}^{o})_{real}$ $JMol^{-1}K^{-1}$	ΔS_{rc}^{o} $JMol^{-1}K^{-1}$	$(\Delta H_{\neq}^{o})_{ideal}$ $kJMol^{-1}$	$(\Delta S_{\neq}^{o})_{ideal}$ $JMol^{-1}K^{-1}$
n=5						
0.1M		68.8	96.2	17.1	70.3	101.3
1.0M		52.8	30.4	19.3	54.6	36.6
n=10						
0.1M		52.1	24.8	21.3	52.9	27.8
1.0M		40.9	-11.8	20.6	42.4	-6.9
n=15						
0.1M	T<285K	10.3	-113.3	16.5	11.2	-110.4
	T>285K	50.2	20.4	21.0	51.1	23.4
1.0M		36.1	-25.9	17.3	36.8	-23.5
n=20						
0.1M		43.1	0.6	19.3	43.9	3.3
1.0M		34.1	-31.7	19.8	35.2	-28.1
n=25						
0.1M		38.4	-15.0	19.2	39.0	-12.9
1.0M		32.9	-35.2	18.6	33.7	-32.5

Table 4.7.4.1 Thermodynamic Parameters for the Heterogeneous Electron Transfer Reaction of the Os(II/III) Couple in $[Os(bipy)_2(PVP)_nCl]Cl$ polymers in H_2SO_4

Loading	$(\Delta H_{\neq}^{o})_{real}$ $kJMol^{-1}$	$(\Delta S_{\neq}^{o})_{real}$ $JMol^{-1}K^{-1}$	ΔS_{rc}^{o} $JMol^{-1}K^{-1}$	$(\Delta H_{\neq}^{o})_{ideal}$ $kJMol^{-1}$	$(\Delta S_{\neq}^{o})_{ideal}$ $JMol^{-1}K^{-1}$
n=5					
0.1M	40.2	-8.8	20.1	42.1	-2.5
1.0M	22.3	-66.9	17.9	24.9	-58.1
n=10					
0.1M	25.1	-54.8	19.2	26.9	-48.6
1.0M	33.6	-27.1	20.2	36.4	-17.8
n=15					
0.1M	20.1	-71.3	21.0	22.3	-63.9
1.0M	37.5	-13.0	18.6	40.2	-3.9
n=20					
0.1M	17.5	-79.5	20.1	19.7	-72.3
1.0M	39.2	-8.0	20.1	41.9	11.1
n=25					
0.1M	16.3	-82.4	18.5	18.6	-74.6
1.0M	41.0	-1.2	19.5	43.5	7.0

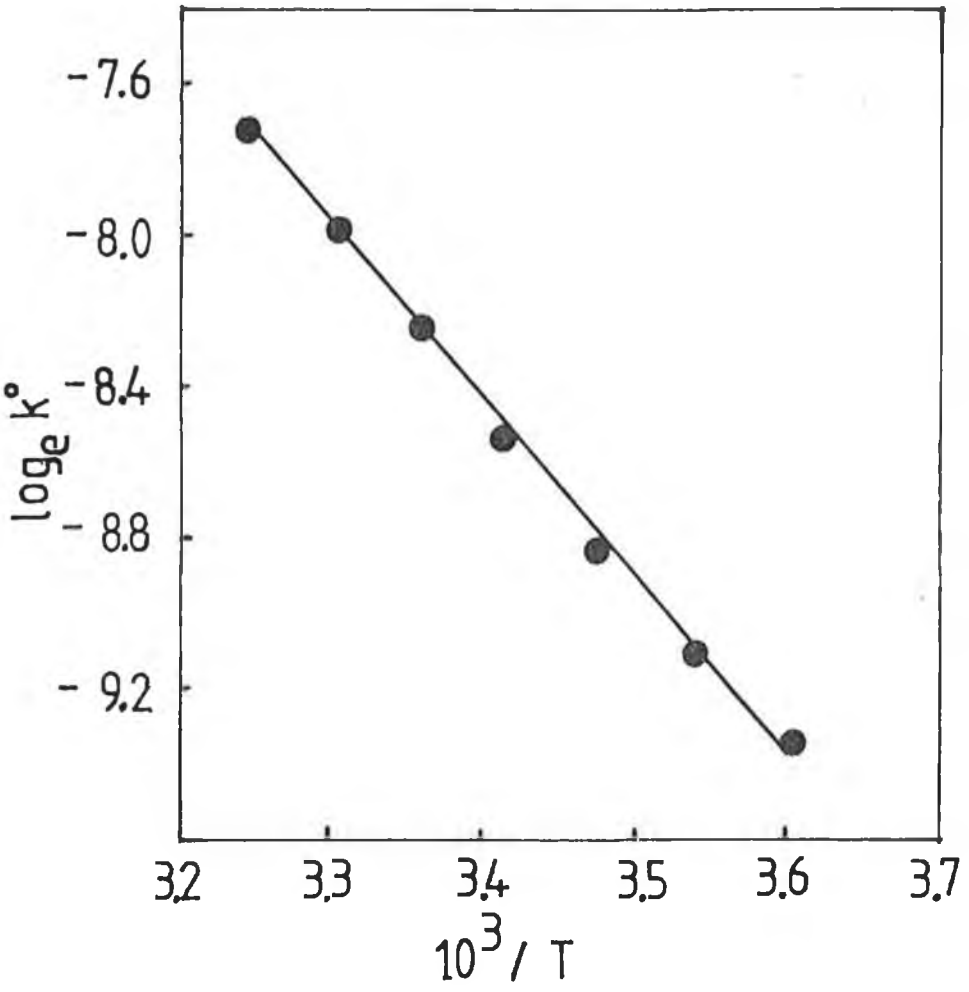

Figure 4.7.4.1 Temperature dependence of k^o for $[Os(bipy)_2(PVP)_{10}Cl]Cl$ modified electrodes. Electrolyte 0.1 M H_2SO_4. Surface coverage 2 x 10^{-8} molcm^{-2}.

Section 4.8 Discussion of Heterogeneous Kinetics.

The results obtained show that for $[Os(bipy)_2(PVP)_nCl]Cl$ modified electrodes the heterogeneous kinetics are influenced by both redox site loading and the nature of the electrolyte solution. For all electrolytes and redox sites loadings k^o is typically an order of magnitude less than values obtained for electroactive species in solution [44]. Such behaviour has been previously reported for several other systems. Partial blocking of the electrode surface by the modifying film, as the explanation of the reduced k^o, has been considered by Saveant and co-workers [48,49]. k^o for a modified electrode is considered to be the product of $(1-\theta)$ and k^o for heterogeneous electron transfer at the active sites, where θ is the surface coverage of active sites. Since the polymer backbone is, for the osmium containing polymer films described here, nonconducting, heterogeneous electron transfer can only occur between the electrode material and the osmium centre. As the redox site concentration is increased the intersite separation decreases and so the number of sites at which heterogeneous electron transfer can take place should be increased, thus increasing k^o. However, k^o only increases with increasing redox site loading up to n = 10 or n = 15 depending on the electrolyte concentration. This suggests that the Saveant model cannot fully explain the results obtained in this work. Uncompensated resistance can also cause reduced values of k^o to be observed [50-52]. However, in this contribution uncompensated resistance was routinely compensated for using positive feedback circuitry. The residual uncompensated resistance is estimated to cause at most a 12 - 15% error on k^o.

The effect of redox site loading and electrolyte concentration on k^o closely follows that observed previously for D_{CT} as measured by potential

step. Figure 4.8.1 shows the correlation of log k^o and log $D_{CT}(PS)$. This plot suggests that the effect of changing the redox site and electrolyte concentration, similarly affects both the rate determining processes of the heterogeneous electron-transfer reaction and the homogeneous charge transport diffusion process occurring within the film [53]. This interpretation is supported by the thermodynamic data.

In 0.1 M electrolytes except for the 1:15 loading in 0.1 M $HClO_4$ both $(\Delta H_{\ddagger}^{o})_{real}$ and $(\Delta S_{\ddagger}^{o})_{real}$ increase as the redox site loading is increased, the enthalpy becoming more positive and the entropy becoming less negative (see Tables 4.7.2.1 - 4.7.4.1). For the 1:15 loading in 0.1 M $HClO_4$ a dual slope behaviour is observed. Below 285 K both the enthalpy and entropy terms are less than those values observed for the other electrolytes, while above this temperature the enthalpy and entropy terms become more positive and follow the same trend observed for the other 0.1 M electrolytes. In 1.0 M $HClO_4$ both $(\Delta H_{\ddagger}^{o})_{real}$ and $(\Delta S_{\ddagger}^{o})_{real}$ show similar increases to those observed in 0.1 M electrolytes. However, in both 1.0 M HCl and 1.0 M H_2SO_4 the trend is reversed with both the enthalpy and entropy terms decreasing with increasing redox site loading. This behaviour appears to be related to the homogeneous charge transport behaviour discussed previously. In 0.1 M electrolytes the homogeneous charge transport rate ($D_{CT}(PS)$) was insensitive to redox site loadings showed low activation energies coupled to negative entropy terms. This suggested an ion transport limitation for all loadings, which became more apparent at the highest loadings. The fact that the homogeneous and heterogeneous entropy terms are both negative suggests that both processes are associated with the availability of charge compensating counterion within the film. The homogeneous charge

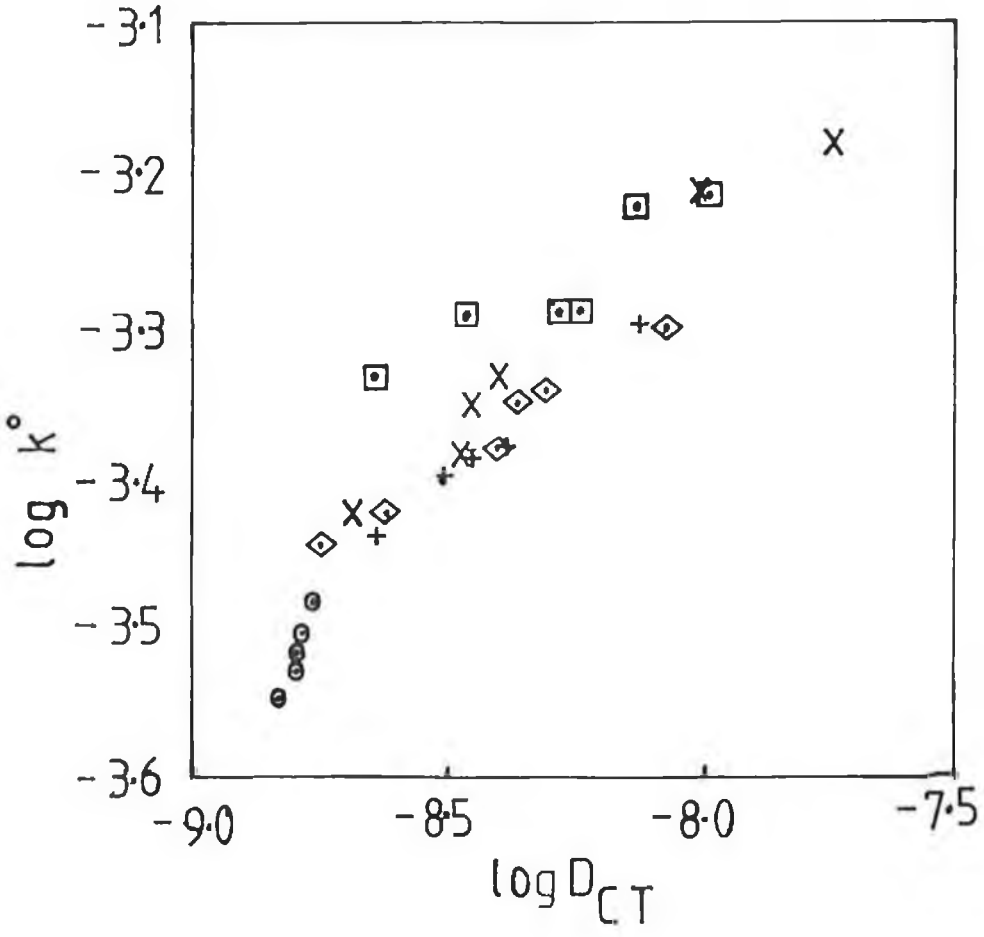

Figure 4.8.1 Correlation of k^0 and $D_{CT}(PS)$ for $[Os(bipy)_2(PVP)_nCl]Cl$ modified electrodes. The supporting electrolyte concentrations are 0.1, 0.2, 0.4, 0.6, 0.8 and 1.0 M HCl. ⊙ n = 5, × n = 10, ⊡ n = 15, ◇ n = 20 and + n = 25.

transport results suggested, that in 1.0 M sulphuric and hydrochloric acids the limitation of ion transport dictated by Donnan exclusion [28,54] was removed for all loadings except 1:5. This breakdown of Donnan exclusion causes in an influx of ions into the film resulting in the rapid establishment of equilibrium and a rapid charge transport rate. This process of ion influx occurring at high electrolyte concentrations is also observed for the heterogeneous kinetics. The entropy and enthalpy terms of heterogeneous electron transfer become less positive with increased redox site loading for 1.0 M HCl and H_2SO_4 because the ion influx affects the formation of the double layer. The fact that in perchloric acid the effect of redox site loading is similar in both 0.1 and 1.0 M electrolyte indicates that the double layer formation is similar. This suggests that the films are compact and that the ion population within the film is similar in 0.1 and 1.0 M perchloric acid, which is in agreement with the homogeneous charge transport results.

As observed in other systems $(\Delta H_{\neq}^{o})_{real}$ and $(\Delta S_{\neq}^{o})_{real}$ follow a linear relation [53]. This behaviour appears significant since, despite the differing trends observed in 1.0 M electrolytes, the values obtained from all electrolytes lie on a single line as illustrated in Figure 4.8.2. This observation suggests that a single process namely ion movement dictates the behaviour observed.

The reaction entropy (ΔS_{rc}^{o}) is considered to be sensitive to changes in the solvent polarisation required to allow electron transfer [55,56]. However, for all electrolytes examined here, a positive reaction entropy term of similar magnitude for all redox site loadings was obtained. Such positive entropy terms have been previously reported [57] and attributed to more extensive solvent ordering in the oxidised state. For the present case

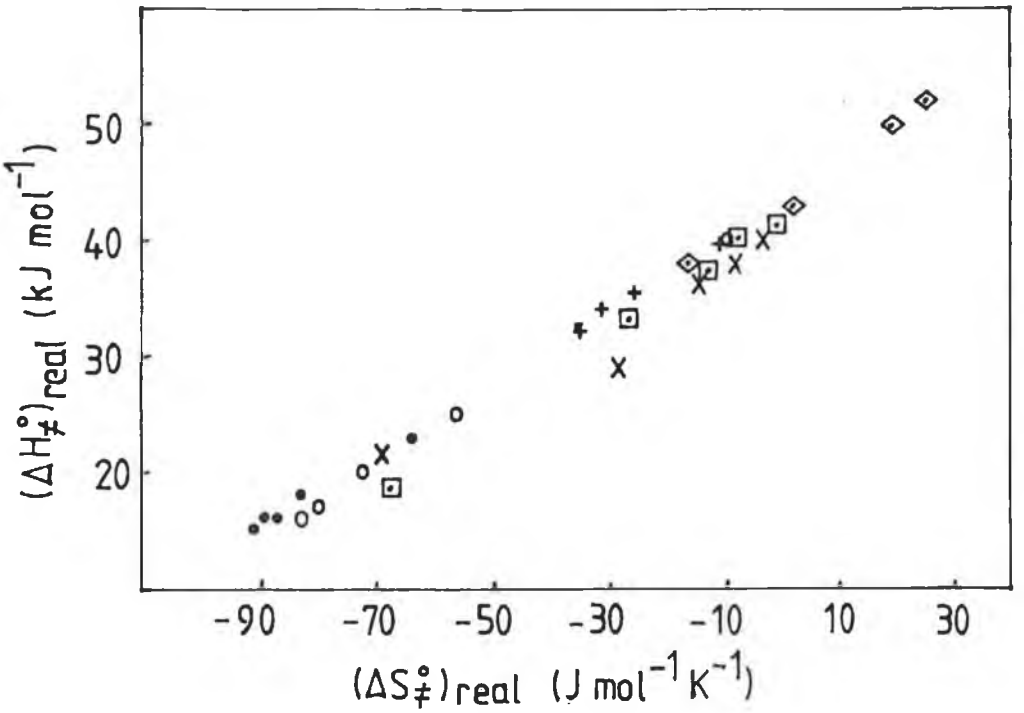

Figure 4.8.2 Correlation of $(\Delta H_{\neq}^{o})_{real}$ and $(\Delta S_{\neq}^{o})_{real}$ for the heterogeneous electron transfer reaction of Os(II/III) within $[Os(bipy)_2(PVP)_nCl]Cl$ modified electrodes. ● 0.1 M HCl, × 1.0 M HCl, ◈ 0.1 M $HClO_4$, + 1.0 M $HClO_4$, o 0.1 M H_2SO_4 and ⊡ 1.0 M H_2SO_4.

we suggest that increased polarisation of water molecules adjacent to the aromatic rings of the osmium complex occurs in the higher oxidation state. The values obtained for the reaction entropy and the fact that they are relatively constant is in qualitative agreement with the Born model discussed above. The Born model gives a value of 27 $JMol^{-1}K^{-1}$ for (ΔS_{rc}^{o}) where a_{ox} = a_{red} = 7.5 A (Section 1.4.2, Equation 18). The fact that the reaction entropy remains constant when the electrolyte is changed or the redox site loading increased suggests that the local chemical microenvironment of the osmium centre remains largely unchanged as the redox site loading is varied. It also appears, that the increased influx of charge compensating which accompanies the breakdown of Donnan exclusion does not significantly alter the solvation of the redox centre. This emphasises the importance of considering not only the redox properties of the electroactive centre, but also the physicochemical properties of the polymeric matrix. The observation that k^{o} and $D_{CT}(PS)$ are sensitive to both redox site and electrolyte concentration while (ΔS_{rc}^{o}) is not, suggests that it is largely changes in the polymer phase which are responsible for the ion availability within the film and hence, the observed variations of k^{o}.

The transfer coefficient for a model monomeric compound ($[Os(bipy)_2PicCl]PF_6$, where Pic = 4-Picoline) at a bare electrode is 0.5±0.08. This value is similar to those obtained for the modified electrodes in high concentrations of sulphuric acid again suggesting, as discussed in the case of homogeneous charge transport, a film in which charge compensating counterion is freely available. It is important to note that where low transfer coefficients are observed e.g in perchloric acid the sum of α_a and α_c is still close to unity. This suggests that Butler-Volmer kinetics operate even in high redox site loading/low electrolyte concentration

combinations. Given that the transfer coefficient can yield information as to the position of the reaction site with respect to the outer Helmholtz plane, the similarity of the transfer coefficient in sulphuric acid for the solution and polymer confined species tends to suggest that the position of the reacting transition state with respect to the electrode is similar in both cases. In general the point of electron exchange is considered to be at this outer Helmholtz plane, therefore the heterogeneous electron exchange occurs over several angstroms and the double layer is formed at the electrode/film interface not at the film electrolyte interface.

Section 4.9 Concluding Remarks.

The stability and ideality of the materials reported here are important properties for practical applications. The results show that a complete understanding of charge transport through these materials is possible only by a systematic variation of both the active site and the electrolyte concentration. The incorporation of these redox active centres, particularly at low loadings gives a method of examining internal polymer structure as a function of the contacting solution, information which is difficult to obtain by any other means.

The use of electrochemical techniques which operate on different timescales, allows the nature of the equilibria present to be assessed. The data obtained suggest that total equilibrium of all mobile species (electrons, ions and polymer chains) occurs only at longer times and that conventional short timescale chronoamperometry may lead to the establishment of only redox or electronic equilibrium. The origin of these kinetic barriers stems mainly from the physicochemical properties of the polymer phase. In sulphuric acid, an electrolyte which is expected to protonate the uncoordinated pyridine units of the polymer backbone, hence inducing film swelling, the difference between D_{CT}(PS) and D_{CT}(CV) is minimal. This in conjunction with the thermodynamic data suggests that rapid equilibrium can be established in this electrolyte. It is not unrealistic to assume that the nature of the equilibrium established can be time dependent. In the potential step methods the Cottrell equation is valid for only a percentage of the total film thickness, typically 40-60%, while in the cyclic voltammetry experiment considerably more of the total film thickness will undergo a redox reaction. This means that where there are kinetic barriers to ion movement, for example by Donnan exclusion, equilibrium

may not be established in the time domain of the potential step measurements. For the cyclic voltammetry experiment counterion movement will be required both within the film and across the film/electrolyte interface, but the longer timescale will allow thermodynamic equilibrium to be established. The suggestion that charge can be propagated at a rate, which is independent of, and larger than, that resulting in total equilibrium is of considerable significance, since it has previously been assumed in the literature that electron and mass transfer processes cannot be decoupled.

The effect of electrolyte type and concentration is typically to influence directly the ion availability within the film as dictated by Donnan exclusion. However, the electrolyte solution also alters the film swelling and consequentially the ease of ion and polymer chain movement. Electron self exchange as the rate determining step is not observed for this system. At the highest redox site loading where electron self exchange would be most favoured, charge compensating counterion motion is always observed as the rate limiting step. An increase in the intersite separation causes either ion or polymer chain motion to control D_{CT}.

k^o increases with increasing redox site loading only for low loadings, typically up to 1:10. The decrease observed for the 1:5 loading for all electrolytes suggests, that models in which the partial blocking of the electrode surface by nonconducting material, is responsible for the decreased k^o observed at modified electrodes are incomplete. The linear relation between the homogeneous charge transport rate and the rate of heterogeneous electron transfer suggest that similar processes, such as ion transport play important roles for both. The importance of ion availability in the formation of the double layer is clearly shown by the breakdown of Donnan potential which

causes an influx of charge compensating counterion resulting in an enhanced k^o in high concentrations of electrolyte. The thermodynamic data presented support this view with redox site loading having a distinctly different effect on the entropy and enthalpy terms in 0.1 and 1.0 M HCl and H_2SO_4. In perchlorate media heterogeneous electron transfer proceeds similarly in both 0.1 and 1.0 M electrolyte, suggesting, as concluded from the homogeneous charge transport data, that the films are rather compact. The dual slope behaviour for k^o for the 1:15 loading in 0.1 M perchloric acid is certainly noteworthy and is attributed to specific interaction of perchlorate anion and the PVP backbone, most likely resulting in film dehydration.

The fact that the reaction entropy remains constant as both the redox site and electrolyte concentrations are varied, indicates that the local microenvironment of the osmium(II/III) couple remains unaltered. This is a significant result since it emphasises the influence that the physicochemical properties of the polymer phase have on the observed charge transport behaviour of these modified electrodes.

Section 4.10 References.

1. R. W. Murray, Electroanalytical Chemistry; A. J. Bard, Ed.; Dekker: New York, 1983; Vol. 13, p. 191.
2. R. W. Murray, Annu. Rev. Mater. Sci. 1984, 14, 145
3. W. J. Albery and A. R. Hillman, Annu. Rep. Prog. Chem. Sect. C 1981, 377
4. L. R. Faulkner, Electrochim. Acta. 1989, 34, 1699
5. J. A. Cox and P. J. Kulesza, J. Electroanal. Chem. 1984, 175, 105
6. P. Denisevich, K. W. Willman and R. W. Murray, J. Am. Chem. Soc. 1981, 103, 4727
7. P. V. Kamat, M. A. Fox and A. J. Fatiadi, J. Am. Chem. Soc. 1984, 106, 1191
8. T. Ohsawa, K. Kaneko and K. Yoshino, Jap. J. Appl. Phys. 1984, 23, L663
9. A. R. Guadalupe, D. A. Usifer and K. T. Potts, H. C. Hurrell, A. E. Mogstad, H. D. Abruna, J. Am. Chem. Soc. 1988, 110, 3462
10. J. S. Facci, R. H. Schmehl and R. W. Murray, J. Am. Chem. Soc. 1982, 104, 4959
11. G. Inzelt, J. Backsai, J. Q. Chambers and R. W. Day, J. Electroanal. Chem. 1986, 201, 301
12. J. C. Jernigan and R. W. Murray, J. Am. Chem. Soc. 1987, 109, 1738
13. B. A. White and R. W. Murray, J. Am. Chem. Soc. 1987, 110, 2576
14. C. E. D. Chidsey and R. W. Murray, J. Phys. Chem. 1986, 90, 1479
15. P. G. Pickup, W. Kutner, C. R. Leidner and R. W. Murray, J. Am. Chem. Soc. 1984, 106, 1991

16. N. Oyama, T. Ohsaka, T. Ushirogouchi, S. Sanpei and S. Nakamura, Bull. Chem. Soc. Jpn. 1988, 61, 3103

17. R. Lange and K. Doblhofer, J. Electroanal. Chem. 1987, 237, 13

18. C. P. Andrieux and J. M. Saveant, J. Phys. Chem. 1988, 92, 6761

19. A. R. Hillman, Electrochemical Science and Technology of Polymers R. G. Linford, Ed; Elsevier Applied Science, Amsterdam, Chap. 5, Vol. 1, p. 103

20. F. G. Cottrell, Z. Physik. Chem. 1902, 42, 385

21. K. Aoki, K. Tokuda and H. Matsuda, J. Electroanal. Chem. 1983, 146, 417

22. A. Sevcik, Collect. Czech. Chem. Commun. 1948, 44, 327

23. S. M. Oh and L. R. Faulkner, J. Electroanal. Chem. 1989, 269, 77

24. P. Daum, J. R. Lenhard, D. R. Rolison and R. W. Murray, J. Am. Chem. Soc. 1980, 102, 4649

25. S. Bruckenstein, C. P. Wilde, M. Shay, A. R. Hillman and D. C. Loveday, J. Electroanal. Chem. 1989, 258, 457

26. G. Horanyi and G. Inzelt, J. Electroanal. Chem. 1988, 257, 311

27. S. Bruckenstein, A. R. Hillman and M. J. Swann, J. Electrochem. Soc., 1990, 137, 1323

28. H. Braun, W. Storck and K.Doblhofer, J. Electrochem. Soc. 1983, 130, 807

29. S. M. Oh and L. R. Faulkner, J. Am. Chem. Soc. 1989, 111, 5613

30. H. Dahms, J. Phys. Chem. 1968, 72, 362

31. I. Ruff, Electrochim. Acta, 1970, 15, 1059

32. I. Ruff and I. Koroisi-Odor, Inorg. Chem. 1970, 9, 168

33. I. Ruff and V. J. Friedrich, J. Phys. Chem. 1971, 75, 3297

34. M. E. G. Lyons, H. G. Fay, T. McCabe, J. Corish, J. G. Vos and A. J. Kelly, J. Chem. Soc., Faraday Trans. in press

35. M. E. G. Lyons, H. G. Fay, J. G. Vos and A. J. Kelly, J. Electroanal. Chem. 1988, 250, 207

36. R. J. Forster, A. J. Kelly, J. G. Vos and M. E. G. Lyons, J. Electroanal. Chem. 1989, 270, 365

37. T. Ohsaka, N. Oyama, S. Yamaguchi and H. Matsuda, Bull. Chem. Soc. Jpn. 1981, 54, 2475

38. K. J. Vetter, Electrochemical Kinetics, (Academic Press, New York and London 1987) p. 107

39. H. Matsuda, Bull. Chem. Soc. Jpn. 1980, 53, 3439

40. M. J. Weaver, J. Phys. Chem. 1976, 83, 2645

41. J. T. Hupp and M. J. Weaver, J. Electroanal. Chem. 1983, 145, 43

42. N. Sutin, M. J. Weaver and E. L. Yee, Inorg. Chem. 1980, 19, 1096

43. E. L. Yee, R. J. Cave, K. L. Guyer, P. D. Tyma and M. J. Weaver, J. Am. Chem. Soc. 1979, 101, 1131

44. S. Yamaguchi, H. Matsuda, T. Ohsaka and N. Oyama, Bull. Chem. Soc. Jpn., 1983, 56, 2952

45. T. Ohsaka, T. Okajima and N. Oyama, J. Electroanal. Chem. 1986, 215, 191

46. T. Ohsaka, S. Kunimura and N. Oyama, Electrochim. Acta. 1988, 33, 639

47. T. Ohsaka, M. Nakanishi, O. Hatozaki and N. Oyama, Electrochim. Acta. 1990, 35, 63

48. C. Amatore, J. M. Saveant and D. Tessier, J. Electroanal. Chem. 1983, 146, 37

49. C. Amatore, J. M. Saveant and D. Tessier, J. Electroanal. Chem. 1983, 147, 39

50. L. Roullier and E. Laviron, J. Electroanal. Chem. 1983, 157. 193

51. N. R. De Tacconi, A. J. Calandra and A. J. Arvia, Electrochim. Acta. 1973, 18, 571

52. T. W. Rosanski and D. H. Evans, J. Electroanal. Chem. 1976, 72, 277

53. N. Oyama, T. Ohsaka, H. Yamamoto and M. Kaneko, J. Phys. Chem. 1986, 90, 3850

54. K. Doblhofer and R. D. Armstrong, Electrochim. Acta. 1988, 33, 453

55. H. Y. Liu, J. T. Hupp and M. J. Weaver, J. Electroanal. chem. 1984, 179, 219

56. T. T. Li, K. L. Guyer, S. W. Barr and M. J. Weaver, J. Electroanal. Chem. 1984, 164, 27

57. T. Ohsaka, H. Yamamoto, N. Oyama, J. Phys. Chem. 1987, 91, 3775

CHAPTER 5

Electrolyte and Temperature Effects on Homogeneous and Heterogeneous Charge Transport Through Films of $[Os(bipy)_2(PVI)_nCl]Cl$

Section 5.1 Introduction

Polymer modified electrodes have been used to model electron transfer in biological systems and in particular to investigate the effects of electron range hopping [1,2]. The interest in polymers containing the imidazole and imidazole like units has arisen in part because many proteins contain imidazole rings in the form of L-Histidine [3]. These groups are thought to be responsible for the buffering capacity of proteins in the physiological pH range, and they also appear to be active sites for metal binding. Interest in the catalytic properties has also been generated by the occurrence of imidazole units in several hydrolytic enzymes. Indeed, many synthetic polymers based on the imidazole unit have shown properties, such as high reaction rates based on co-operative effects, saturation kinetics and selective inhibition generally associated with enzyme catalysed reactions [4-6].

In this chapter the electron transfer reactions for both homogeneous charge propagation within the film, and the heterogeneous electron transfer from the underlying electrode into the film has been examined in a variety of electrolytes over the concentration range 0.1 to 1.0 M. The loading of $[Os(bipy)_2Cl]^+$ to imidazole units within the film has been varied from 1:5 to 1:25. As well as this, the effect of temperature and experimental timescale has been considered. The gives useful information as to the effect of electron transfer distance on the charge transport rate and the nature of the rate limiting step, as well as, allowing fundamental parameters to be evaluated and the modified electrodes response to be optimised.

Data for charge transport through thin films of poly(4-vinylpyridine) containing the $[Os(bipy)_2Cl]^+$ redox centre was presented in chapter 4 and this clearly showed that factors such as the nature of the supporting

electrolyte, its concentration, and the redox site loading clearly influenced the electrochemical properties of the modified electrodes.
Poly(N-vinylimidazole) is an essentially monofunctional polybase with a pK_a of between 3.2 in chloride media and 4.2 in p-Toluene-sulphonate [7]. In this chapter the effect of electrolytes whose pH is above and below this pK_a on both the homogeneous charge transport and heterogeneous electron transfer processes of electrodes modified with osmium containing poly(N-vinylimidazole) is investigated.

Section 5.2 Experimental

Materials. $[Os(bipy)_2(PVI)_nCl]Cl$ polymers, where n = 5, 10, 15, 20 and 25 were prepared as described previously in chapter 2.

Apparatus and procedures. Electrochemical measurements were performed using an E. G. & G. Model 273 potentiostat/ galvanostat as described in chapter 3.

Surface coverages were estimated by graphical integration of the background corrected slow sweep rate cyclic voltammograms (1 mV/s), and were typically 2 - 4 x 10^{-8} molcm^{-2}. The quantity of osmium immobilised on the electrode surface was kept constant as the loading was varied. This means that the layer thickness for the 1:25 loading is approximately 3.5 times greater than the 1:5 loading. However, the same results within experimental error are obtained for homogeneous charge transport when layer thickness is kept constant. Where the layer thickness is varied more extremely D_{CT} typically decreases with increasing film thickness (see chapter 3 for further discussion of layer thickness effects). The advantage of keeping the quantity of osmium

on the electrode constant is that a high Faradaic to capacitive current ratio is maintained where the electrolyte, redox site concentrations and temperature are low. Layer thickness was estimated from the individual densities of the dry metallopolymers as measured by flotation in non swelling solvents, namely petroleum ether and dichloromethane; n = 25, 0.918 g/cm^3; n = 20, 0.817 g/cm^3; n = 15, 0.811 g/cm^3; n = 10, 0.905 g/cm^3 and n = 5 1.032 g/cm^3. These gave a value for the maximum concentration of osmium centres within the film as follows n = 25, 0.35 M; n = 20, 0.37 M; n = 15, 0.45 M; n = 10, 0.65 M and n = 5, 1.05 M. These values have been used to calculate D_{CT} from the experimentally determined $D_{CT}{}^{1/2}C$.

In studies where the electrolyte concentration was varied, all the experiments were carried out with fresh coatings. This avoids possible problems from "memory effects" where the rate of charge transport through a film would be dependent on the electrolytes to which the electrode had previously been exposed. The values for the diffusion coefficients, and activation parameters are reproducible to within $\pm$ 2% on a single coating and to $\pm$ 9% between coatings.

Section 5.3 Results: The Effect of Electrolyte and Active Site Concentration on the Rate of Homogeneous Charge Transport.

Section 5.3.1 General:

Glassy carbon electrodes modified with $[Os(bipy)_2(PVI)_nCl]Cl$ polymers are stable to photolysis in both aqueous and non aqueous media unlike the previously reported ruthenium analogues [8]. The slow sweep rate linear sweep voltammetry behaviour for $[Os(bipy)_2(PVI)_5Cl]Cl$ in 0.1 M H_2SO_4 is shown in Figure 5.3.1.1. This cyclic voltammogram is typical of a

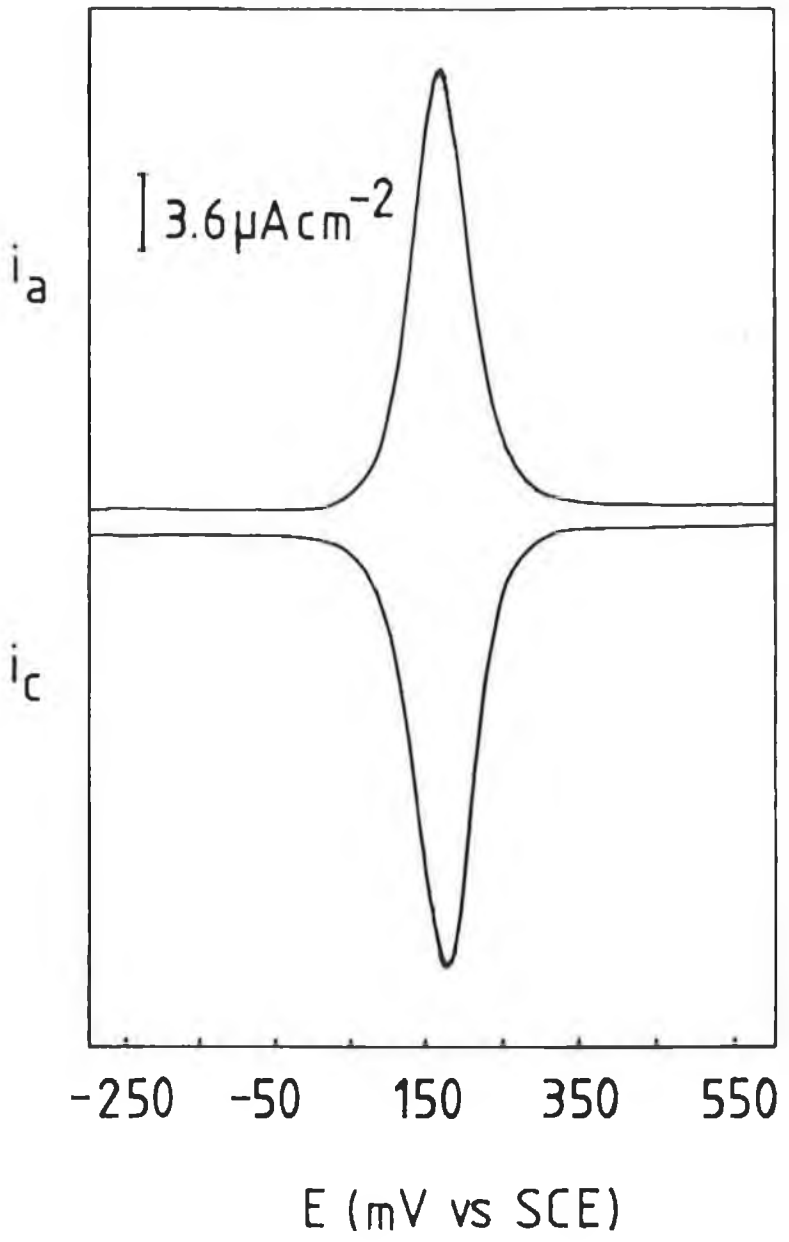

Figure 5.3.1.1 Linear sweep voltammogram for $[Os(bipy)_2(PVI)_5Cl]Cl$ modified electrodes in 0.1 M H_2SO_4. Sweep rate 1 mV/s.

reversible, single electron redox reaction of a surface bound species where significant interaction between the redox centres is absent [9]. Such a response is observed for all loadings and electrolytes except perchloric acid and lithium perchlorate where there is tendency for an equilibrium response to occur only at sweep rates lower than 1 mV/s. This results in the anodic and cathodic branches of the cyclic voltammogram failing to converge, in such situations E^0 is taken as the midpoint of the anodic and cathodic branches of the slow sweep rate cyclic voltammogram. A typical example of this behaviour is given for $[Os(bipy)_2(PVI)_5Cl]Cl$ in 0.1 M perchloric acid in Figure 5.3.1.2. For sweep rates of 100 mV/s or greater, linear sweep voltammograms show apparent semi-infinite diffusion behaviour as discussed in section 1.3.1. The charge passed during a potential sweep in the potential region of the redox couple, recorded at 1 mV/s, is between 95 and 105% of that anticipated from the amount of material placed on the electrode surface.

Section 5.3.2 Hydrochloric Acid

The effect of increased hydrochloric acid concentration and redox site loading on $D_{CT}(PS)$ is given in Table 5.3.2.1. $D_{CT}(PS)$ increases moderately with increasing supporting electrolyte concentration. This increase is typically quasi-linear with no sharp rises occurring between different HCl concentrations. As the redox site loading is increased $D_{CT}(PS)$ decreases, e.g in 0.1 M hydrochloric acid $D_{CT}(PS)$ decreases from 1.50×10^{-9} to 0.5×10^{-9} cm^2s^{-1} as the redox loading is increased from 1:25 to 1:5.

In certain systems $D_{CT}(CV)$ is comparable to $D_{CT}(PS)$ e.g for n = 15 in 1.0 M hydrochloric acid $D_{CT}(PS)$ is $1.62 \pm 0.14 \times 10^{-9}$ cm^2s^{-1} while

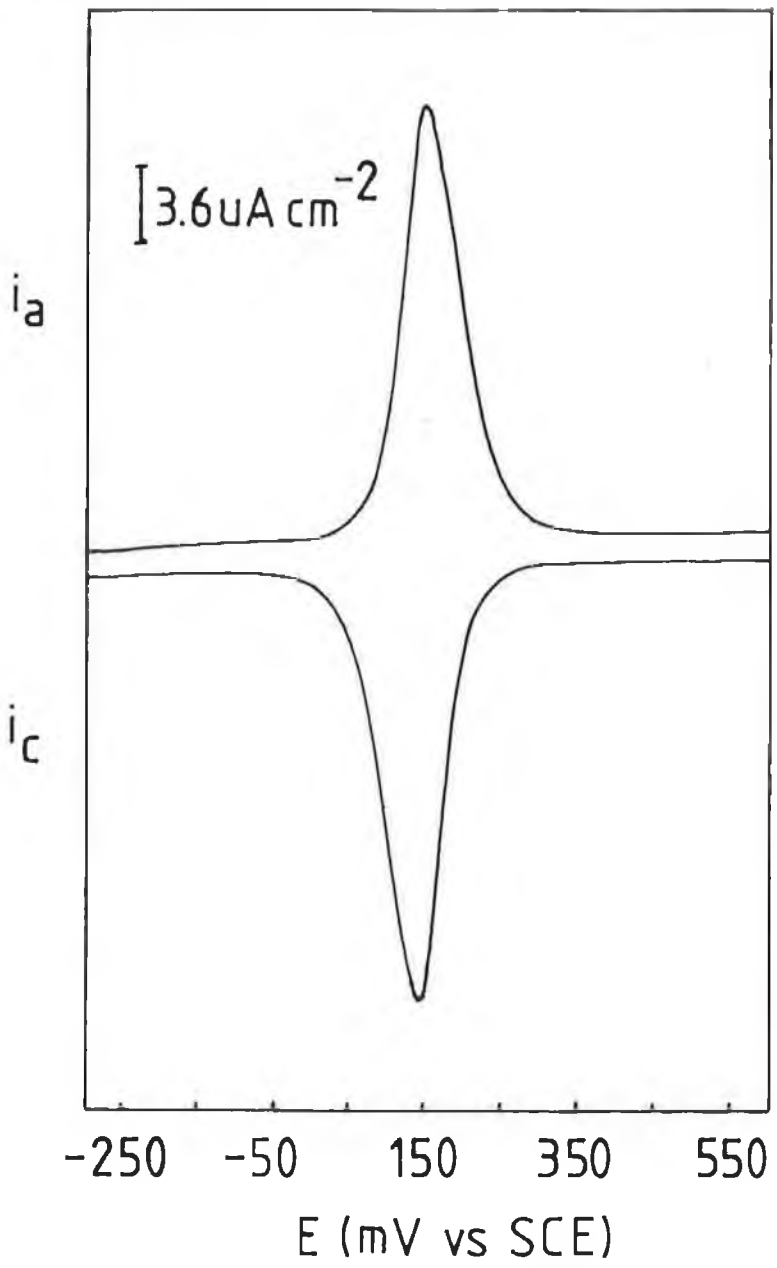

Figure 5.3.1.2 Linear sweep voltammogram for $[Os(bipy)_2(PVI)_5Cl]Cl$ modified electrodes in 0.1 M $HClO_4$. Sweep rate 1 mV/s.

Table 5.3.2.1 The effect of concentration of hydrochloric acid supporting electrolyte and redox site loading on charge transport parameters of $[Os(bipy)_2(PVI)_nCl]Cl$ modified electrodes.

Loading	Conc. M	D_{CT}(PS) $*10^9$ cm^2s^{-1}	D_{CT}(CV) $*10^{10}$ cm^2s^{-1}	E^o V
n=5	0.1	0.46	2.25	0.190
	0.2	0.61	2.25	0.185
	0.4	0.69	2.81	0.195
	0.6	0.83	3.12	0.155
	0.8	1.02	3.85	0.125
	1.0	1.15	4.14	0.130
n=10	0.1	0.75	2.30	0.165
	0.2	0.87	3.01	0.170
	0.4	1.05	5.20	0.180
	0.6	1.14	5.73	0.180
	0.8	1.14	7.92	0.175
	1.0	1.23	9.65	0.175
n=15	0.1	1.03	2.60	0.150
	0.2	1.11	3.45	0.140
	0.4	1.21	5.78	0.145
	0.6	1.38	6.53	0.140
	0.8	1.48	9.53	0.145
	1.0	1.62	11.02	0.150
n=20	0.1	1.26	2.91	0.150
	0.2	1.34	3.49	0.150
	0.4	1.46	5.83	0.145
	0.6	1.65	6.50	0.145
	0.8	1.88	8.78	0.140
	1.0	2.04	9.61	0.140
n=25	0.1	1.50	3.17	0.145
	0.2	1.62	3.54	0.140
	0.4	1.78	6.13	0.140
	0.6	1.91	6.48	0.140
	0.8	2.11	7.09	0.140
	1.0	2.27	7.97	0.140

D_{CT}(CV) is 1.02±0.08 x 10^{-9} cm^2s^{-1}. D_{CT}(CV) increases considerably with increasing HCl concentration where $10 \leq n \leq 25$, while for n = 5 D_{CT}(CV) is relatively less sensitive to electrolyte concentration. It is only in 0.8 M and 1.0 M hydrochloric acid that D_{CT}(CV) increases as the osmium to imidazole ratio is increased from 1:25 to 1:15, in all other electrolyte concentrations and redox site loadings D_{CT}(CV) decreases.

The formal potential of the Os(II/III) oxidation remains constant for a given loading as the HCl concentration is increased, with the exception of n = 5, where E^o decreases sharply between 0.4 and 0.6 M.

Section 5.3.3 Sodium Chloride

The effect of NaCl concentration on both D_{CT}(PS) and D_{CT}(CV) is given in Table 5.3.3.1. The rates of charge transport using sodium chloride as supporting electrolyte are comparable and indeed higher to those observed in hydrochloric acid. For all the loadings examined both D_{CT}(PS) and D_{CT}(CV) increase as the concentration of sodium chloride increases, with a significant increase in the charge propagation rate being observed for all loadings between 0.1 and 0.2 M electrolyte. This behaviour is illustrated in Figure 5.3.3.1. The effect of osmium loading on D_{CT}(PS) is distinctly different in 0.1 M sodium chloride to that observed at higher concentrations. D_{CT}(PS) decreases linearly with increased redox site loading from a value of 1.5 x 10^{-9} to 0.33 x 10^{-9} cm^2s^{-1} as the osmium loading is increased from 1:25 to 1:5. For concentrations of sodium chloride of 0.2 M, or greater, an increased osmium content initially increases D_{CT}(PS) before decreasing at the 1:5 loading.

D_{CT}(CV) is significantly lower than D_{CT}(PS), e.g for $[Os(bipy)_2(PVI)_{10}Cl]Cl$ in 1.0 M sodium chloride D_{CT}(PS) is 3.58 x 10^{-9}

Table 5.3.3.1 The effect of concentration of sodium chloride supporting electrolyte and redox site loading on charge transport parameters of $[Os(bipy)_2(PVI)_nCl]Cl$ modified electrodes.

Loading	Conc. M	D_{CT}(PS) $*10^9$ cm^2s^{-1}	D_{CT}(CV) $*10^{10}$ cm^2s^{-1}	E^o V
n=5	0.1	0.33	0.24	0.195
	0.2	1.15	0.24	0.190
	0.4	1.28	1.49	0.155
	0.6	1.63	1.72	0.150
	0.8	1.91	2.04	0.150
	1.0	2.56	2.31	0.150
n=10	0.1	1.01	3.46	0.175
	0.2	2.91	3.76	0.175
	0.4	3.01	4.29	0.175
	0.6	3.23	5.02	0.175
	0.8	3.29	5.50	0.160
	1.0	3.58	6.10	0.160
n=15	0.1	1.20	2.76	0.165
	0.2	2.31	3.11	0.155
	0.4	2.44	3.52	0.160
	0.6	2.67	4.09	0.155
	0.8	2.91	4.80	0.155
	1.0	3.41	5.09	0.155
n=20	0.1	1.34	2.45	0.170
	0.2	1.92	2.78	0.170
	0.4	2.20	3.39	0.165
	0.6	2.39	3.95	0.155
	0.8	2.81	4.67	0.160
	1.0	3.21	5.00	0.155
n=25	0.1	1.50	1.92	0.165
	0.2	1.62	2.41	0.165
	0.4	1.85	3.25	0.150
	0.6	2.07	3.86	0.150
	0.8	2.68	4.51	0.150
	1.0	3.21	4.93	0.150

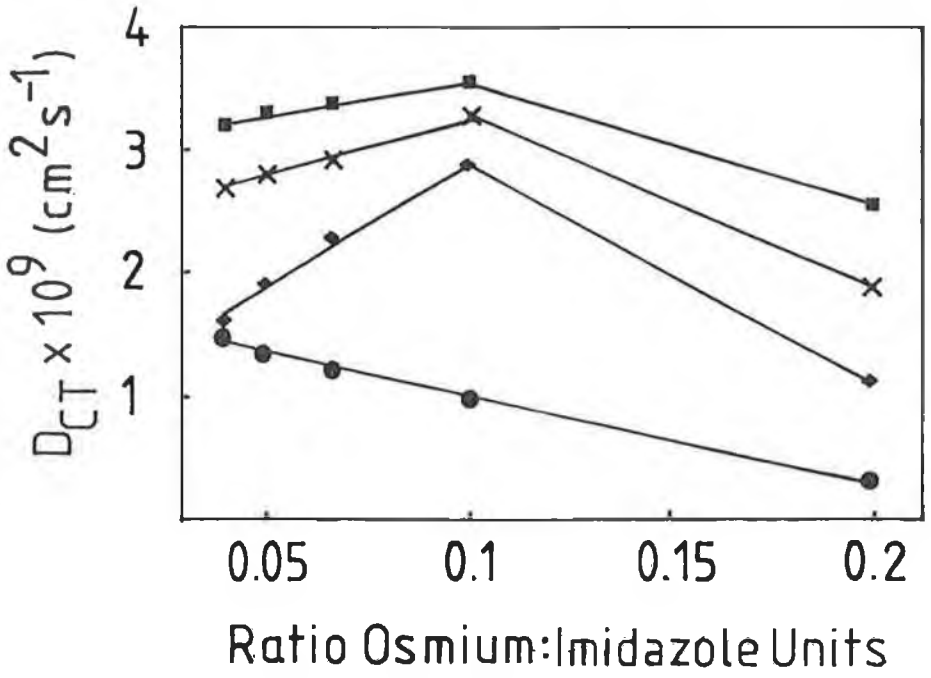

Figure 5.3.3.1 The effect of redox site concentration and NaCl concentration on $D_{CT}(PS)$ for $[Os(bipy)_2(PVI)_nCl]Cl$ modified electrodes. The electrolyte concentrations are, from top to bottom, 1.0 M, 0.8 M, 0.2 M and 0.1 M.

cm^2s^{-1} while $D_{CT}(CV)$ is 6.1 x 10^{-10} cm^2s^{-1} (Table 5.3.3.1). As the sodium chloride concentration is increased $D_{CT}(CV)$ increases approximately linearly for all loadings. An increase in redox site loading from 1:25 results in an increased $D_{CT}(CV)$ up to 1:10 loading.

Section 5.3.4 Sulphuric Acid

Charge transport rates in sulphuric acid as measured by potential step methods are amongst the highest observed for these modified electrodes, reaching a maximum at the 1:10 loading in 1.0 M sulphuric acid of 2 x 10^{-8} cm^2s^{-1} (Table 5.3.4.1). Both $D_{CT}(PS)$ and $D_{CT}(CV)$ increase as the concentration of sulphuric acid as supporting electrolyte is increased. The sensitivity of $D_{CT}(PS)$ to increases in sulphuric acid concentration depends on the redox site loading. With the exception of n=10 and 15 the effect of an increased sulphuric acid concentration is to increase $D_{CT}(PS)$ in a quasi-linear manner. For the 1:15 and 1:10 loadings however, a different behaviour is observed. Below 0.6 M sulphuric acid $D_{CT}(PS)$ is relatively insensitive to the sulphuric acid concentration, while above this concentration $D_{CT}(PS)$ increases more significantly e.g $D_{CT}(PS)$ in 0.4 M sulphuric acid is 4.6 x 10^{-9} cm^2s^{-1} while at 1.0 M D_{CT} is 2 x 10^{-8} cm^2s^{-1}. An increased redox site loading increases $D_{CT}(PS)$ for loadings between 1:25 and 1:10 after which it decreases.

The effect of redox site loading and sulphuric acid concentration on $D_{CT}(CV)$ is given in Table 5.3.4.1 and shown in Figure 5.3.4.1. $D_{CT}(PS)$ and $D_{CT}(CV)$ are comparable for low loadings e.g for the 1:25 system with 1.0 M electrolyte $D_{CT}(PS)$ is 1.15 x 10^{-9} cm^2s^{-1} while $D_{CT}(CV)$ is 1.08 x 10^{-9} cm^2s^{-1}. For higher loadings the rate of charge transport

Table 5.3.4.1 The effect of concentration of sulphuric acid supporting electrolyte and redox site loading on charge transport parameters of $[Os(bipy)_2(PVI)_nCl]Cl$ modified electrodes.

Loading	Conc. M	D_{CT}(PS) $*10^9$ cm^2s^{-1}	D_{CT}(CV) $*10^{10}$ cm^2s^{-1}	E^o V
n=5	0.1	1.18	3.88	0.175
	0.2	1.37	4.00	0.170
	0.4	1.46	4.35	0.170
	0.6	1.54	4.30	0.145
	0.8	2.18	4.43	0.145
	1.0	2.25	4.53	0.150
n=10	0.1	2.97	1.83	0.145
	0.2	3.70	1.97	0.155
	0.4	4.64	2.09	0.175
	0.6	8.91	2.40	0.190
	0.8	14.1	2.60	0.190
	1.0	20.1	2.70	0.205
n=15	0.1	2.01	1.74	0.165
	0.2	2.67	2.53	0.160
	0.4	3.12	3.11	0.160
	0.6	5.47	6.62	0.140
	0.8	8.53	8.34	0.135
	1.0	11.00	9.98	0.135
n=20	0.1	1.23	2.54	0.165
	0.2	1.46	3.37	0.160
	0.4	1.72	6.31	0.155
	0.6	1.91	8.09	0.155
	0.8	2.85	8.85	0.145
	1.0	3.10	10.42	0.150
n=25	0.1	0.51	2.70	0.170
	0.2	0.60	3.51	0.145
	0.4	0.75	6.72	0.145
	0.6	0.91	8.25	0.150
	0.8	1.08	9.05	0.135
	1.0	1.15	10.81	0.140

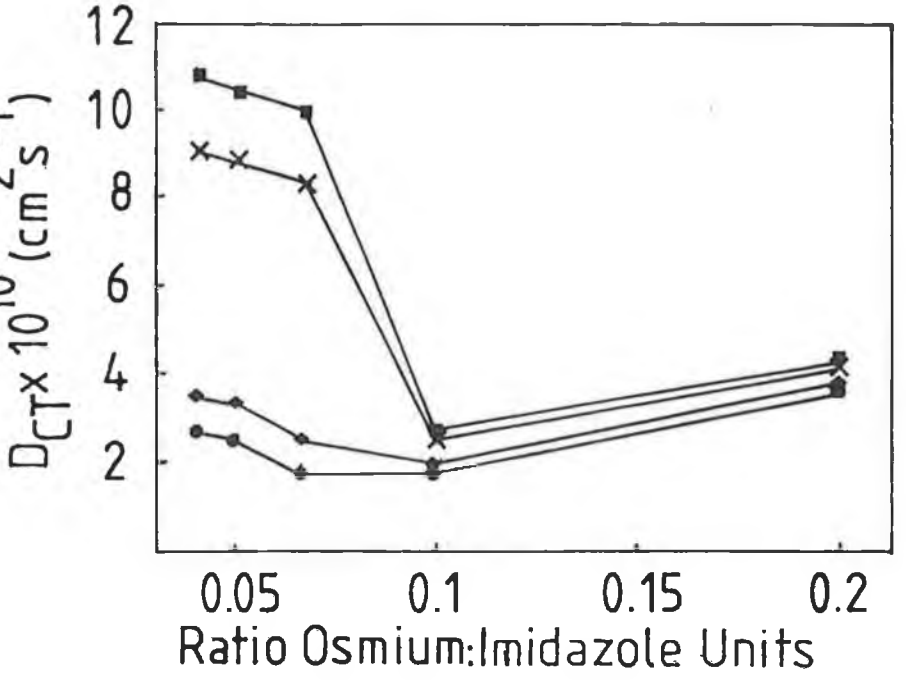

Figure 5.3.4.1 The effect of redox site concentration and H_2SO_4 concentration on D_{CT}(CV) for $[Os(bipy)_2(PVI)_nCl]Cl$ modified electrodes. The electrolyte concentrations are, from top to bottom, 1.0 M, 0.8 M, 0.2 M and 0.1 M.

observed becomes more dependent on the experimental technique employed to measure it; e.g for the 1:5 system in 0.1 M sulphuric acid D_{CT}(PS) is 1.18 x 10^{-9} cm^2s^{-1} while D_{CT}(CV) is 0.38 x 10^{-9} cm^2s^{-1}. As the sulphuric acid concentration is increased then D_{CT}(CV) also increases for all loadings. However, a significant proportion of the increase occurs between 0.2 and 0.6 M except for the 1:10 and 1:5 loadings where D_{CT}(CV) is relatively less sensitive to increased sulphuric acid concentration. As the redox site loading is increased from 1:25 the rate of homogeneous charge transport decreases. This decreases continues with increasing active site loading until n = 5 where D_{CT}(CV) increases moderately.

Section 5.3.5 Potassium Sulphate

The effect of redox site loading and potassium sulphate concentration over the range 0.1 to 0.6 M is given in Table 5.3.5.1 and shown in Figure 5.3.5.1. This figure shows that for all redox site loadings an increase in potassium sulphate concentration increases D_{CT}(PS). Where n = 25 and n = 5 a quasi-linear increase of D_{CT}(PS) with potassium sulphate concentration is observed and the rate of charge transport is relatively less sensitive to electrolyte concentration. For intermediate loadings, (where n = 20, 15 or 10), D_{CT}(PS) increases more significantly with much of this increase occurring between 0.2 and 0.4 M potassium sulphate. D_{CT}(PS) increases as the osmium loading is increased from 1:25 to 1:10 after which D_{CT}(PS) decreases for the 1:5 loading.

The charge transport rates measured by cyclic voltammetry are less than those recorded using potential step measurements (Table 5.3.5.1). As observed in the potential step experiments D_{CT}(CV) also increases as the

Table 5.3.5.1 The effect of concentration of potassium sulphate supporting electrolyte and redox site loading on charge transport parameters of $[Os(bipy)_2(PVI)_nCl]Cl$ modified electrodes.

Loading	Conc. M	D_{CT}(PS) $*10^9$ cm^2s^{-1}	D_{CT}(CV) $*10^{10}$ cm^2s^{-1}	E^o V
n=5	0.1	0.25	0.06	0.185
	0.2	0.39	0.15	0.185
	0.4	0.59	0.17	0.185
	0.6	0.81	0.21	0.180
n=10	0.1	4.37	1.71	0.165
	0.2	6.42	1.86	0.170
	0.4	10.93	2.28	0.170
	0.6	14.12	2.80	0.175
n=15	0.1	3.04	2.92	0.185
	0.2	4.07	3.35	0.180
	0.4	8.46	3.71	0.175
	0.6	9.46	4.37	0.170
n=20	0.1	1.87	5.45	0.180
	0.2	2.81	5.78	0.175
	0.4	5.11	6.47	0.175
	0.6	6.20	6.56	0.165
n=25	0.1	0.94	7.92	0.180
	0.2	1.45	8.37	0.175
	0.4	1.87	9.05	0.170
	0.6	2.71	9.10	0.170

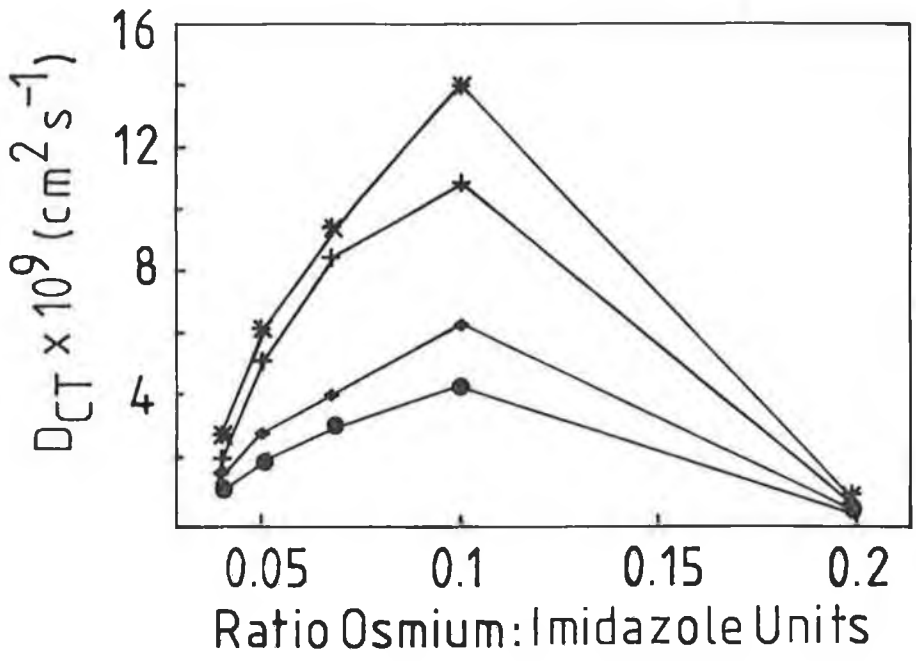

Figure 5.3.5.1 The effect of redox site concentration and K_2SO_4 concentration on D_{CT}(PS) for $[Os(bipy)_2(PVI)_nCl]Cl$ modified electrodes. The electrolyte concentrations are, from top to bottom, 0.6, 0.4, 0.2 and 0.1 M.

electrolyte concentration is increased. The effect of redox site concentration on D_{CT}(CV) is, however, different to that observed using potential step, with D_{CT}(CV) decreasing with increasing redox site loading over the whole range examined.

Section 5.3.6 Toluene-4-sulphonic Acid

Table 5.3.6.1 gives the dependence of both D_{CT}(PS) and D_{CT}(CV) on redox site loading as the concentration of toluene-4-sulphonic acid as supporting electrolyte is varied over the range 0.1 to 1.0 M. This table shows that the rates of homogeneous charge transport are amongst the highest obtained for these films. The effect of increased p-TSA concentration is to increase D_{CT}(PS). A significant increase in D_{CT}(PS) occurs between 0.8 and 1.0 M p-TSA. The effect of increased redox site loading is to linearly increase the charge transport rate over the whole loading range examined. This behaviour is shown in Figure 5.3.6.1. This is the only electrolyte which shows this behaviour over the whole loading range examined and for all electrolyte concentrations. It is to be noted that the overall increase in D_{CT}(PS) with redox site loading (a maximum factor of 1.7 from 1:25 to 1:5 loadings) is not as significant as that observed in other electrolytes.

D_{CT}(CV) shows a near linear variation with p-TSA concentration (Table 5.3.6.1). The maximum variation, which occurs for the 1:25 loading is a factor of 1.9 between 0.1 and 1.0 M electrolyte. An increase in the active site loading, results in a considerably enhanced charge propagation rate. This variation is linear over the whole loading range and is illustrated in Figure 5.3.6.2. The maximum charge transport rate is 1.3×10^{-9} cm^2s^{-1} attained

Table 5.3.6.1 The effect of concentration of toluene sulphonic acid supporting electrolyte and redox site loading on charge transport parameters of $[Os(bipy)_2(PVI)_nCl]Cl$ modified electrodes.

Loading	Conc. M	D_{CT}(PS) $*10^9$ cm^2s^{-1}	D_{CT}(CV) $*10^{10}$ cm^2s^{-1}	E^o V
n=5	0.1	1.85	10.50	0.220
	0.2	2.12	11.12	0.200
	0.4	3.05	11.54	0.175
	0.6	4.00	11.98	0.170
	0.8	4.22	12.52	0.175
	1.0	7.15	13.08	0.170
n=10	0.1	1.45	5.89	0.220
	0.2	1.75	6.14	0.225
	0.4	2.60	7.11	0.215
	0.6	3.40	7.29	0.195
	0.8	3.56	7.59	0.185
	1.0	6.75	7.89	0.185
n=15	0.1	1.20	4.48	0.190
	0.2	1.52	4.66	0.185
	0.4	2.31	4.81	0.190
	0.6	3.05	5.17	0.195
	0.8	3.25	5.34	0.195
	1.0	6.55	5.62	0.195
n=20	0.1	1.16	3.45	0.195
	0.2	1.47	3.71	0.190
	0.4	2.23	4.00	0.190
	0.6	2.97	4.39	0.180
	0.8	3.18	4.76	0.175
	1.0	6.47	5.03	0.170
n=25	0.1	1.09	2.36	0.190
	0.2	1.35	2.57	0.195
	0.4	2.11	3.20	0.200
	0.6	2.81	3.77	0.185
	0.8	3.00	4.14	0.170
	1.0	6.28	4.43	0.170

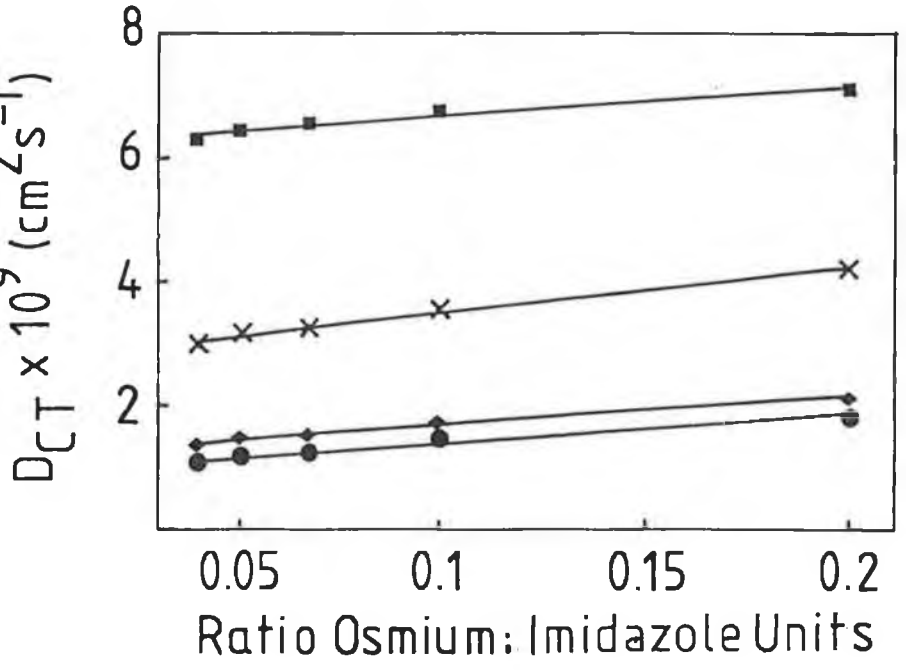

Figure 5.3.6.1 The effect of redox site concentration and toluene-4-sulphonic acid concentration on D_{CT}(PS) for $[Os(bipy)_2(PVI)_nCl]Cl$ modified electrodes. The electrolyte concentrations are, from top to bottom, 1.0, 0.8, 0.2 and 0.1 M.

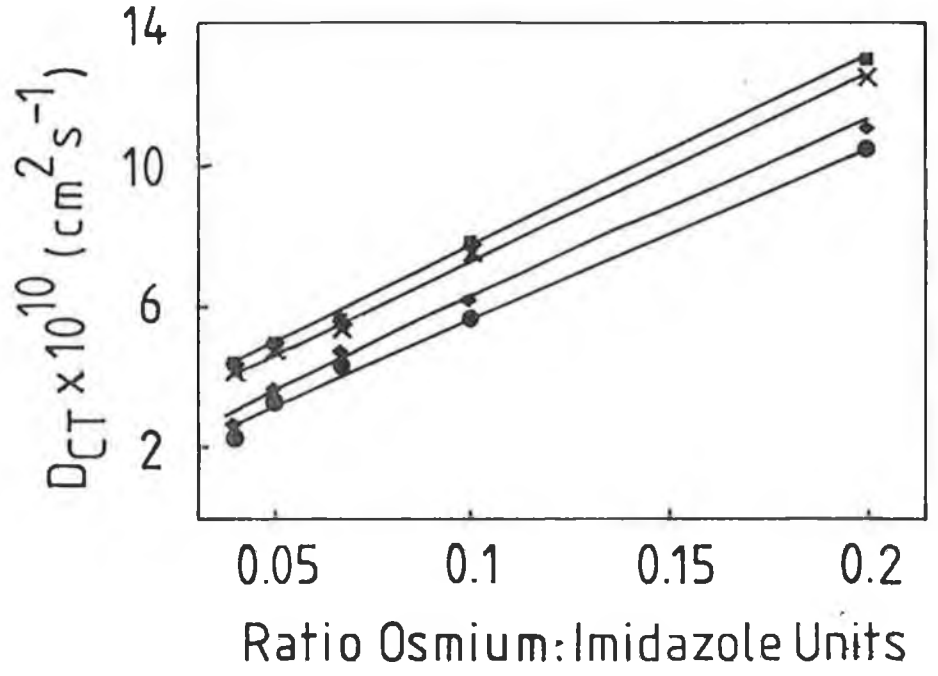

Figure 5.3.6.2 The effect of redox site concentration and toluene-4-sulphonic acid concentration on D_{CT}(CV) for $[Os(bipy)_2(PVI)_nCl]Cl$ modified electrodes. The electrolyte concentrations are, from top to bottom, 1.0, 0.8, 0.2 and 0.1 M.

at the 1:5 loading in 1.0 M p-TSA. D_{CT}(CV) increases by a factor of between 3 and 4.5 depending on the electrolyte concentration as the redox loading is increased from 1:25 to 1:5.

Section 5.3.7 Perchloric Acid

The effect of redox site loading in perchloric acid is given in Table 5.3.7.1 and is illustrated in Figure 5.3.7.1. An increase in $HClO_4$ concentration increases D_{CT}(PS). For loadings in the range 1:25 to 1:10 this increase in significant, while for the 1:5 loading it is less so. For films where $25 \geq n \geq 10$ D_{CT}(PS) increases most significantly between 0.6 and 1.0 M electrolyte. The effect of increased active site loading is to enhance the charge transport rate over the range 1:25 to 1:10 before suppressing it at the 1:5 loading.

The response of D_{CT}(CV) to changes in the perchloric acid and osmium concentration within the film is given in Table 5.3.7.1 and illustrated in Figure 5.3.7.2. D_{CT}(CV) decreases as the concentration of perchlorate is increased. As well as this, D_{CT}(CV) is sluggish compared to other electrolytes, the maximum charge transport rate being 9 x 10^{-11} cm^2s^{-1}. The decrease in D_{CT} with increasing perchlorate concentration is most apparent for low redox site loadings i.e 1:25 - 1:15 while for the 1:10 and 1:5 loadings the effect is less pronounced. As the redox site concentration is increased from 1:25 to 1:15, D_{CT}(CV) is insensitive to the fixed site concentration before decreasing sharply at the 1:10 loading.

Table 5.3.7.1 The effect of concentration of perchloric acid supporting electrolyte and redox site loading on charge transport parameters of $[Os(bipy)_2(PVI)_nCl]Cl$ modified electrodes.

Loading	Conc. M	D_{CT}(PS) $*10^9$ cm^2s^{-1}	D_{CT}(CV) $*10^{10}$ cm^2s^{-1}	E^o V
n=5	0.1	0.48	0.44	0.160
	0.2	0.48	0.44	0.155
	0.4	0.48	0.43	0.125
	0.6	0.50	0.42	0.115
	0.8	0.60	0.41	0.115
	1.0	0.68	0.34	0.115
n=10	0.1	2.86	2.06	0.155
	0.2	2.86	1.45	0.155
	0.4	3.10	1.43	0.125
	0.6	3.93	1.40	0.125
	0.8	5.30	1.40	0.130
	1.0	6.01	1.35	0.130
n=15	0.1	0.89	8.76	0.140
	0.2	1.12	5.89	0.130
	0.4	1.31	4.84	0.140
	0.6	1.43	3.73	0.125
	0.8	1.79	3.09	0.115
	1.0	3.64	2.73	0.115
n=20	0.1	0.75	8.89	0.150
	0.2	0.93	6.43	0.140
	0.4	1.01	5.09	0.135
	0.6	1.11	4.45	0.130
	0.8	1.32	3.25	0.120
	1.0	2.58	3.03	0.115
n=25	0.1	0.57	9.01	0.160
	0.2	0.65	6.94	0.150
	0.4	0.66	5.37	0.130
	0.6	0.74	4.89	0.120
	0.8	0.80	3.42	0.100
	1.0	1.82	3.32	0.100

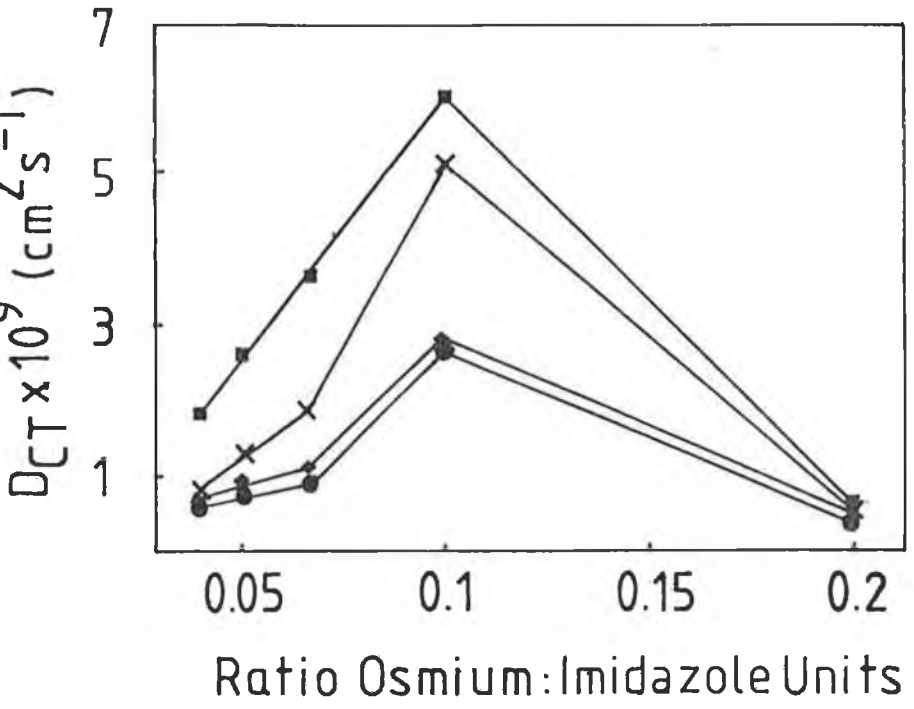

Figure 5.3.7.1 The effect of redox site concentration and $HClO_4$ concentration on D_{CT}(PS) for $[Os(bipy)_2(PVI)_nCl]Cl$ modified electrodes. The electrolyte concentrations are, from top to bottom, 1.0, 0.8, 0.2 and 0.1 M.

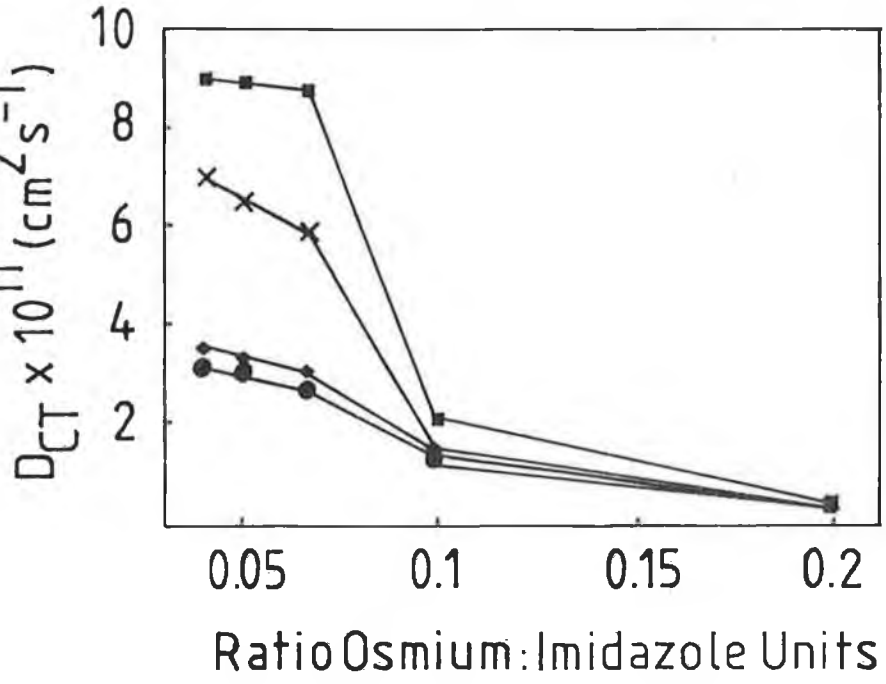

Figure 5.3.7.2 The effect of redox site concentration and $HClO_4$ concentration on D_{CT}(CV) for $[Os(bipy)_2(PVI)_nCl]Cl$ modified electrodes. The electrolyte concentrations are, from top to bottom, 1.0, 0.8, 0.2 and 0.1 M.

Section 5.3.8 Lithium Perchlorate

D_{CT}(PS) increases as the lithium perchlorate concentration is raised, most noticably between 0.8 and 1.0 M where $25 \geq n \geq 10$ (Table 5.3.8.1). As the redox site loading is increased from 1:25 D_{CT}(PS) initially increases before decreasing for the 1:10 and 1:5 loadings.

The rate of charge transport measured using cyclic voltammetry is approximately an order of magnitude less than that observed using potential step (Table 5.3.8.1). As observed for perchloric acid an increase in the lithium perchlorate concentration decreases D_{CT}(CV). As the redox site loading is increased D_{CT}(CV) initially increases linearly before decreasing at the 1:5 loading.

Section 5.4 Activation Parameters For Homogeneous Charge Transport

As discussed previously for osmium containing poly(4-vinylpyridine) films variable temperature chronoamperometry and cyclic voltammetry can be used to measure the activation parameters for the homogeneous charge transport process. The measured activation energies and entropies can be useful in the diagnosis of the rate determining step in the charge transport process [10,11]. Like the poly(4-vinylpyridine) films discussed in chapter 4, the poly(N-vinylimidazole) metallopolymers discussed here are compatible with a wide range of temperatures. Therefore, thermodynamic parameters have been evaluated from both potential step and cyclic voltammetry data for the above electrolytes at the various loadings over the temperature range 276-310 K.

Table 5.3.8.1 The effect of concentration of lithium perchlorate supporting electrolyte and redox site loading on charge transport parameters of $[Os(bipy)_2(PVI)_nCl]Cl$ modified electrodes.

Loading	Conc. M	D_{CT}(PS) $*10^9$ cm^2s^{-1}	D_{CT}(CV) $*10^{10}$ cm^2s^{-1}	E^o V
n=5	0.1	0.35	0.34	0.180
	0.2	0.37	0.32	0.155
	0.4	0.48	0.29	0.145
	0.6	0.65	0.25	0.135
	0.8	0.82	0.24	0.125
	1.0	1.09	0.20	0.130
n=10	0.1	1.33	3.50	0.165
	0.2	1.68	2.73	0.165
	0.4	1.67	2.15	0.170
	0.6	1.78	2.03	0.145
	0.8	1.93	1.81	0.145
	1.0	2.87	1.67	0.145
n=15	0.1	1.62	2.26	0.135
	0.2	1.66	1.72	0.130
	0.4	1.72	1.54	0.130
	0.6	1.79	1.33	0.125
	0.8	2.06	1.11	0.125
	1.0	3.66	0.95	0.125
n=20	0.1	1.21	1.55	0.140
	0.2	1.24	1.14	0.135
	0.4	1.40	1.02	0.130
	0.6	1.45	0.90	0.130
	0.8	1.64	0.77	0.130
	1.0	3.01	0.67	0.130
n=25	0.1	0.81	0.87	0.155
	0.2	0.82	0.55	0.145
	0.4	1.07	0.51	0.130
	0.6	1.13	0.46	0.110
	0.8	1.21	0.43	0.115
	1.0	2.32	0.39	0.115

Section 5.4.1 Hydrochloric Acid

The activation energy for charge transport through $[Os(bipy)_2(PVI)_nCl]Cl$ films in contact with 0.1 and 1.0 M hydrochloric acid has been measured and the data given in Table 5.4.1.1. The activation energies are between 20 and 45 kJ/Mol and increase as the osmium loading of the film increases. The entropy terms at all loadings are negative. The magnitude and behaviour of the activation energy is similar in both 0.1 and 1.0 M hydrochloric acid as supporting electrolyte. The increase in E_a(CV) relates to the decrease in D_{CT}(PS) discussed previously (section 5.3.2.1).

The effect of redox site loading on E_a(CV) is illustrated in Figure 5.4.1.1, and is distinctly different to that observed previously via potential step. The response is similar in both 0.1 and 1.0 M electrolyte. For redox site loadings between 1:25 and 1:15 the activation energy is large (>100 kJ/Mol) and decreases marginally in both 0.1 and 1.0 M hydrochloric acid as n is varied from 25 to 15. The entropy terms coupled to these activation energies are positive. At the 1:10 and 1:5 loadings the activation energy is considerably decreased to a value of 15 - 40 kJ/Mol. This reduced activation energy is coupled to a negative entropy term.

Section 5.4.2 Sodium Chloride

E_a(PS) shows little variation with redox site loading in 0.1 M sodium chloride, maintaining a value of 12.5±1 kJ/Mol (Table 5.4.2.1). In 0.1 M sodium chloride E_a(PS) shows more variation with redox site loading. E_a(PS) decreases linearly from 24 kJ/Mol where n = 25 to 15.1 kJ/Mol where n = 15. For $25 \geq n \geq 5$ E_a(PS) is similar to that observed in 0.1 M sodium chloride, with a value of 14.5±0.6 kJ/Mol. The entropy terms are all negative at both

Table 5.4.1.1 Activation parameters for charge transport through $[Os(bipy)_2(PVI)_nCl]Cl$ films as obtained by potential step methods in hydrochloric acid.

Loading	Conc.	E_a kJ/Mol	$\Delta H^{\neq}$ kJ/Mol	$\Delta S^{\neq}$ $JMol^{-1}K^{-1}$	$\Delta G^{\neq}$ kJ/Mol
n=5	0.1 M	45.1	42.6	-16.2	47.4
	1.0 M	43.1	40.6	-15.3	45.2
n=10	0.1 M	42.9	40.4	-31.1	49.7
	1.0 M	37.6	35.1	-44.8	48.5
n=15	0.1 M	38.8	36.3	-48.9	50.9
	1.0 M	33.7	31.2	-62.3	49.7
n=20	0.1 M	30.5	28.0	-79.9	54.3
	1.0 M	26.9	24.4	-87.9	50.6
n=25	0.1 M	21.9	19.5	-111.0	52.6
	1.0 M	19.0	16.5	-117.3	51.5

Table 5.4.1.2 Activation parameters for charge transport through $[Os(bipy)_2(PVI)_nCl]Cl$ films as obtained by cyclic voltammetry in hydrochloric acid.

Loading	Conc.	E_a	$\Delta H^{\ddagger}$	$\Delta S^{\ddagger}$	$\Delta G^{\ddagger}$
		kJ/Mol	kJ/Mol	$JMol^{-1}K^{-1}$	kJ/Mol
n=5	0.1 M	14.7	17.9	-96.9	46.8
	1.0 M	24.0	21.6	-83.8	46.5
n=10	0.1 M	31.2	28.7	-80.2	52.6
	1.0 M	40.8	38.3	-36.1	49.1
n=15	0.1 M	99.0	96.5	140.5	54.6
	1.0 M	124.7	122.2	227.3	54.5
n=20	0.1 M	110.1	107.6	176.2	55.1
	1.0 M	131.7	129.2	256.8	52.6
n=25	0.1 M	114.6	112.1	182.8	57.6
	1.0 M	134.6	132.1	261.9	54.1

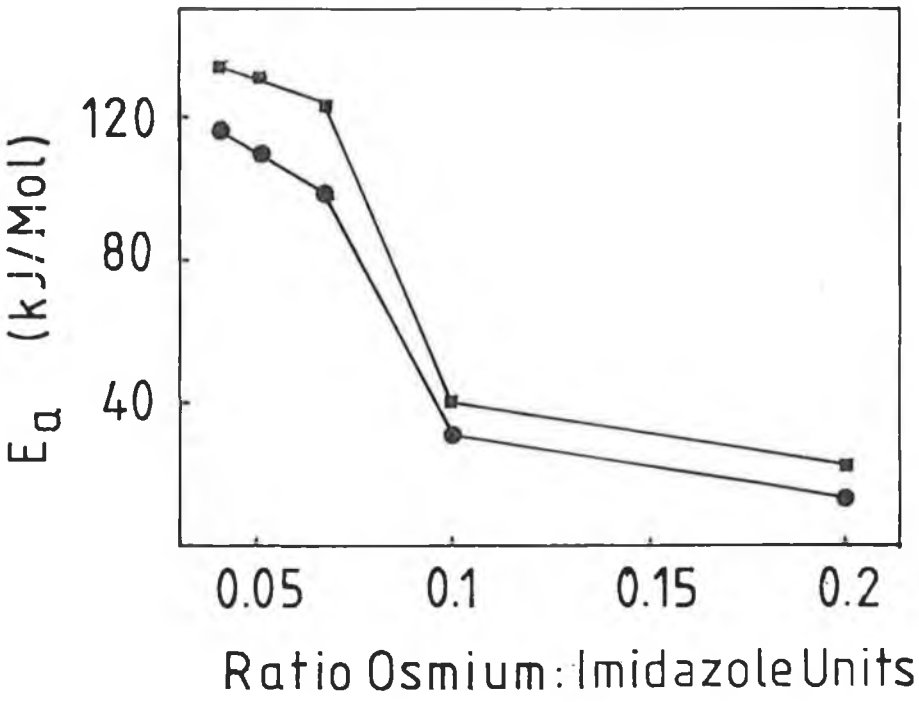

Figure 5.4.1.1 The effect of redox site loading on the activation energy in ● 0.1 M HCl and ■ 1.0 M HCl as measured by linear sweep voltammetry.

Table 5.4.2.1 Activation parameters for charge transport through $[Os(bipy)_2(PVI)_nCl]Cl$ films as obtained by potential step methods in sodium chloride.

Loading	Conc.	E_a kJ/Mol	$\Delta H^{\ddagger}$ kJ/Mol	$\Delta S^{\ddagger}$ $JMol^{-1}K^{-1}$	$\Delta G^{\ddagger}$ kJ/Mol
n=5	0.1 M	12.1	9.6	-129.7	48.3
	1.0 M	13.6	11.1	-107.7	43.2
n=10	0.1 M	13.8	11.3	-126.3	49.0
	1.0 M	14.7	12.2	-112.7	45.8
n=15	0.1 M	13.3	10.8	-133.2	50.5
	1.0 M	15.1	12.6	-118.5	47.9
n=20	0.1 M	11.5	9.0	-143.1	51.7
	1.0 M	20.2	17.7	-106.7	49.5
n=25	0.1 M	11.9	9.4	-144.6	52.5
	1.0 M	24.0	21.5	-97.6	50.6

Table 5.4.2.2 Activation parameters for charge transport through $[Os(bipy)_2(PVI)_nCl]Cl$ films as obtained by cyclic voltammetry in sodium chloride.

Loading	Conc.	E_a	$\Delta H^{\ddagger}$	$\Delta S^{\ddagger}$	$\Delta G^{\ddagger}$
		kJ/Mol	kJ/Mol	$JMol^{-1}K^{-1}$	kJ/Mol
n=5	0.1 M	35.8	31.1	-63.1	49.9
	1.0 M	61.2	58.6	29.2	49.0
n=10	0.1 M	42.2	39.8	-39.5	51.6
	1.0 M	61.3	58.8	28.9	50.2
n=15	0.1 M	114.6	112.1	191.4	55.1
	1.0 M	61.6	59.1	21.7	52.6
n=20	0.1 M	116.2	113.7	193.2	56.1
	1.0 M	128.9	126.4	242.5	54.1
n=25	0.1 M	116.4	114.0	188.6	57.8
	1.0 M	134.3	131.8	256.9	55.2

electrolyte concentrations although the entropy is more negative in 0.1 M electrolyte.

E_a(CV) values are more sensitive to redox site loading than those obtained using potential step methods (Table 5.4.2.2). With 0.1 M sodium chloride as supporting electrolyte E_a(CV) is large for $25 \geq n \geq 15$ (115.7±1.1 kJ/Mol) and is associated with positive entropy terms. For n = 10 and n = 5 a reduced activation energy is obtained (33.5±2.5 kJ/Mol) together with negative entropy terms. In 1.0 M sodium chloride the activation energy is large for the 1:25 and 1:20 loadings (131.5±2.5 kJ/Mol) before decreasing to 61.3±0.2 kJ/Mol where $15 \geq n \geq 5$. The entropy terms are positive for all redox site loadings in 1.0 M sodium chloride.

Section 5.4.3 Sulphuric Acid

E_a(PS) remains constant for all redox site loadings with a value of 39.6±3.6 kJ/Mol which is coupled to a negative entropy term. In 1.0 M sulphuric acid the activation energy decreases linearly from 71 kJ/Mol for the 1:25 loading to 32 kJ/Mol for the 1:5 loading. Where $25 \geq n \geq 10$ the entropy terms are positive, while for n = 5 a negative entropy is observed.

E_a(CV) remains constant at a value of 51.1±4 kJ/Mol for all redox site loadings in 0.1 M sulphuric acid. These activation energies are coupled to negative entropy terms which show little dependence on active site loading. In 0.6 M H_2SO_4 two distinct behaviours are observed depending on the redox site loading. For $25 \leq n \leq 15$ E_a(CV) is large (98.2±10.9 kJ/Mol) and is coupled to a positive entropy term. The 1:10 and 1:5 loadings have lower activation energies (47.9±1 kJ/Mol) and are coupled to negative entropy terms.

Table 5.4.3.1 Activation parameters for charge transport through $[Os(bipy)_2(PVI)_nCl]Cl$ films as obtained by potential step methods in sulphuric acid.

Loading	Conc.	E_a kJ/Mol	$\Delta H^{\ddagger}$ kJ/Mol	$\Delta S^{\ddagger}$ $JMol^{-1}K^{-1}$	$\Delta G^{\ddagger}$ kJ/Mol
n=5	0.1 M	38.9	36.4	-29.2	45.1
	1.0 M	32.1	29.6	-46.6	43.5
n=10	0.1 M	37.6	35.1	-37.1	46.2
	1.0 M	59.9	57.4	53.3	41.5
n=15	0.1 M	35.2	32.7	-55.5	49.2
	1.0 M	63.8	61.3	54.6	45.0
n=20	0.1 M	43.3	40.8	-37.1	51.8
	1.0 M	64.8	62.3	42.7	49.6
n=25	0.1 M	43.3	40.8	-48.2	55.1
	1.0 M	70.9	68.4	51.2	53.1

Table 5.4.3.2 Activation parameters for charge transport through $[Os(bipy)_2(PVI)_nCl]Cl$ films as obtained by cyclic voltammetry in sulphuric acid.

Loading	Conc.	E_a	$\Delta H^{\neq}$	$\Delta S^{\neq}$	$\Delta G^{\neq}$
		kJ/Mol	kJ/Mol	$JMol^{-1}K^{-1}$	kJ/Mol
n=5	0.1 M	43.4	40.9	-23.5	47.9
	1.0 M	48.9	46.4	-3.67	47.5
n=10	0.1 M	51.0	48.5	-15.7	53.2
	1.0 M	46.8	44.3	-26.4	52.2
n=15	0.1 M	52.3	49.8	-18.4	55.3
	1.0 M	92.8	90.3	132.0	50.9
n=20	0.1 M	53.6	51.1	-15.8	55.8
	1.0 M	92.8	92.5	127.6	54.5
n=25	0.1 M	55.1	52.6	-13.8	56.7
	1.0 M	109.1	106.6	178.8	53.5

Section 5.4.4 Potassium Sulphate

In contrast to the other electrolyte systems examined, the activation energy in high electrolyte concentration (0.6 M) is less than that observed in 0.1 M electrolyte (Table 5.4.4.1). In 0.6 M potassium sulphate the activation energy is low and constant with a value of 17.7±2.4 kJ/Mol. In 0.1 M electrolyte the activation energy steadily increases as the redox site loading is increased. For the 1:25 loading E_a is 23.6 kJ/Mol, which increases to a maximum of 35.9 kJ/Mol at the 1:5 loading. In both electrolyte concentrations the entropies are negative. The free energy terms also show some dependence on redox site loading. At low loadings the Gibbs free energy term is approximately 50 kJ/Mol which reduces to 45 kJ/Mol for the 1:15 to 1:5 loadings.

The values obtained for E_a(CV) in both 0.1 and 0.6 M potassium sulphate are the same. As n is varied from 25 to 10 E_a(CV) decreases systematically from 17.5 kJ/Mol to 5.8 kJ/Mol and remains at this value for the 1:5 loading (Table 5.4.4.2). These activation energies are coupled to negative entropy terms. The free energy term shows no systematic variation with redox site loading, maintaining a value of 54.1±4 kJ/Mol.

Section 5.4.5 Toluene-4-sulphonic Acid

E_a(PS) decreases steadily from 37.1 kJ/Mol to 8.7 kJ/Mol in 0.1 M p-TSA and from 32.5 kJ/Mol to 14.0 kJ/Mol as the redox site loading is increased from 1:25 to 1:5. This behaviour is illustrated in Figure 5.4.5.1. In both concentrations of supporting electrolyte the entropy terms remain negative for all loadings examined.

Table 5.4.4.1 Activation parameters for charge transport through $[Os(bipy)_2(PVI)_nCl]Cl$ films as obtained by potential step methods in potassium sulphate.

Loading	Conc.	E_a kJ/Mol	$\Delta H^{\neq}$ kJ/Mol	$\Delta S^{\neq}$ $JMol^{-1}K^{-1}$	$\Delta G^{\neq}$ kJ/Mol
n=5	0.1 M	35.9	33.4	-52.2	48.9
	0.6 M	20.1	17.6	-95.4	46.0
n=10	0.1 M	32.3	29.8	-52.0	45.3
	0.6 M	17.8	15.3	-90.9	42.4
n=15	0.1 M	28.7	26.2	-73.8	48.2
	0.6 M	16.3	13.8	-106.0	45.4
n=20	0.1 M	25.9	23.4	-92.1	50.8
	0.6 M	16.5	14.0	-113.6	47.9
n=25	0.1 M	23.6	21.1	-109.2	53.6
	0.6 M	17.7	15.2	-120.2	51.0

Table 5.4.4.2 Activation parameters for charge transport through $[Os(bipy)_2(PVI)_nCl]Cl$ films as obtained by cyclic voltammetry in potassium sulphate.

Loading	Conc.	E_a kJ/Mol	$\Delta H^{\ddagger}$ kJ/Mol	$\Delta S^{\ddagger}$ $JMol^{-1}K^{-1}$	$\Delta G^{\ddagger}$ kJ/Mol
n=5	0.1 M	5.5	3.0	-185.2	58.2
	0.6 M	5.1	2.6	-176.1	55.1
n=10	0.1 M	5.8	3.3	-167.9	53.3
	0.6 M	5.8	3.3	-163.8	52.1
n=15	0.1 M	11.1	8.6	-152.4	54.0
	0.6 M	9.6	7.1	-154.0	53.0
n=20	0.1 M	13.7	11.2	-143.2	53.9
	0.6 M	14.1	11.6	-140.3	53.4
n=25	0.1 M	17.5	15.0	-131.1	54.0
	0.6 M	17.8	15.3	-128.9	53.7

Table 5.4.5.1 Activation parameters for charge transport through $[Os(bipy)_2(PVI)_nCl]Cl$ films as obtained by potential step methods in toluene sulphonic acid.

Loading	Conc.	E_a kJ/Mol	$\Delta H^{\ddagger}$ kJ/Mol	$\Delta S^{\ddagger}$ $JMol^{-1}K^{-1}$	$\Delta G^{\ddagger}$ kJ/Mol
n=5	0.1 M	14.0	11.5	-97.9	40.6
	1.0 M	8.7	6.2	-126.7	44.0
n=10	0.1 M	27.1	24.6	-65.8	44.2
	1.0 M	22.1	19.6	-95.7	48.1
n=15	0.1 M	32.9	30.4	-67.5	50.5
	1.0 M	28.4	25.9	-68.6	46.3
n=20	0.1 M	35.1	32.6	-65.2	52.0
	1.0 M	30.2	27.7	-67.3	47.8
n=25	0.1 M	37.1	34.6	-62.6	53.3
	1.0 M	32.5	30.0	-63.4	48.9

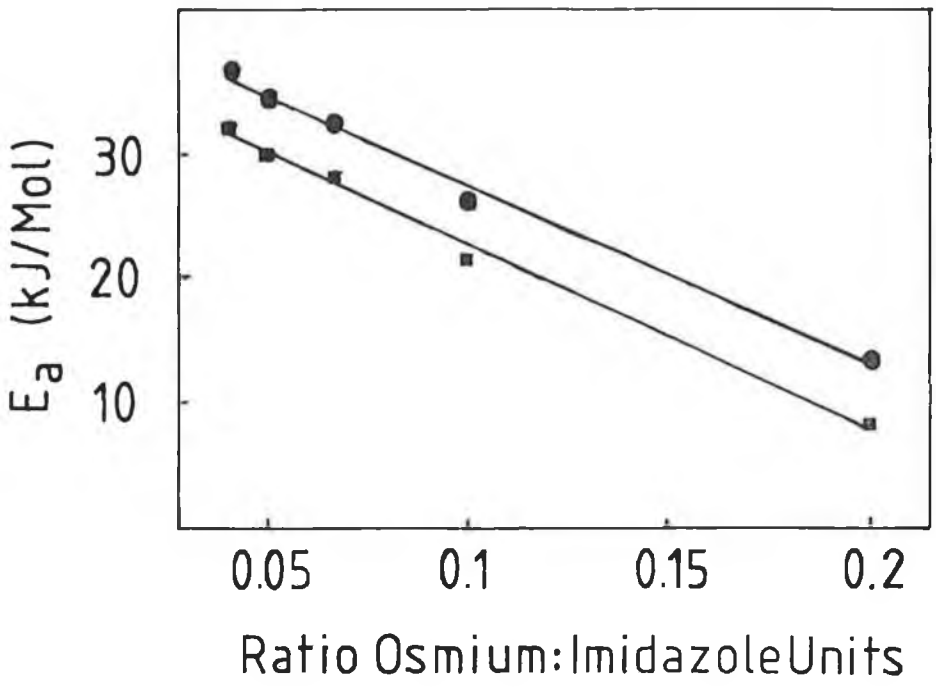

Figure 5.4.5.1 The effect of redox site loading on the activation energy in ● 0.1 and ■ 1.0 M toluene-4-sulphonic acid as measured by potential step.

Table 5.4.5.2 Activation parameters for charge transport through $[Os(bipy)_2(PVI)_nCl]Cl$ films as obtained by cyclic voltammetry in toluene sulphonic acid.

Loading	Conc.	E_a kJ/Mol	$\Delta H^{\ddagger}$ kJ/Mol	$\Delta S^{\ddagger}$ $JMol^{-1}K^{-1}$	$\Delta G^{\ddagger}$ kJ/Mol
n=5	0.1 M	18.3	15.8	-99.5	45.4
	1.0 M	40.1	37.6	-24.7	44.9
n=10	0.1 M	25.4	22.9	-91.8	50.3
	1.0 M	37.8	35.3	-47.8	49.5
n=15	0.1 M	28.4	25.9	-90.8	52.9
	1.0 M	32.9	30.4	-73.8	52.4
n=20	0.1 M	28.7	26.2	-96.7	55.0
	1.0 M	37.0	34.5	-65.7	54.1
n=25	0.1 M	29.2	26.7	-101.9	57.1
	1.0 M	37.7	33.2	-68.1	53.5

The effect of redox site loading on E_a(CV) is less than that observed for E_a(PS) (see Table 5.4.5.2). In 0.1 M p-TSA the activation energy shows a linear decrease from 29 kJ/Mol to 18 kJ/Mol as the redox site loading is increased from 1:25 to 1:5. In 1.0 M electrolyte the activation energy is largely unaffected by changes in the active site concentration maintaining a value of 37.1±3 kJ/Mol. The activation entropies are negative for all loadings.

Section 5.4.6 Perchloric Acid

The effect of redox site loading on E_a(PS) is similar in 0.1 and 1.0 M perchloric acid and Figure 5.4.6.1 illustrates the observed behaviour. For $25 \geq n \geq 15$ the activation energy is large (69.4±2.8 kJ/Mol) and associated with positive entropy terms. This value drops to 25.7±2.5 kJ/Mol for loadings of 1:10 and 1:5 with negative entropy terms.

In 0.1 M perchloric acid E_a(CV) for the 1:25 to 1:15 loadings are large, 103.3±2 kJ/Mol, before decreasing to 26±2.6 kJ/Mol for the 1:5 loading. Where $25 \geq n \geq 15$ the entropy terms are positive, while for n = 10 and n = 5 the entropy terms are negative. The transition loading of 1:10 shows dual slope behaviour observed previously for $[Os(bipy)_2(PVP)_nCl]Cl$ films in contact with perchlorate salts. Two activation energies are obtained, for temperatures above 285 K the activation energy is 84.5 kJ/Mol with a positive entropy term. For temperatures below 285 K a negative entropy term is observed with an activation energy of 34.2 kJ/Mol. In 1.0 M perchloric acid a high activation energy (145.6±18 kJ/Mol) is obtained where $25 \geq n \geq 15$. For n = 10 the activation energy is reduced to 69 kJ/Mol. These activation energies are coupled to

Table 5.4.6.1 Activation parameters for charge transport through $[Os(bipy)_2(PVI)_nCl]Cl$ films as obtained by potential step methods in perchloric acid.

Loading	Conc.	E_a	$\Delta H^{\neq}$	$\Delta S^{\neq}$	$\Delta G^{\neq}$
		kJ/Mol	kJ/Mol	$JMol^{-1}K^{-1}$	kJ/Mol
n=5	0.1 M	22.9	20.4	-90.4	47.3
	1.0 M	25.9	23.4	-77.4	46.5
n=10	0.1 M	25.8	23.3	-77.3	46.3
	1.0 M	28.2	25.7	-63.1	44.5
n=15	0.1 M	67.7	65.2	46.8	51.2
	1.0 M	72.2	69.7	73.6	47.8
n=20	0.1 M	66.4	63.9	36.2	53.1
	1.0 M	69.8	67.3	57.9	50.0
n=25	0.1 M	68.9	66.4	38.6	54.9
	1.0 M	71.3	68.8	56.3	52.0

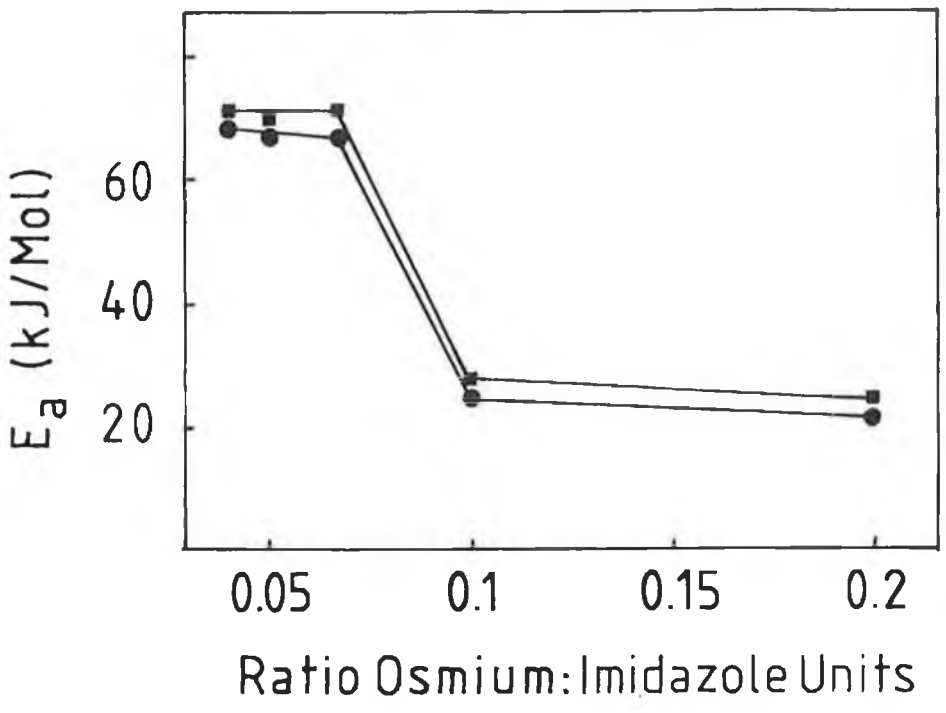

Figure 5.4.6.1 The effect of redox site loading on the activation energy in ● 0.1 M and ■ 1.0 M $HClO_4$ as measured by potential step.

Table 5.4.6.2 Activation parameters for charge transport through $[Os(bipy)_2(PVI)_nCl]Cl$ films as obtained by cyclic voltammetry in perchloric acid.

Loading	Conc.		E_a kJ/Mol	$\Delta H^{\ddagger}$ kJ/Mol	$\Delta S^{\ddagger}$ $JMol^{-1}K^{-1}$	$\Delta G^{\ddagger}$ kJ/Mol
n=5	0.1 M		28.7	26.2	-90.8	53.2
	1.0 M		23.4	20.9	-110.7	53.9
n=10	0.1 M	T<285K	34.2	31.7	-71.5	53.0
		T>285K	84.5	82.0	97.8	54.3
	1.0 M		69.3	66.8	43.3	53.9
n=15	0.1 M		105.3	102.8	172.9	51.3
	1.0 M		127.6	125.1	238.0	54.2
n=20	0.1 M		103.5	101.0	162.2	52.6
	1.0 M		150.6	148.1	290.5	61.5
n=25	0.1 M		101.2	98.7	150.8	53.8
	1.0 M		158.5	156.0	322.5	59.9

positive entropy terms. When n = 5 E_a(CV) is reduced to 23.4 kJ/Mol which is associated with a negative entropy.

Section 5.4.7 Lithium Perchlorate

The activation energy as measured by potential step is insensitive to redox site loading in both 0.1 and 1.0 M lithium perchlorate. In 0.1 M lithium perchlorate the activation energy is 18.8±3.7kJ/Mol while in 1.0M electrolyte the activation energy is 28.2±3.2 kJ/Mol. In both concentrations of supporting electrolyte the activation energies are coupled to negative entropy terms for all loadings.

As observed using potential step E_a(CV) shows a similar dependence on redox site loading in both 0.1 and 1.0 M lithium perchlorate. At low redox site loading ($25 \geq n \geq 15$), the activation energy is high (127.1±4.8 kJ/Mol) and is coupled to a positive entropy term. For the 1:5 loading both concentrations of lithium perchlorate give an activation energy of 15.9 kJ/Mol with negative entropy terms. The 1:10 loading represents a transition loading with an activation energy of 64 kJ/Mol in 1.0 M lithium perchlorate and a positive entropy. The activation energy in 0.1 M electrolyte is 40 kJ/Mol with a negative entropy term indicating that an ordering process limits the rate of charge propagation.

Table 5.4.7.1 Activation parameters for charge transport through $[Os(bipy)_2(PVI)_nCl]Cl$ films as obtained by potential step methods in lithium perchlorate.

Loading	Conc.	E_a kJ/Mol	$\Delta H^{\ddagger}$ kJ/Mol	$\Delta S^{\ddagger}$ $JMol^{-1}K^{-1}$	$\Delta G^{\ddagger}$ kJ/Mol
n=5	0.1 M	20.8	18.3	-100.0	48.1
	1.0 M	27.6	25.1	-67.8	45.3
n=10	0.1 M	18.9	16.4	-106.8	48.2
	1.0 M	28.8	26.3	-67.2	46.3
n=15	0.1 M	15.1	12.6	-124.7	49.8
	1.0 M	31.4	28.9	-63.2	47.7
n=20	0.1 M	17.7	15.2	-123.2	51.9
	1.0 M	27.9	25.4	-81.4	49.6
n=25	0.1 M	21.5	19.0	-117.5	54.0
	1.0 M	25.4	22.9	-95.6	51.4

Table 5.4.7.2 Activation parameters for charge transport through $[Os(bipy)_2(PVI)_nCl]Cl$ films as obtained by cyclic voltammetry in lithium perchlorate.

Loading	Conc.	E_a kJ/Mol	$\Delta H^{\ddagger}$ kJ/Mol	$\Delta S^{\ddagger}$ $JMol^{-1}K^{-1}$	$\Delta G^{\ddagger}$ kJ/Mol
n=5	0.1 M	15.9	13.4	-135.9	53.9
	1.0 M	15.9	13.4	-121.2	49.5
n=10	0.1 M	40.5	38.0	-51.6	53.4
	1.0 M	64.2	61.7	34.0	51.5
n=15	0.1 M	120.6	118.1	212.9	54.6
	1.0 M	124.7	122.2	219.5	56.8
n=20	0.1 M	126.7	124.2	225.5	57.0
	1.0 M	127.9	125.4	222.6	59.1
n=25	0.1 M	130.9	128.4	231.1	59.6
	1.0 M	131.9	129.4	227.7	61.5

Section 5.5 Electrolyte and Redox Site Loading Effects on Heterogeneous Electron Transfer Reactions

A linear correlation of the homogeneous charge transport rate $D_{CT}(PS)$ and the standard rate constant k^o has been observed for several polymer modified electrodes [11-13]. This behaviour was also observed for the poly(4-vinylpyridine) films discussed in chapter 4. In this section the effect of the redox site loading as well as, the electrolyte type and concentration on the rate of electron transfer from the underlying electrode surface to the immobilised metallopolymer is discussed.

Section 5.5.1 Hydrochloric Acid

k^o increases approximately linearly with increasing HCl concentration for all osmium loadings (Table 5.5.1.1). The effect of an increased active site loading is to decrease k^o, e.g in 0.1 M HCl k^o decreases from 2.90 x 10^{-4} cms^{-1} to 0.97 x 10^{-4} cms^{-1} as the redox site loading is increased from 1:25 to 1:5.

The transfer coefficient α , is dependent on the redox site loading. In 0.1 M HCl α increases from 0.21 to 0.35 as the redox site loading is increased from 1:25 to 1:5. The transfer coefficient also increases with increasing HCl concentration for all redox site loadings.

Section 5.5.2. Sodium Chloride

The rate of heterogeneous electron transfer from the electrode into the $[Os(bipy)_2(PVI)_nCl]Cl$ coatings is more rapid in sodium chloride than in hydrochloric acid (Table 5.5.2.1). k^o increases with increasing osmium loading up to the 1:10 loading, after which k^o decreases.

Table 5.5.1.1 The effect of concentration of hydrochloric acid supporting electrolyte and redox site loading on heterogeneous electron transfer parameters of $[Os(bipy)_2(PVI)_nCl]Cl$ modified electrodes.

Loading	Conc. M	k^o*10^4 cms^{-1}	α
n=5	0.1	0.97	0.35
	0.2	1.11	0.45
	0.4	1.56	0.50
	0.6	2.17	0.45
	0.8	2.96	0.45
	1.0	3.81	0.45
n=10	0.1	1.68	0.32
	0.2	1.94	0.34
	0.4	2.31	0.33
	0.6	2.69	0.35
	0.8	2.96	0.40
	1.0	3.81	0.38
n=15	0.1	2.40	0.30
	0.2	2.87	0.30
	0.4	3.10	0.31
	0.6	3.35	0.31
	0.8	3.57	0.31
	1.0	3.93	0.31
n=20			
	0.1	2.72	0.29
	0.2	3.09	0.32
	0.4	3.28	0.35
	0.6	3.61	0.38
	0.8	3.81	0.36
	1.0	4.12	0.36
n=25	0.1	2.90	0.21
	0.2	3.25	0.35
	0.4	3.45	0.32
	0.6	3.90	0.32
	0.8	4.18	0.33
	1.0	4.38	0.33

Table 5.5.2.1 The effect of concentration of sodium chloride supporting electrolyte and redox site loading on heterogeneous electron transfer parameters of $[Os(bipy)_2(PVI)_nCl]Cl$ modified electrodes.

Loading	Conc. M	k^o*10^4 cms^{-1}	α
n=5	0.1	1.08	0.25
	0.2	1.10	0.25
	0.4	1.35	0.33
	0.6	1.77	0.33
	0.8	1.84	0.33
	1.0	2.12	0.35
n=10	0.1	3.10	0.28
	0.2	3.80	0.32
	0.4	4.62	0.35
	0.6	4.93	0.41
	0.8	5.34	0.40
	1.0	5.72	0.40
n=15	0.1	2.58	0.30
	0.2	3.10	0.30
	0.4	3.85	0.30
	0.6	4.56	0.35
	0.8	4.85	0.40
	1.0	4.97	0.40
n=20	0.1	2.23	0.31
	0.2	2.51	0.32
	0.4	3.04	0.34
	0.6	3.65	0.35
	0.8	4.01	0.40
	1.0	4.25	0.40
n=25	0.1	1.75	0.31
	0.2	1.92	0.32
	0.4	2.35	0.35
	0.6	2.75	0.37
	0.8	3.10	0.36
	1.0	3.55	0.37

The effect of increasing NaCl concentration is to monotonically increase k^o for all loadings.

The transfer coefficient is insensitive to redox site loading, it does however, increase with increasing electrolyte concentration from a value of 0.29 ± 0.04 in 0.1 M NaCl to 0.39 ± 0.04 in 1.0 M NaCl.

Section 5.5.3 Sulphuric Acid

k^o increases as the electrolyte concentration is increased. For $25\geq n\geq 15$ much of the overall increase occurs between 0.6 and 0.8 M sulphuric acid. The 1:10 loading is more sensitive to the sulphuric acid concentration increasing from 4.50×10^{-4} cms^{-1} to 7.15×10^{-4} cms^{-1} on going from 0.1 to 1.0 M H_2SO_4. The 1:5 loading is less sensitive to changes in electrolyte concentration (Table 5.5.3.1). An increased redox site loading increases k^o until the 1:10 loading after which k^o decreases. These trends closely follow those discussed earlier for $D_{CT}(PS)$.

α is insensitive to both active site and electrolyte concentrations, maintaining a value of 0.47 ± 0.06. This is close to the theoretical value of 0.5 expected for a single electron, reversible reaction.

Section 5.5.4 Potassium Sulphate

k^o shows the same dependence on electrolyte concentration and redox site loading as that observed previously for $D_{CT}(PS)$. k^o increases almost monotonically as the electrolyte concentration is raised for all loadings except 1:10 where a significant increase occurs between 0.2 and 0.4 M potassium sulphate (Table 5.5.4.1). An increased $[Os(bipy)_2Cl]^+$ loading enhances k^o over the range 1:25 to 1:10 after which point k^o decreases.

Table 5.5.3.1 The effect of concentration of sulphuric acid supporting electrolyte and redox site loading on heterogeneous electron transfer parameters of $[Os(bipy)_2(PVI)_nCl]Cl$ modified electrodes.

Loading	Conc. M	k^o*10^4 cms^{-1}	α
n=5	0.1	3.65	0.45
	0.2	3.48	0.41
	0.4	3.81	0.42
	0.6	3.85	0.47
	0.8	3.90	0.51
	1.0	3.95	0.51
n=10	0.1	4.50	0.44
	0.2	5.11	0.47
	0.4	5.48	0.44
	0.6	6.21	0.50
	0.8	6.43	0.48
	1.0	7.15	0.49
n=15	0.1	3.24	0.45
	0.2	3.39	0.45
	0.4	3.43	0.46
	0.6	3.53	0.46
	0.8	4.30	0.48
	1.00	4.42	0.48
n=20	0.1	3.01	0.44
	0.2	3.18	0.44
	0.4	3.26	0.48
	0.6	3.39	0.45
	0.8	3.87	0.46
	1.0	3.98	0.48
n=25	0.1	2.78	0.45
	0.2	2.87	0.45
	0.4	3.09	0.46
	0.6	3.19	0.46
	0.8	3.56	0.50
	1.0	3.78	0.50

Table 5.5.4.1 The effect of concentration of potassium sulphate supporting electrolyte and redox site loading on heterogeneous electron transfer parameters of $[Os(bipy)_2(PVI)_nCl]Cl$ modified electrodes.

Loading	Conc. M	k^o*10^4 cms^{-1}	α
n=5	0.1	1.32	0.25
	0.2	1.41	0.34
	0.4	1.53	0.34
	0.6	2.43	0.49
n=10	0.1	3.71	0.27
	0.2	3.84	0.30
	0.4	5.15	0.34
	0.6	5.75	0.37
n=15	0.1	1.89	0.26
	0.2	2.19	0.32
	0.4	2.67	0.37
	0.6	3.28	0.44
n=20	0.1	1.43	0.30
	0.2	1.67	0.34
	0.4	1.82	0.35
	0.6	2.25	0.40
n=25	0.1	1.26	0.30
	0.2	1.43	0.31
	0.4	1.62	0.32
	0.6	2.10	0.34

The transfer coefficient is insensitive to redox site loading in 0.1 M K_2SO_4, maintaining a value of 0.28±0.03. As the electrolyte concentration is increased increases, the nature of this increase is however, dependent on the redox site loading. For the 1:5 loading α reaches a value of 0.49 in 1.0 M potassium sulphate.

Section 5.5.5 Toluene-4-sulphonic Acid

Figure 5.5.5.1 shows the effect of p-TSA concentration and redox site loading on k^o. k^o increases with increasing redox site loading in low electrolyte concentrations while in 1.0 M p-TSA k^o is insensitive to the films osmium content (Table 5.5.5.1). The rate of heterogeneous electron transfer increases with increasing electrolyte with much of the increase occurring between 0.6 and 0.8 M p-TSA for all redox site loading.

The transfer coefficient is insensitive to both redox site, and electrolyte concentration maintaining a value of 0.44±0.04 for all active site / electrolyte combinations.

Section 5.5.6 Perchloric Acid

Table 5.5.6.1 gives the dependence of the heterogeneous electron transfer parameters on both the concentration of $HClO_4$ and redox site loading. In 0.1 M electrolyte k^o increases linearly with increasing redox site loading. For higher concentrations of electrolyte k^o increases for $25 \geq n \geq 15$ before decreasing for higher loadings. k^o increases with increased perchloric acid concentration for all loadings, this increase is however, larger for the 1:15 loading.

The transfer coefficient also shows a disjoint behaviour around the 1:15 loading. For loadings higher than 1:15 α approaches the theoretical

Table 5.5.5.1 The effect of concentration of toluene sulphonic acid supporting electrolyte and redox site loading on heterogeneous electron transfer parameters of $[Os(bipy)_2(PVI)_nCl]Cl$ modified electrodes.

Loading	Conc. M	k^o*10^4 cms^{-1}	α
n=5	0.1	4.21	0.44
	0.2	4.72	0.45
	0.4	5.65	0.45
	0.6	6.00	0.45
	0.8	7.60	0.45
	1.0	8.23	0.44
n=10	0.1	3.98	0.44
	0.2	4.51	0.44
	0.4	5.23	0.45
	0.6	5.71	0.45
	0.8	7.45	0.45
	1.0	7.89	0.45
n=15	0.1	3.72	0.44
	0.2	4.27	0.44
	0.4	4.78	0.45
	0.6	5.54	0.44
	0.8	7.39	0.45
	1.0	7.62	0.44
n=20	0.1	3.18	0.45
	0.2	3.90	0.44
	0.4	4.54	0.45
	0.6	5.49	0.48
	0.8	7.36	0.48
	1.0	7.56	0.48
n=25	0.1	2.60	0.40
	0.2	3.37	0.40
	0.4	4.32	0.41
	0.6	5.45	0.40
	0.8	7.20	0.41
	1.0	7.50	0.41

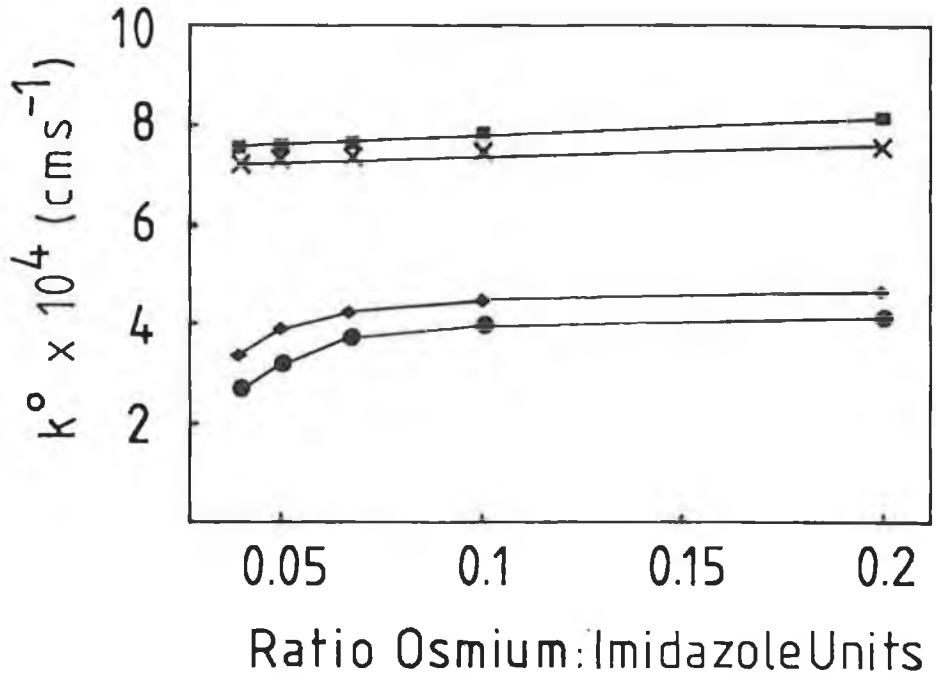

Figure 5.5.5.1 The effect of redox site concentration and toluene-4-sulphonic acid concentration on k^o for $[Os(bipy)_2(PVI)_nCl]Cl$ modified electrodes. The electrolyte concentrations are, from top to bottom, 1.0, 0.8, 0.2 and 0.1 M.

Table 5.5.6.1 The effect of concentration of perchloric acid supporting electrolyte and redox site loading on heterogeneous electron transfer parameters of $[Os(bipy)_2(PVI)_nCl]Cl$ modified electrodes.

Loading	Conc. M	k^o*10^4 cms^{-1}	α
n=5	0.1	1.72	0.47
	0.2	1.80	0.45
	0.4	1.86	0.45
	0.6	1.90	0.46
	0.8	2.19	0.46
	1.0	2.22	0.48
n=10	0.1	1.25	0.45
	0.2	1.96	0.45
	0.4	2.00	0.45
	0.6	2.21	0.46
	0.8	2.55	0.48
	1.0	2.71	0.47
n=15	0.1	0.84	0.35
	0.2	2.16	0.36
	0.4	2.30	0.38
	0.6	2.44	0.37
	0.8	2.87	0.37
	1.0	3.12	0.38
n=20	0.1	0.66	0.36
	0.2	1.43	0.35
	0.4	1.50	0.37
	0.6	1.55	0.36
	0.8	1.90	0.37
	1.0	2.20	0.38
n=25	0.1	0.53	0.35
	0.2	0.69	0.35
	0.4	0.82	0.34
	0.6	0.92	0.35
	0.8	1.05	0.35
	1.0	1.11	0.38

value of 0.5 expected for reversible single electron reactions, while for lower loadings it is suppressed to approximately 0.35.

Section 5.5.7 Lithium Perchlorate

In all concentrations of $LiClO_4$ k^o increases with increasing redox site loading for $25 \geq n \geq 15$ before decreasing at the 1:10 and 1:5 loadings respectively for low and high electrolyte concentrations. k^o shows a nearly linear increase as the electrolyte concentration is increased (Table 5.5.7.1). Where n = 15 and n = 10 k^o increases significantly between 0.2 and 0.4 M $LiClO_4$, for other loadings k^o increases in a near linear manner with increasing electrolyte concentration.

The transfer coefficient only approaches the theoretical value of 0.5 for the 1:5 loading in 0.8 and 1.0 M electrolyte. For lower loadings and electrolyte concentrations α has a value of approximately 0.35.

Table 5.5.7.1 The effect of concentration of lithium perchlorate supporting electrolyte and redox site loading on heterogeneous electron transfer parameters of $[Os(bipy)_2(PVI)_nCl]Cl$ modified electrodes.

Loading	Conc. M	k^o*10^4 cms^{-1}	α
n=5	0.1	1.10	0.35
	0.2	1.23	0.38
	0.4	1.34	0.39
	0.6	1.55	0.42
	0.8	1.61	0.45
	1.0	1.81	0.45
n=10	0.1	2.04	0.35
	0.2	2.53	0.36
	0.4	3.04	0.37
	0.6	3.19	0.36
	0.8	3.43	0.35
	1.0	3.69	0.36
n=15	0.1	2.19	0.35
	0.2	2.70	0.35
	0.4	3.19	0.35
	0.6	3.34	0.35
	0.8	3.48	0.35
	1.0	3.60	0.35
n=20	0.1	1.43	0.35
	0.2	1.55	0.35
	0.4	1.71	0.36
	0.6	1.90	0.36
	0.8	2.01	0.36
	1.0	2.21	0.38
n=25	0.1	0.83	0.35
	0.2	0.90	0.35
	0.4	1.04	0.35
	0.6	1.05	0.35
	0.8	1.41	0.35
	1.0	1.51	0.35

Section 5.6 Discussion of Homogeneous and Heterogeneous Charge Transport

The rates of homogeneous charge transport through $[Os(bipy)_2(PVI)_nCl]Cl$ films and from the electrode into such coatings is clearly dependent on the electrolyte type, its concentration and the redox site loading. In general for the above systems the rate of charge transport is also dependent on the timescale of the method used to evaluate it. A similar result was obtained for poly(4-vinylpyridine) films containing the $[Os(bipy)_2Cl]^+$ redox centre examined in this work. Both potential step and sweep experiments did, however, give the same result for several systems notably in sulphuric acid. As discussed previously the difference between $D_{CT}(PS)$ and $D_{CT}(CV)$ can arise because CV measurements are made at a longer timescale where equilibrium of all mobile species is more likely to be established.

In the short timescale potential step experiments species resident within the film are used to maintain electroneutrality within the film. This leads to the establishment of a kinetic equilibrium involving only highly mobile species within the film. This situation occurs because of the instantaneous demands of electroneutrality on oxidation of the redox centre [14]. Where the supporting electrolyte concentration is high there may be a large excess of charge compensating counterion within the film, in such circumstances the potential step measurements may involve an equilibrium of ions within the film as well as electrons. In low concentrations of electrolyte, processes such as Donnan exclusion may operate leading to an ion shortage within the film, and a kinetic situation involving only redox equilibrium [15] is established.

In contrast, at longer times a thermodynamic equilibrium will be established, in which all mobile species will reach equilibrium. This process, in contrast to the short timescale measurements will involve charge compensating counterion motion within the film, across the film/electrolyte boundary and in solution. The nature of the equilibrium observed using these electrochemical methods will be dependent on the magnitude of the potential gradient, charge compensating counterion availability, the extent of film swelling and the work terms associated with the swelling involved in the forced inclusion of charge compensating counterion as dictated by electroneutrality.

This means that where thermodynamic equilibrium is established very rapidly, the rate of homogeneous charge transport as measured by potential step and sweep methods will be similar. Such a situation appears for sulphuric acid, e.g in 1.0 M H_2SO_4 $D_{CT}(PS)$ for $[Os(bipy)_2(PVI)_{25}Cl]Cl$ is 1.15 x 10^{-9} cm^2s^{-1} while $D_{CT}(CV)$ is 1.08 x 10^{-9} cm^2s^{-1}. It is conceivable that a situation could arise in which a thermodynamic equilibrium could not be established even under cyclic voltammetry conditions, in these circumstances $D_{CT}(PS)$ and $D_{CT}(CV)$ could again agree, such a response does not however, appear to be observed for these films.

It is possible to maintain electroneutrality within the film during the oxidation cycle by ingress of a negatively charged counterion or egress of a positively charged co-ion. It is possible, therefore, that depending on the pH of the supporting electrolyte H^+ transport out of the film could play a role in the charge transport process. For the films discussed here such a process appears unlikely since $D_{CT}(PS)$ is similar at both pH 1 and pH 7.

Furthermore, the rate of charge transport is independent of the cation type, eg the same D_{CT}(PS) and D_{CT}(CV) values are observed in TeapCl, NaCl, LiCl and KCl. These observations strongly suggest that only anion transport is significant in determining the rate of charge transport for these films. It is possible that the species contributing to the equilibrium established are different at different timescales. It has been suggested that for polythionine films protonic species dominate the short timescale response, while at longer times all mobile species reach equilibrium populations [16].

An alternative explanation of the differences observed between D_{CT}(PS) and D_{CT}(CV) is that differential film swelling occurs through the film thickness. This involves a model in which that portion of the film adjacent to the electrode is smooth, homogeneous and less swollen than that portion in direct contact with the supporting electrolyte. The exterior region would therefore, have a lower fixed site concentration leading to an underestimation of the charge transport rate. Such a process is considered unlikely, since the difference between D_{CT}(PS) and D_{CT}(CV) can be as large as a factor of 450. This would require differential swelling between the inner and outer regions of the film of over 2000 %. Such a large difference in concentration seems unlikely. Furthermore, it is in electrolytes which are expected to protonate the free nitrogens of the polymer backbone and induce film swelling, where D_{CT}(PS) and D_{CT}(CV) are similar.

The rate of homogeneous charge transport through these materials immobilised on electrode surfaces is clearly related to the nature and concentration of charge compensating counterion in solution. Unlike other systems, D_{CT} is not directly related to the anion size or molar volume [17]. This point is emphasised by the D_{CT} values obtained in p-TSA. The molar

volume per unit charge of this anion is considerably larger, than for example sulphate, the rate of charge transport is however, considerably faster. This suggests that other properties of the electrolyte solution such as swelling ability exert more influence over D_{CT} than does anion size or volume.

In general, for both D_{CT}(PS) and D_{CT}(CV) the rate of charge transport is insensitive to electrolyte concentration in all electrolytes examined at high redox site loadings. Furthermore, the activation energies associated with this process is generally quite low 15-40 kJ/Mol and is coupled to a negative entropy term. These observations strongly suggest that ion transport and availability directly influences charge transport for these systems. For the other limiting case of low redox site loading / high electrolyte concentration both D_{CT}(PS) and D_{CT}(CV) are sensitive to the electrolyte concentration show high activation energies and positive entropy terms. These positive entropy terms are associated with a disordering process limiting the rate of charge transport [18]. For these cases, it appears therefore, that segmental polymer chain motion limits D_{CT}. That such a rate limiting step should be observed is reasonable since the intersite separation will be of the order of 65 A [19], thus requiring movement of the polymer chains to which the redox centres are bound for electron self exchange.

In practice the observation of these limiting cases depends on factors such as the operation of Donnan exclusion, film swelling and the ease of anion transport within the film. In HCl for example, D_{CT}(PS) is insensitive to redox site loading, (some decrease is observed but this may be a consequence of

overestimating the fixed site concentration for high loadings), E_a(PS) is low and coupled to a negative entropy for all loadings. These observations suggest that ion transport represents the rate determining step. In cyclic voltammetry experiments two limiting cases, as discussed above are observed. For low loadings D_{CT}(CV) is sensitive to electrolyte concentration and has large activation energies coupled to positive entropies which suggests segmental polymer chain motion as the rate determining event. In contrast, as the active site loading is increased to 1:10 and 1:5 D_{CT}(CV) is less sensitive to HCl concentration and has a reduced activation energy and negative entropy terms. These observations suggest an ion transport limitation as expected. NaCl shows a similar behaviour with the exception that D_{CT}(CV) is limited by polymer chain movement for all loadings in 1.0 M NaCl.

In H_2SO_4 as supporting electrolyte D_{CT}(PS) and D_{CT}(CV) are more similar than in other electrolytes. As well as this, the nature of the rate determining steps as measured by potential step and sweep methods are the same (vide infra). In 0.1 M electrolyte both D_{CT}(PS) and D_{CT}(CV) are insensitive to redox site loading. The activation energies are of similar magnitude (35-55 kJ/Mol) and are coupled to negative entropy terms suggesting an ion transport limitation. In 1.0 M sulphuric acid both D_{CT}(PS) and D_{CT}(CV) are more sensitive to electrolyte concentration. Where $25 \geq n \geq 10$ D_{CT}(PS) shows large activation energies and positive entropies indicating that charge transport is limited by segmental polymer chain motion. For higher redox site loadings E_a(PS) is reduced and coupled to a negative entropy term. This suggests that ion movement is the rate determining step. In the case of the cyclic voltammetry experiments a similar behaviour is observed except that the change in the rate determining event occurs at the 1:15

loading.

Both K_2SO_4 and p-TSA exhibit low activation energies coupled to negative entropy terms for all loadings and electrolyte concentrations. This strongly suggests an ion transport limitations for all loadings in both 0.1 and 1.0 M electrolytes. The response of both D_{CT}(PS) and D_{CT}(CV) to changes in electrolyte and redox site loading is distinctly different in both electrolytes. In K_2SO_4 D_{CT}(PS) initially increases with increasing redox site loading before decreasing at the 1:5 loading. In p-TSA D_{CT}(PS) increases over the whole redox loading range examined. The cyclic voltammetry experiments also shows a different behaviour in the two electrolytes. In K_2SO_4 D_{CT}(CV) decreases systematically with increasing redox site loading, this process being reflected in an increased activation energy. In contrast, in p-TSA, D_{CT}(CV) increases linearly with increasing osmium content within the film and the activation energy remains invariant. These observations clearly show that the observed charge transport rate and dependency on electrolyte and active site concentration is a product not only of the rate determining event, but also, of factors such as film swelling and anion mobility.

The charge transport behaviour of these modified electrodes is unusual in that D_{CT}(CV) decreases with increasing perchlorate concentration. As discussed previously (chapter 4) the perchlorate salts of these materials are insoluble in aqueous media. The dependence of E_a(PS) on redox site loading is similar in both 0.1 and 1.0 M perchloric acid. For $25 \geq n \geq 15$ the activation energy is large and is coupled to positive entropy terms. When the active site loading is increased to 1:10 and 1:5 the activation energy is reduced and is coupled to a negative entropy term. These observations suggest that charge

transport is limited by polymer chain and ion movement at low and high redox site loadings respectively. In 1.0 M perchloric acid the response as observed using cyclic voltammetry is similar except that the transition from polymer chain to ion movement occurs at the 1:10 loading. In 0.1 M $HClO_4$ $D_{CT}(CV)$ is again limited by polymer chain movement for $25 \geq n \geq 15$ and by ion transport for the 1:5 loading. The intermediate loading of 1:10 shows dual slope behaviour observed previously for the poly(4-vinylpyridine) films (chapter 4). For temperatures greater than 285 K $E_a(CV)$ is large and coupled to a positive entropy term, below this temperature $E_a(CV)$ is reduced and associated with a negative entropy. These observations suggest that polymer chain movement limits $D_{CT}(CV)$ for temperatures above 285 K while below this temperature ion transport is the rate determining step. In lithium perchlorate the short timescale potential step measurements all show small activation energies and negative entropy terms suggesting an ion transport limitation. The activation energy response observed via cyclic voltammetry is similar in both 0.1 and 1.0 M $LiClO_4$. For $25 \geq n \geq 15$ a large activation, positive entropy behaviour is observed indicating polymer chain movement limits $D_{CT}(CV)$. At the highest loading examined (1:5) $E_a(CV)$ is reduced and associated with negative entropy terms suggesting an ion transport limitation. The 1:10 loading shows polymer chain and ion movement at high and low electrolyte concentrations respectively.

The rate of heterogeneous electron transfer measured as k^o is similarly affected by changes in the electrolyte and redox site concentration as $D_{CT}(PS)$. This behaviour is significant since it implies that processes such as ion movement similarly affect both homogeneous and heterogeneous charge transfer [12,13,20]. This suggests that the deposited film controls the concentration of electrolyte at the film / electrode interface and that this

process influences the formation of the electrical double layer and hence k^o and α. Significantly the dependence of D_{CT}(PS) and k^o on the fixed site concentration is not reflected in the transfer coefficient [21]. α is typically more sensitive to electrolyte concentration than the fixed site concentration again suggesting that ion availability within the film as dictated largely by the films Donnan potential directly influences the heterogeneous kinetics.

Section 5.7 Concluding Remarks.

The redox behaviour of $[Os(bipy)_2(PVI)_nCl]Cl$ immobilised on glassy carbon electrodes is nearly ideally reversible for all loadings and electrolytes except for those based on perchlorate. The rate of charge transport through these films is dependent on the supporting electrolyte solution, the redox site loading and the experimental timescale. Significantly, both $D_{CT}(PS)$ and $D_{CT}(CV)$ are less sensitive to changes in the pH of the supporting electrolyte, neither is there a direct relationship between D_{CT} and the anion molar volume. The optimum rate of homogeneous charge transport is not attained for the highest redox site loading except in the case of toluene sulphonic acid.

The rate of heterogeneous electron transfer is also dependent on the ion population within the film, which in certain cases appears to be dictated by Donnan exclusion. The formation of the double layer and symmetry of the energy barrier to electron transfer also appears to be controlled more by the nature of the supporting electrolyte than the redox site loading.

Section 5.8 References

1. T. T. Li and M. J. Weaver, J. Am. Chem. Soc., 1984, 106, 6107
2. J. R. Miller, L. T. Calcaterra and G. L. Closs, J. Am. Chem. Soc., 1984, 106, 1722
3. E. J. Cohn and J. T. Edsall in "Proteins Amino Acids and Peptides", Rheinhold Publishing Corp., New York, 1943
4. T. Kunitake, F. Shimada and C. Aso, J. Am. Chem. Soc., 1969, 91, 2716
5. C. G. Overberger, J. C. Salamone and S. Yaroslavsky, J. Am. Chem. Soc., 1967, 89, 6231
6. J. L. Lippert, J. A. Robertson, J. R. Havens and J. S. Tan, Macromols., 1985, 18, 63
7. P. Ferruti and R. Barbucci, Adv. Polym. Sci., 1984, 58, 55
8. S. M. Geraty and J. G. Vos, J. Chem. Soc. Dalton Trans., 1987, 3073
9. A. P. Brown and F. C. Anson, Anal. Chem., 1977, 49, 1589
10. M. E. G. Lyons, H. G. Fay, J. G. Vos and A. J. Kelly, J. Electroanal. Chem., 1988, 250, 207
11. P. Daum, J. R. Lenhard, D. Rolison and R. W. Murray, J. Am. Chem. Soc., 1980, 102, 4649
12. H. Daifuku, K. Aoki, K. Tokuda and H. Matsuda, J. Electroanal. Chem., 1985, 183, 1
13. N. Oyama, T. Ohsaka, M. Kaneko, K. Sato and H. Matsuda, J. Am. Chem. Soc., 1983, 105, 6003
14. S. B. Khoo, J. K. Foley and S. Pons, J. Electroanal. Chem., 1986, 215, 273
15. S. Bruckenstein and A. R. Hillman, J. Phys. Chem., 1988, 92, 4837
16. S. Bruckenstein, A. R. Hillman and M. J. Swann, J. Electrochem. Soc., 1990, 137, 1323

17. W. G. Albery, M. G. Boutelle, P. J. Colby and A. R. Hillman, J. Electroanal. Chem., 1982, 133, 135

18. S. M. Oh and L. R. Faulkner, J. Am. Chem. Soc., 1989, 111, 5613

19. D. P. Rillema, D. S. Jones and H. A. Levy, J. Chem. Soc. Chem. Commun., 1979, 849

20. T. Ohsaka, S. Kunimura and N. Oyama, Electrochim. Acta, 1988, 33, 639

21. N. Oyama, T. Ohsaka and T. Ushirogouchi, J. Phys. Chem., 1984, 88, 5274

CHAPTER 6

Charge Transport Properties of Poly(N-vinylimidazole) Polymers Containing $[Os(N)_6]^{2+/3+}$ Moieties

Section 6.1 Introduction

The investigation of metallopolymers as electrode modifiers is one of the more active areas in contemporary electrochemistry [1-3]. Through these investigations it is becomingly increasingly apparent that the physicochemical properties of the polymer phase exert considerable influence on the electrochemical properties of the modified electrodes [4-6]. In previous chapters the effect of changes in the nature and concentration of the supporting electrolyte, the redox site loading and the nature of the polymer backbone were explored. These studies clearly showed that D_{CT} is influenced by these parameters and by the experimental timescale. In this chapter the effect of altering the nature of the coordinated site from mono to bis coordination is examined for the case of $[Os(bipy)_2(PVI)_{10}](Cl)_2$ films. The presence of $[Os(N)_6]^{2+/3+}$ centres within the polymer matrix is expected to increase the structural rigidity of the matrix. It is anticipated that the measurement of charge transport parameters for this material will give useful information about the local microenvironment of the redox centre and hence about the polymer matrix. In temperature dependent measurements, the immobile redox centre acts as an internal sensor giving information about segmental polymer chain motion and about the movement of anionic species through the matrix. This is valuable information which is difficult to obtain by other methods.

The influence of the supporting electrolyte on the heterogeneous kinetics is also considered.

Section 6.2 Experimental

Materials $[Os(bipy)_2(PVI)_{10}](Cl)_2$ was prepared as described previously in chapter 2. The density of the metallopolymer was estimated in dichloromethane/petroleum ether mixture as 1.07 g/cm^3, this gives a maximum concentration of 0.71 M for osmium centres within the film. The separation of the redox centres is taken as 25 Å.

Apparatus and procedures Electrochemical measurements were performed using an E. G. & G. Model 273 potentiostat/ galvanostat and the experimental methods outlined in chapter 3.

The values for the diffusion coefficients, heterogeneous electron transfer rates and activation parameters are reproducible to within ± 2% on a single coating and to ± 10% between coatings. Transfer coefficients are accurate to ±0.05.

Section 6.3 Results: The Effect of Electrolyte Concentration on the Rate of Homogeneous and Heterogeneous Charge Transfer Reactions of $[Os(bipy)_2(PVI)_{10}](Cl)_2$ Films.

Section 6.3.1 General layer properties. When deposited from methanolic solutions onto glassy carbon electrodes, the metallopolymer shows the expected single eleetron redox behaviour in all electrolytes examined (see Figure 6.3.1.1). The Os(II/III) redox couple is observed at about 420 mV vs SCE, depending on the electrolyte, and is photochemically and thermally stable. The formal peak potential observed in CH_3CN/0.1 M TEAP of 450 mV vs SCE is

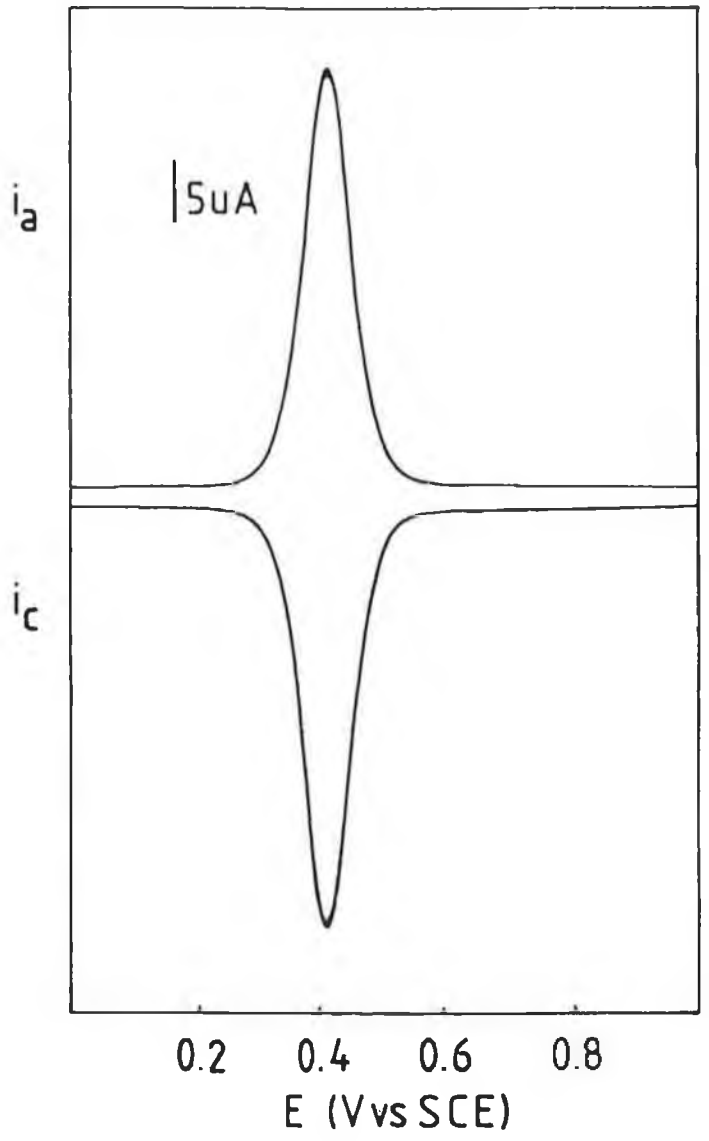

Figure 6.3.1.1 Cyclic voltammogram of $[Os(bipy)_2(PVI)_{10}](Cl)_2$ on a glassy carbon electrode. Scan rate 5 mV/s. 0.1 M HCl as supporting electrolyte. Surface coverage 1.7×10^{-8} molcm^{-2}.

similar to that observed for the analogous mononuclear model compound $[Os(bipy)_2(Meim)_2]^{2+}$ (E_0 = 475 mV Meim = N-methylimidazole) and is indicative of the presence of an $[Os(N_6)]^{2+}$ moiety [7]. The electrochemical data, together with electronic spectra and the synthetic conditions are consistent with a molecular formula $[Os(bipy)_2(PVI)_{10}](Cl)_2$, where of the ten PVI units present per osmium atom, two are coordinatively bound to the metal centre.

Potential step chronoamperometry and sampled current voltammetry have been used, as described in sections 1.3.2 and 1.3.3 to evaluate homogeneous charge transport rates ($D_{CT}(PS)$). Cyclic voltammetry performed under semi-infinite diffusion conditions has also been used, as described in section 1.3.1, to calculate a homogeneous charge transport rate labelled $D_{CT}(CV)$.

Sampled current voltammetry has also been utilised to examine the rate of heterogeneous electron transfer from the glassy carbon electrode into the modifying film. A typical sampled current voltammogram is illustrated in Figure 6.3.1.2. These sigmoid shaped waves are similar to those observed at unmodified electrodes for solution phase reactants. The cathodic currents increase with decreasing sampling time τ and at the same time the half wave potentials of the voltammograms for the oxidation process shift in a positive direction with decreasing sampling time. This behaviour is accepted as being indicative of Butler-Volmer kinetics [8] and the conventional analysis for sampled current voltammograms as described in section 1.3.3 can, therefore, be used.

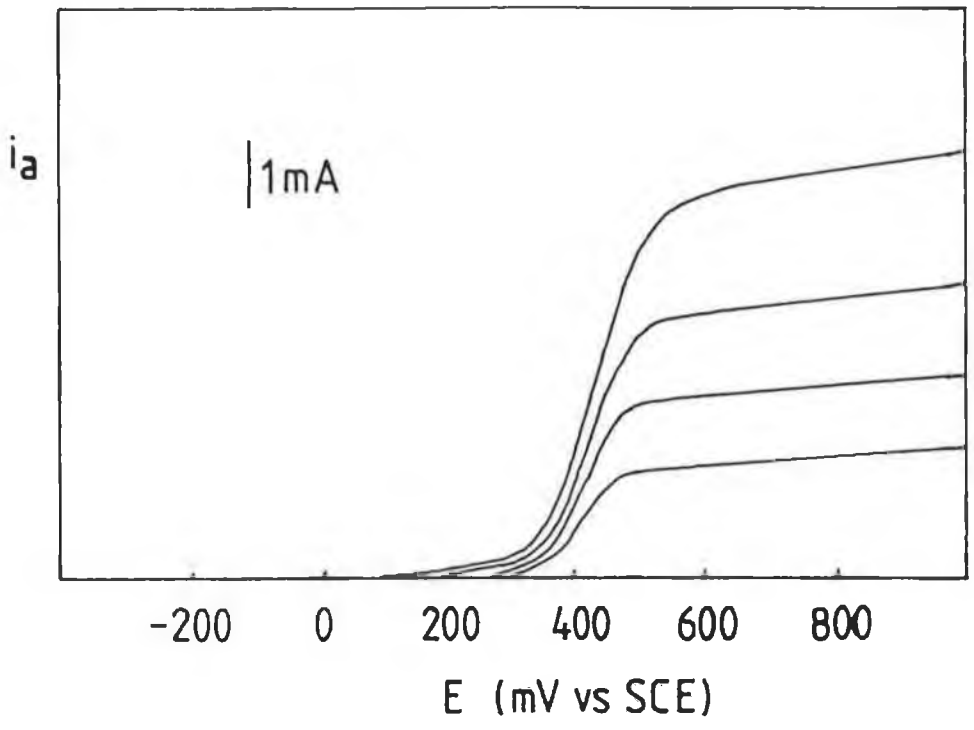

Figure 6.3.1.2 Typical sampled current voltammograms for the Os(II/III) oxidation within $[Os(bipy)_2(PVI)_{10}](Cl)_2$ films. Electrolyte 0.1 M HCl. Sampling times are, from top to bottom, 1, 2, 4 and 10 ms. Surface coverage 2 x 10^{-8} molcm^{-2}.

Section 6.3.2 Chloride Based Electrolytes

In hydrochloric acid both $D_{CT}(PS)$ and $D_{CT}(CV)$ increase linearly as the electrolyte concentration is increased (see Table 6.3.2.1). $D_{CT}(CV)$ is, however, more sensitive to HCl concentration. The rate of homogeneous charge transport in NaCl is similar to that observed in HCl. Both $D_{CT}(PS)$ and $D_{CT}(CV)$ show a more rapid increase as the NaCl concentration is increased above 0.6 M. The rate of heterogeneous electron transfer is approximately 1.5 x 10^{-4} cms^{-1} and is similar for all electrolyte concentrations in both HCl and NaCl.

The transfer coefficient increases in HCl from 0.2 in 0.1 M HCl to 0.32 in 1.0 M HCl. In NaCl it remains approximately constant at a value of 0.19 ± 0.02.

Section 6.3.3 Sulphate Based Electrolytes

$D_{CT}(PS)$ increases linearly from 4.17 x 10^{-10} cm^2s^{-1} to 8.25 x 10^{-10} cm^2s^{-1} as the sulphuric acid concentration is increased from 0.1 to 1.0 M as shown in Figure 6.3.3.1 (Table 6.3.3.1). $D_{CT}(CV)$ also increases linearly with increasing electrolyte concentration. The overall change is, however, significantly larger than that observed using potential step methods, with $D_{CT}(CV)$ increasing by a factor of 5 over the 0.1 to 1.0 M concentration range. The effect of an increase of the pH of the supporting electrolyte to 7 on the rate of charge propagation has been examined using potassium sulphate as supporting electrolyte. $D_{CT}(PS)$ is of comparable magnitude to that observed in sulphuric acid. However, $D_{CT}(CV)$ is reduced by a factor of approximately 10 compared to the H_2SO_4 values. Both $D_{CT}(PS)$ and $D_{CT}(CV)$ values increase as the potassium sulphate concentration is increased. As observed for

Table 6.3.2.1: The effect of concentration of chloride based supporting electrolytes on charge transport parameters of $[Os(bipy)_2(PVI)_{10}](Cl)_2$ modified electrodes.

Electro-lyte	Conc. M	D_{CT}(PS) $*10^{10}$ cm^2s^{-1}	k^o $*10^4$ cms^{-1}	α	D_{CT}(CV) $*10^{11}$ cm^2s^{-1}	E^o V
HCl	0.1	5.22	1.67	0.20	4.35	0.415
	0.2	5.62	1.60	0.20	7.45	0.395
	0.4	5.76	1.70	0.27	8.05	0.385
	0.6	6.15	1.57	0.34	10.50	0.390
	0.8	6.61	1.62	0.32	10.50	0.390
	1.0	7.06	1.94	0.32	13.80	0.385
NaCl	0.1	5.58	1.17	0.20	3.16	0.395
	0.2	5.96	1.29	0.19	3.69	0.400
	0.4	6.10	1.27	0.21	3.91	0.390
	0.6	6.57	1.42	0.18	4.86	0.390
	0.8	8.49	1.57	0.18	7.31	0.390
	1.0	11.10	1.52	0.19	8.88	0.395

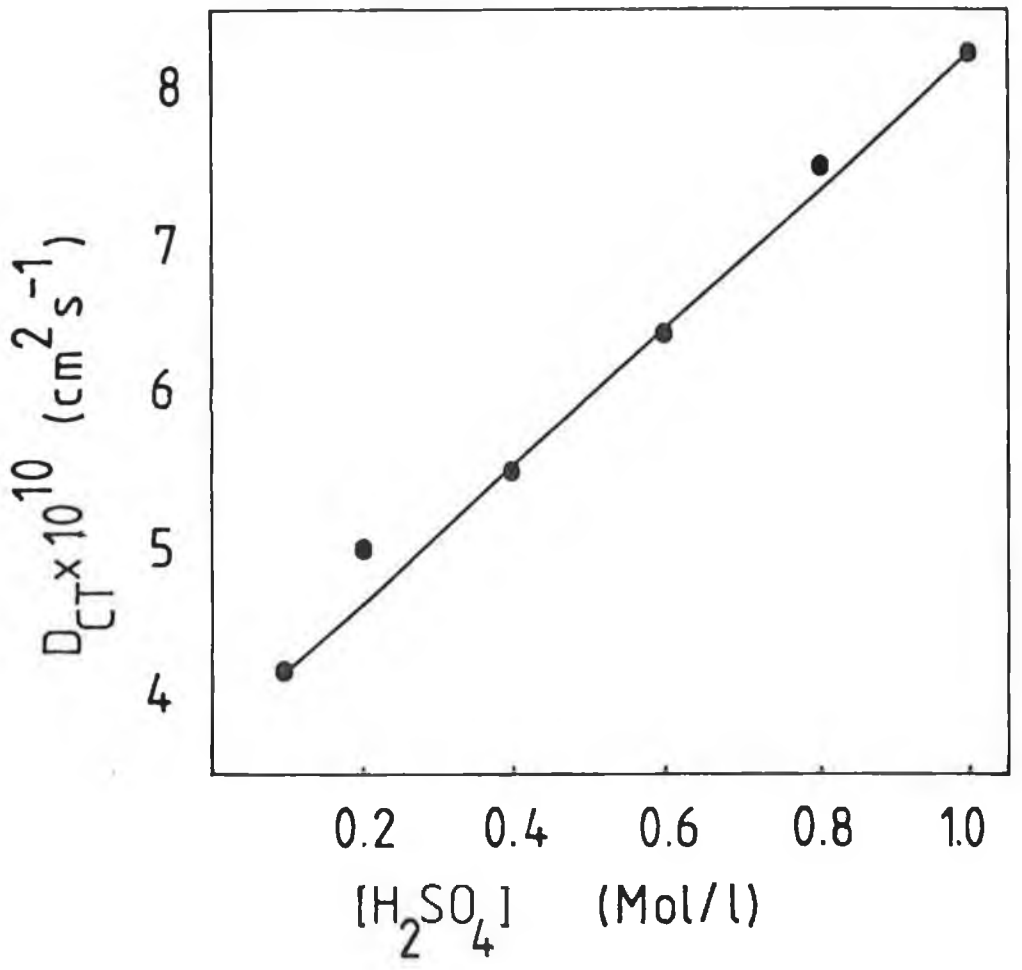

Figure 6.3.3.1 The effect of sulphuric acid concentration on D_{CT}(PS) for thin films of $[Os(bipy)_2(PVI)_{10}](Cl)_2$.

Table 6.3.3.1 The effect of concentration of sulphate based supporting electrolytes on charge transport parameters of $[Os(bipy)_2(PVI)_{10}](Cl)_2$ modified electrodes.

Electro-lyte	Conc. M	D_{CT}(PS) $*10^{10}$ cm^2s^{-1}	k^o $*10^4$ cms^{-1}	α	D_{CT}(CV) $*10^{11}$ cm^2s^{-1}	E^o V
H_2SO_4	0.1	4.17	1.71	0.45	5.90	0.400
	0.2	5.03	1.85	0.45	9.30	0.380
	0.4	5.48	1.64	0.45	19.03	0.390
	0.6	6.39	1.57	0.45	20.06	0.390
	0.8	7.52	1.68	0.45	25.16	0.385
	1.0	8.25	1.58	0.45	29.05	0.380
K_2SO_4	0.1	3.34	0.64	0.40	0.29	0.420
	0.2	6.17	0.88	0.40	0.44	0.430
	0.4	6.90	1.24	0.41	0.81	0.420
	0.6	8.74	1.62	0.39	1.16	0.415

sulphuric acid, the increase observed in $D_{CT}(CV)$ is relatively larger than that observed for $D_{CT}(PS)$.

The rate of heterogeneous electron transfer remains approximately constant ($1.67 \pm 0.18 \times 10^{-4}$ cms^{-1}) as the sulphuric acid concentration is increased. In contrast k^o increases as the potassium sulphate concentration is increased. The transfer coefficient is insensitive to either sulphuric acid (0.45) or potassium sulphate (0.40 ± 0.01) concentration.

Section 6.3.4 Toluene-4-Sulphonic Acid Electrolyte

$D_{CT}(PS)$ increases from 16.5×10^{-10} cm^2s^{-1} to 23.5×10^{-10} cm^2s^{-1} upon changing the electrolyte concentration from 0.1 to 1.0 M electrolyte (Table 6.3.4.1). $D_{CT}(CV)$ increases from 0.61×10^{-10} cm^2s^{-1} to 2.22×10^{-10} cm^2s^{-1} on going from 0.1 to 0.2 M pTSA, after which point $D_{CT}(CV)$ is rather insensitive to further increase in the electrolyte concentration. The rate of heterogeneous electron transfer is not greatly affected by electrolyte concentration. The transfer coefficient does increase from 0.35 to 0.41 from 0.1 to 1.0 M pTSA.

Section 6.3.5 Perchlorate Based Electrolytes

In contrast with the other electrolyte systems examined an increased perchlorate concentration decreases both $D_{CT}(PS)$ and $D_{CT}(CV)$. The $D_{CT}(PS)$ values are significantly larger than those observed for the other electrolytes (Table 6.3.5.1). However, $D_{CT}(PS)$ decreases from 4.05×10^{-9} cm^2s^{-1} to 1.05×10^{-9} cm^2s^{-1} when the perchloric acid concentration is increased from 0.1 to 1.0 M. The difference between $D_{CT}(PS)$ and $D_{CT}(CV)$ is larger than that observed for the other electrolytes examined, approximately

Table 6.3.4.1 The effect of concentration of p-Toluene sulphonic acid as supporting electrolyte on charge transport parameters of $[Os(bipy)_2(PVI)_{10}](Cl)_2$ modified electrodes.

Electro-lyte	Conc. M	D_{CT}(PS) $*10^{10}$ cm^2s^{-1}	k^o $*10^4$ cms^{-1}	α	D_{CT}(CV) $*10^{11}$ cm^2s^{-1}	E^o V
pTSA	0.1	16.5	2.21	0.35	6.17	0.410
	0.2	16.8	2.21	0.35	22.23	0.455
	0.4	17.5	2.31	0.35	23.06	0.440
	0.6	18.9	2.10	0.40	24.11	0.430
	0.8	21.0	2.35	0.40	25.89	0.425
	1.0	23.5	2.40	0.41	26.07	0.420

Table 6.3.5.1 The effect of concentration of perchlorate based supporting electrolytes on charge transport parameters of $[Os(bipy)_2(PVI)_{10}](Cl)_2$ modified electrodes.

Electro-lyte	Conc. M	D_{CT}(PS) $*10^{10}$ cm^2s^{-1}	k^o $*10^4$ cms^{-1}	α	D_{CT}(CV) $*10^{11}$ cm^2s^{-1}	E^o V
$HClO_4$	0.1	40.5	2.48	0.20	4.74	0.415
	0.2	39.8	2.45	0.18	4.80	0.415
	0.4	33.0	2.34	0.14	3.59	0.415
	0.6	30.9	2.29	0.13	2.62	0.410
	0.8	26.4	2.12	0.14	2.51	0.400
	1.0	10.5	1.57	0.11	2.10	0.395
$LiClO_4$	0.1	38.4	2.51	0.18	8.91	0.435
	0.2	38.2	2.45	0.20	6.86	0.415
	0.4	39.3	2.40	0.18	5.25	0.415
	0.6	20.2	2.01	0.15	4.85	0.415
	0.8	19.8	1.97	0.15	4.11	0.420
	1.0	19.7	1.93	0.14	3.53	0.420

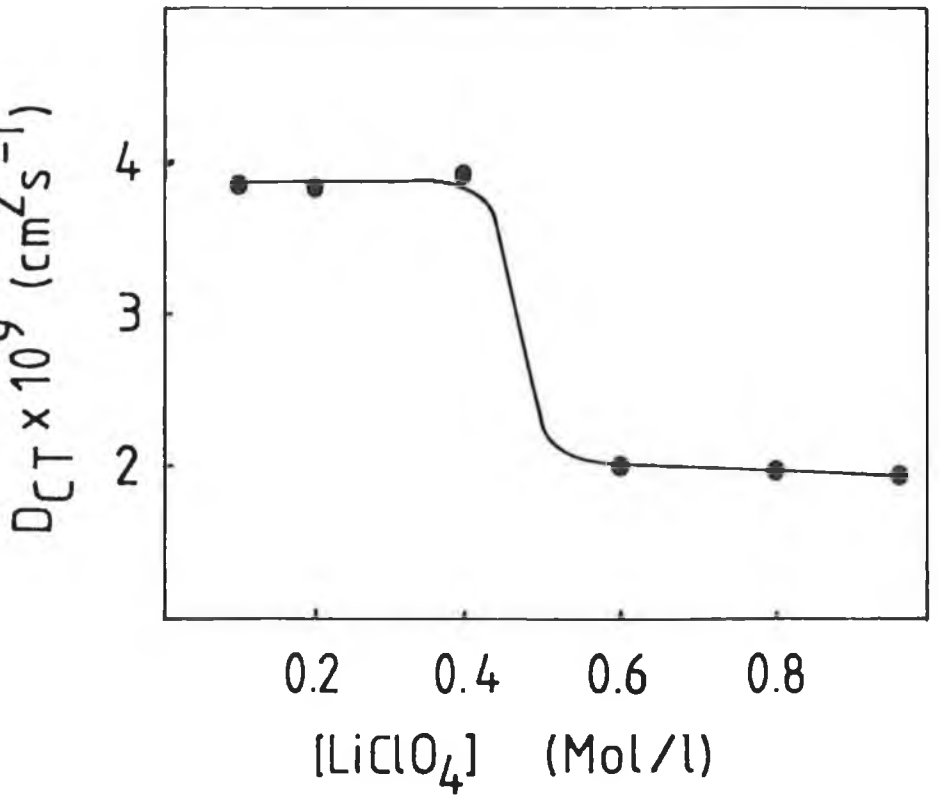

Figure 6.3.5.1 The effect of lithium perchlorate concentration on $D_{CT}(PS)$ for thin films of $[Os(bipy)_2(PVI)_{10}](Cl)_2$.

a factor of 100. D_{CT}(CV) also decreases from 4.74 x 10^{-11} cm^2s^{-1} to 2.10 x 10^{-11} cm^2s^{-1} over the 0.1 to 1.0 M concentration range with much of this decrease occurring between 0.2 and 0.6 M perchloric acid.

Charge transport rates in lithium perchlorate are of similar magnitude to those observed in perchloric acid. The effect of lithium perchlorate concentration on D_{CT}(PS) is illustrated in Figure 6.3.5.1. This figure shows that D_{CT}(PS) is insensitive to $LiClO_4$ concentration over the 0.1 to 0.4 M range, but decreases for the 0.6 M concentration after which point D_{CT}(PS) is again insensitive to lithium perchlorate concentration. D_{CT}(CV) decreases from 8.91 x 10^{-11} to 3.53 x 10^{-11} cm^2s^{-1} when the lithium perchlorate concentration is increased from 0.1 to 1.0 M (Table 6.3.5.1).

The rate of heterogeneous charge transfer decreases as the perchloric acid concentration is increased, reducing from 2.48 x 10^{-4} cms^{-1} to 1.57 x 10^{-4} cms^{-1}. In lithium perchlorate k^o shows a similar decrease from 2.51 x 10^{-4} cms^{-1} to 1.93 x 10^{-4} cms^{-1} on going from 0.1 to 1.0 M electrolyte. In both electrolytes the transfer coefficient decreases from a value of approximately 0.20 to 0.11 on going from 0.1 to 1.0 M electrolyte.

Section 6.4 Determination of Activation Parameters

The evaluation of thermodynamic parameters can be useful in the identification of the rate determining step of the charge transport process [9-11] and can provide useful information as to temperature effects on polymer morphology. Activation energies have been evaluated in both 0.1 and 1.0 M electrolytes by varying the temperature of the contacting electrolyte over the range 278-303 K in accordance with the methods described in section 3.4 and the results presented in tables 6.4.1 and 6.4.2.

Table 6.4.1 : Activation parameters for charge transport through $[Os(bipy)_2(PVI)_{10}](Cl)_2$ films as obtained by potential step methods.

Electrolyte		$E_a(PS)$ kJ/Mol	$\Delta H(PS)^{\ddagger}$ kJ/Mol	$\Delta S(PS)^{\ddagger}$ $JMol^{-1}K^{-1}$	$\Delta G(PS)^{\ddagger}$ kJ/Mol
HCl	0.1 M	23.8	21.3	-98.2	50.6
	1.0 M	6.6	4.1	-153.4	49.8
NaCl	0.1 M	19.3	16.8	-112.7	50.4
	1.0 M	3.9	1.4	-158.7	48.7
H_2SO_4	0.1 M	15.8	13.3	-126.9	51.1
	1.0 M	14.6	12.1	-125.2	49.5
K_2SO_4	0.1 M	13.7	11.2	-135.8	51.7
	0.6 M	12.8	10.3	-139.2	49.3
pTSA	0.1 M	26.4	23.9	-79.9	47.7
	1.0 M	9.3	6.8	-134.3	46.9
$HClO_4$	0.1 M	9.8	7.3	-128.1	45.5
	1.0 M	3.6	1.1	-160.2	48.9
$LiClO_4$	0.1 M	15.4	12.9	-109.8	45.6
	1.0 M	36.3	33.8	-45.2	47.3

Table 6.4.2 : Activation parameters for charge transport through $[Os(bipy)_2(PVI)_{10}](Cl)_2$ films as obtained by cyclic voltammetry.

Electrolyte		$E_a(CV)$ kJ/Mol	$\Delta H(CV)^{\ddagger}$ kJ/Mol	$\Delta S(CV)^{\ddagger}$ $JMol^{-1}K^{-1}$	$\Delta G(CV)^{\ddagger}$ kJ/Mol
HCl	0.1 M	104.6	102.1	152.3	56.7
	1.0 M	65.4	62.9	30.4	53.9
NaCl	0.1 M	88.4	85.9	95.3	57.5
	1.0 M	65.4	62.9	26.7	54.9
H_2SO_4	0.1 M	15.8	13.3	-143.1	56.0
	1.0 M	110.1	107.7	186.5	52.0
K_2SO_4	0.1 M	35.6	33.1	-101.7	63.4
	0.6 M	91.5	89.0	97.4	60.0
pTSA	0.1 M	26.1	23.6	-108.2	55.9
	1.0 M	65.7	63.2	36.6	52.3
$HClO_4$	0.1 M	98.2	95.7	131.5	56.5
	1.0 M	102.3	99.8	138.5	58.5
$LiClO_4$	0.1 M	107.5	105.0	167.6	55.0
	1.0 M	47.9	45.4	-36.7	57.2

Section 6.4.1 Chloride Based Electrolytes.

In 0.1 M HCl E_a(PS) is 23.6 kJ/Mol, a value which decreases to 6.6 kJ/Mol in 1.0 M electrolyte. Both of these activation energies are coupled to negative entropy terms. This is in contrast to the cyclic voltammetry values which show positive entropy terms in both 0.1 and 1.0 M HCl. As observed for E_a(PS), E_a(CV) is reduced in the higher concentration of electrolyte.

In sodium chloride a similar behaviour is observed. Both E_a(PS) and E_a(CV) are reduced in 1.0 M NaCl compared to 0.1 M NaCl. The cyclic voltammetry measurements show positive entropy terms, while variable temperature chronoamperometry show negative entropy terms.

Section 6.4.2 Sulphate Based Electrolytes.

E_a(PS) is insensitive to the electrolyte concentration in both sulphuric acid and potassium sulphate. In both 0.1 and 1.0 M sulphuric acid, E_a(PS) is 15.2 $\pm$ 0.6 kJ/Mol, while for the same concentrations of potassium sulphate E_a(PS) is 13.3 $\pm$ 0.5 kJ/Mol. These activation energies are coupled to negative entropy terms. The cyclic voltammetry values are larger and show differences between the 0.1 and 1.0 M values. In 0.1 M sulphuric acid the activation energy is low (15.8 kJ/Mol) and coupled to a negative entropy term. This increases to 110.1 kJ/Mol and the entropy term becomes positive in 1.0 M sulphuric acid. A similar response is observed in potassium sulphate with E_a(CV) increasing from 35.6 to 91.5 kJ/Mol on increasing the K_2SO_4 concentration from 0.1 to 1.0 M. The entropy term changes from negative to positive over this concentration range.

Section 6.4.3 Toluene-4-Sulphonic Acid

In pTSA E_a(PS) decreases from 26.4 to 9.3 kJ/Mol on going from 0.1 to 1.0 M electrolyte. Both activation energies are coupled to negative entropy terms. When examined using variable temperature cyclic voltammetry the activation energy shows an increase from 26.1 to 65.7 kJ/Mol on going from 0.1 to 1.0 M pTSA. This is connected to a change of the sign of the entropy term from negative to positive.

Section 6.4.4 Perchlorate Based Electrolytes.

In perchloric acid E_a(PS) is lower than observed for other electrolytes. In 0.1 M perchloric acid E_a(PS) is 9.8 kJ/Mol, which decreases to 3.6 kJ/Mol in 1.0 M electrolyte. The entropy terms are both negative. E_a(CV) values are larger than those observed using potential step methods. E_a(CV) values in both 0.1 and 1.0 M $HClO_4$ are similar at 100.2 $\pm$ 2 kJ/Mol and are coupled to positive entropy terms.

The effect of lithium perchlorate on E_a(PS) is different to that observed for other electrolytes examined, with E_a(PS) increasing as the electrolyte concentration is increased. In 0.1 M $LiClO_4$ E_a(PS) is 15.4 kJ/Mol which increases to 36.3 kJ/Mol in 1.0 M $LiClO_4$. These activation energies are coupled to negative entropy terms. E_a(CV) decreases as the lithium perchlorate concentration is increased. The entropy is positive in 0.1 M $LiClO_4$ and becomes negative in 1.0 M electrolyte.

Section 6.5 Discussion of Homogeneous and Heterogeneous Charge Transfer

The results presented show that the rate of homogeneous charge transport through these osmium containing poly(N-vinylimidazole) films is dependent on the nature of the charge compensating counterion in the electrolyte solution and its concentration. The results also suggest that the rate of homogeneous charge transport through these metallopolymer films is dependent on the timescale of the experiment. D_{CT}(CV) is always less than D_{CT}(PS), the difference between the two rates is, however, significantly affected by the nature and concentration of the electrolyte.

For all electrolytes, except those based on perchlorate anion, D_{CT}(PS) shows only small increases as the electrolyte concentration is increased. This insensitivity to electrolyte concentration, suggests that the rate controlling step of the charge propagation process, as determined by short timescale potential step measurements, remains unaltered over the 0.1 to 1.0 M concentration range. The thermodynamic data support this interpretation. E_a(PS) decreases with increasing electrolyte concentration and remains coupled to negative entropy terms. Negative entropy terms have been previously reported for related osmium and ruthenium systems [12-13], as well as, for other redox polymers [14] and have been associated with ordering processes namely ion or electron movement. The negative entropy terms reported here suggest that for the Os(II/III) oxidation an ordering process occurs in the polymer matrix in a localised region around the redox centre. The rate of electron self exchange has been measured using steady state methods [15] for related osmium [16] and ruthenium polymers [17] and is typically substantially higher (10^{-8}-10^{-6} cm^2s^{-1}) than the charge transport rates measured here. Therefore, the relatively low values of D_{CT}(PS), in conjunction with

the low activation energy, negative entropy terms and the sensitivity of D_{CT}(PS) to the nature of the electrolyte anion, strongly suggest that charge compensating counterion motion within the film limits D_{CT}(PS).

In contrast, D_{CT}(CV) while being significantly less than D_{CT}(PS), by at least an order of magnitude, is more sensitive to electrolyte concentration. The activation energies are larger and are frequently associated with positive entropy, suggesting that disordering processes limit D_{CT}(CV). These observations suggest that the nature of the equilibrium established and the rate determining step are different to those observed previously for potential step measurements. In chloride based electrolytes E_a(CV) is large and coupled to a positive entropy term in both 0.1 and 1.0 M electrolyte. In 0.1 M sulphate and pTSA electrolytes E_a(CV) is of similar magnitude to the relevant E_a(PS) values and are associated with negative entropy terms. In 1.0 M electrolyte the activation energy increases sharply and the entropy term becomes positive. This suggests that for high concentrations of non perchlorate electrolytes where large activation energies and positive entropy terms are observed, polymer chain motion limits D_{CT}(CV) [12,13].

These observations suggest, therefore, that in the non-perchlorate electrolytes a kinetic equilibrium, i.e an equilibrium on this short timescale, is established within the film, such that ion movement within the film limits D_{CT}(PS). In contrast, for high electrolyte concentrations, the cyclic voltammetry situation involves a thermodynamic equilibrium in which all mobile species including electrons, ions and polymer chains contribute to the observed charge transport rate.

The anion molar volumes of the electrolytes examined are different. Both chloride and sulphate anions have similar molar volumes [18] and charge transport rates. Toluene-4-sulphonic acid, however, has a larger molar volume and yet in pTSA both D_{CT}(PS) and D_{CT}(CV) are larger than those observed for the chloride and sulphate based electrolytes. This observation suggests that it is not the anion size which dictates the permeation of the required charge compensating counterion. Donnan exclusion is expected to be observed for non porous films, this acts to exclude co-ions from the film where the electrolyte concentration is below the fixed site concentration. This can indirectly lower the total quantity of charge compensating counterion resident within the film. This can cause an ion shortage within the film and hence a suppressed D_{CT} [19]. For the films discussed here however, the fact that D_{CT}(PS) varies monotonically with electrolyte concentration, and that little variation in the formal potential is observed, discounts such a process occurring for the non-perchlorate electrolytes.

Unlike the poly(4-vinylpyridine) films reported previously [20] and discussed in chapter 4, pH has little effect on the charge propagation rate. The pK_a of poly(N-vinylimidazole) lies between 3.00 for chloride solutions to 4.18 for p-toluene-sulphonate solutions [21]. It is has previously been observed that where the electrolyte pH was below the pK_a of the polymer backbone, that protonation of the uncoordinated nitrogens resulted in film swelling and a more porous coating. This resulted in a greater ion availability and hence a more rapid charge transport rate. The fact that such an effect is not observed for the present case suggests an open film structure [22].

The behaviour in perchlorate based electrolytes is significantly different to that observed for the other electrolytes. Both D_{CT}(PS) and D_{CT}(CV) decrease as the perchlorate concentration is increased. The difference between D_{CT}(PS) and D_{CT}(CV) is also considerably larger, approximately a factor of 100. This suggests that the nature of the equilibrium established is distinctly different for the two techniques. The thermodynamic data support this interpretation. E_a(PS) is low (4-36 kJ/Mol) for both perchloric acid and lithium perchlorate electrolytes. This coupled to negative entropy terms suggests that ion transport limits D_{CT}(PS). In perchloric acid E_a(CV) is considerably larger (100 kJ/Mol) and coupled to positive entropy terms. This suggests that a disordering process, namely disruptive segmental polymer chain motion, limits D_{CT}(CV). In 0.1 M lithium perchlorate E_a(CV) is of similar magnitude (107.5 kJ/Mol) and is also coupled to a positive entropy term. In 1.0 M electrolyte E_a(CV) is reduced to 47.9 kJ/Mol and is coupled to a negative entropy term. This suggests that in $LiClO_4$ the rate determining step is polymer chain movement in low electrolyte concentration and ion transport in 1.0 M solutions.

In perchlorate solutions the film appears to act as a semipermeable membrane. Figure 6.3.5.1 shows that D_{CT}(PS) is insensitive to changes in the lithium perchlorate over the concentration range 0.1 to 0.4 M after which D_{CT}(PS) decreases sharply to a constant value for perchlorate concentrations between 0.6 and 1.0 M. The concentration at which D_{CT}(PS) decreases is approximately the concentration of osmium sites within the film. This suggests that Donnan exclusion may be the cause of this behaviour. However, in normal circumstances a breakdown of Donnan exclusion results in an enhanced D_{CT}. The fact that D_{CT}(PS) decreases at this concentration and that D_{CT}(PS) and

D_{CT}(CV) decrease as the perchlorate concentration is increased suggests that there is a specific interaction of the perchlorate anion and the film. It has previously been reported that poly(4-vinylpyridine) films become dehydrated and compact when exposed to perchlorate containing solutions [23], and the formation of crosslinks has also been proposed in perchlorate media [24]. The results presented suggest therefore, that as the perchlorate concentration is increased and exceeds the fixed site concentration Donnan exclusion breaks down. This would normally increase D_{CT}, but such an influx of perchlorate ion makes the film more compact, thus hindering ion transport and hence suppressing D_{CT}. The negative entropy observed in 1.0 M $LiClO_4$ using cyclic voltammetry supports this interpretation of impeded ion transport, since it reflects an ion shortage even at long timescales and high electrolyte concentrations.

For osmium and ruthenium containing polymers in which [M(N_5)Cl] (M = Os, Ru) moieties were immobilised, charge transport rates were considerably more sensitive to changes in the concentration of the supporting electrolyte [28, 20]. Thermodynamic parameters suggested that the films became swollen and adopted an extended configuration only in low pH electrolytes of high concentration. The [Os(bipy)$_2$(PVI)$_{10}$](Cl)$_2$ films described here appear to be significantly porous for all non perchlorate based electrolytes, and rather insensitive to the supporting electrolyte concentration. This is somewhat surprising given the the bis coordination might be expected to result in a less soluble film. We suggest that it is the structural rigidity of the metallopolymer which is responsible for the porous nature of the films. For films where the redox centre is coordinated to a single monomer unit [20] it appears that there is sufficient flexibility for the polymer chains to adopt

their lowest energy state. In contrast, for the bis-coordinated materials discussed in this chapter, the intra chain coordination of the metal centre, means that sites must maintain their relative geometry thus leading to a more porous film.

A feature of the poly(N-vinylimidazole) polymers which has attracted attention is their high internal buffering capacity [21]. This internal buffering may also be present in these metallopolymers. Such a buffering capacity would prevent changes in the concentration of the contacting electrolyte being directly transferred to within the film. This would explain the insensitivity of D_{CT} to changes in the electrolyte concentration.

It has previously been noted that similar trends are observed for both homogeneous and heterogeneous electron transport rates as the electrolyte concentration is changed. We have reported on this behaviour recently for osmium containing poly(4-vinylpyridine) films [13] and this was discussed in chapter 4. The immobilised films acted as semipermeable membranes and as the electrolyte concentration was increased the anion population within the film increased thus altering the dynamics of double layer formation. This resulted in $D_{CT}(PS)$ and k^o both increasing as the electrolyte concentration was increased. For the poly(N-vinylimidazole) metallopolymers reported here, $D_{CT}(PS)$ and k^o appear related. k^o shows a similar dependence on the nature of the electrolyte anion as does $D_{CT}(PS)$; with the largest D_{CT} and k^o values being observed for the perchlorate based electrolytes. In all non perchlorate electrolytes k^o, as observed for $D_{CT}(PS)$, does not vary significantly with increasing electrolyte concentration. In perchlorate media however, a linear variation of log k^o and log $D_{CT}(PS)$ is observed as illustrated in Figure 6.5.1. This type of dependence has been reported for

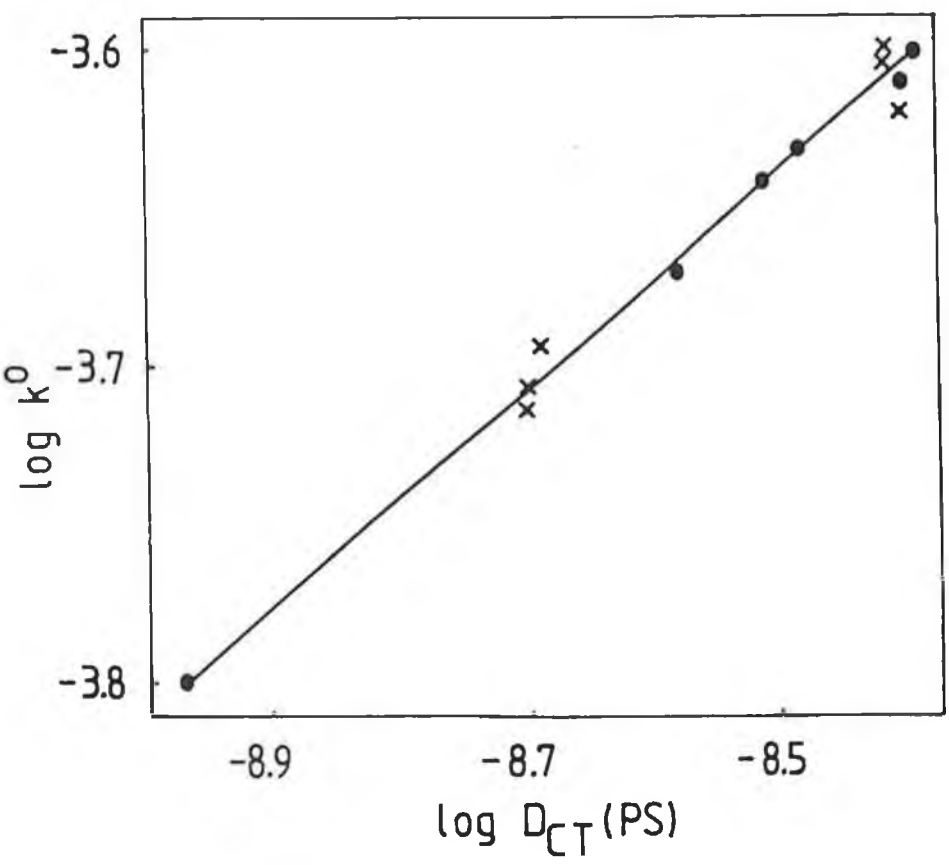

Figure 6.5.1 Correlation of $D_{CT}(PS)$ and k^o for $[Os(bipy)_2(PVI)_{10}](Cl)_2$ modified electrodes. • $HClO_4$ and x $LiClO_4$ as supporting electrolyte.

other osmium containing polymers [13]. This suggests that processes such as charge compensating counterion motion similarly affect the homogeneous and heterogeneous charge transfer processes. It is significant that it is only in perchlorate media, where evidence of Donnan exclusion was observed, that this behaviour occurs. For the other electrolytes, k^o is rather insensitive to electrolyte concentration. This suggests that the double layer formation is similar for all electrolyte concentrations. This is in agreement with the homogeneous charge transport data presented earlier, since it suggests that the population of charge compensating counterion within the film is similar at all electrolyte concentrations, which in turn suggests a porous film structure.

The transfer coefficient data also show a dependence on the nature and concentration of charge compensating counterion. In sodium chloride α is insensitive to electrolyte concentration and remains constant at 0.2 ± 0.01 suggesting a asymmetric barrier to electron exchange. In hydrochloric acid α increases with increasing electrolyte concentration. The transfer coefficient is larger in sulphate and pTSA electrolytes approaching the theoretical value of 0.5 in high concentrations of electrolyte. In perchlorate media the transfer coefficient is low and decreases with increasing electrolyte concentration. As discussed previously for $D_{CT}(PS)$ and k_o this is considered to be related to the availability of anion within the film.

Section 6.6 References.

1. A. R. Hillman, Electrochemical Science and Technology of Polymers, R. G. Linford, ed. (Elsevier Applied Science, Amsterdam) Chap. 5, Vol. 1, p. 103
2. R. W. Murray, Electroanalytical Chemistry, A. J. Bard, ed. (Dekker, New York, 1983) vol. 13, p. 191
3. L. R. Faulkner, Electrochim. Acta., 1989, 34, 1699
4. G. Inzelt, Electrochim. Acta., 1989, 34, 83
5. A. H. Schroeder and F. B. Kaufman, J. Electroanal. Chem., 1980, 113, 209
6. F. B. Kaufman, A. H. Schroeder, E. M. Engler, S. R. Kramer and J. Q. Chambers, J. Am. Chem. Soc., 1980, 102, 483
7. E. M. Kober, J. V. Caspar, B. P. Sullivan and T. J. Meyer, Inorg. Chem., 1988, 27, 4587
8. K. J. Vetter, Electrochemical Kinetics, (Academic Press, New York and London 1987) p. 107
9. J. Q. Chambers and G. Inzelt, Anal. Chem., 1985, 57, 1117
10. G. Inzelt, L Szabo, J. Q. Chambers and R. W. Day, J. Electroanal. Chem., 1988, 201, 301
11. T. Ohsaka, H. Yamamoto and N. Oyama, J. Phys. Chem., 1987, 91, 3775
12. M. E. G. Lyons, H. G. Fay, J. G. Vos and A. J. Kelly, J. Electroanal. Chem., 1988, 250, 207
13. R. J. Forster, M. E. G. Lyons and J. G. Vos, submitted for publication
14. P. Daum, J. R. Lenhard, D. Rolison and R. W. Murray, J. Am. Chem. Soc., 1980, 102, 4649
15. B. A. White and R. W. Murray, J. Am. Chem. Soc., 1987, 109, 2576
16. J. C. Jernigan and R. W. Murray, J. Am. Chem. Soc., 1987, 109, 1738

17. M. E. G. Lyons, H. G. Fay, T. McCabe, J. Corish, J. G. Vos and A. J. Kelly, J. Chem. Soc., Faraday Trans., in press

18. Y. Marcus, Ion Solvation, (Wiley-Interscience, New York)

19. K. Doblhofer and R. D. Armstrong, Electrochim. Acta., 1983, 33, 453

20. R. J. Forster, A. J. Kelly, J. G. Vos and M. E. G. Lyons, J. Electroanal. Chem., 1989, 270, 365

21. P. Ferruti and R. Barbucci, Adv. Polym. Sci., 1984, 58, 55

22. G. Inzelt, J. Backsai, J. Q. Chambers and R. W. Day, J. Electroanal. Chem., 1986, 201, 301

23. S. M. Oh and L. R. Faulkner, J. Am. Chem. Soc., 1989, 111, 5613

24. E. F. Bowden, M. F. Dautartas and J. F. Evans, J. Electroanal. Chem., 1987, 219, 91

CHAPTER 7

Electrocatalysis

by $[Os(bipy)_2(PVP)_{10}Cl]Cl$

Modified Electrodes.

Section 7.1 Introduction

This chapter describes how properties of modified electrodes may be exploited to act as efficient electrocatalysts. Mediated charge transfer forms the basis of many applications including electrochemical synthesis [1-3], oxygen reduction [4-8], analytical applications [9], semiconductor electrochemistry [10-13] and photogalvanic and display devices [14-16]. For those applications involving charge mediation by the modifying layer between the underlying electrode material and a target species in solution, the theory of mediated charge transfer has been extensively studied by many authors and allows mechanistic elucidation and kinetic parameters to be evaluated [17-24]. With the theoretical models discussed below, both qualitative and quantitative information about these processes can be obtained. For the field of analysis it defines a means of optimising electrode response.

Section 7.2 Theoretical and Experimental Implementation of Mediation Processes at Modified Electrodes

The fundamental redox reactions which may occur between a solution species Y and a mediating layer containing the redox couple A/B are shown in Figure 7.2.1.

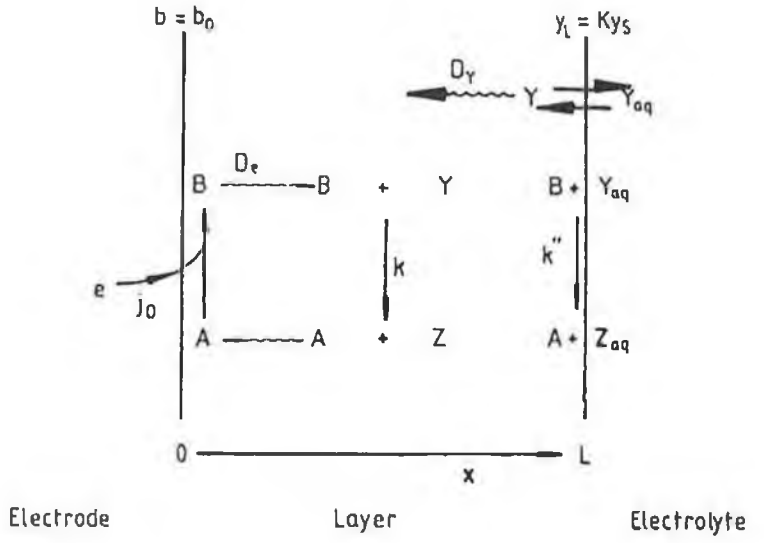

Figure 7.2.1 General model for a modified electrode showing the notation. Four processes are shown, electrode surface reaction (k'_E), partition of substrate into the film (K), mediated reaction in the film (k), and surface mediated reaction (k").

The mediating process can be described by reactions 1 and 2;

$$A + e \text{ -----> } B \qquad (1)$$

$$B + Y \text{ -----> } A + Z \qquad (2)$$

In this example the mediating process involves the reduction of the surface bound redox species A, but for a mediating process based on the oxidation of the surface bound species the same theories can be used. Other, more complex mediating processes, involving reversible mediating reactions, self exchange reactions, additional chemical steps and charge exchange have been considered by Andrieux and Saveant and co-workers [25-30].

Depending on factors such as film morphology, film thickness, the diffusion rate of the electroactive species through the film, electron transfer rate etc. four types of limiting cases may arise [26];

1) electron and substrate diffusion (D_E and D_Y) are so fast that the rate controlling step is the rate, k, of the catalytic reaction.

2) the catalytic reaction is so fast that the rate is controlled by the two diffusion processes, i.e diffusion of electrons and substrate.

3) when diffusion of electrons is faster than diffusion of substrate a pure kinetic situation may arise by mutual compensation of the latter process and the catalytic reaction.

4) in the opposite case a pure kinetic situation may again arise resulting in the mutual compensation of electron diffusion and catalytic reaction.

The fundamental processes involved in the mediating process are identified as charge introduction at the modifying layer/electrode interface, charge introduction at the layer/solution interface and reaction of the target analyte with the modifying layer. Coupled to these reactions one may observe substrate diffusion into the film as dictated by the partition coefficient, K. If the substrate is capable of penetrating the film then the diffusion rate of substrate Y within the layer D_Y will, in all but a few cases, be considerably less than the solution value D_S.

The analysis presented below is that developed by Albery, Hillman and co-workers [17], [31-33]. A similar model describing the mediating process has been developed by Andrieux, Saveant and co-workers [25-30]. The two differ in that the Albery and Hillman model utilises the notion of "reaction layers" to describe two different reaction zones within the film, a) a region where permeating Y is converted to product Z and b) a region of consumption of an electron or B. In this analysis a rate constant k'_{ME} for the modified electrode is utilised, in contrast to Saveant's model where no reaction layers are identified but the mediating process is described via characteristic currents. Alternative models have also been developed [34-35].

To analyse the mediating process for electrocatalytic modified electrodes one has to solve, equations 3 and 4 given certain boundary conditions.

charge transport within film $$D_E \frac{\delta^2 b}{\delta x^2} - kby = 0 \qquad (3)$$

Substrate diffusion in film $$D_y \frac{\delta^2 y}{\delta x^2} - kby = 0 \qquad (4)$$

These equations describe the concentration profiles of both the fixed redox couple and the substrate within the film. In these equations b and y are the concentration in the coating of B and Y respectively. The boundary conditions used are;

1) assuming Marcusian A/B self exchange behaviour, it is assumed that charge introduction at the electrode/layer interface will be more rapid than charge propagation [36]. Thus charge transfer to the electrode/layer interface is not expected to be rate limiting.

2) at x = 0 the concentration of B is b_0, and is controlled by the electrode potential.

3) the modifying layer acts in a catalytic manner, such that any substrate which permeates the layer and reaches the underlaying electrode will not react there, therefore $(\delta y/\delta x)_0=0$. This boundary condition is in agreement with the perception of a modified electrode where the substrate is not reacting directly with the underlaying electrode surface, but where the electrochemical process is controlled

by the mediating layer. It is to be noted that Saveant and co-workers have included in their treatment the reaction of the substrate directly at the electrode surface [25].

4) the partitioning of the substrate Y between the solution and the modifying layer is given by;

$$y_L = K y_s \tag{5}$$

5) the electron flux at the layer/solution interface is related to the kinetics by equation 6;

$$-D_E(\delta b/\delta x)_L = k'' b_L Y_s \tag{6}$$

where b_L is the concentration of B at the interface (X = L).
Using these boundary conditions and equations 1 and 2, the electron flux at the electrode, j_o which is proportional to the current, i, is obtained;

$$j_o = i/FA = -D_E(\delta b/\delta x)_o \tag{7}$$

At this stage an electrochemical rate constant, k'_{ME}, can be introduced [17], which relates the concentration of Y at the layer/solution interface to the electron flux, as in equation 8;

$$j_o = k'_{ME} y_s \tag{8}$$

The rate constant k'_{ME} can be evaluated from the intercept of Koutecky-Levich plots using RDE. The observed current i_F, is thus related to the sum of the fluxes of direct (j_Y) and mediated (j_B) charge transfer and the concentration gradients at the electrode/film interface by :

$$(i_F/nFA) = j_o = j_B + j_y =$$
$$-D_E(\delta b/\delta x)_o + D_y(\delta y/\delta x)_o = k'_{ME}y_s \qquad (9)$$

As discussed earlier an essential concept to be included in this analysis is that of the "reaction layer". The first reaction layer, X_L, defines the distance which Y can travel within the film prior to reacting with B and is given by equation 10:

$$X_L = (D_y/kb_L)^{1/2} \qquad (10)$$

The second reaction layer, X_o, defines the average distance an electron can diffuse before reacting with Y :

$$X_o = (D_E/ky_o)^{1/2} \qquad (11)$$

With the concepts of the electrochemical rate constant and of the reaction layer introduced one can now go back to reactions 3 and 4. Depending on the relative importance of electron and substrate diffusion different approximations for k'_{ME} can be obtained. If $D_Eb_o >> D_yky_s$, i.e. fast electron transport or slow permeation or ineffective partitioning of the substrate, then :

$$\frac{1}{k'_{ME}} = \frac{Y_s L}{D_E b_o} + \frac{1}{k'' b_o + k b_o K X_L \tanh(L/X_L)} \qquad (12)$$

electron transport within layer

surface reaction

layer reaction

If permeation is very fast and/or electron transport within the film is relatively slower then $D_E b_o << D_Y K y_s$ and :

$$\frac{1}{k'_{ME}} = \frac{L}{K D_y} + \frac{k''\tanh(L/X_o) + kKx_o}{kKx_o b_o\{k'' + kKx_o \tanh(L/x_o)\}} \qquad (13)$$

transport of Y across layer

surface reaction

layer reaction

From these two equations it can be deduced that the slower contributions to the mediating reaction, which can be kinetic or diffusional in nature, will determine the magnitude of k'_{ME}. In the limiting case as represented by equation 12 the last term on the right hand side represents the competition between the surface reaction (k") and the layer reaction (k). The flux however may alternatively be limited to a value of $D_E b_o/L$ by electron transport through the film. The position of the reaction layer is reflected in the equation obtained for k'_{ME} in these limiting cases, and will depend on

the ratio between the reaction layer X_L and the layer thickness L. For cases where $X_L >> L$ the whole layer participates in the reaction, this is called the layer (L) case. In the reverse case the reaction occurs in a thin layer at the layer/electrolyte interface, the surface (S) case.

The position of the reaction layer in the second limiting case, as presented in equation 13 can be obtained by similar methods. If the layer thickness $L >> X_0$ then the kinetic term reduces to kKX_0b_0 and the reaction takes place in a layer adjacent to the electrode. This is called the layer/electrode (LE) case. In the reverse situation, when $L >> X_0$, the reaction takes place at the layer/electrolyte interface, the layer/surface (LS) case. For intermediate ratios of L and X_0 the reaction takes place throughout the whole layer.

Another situation arises when neither equation 8 or 9 are valid. This would be the case if the electron and substrate diffusion contributions are of the same magnitude, but can be described as in equation 14;

$$\frac{D_E b_0}{K D_y y_s} \simeq \frac{X_0^2}{X_L^2} \sim 1 \qquad (14)$$

Under such conditions, and if X_0 or X_L is less than L, then the reaction will take place somewhere in the middle of the layer and is controlled by the diffusion rates of both electrons and substrate. This is called the layer/reaction zone (LRZ) case. For this situation the solution for k'_{ME} is given by :

$$\frac{1}{k'_{ME}} = \frac{L}{D_Y K + D_E b_0 / y_s} \qquad (15)$$

From the above equations it can be seen that the LE, LS and S cases (i.e those derived above) can controlled either by the transport or by the kinetic term. So depending on the relative importance of these two terms, these cases can be subdivided in to subclasses. These subclasses are either controlled by transport processes, in which case they are given the label t_e or t_y, depending on whether electron or substrate transport are rate limiting, or by kinetic factors, in which case the labels are k or k". So LEk denotes a mediated reaction that takes place at a layer close to the underlying electrode surface and is controlled kinetically, whereas in the LEt_y case the reaction takes place in the same part of the layer but is controlled by substrate transport. These labels, together with the corresponding rate constant for the various limiting cases have been listed in Table 7.2.1. A diagram depicting the different positions and notations for the reaction layer has been given in Figure 7.2.2.

The equations given above have been used by Albery and co-workers to construct a kinetic zone diagram. An example of such a diagram is given in Figure 7.2.3. "Surface" and "electrode" cases give a third dimension to the diagram but those cases are not of interest in the search for three dimensional sensor devices and therefore only the layer cases are included.

Some parameters, including b_0, y_s and L, given in the above analysis and in Table 7.2.1 can be easily changed, while others such as D_E, D_Y and k are not so readily variable. Results presented in this thesis have

	Expression for charge transfer rate	
Case notation	k'_{ME}	i_F
Sk''	$k''b_0$	—
St_E	$D_E b_0 / Ly_s$	—
LSk	$\kappa k b_0 X_L$	$(i_s i_k)^{1/2}$
LSt_E	$D_E b_0 / Ly_s$	i_E
Lk	$\kappa k b_0 L$	i_k
$LRZt_E t_Y$	$D_E b_0 / Ly_s + \kappa D_Y / L$	$i_E + i_s$
LEk	$\kappa k b_0 X_0$	$(i_E i_k)^{1/2}$
LEt_Y	$\kappa D_Y / L$	i_s
Ek'_E	$\kappa k'_E$	—
Et_Y	$\kappa D_Y / L$	—

Table 7.2.1 Notation and expressions describing behaviour of different cases for Faradaic reactions at polymer modified electrodes.

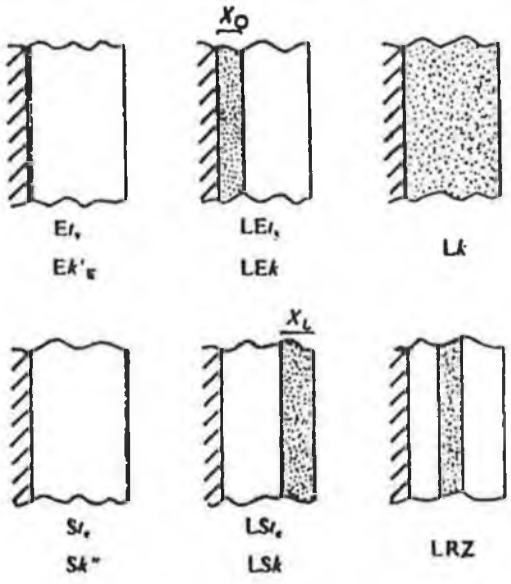

Figure 7.2.2 The location of the reaction in the ten possible cases together with the notation used to distinguish them. The electrode is on the left in each case and the location of the reaction is shown by the shaded region.

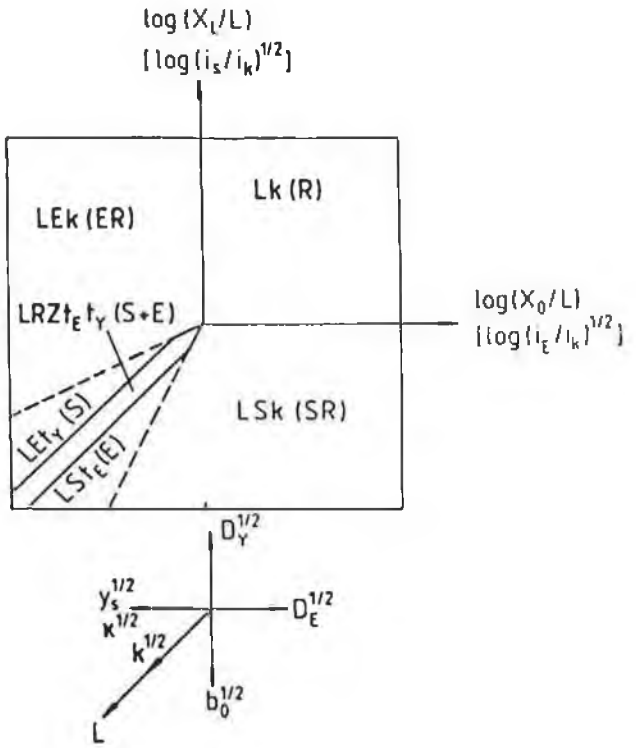

Figure 7.2.3 The effect on k'_{ME} of increasing the surface concentration of mediator b_o. The order of k'_{ME} with respect to b_o is shown by the circled numbers.

sought to show that all of these parameters can be sensitive to changes in the nature of the electrolyte and its concentration as well as temperature.

The Saveant approach [29] leads to the same conclusions as the Albery model but it does not define reaction layers. Instead the mediating processes are described by the characteristic currents i_A, i_S, i_E and i_k. These currents give the contribution to the observed currents by respectively, substrate diffusion from the solution to the electrode surface, substrate diffusion in the film, electron diffusion in the film and finally by the rate of the cross-exchange reaction between the redox centre and the substrate. The equations derived for these characteristic currents and the processes they describe are given in equations 16-19 [37]:

The substrate diffusion from the solution to the film.

$$i_A = FAC^0_A D/d \qquad (16)$$

Substrate diffusion in the film.

$$i_S = FAC^0_A D_S/L \qquad (17)$$

Electron transfer between different redox sites in the film, the electron self exchange process.

$$i_E = FAC^0_P D_E/L \qquad (18)$$

The cross exchange reaction between the redox centre and the substrate in the film.

$$i_K = FAC^o_A kKC_0 L \qquad (19)$$

In these equations F : Faraday constant, C^o_A : bulk concentration of the redox substrate, C^o_P : concentration of the redox site within the film, A : the electrode area, D : diffusion coefficient of the substrate in solution, D_E the charge transport parameter describing electron "diffusion" through the film, D_S substrate diffusion within the film, K : partition coefficient of the substrate between the film and solution, k : second order rate constant describing the mediated reaction between the film and substrate, d : diffusion layer thickness and L the film thickness.

This model has been used successfully to describe the electrochemical properties of modified electrodes [38-40], particularly with respect to important analytical applications.

The conditions for optimum efficiency of catalytic modified electrodes, that is a high value for k'_{ME}/k'_E, the ratio between the electrochemical rate constant for the modified and bare electrode, have been considered by Albery and Hillman [32] and by Saveant and co-workers [26]. In these studies factors such as the thickness of the modifying layer L and limits for the kinetic parameters discussed above have been considered. Where the electrode response has been optimised with respect to electron transport and morphology it is usually found that electron diffusion is faster than substrate diffusion and that the concentration of the surface bound redox couple is larger than that of the substrate.

Because of the "preconditions" discussed above the number of limiting cases to be considered for optimisation of the modified electrode are limited, with the layer cases showing most promise. The optimum efficiency cases are LSk and LEk. LSk corresponds to rapid electron transfer compared to substrate diffusion through the film, the reaction occurring near the layer/electrolyte interface the exact position depending on the mediated reaction rate constant k. In the LEk the mediated reaction occurs close to the underlying electrode material. For the layer cases the magnitude of k'_{ME} will initially increase with the layer thickness (all sites mediate electron transfer under kinetic control) then pass through a maximum before decreasing due to transport limitations of the substrate. These ideal cases correspond to a sufficient amount of mediation sites for substrate consumption combined with efficient substrate or charge diffusion and correspond to the ideal three dimensional modified electrode. For the LSk case the catalytic advantage becomes

$$k'_{ME}/k'_{E} = KX_{L}/l \qquad (20)$$

This can be very large since the reaction layer thickness can be much greater than l, the distance over which electron transfer can take place. It can be clearly seen that for reactions which exhibit slow homogeneous kinetics that a layer reaction is required where Y permeates the film rapidly. This requires an open porous structure for the film which will ensure easy permeation of B, but electron transport must also be rapid to avoid limitations posed by charge transfer.

Finally we wish to consider the two optimum surface and electrode cases Sk" and Ek'_E. In these two limiting cases mediation does not occur throughout the layer and the reaction occurs at the layer/solution and the electrode/layer interface respectively. These limiting cases find only limited application in analysis as the electrochemical reaction is only taking place in a monolayer and cannot therefore be described as three dimensional. In the surface case a practical application can be envisaged only of B is a specific catalyst for the oxidation or reduction of the substrate Y. The electrode case becomes interesting when a favourable partition can be obtained. In that case, even as the reaction is taking place at the underlaying electrode surface, a catalytic effect will be obtained because of the high value of the partition coefficient, K. This particular approach has been used in a number of occasions where preconcentration has been used as a way to construct new sensors.

The experimental determination of the parameters involved in the theoretical described above relies on recognition of the appropriate limiting processes. It is the use of the rotating disk and rotating ring-disk electrodes which provides the means of analysing the kinetics of catalysis at the modified electrode surface. These techniques allow control of the substrate diffusion in solution and thus permit the elucidation of the kinetics and mechanism of the catalytic reaction. By controlling the electrode potential the surface concentration of solution species can be reduced to zero and the current response becomes limited by mass transport and is given by the Levich equation [41].

$$i_{Lev} = 1.554nAFD^{2/3}\nu^{-1/6}{}_y\,\omega^{1/2} \qquad (21)$$

Rotating disk measurements are ideal for the investigation of mediated reactions at electrode surfaces since the rate of mass transport of the substrate is calculable. This has lead to the widespread exploitation of the technique [42-45]. The modified electrode does not usually obey the simple Levich equation since mass transport may not represent the rate limiting process. In this case the limiting current is given by :

$$1/i_{Lim} = 1/i_F + 1/i_{Lev} \qquad (22)$$

or

$$1/i_{Lim} = 1/(nFAk'_{ME}y) +$$

$$1/(1.554nFAD^{2/3}\,\nu^{-1/6}{}_y\,\omega^{1/2})$$

A plot of i^{-1} vs $\omega^{1/2}$ gives a straight line, where the slope is the reciprocal of the Levich slope, the intercept yielding the value of k'_{ME}. Albery and Hillman [17] have published a useful flowchart for the diagnosis of reaction type based on this mode of analysis (see Figure 7.2.4). In this flow chart the functional dependence of k'_{ME} on b_o, y_s and L allows classification of the process.

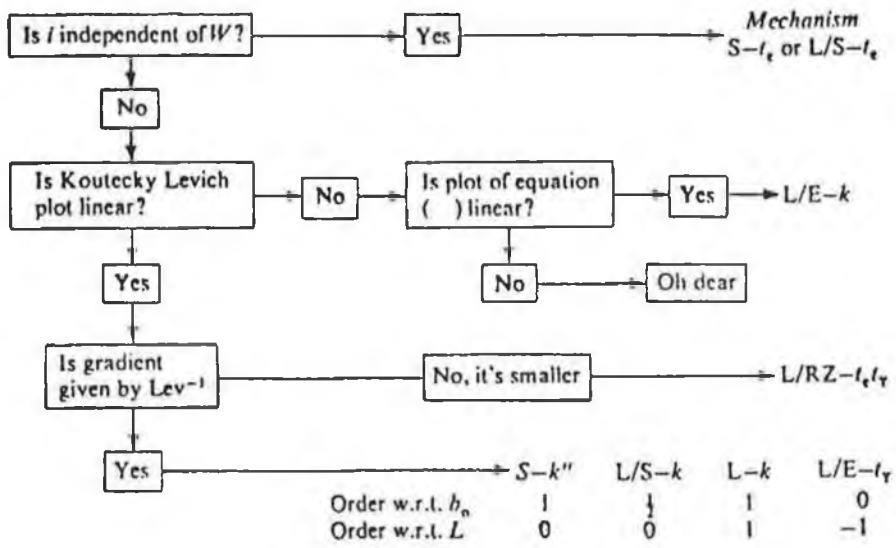

Figure 7.2.4 Diagnosis of mechanism for modified electrodes.

Section 7.3 Experimental. $[Os(bipy)_2(PVP)_{10}Cl]Cl$ was prepared as described in chapter 2. Films of varying thickness were prepared by droplet evaporation or spin coating as described in chapter 3. Rotating disk voltammograms were recorded as detailed in chapter 3.

Section 7.4 Results: Mediated Reduction of $[Fe(H_2O)_6]^{3+}$ by $[Os(bipy)_2(PVP)_{10}Cl]Cl$ in 0.1 M H_2SO_4.

$[Fe(H_2O)_6]^{3+}$ does not undergo a redox reaction at a glassy carbon electrode in the potential region for the Os(III/II) (E^o=250mV) reduction despite a formal potential of 460 mV. Given this formal potential of the $Fe^{2+/3+}$ reaction, it is expected that electrodes modified with $[Os(bipy)_2(PVP)_{10}Cl]Cl$ could mediate the $[Fe(H_2O)_6]^{3+/2+}$ reduction according to equation 24:

$$Fe(III) + Os(II) \longrightarrow Fe(II) + Os(III) \qquad (24)$$

with a 210mV driving force.

Typical rotating disk voltammograms for the mediated reduction of a 0.2 mM $[Fe(H_2O)_6]^{3+}$ by $[Os(bipy)_2(PVP)_{10}Cl]Cl$ modified electrodes are shown in Figure 7.4.1. It is evident from these plots that a mediated reduction of $[Fe(H_2O)_6]^{3+}$ appears in the potential region of the Os(III/II) reduction and that i_L is dependent on the rotation rate ω. Koutecky-Levich plots can be used to analyse this data. Typical plots showing the dependence on layer thickness of this mediated reduction in 0.2 mM $[Fe(H_2O)_6]^{3+}$ are shown in Figure 7.4.2. These plots are linear for the

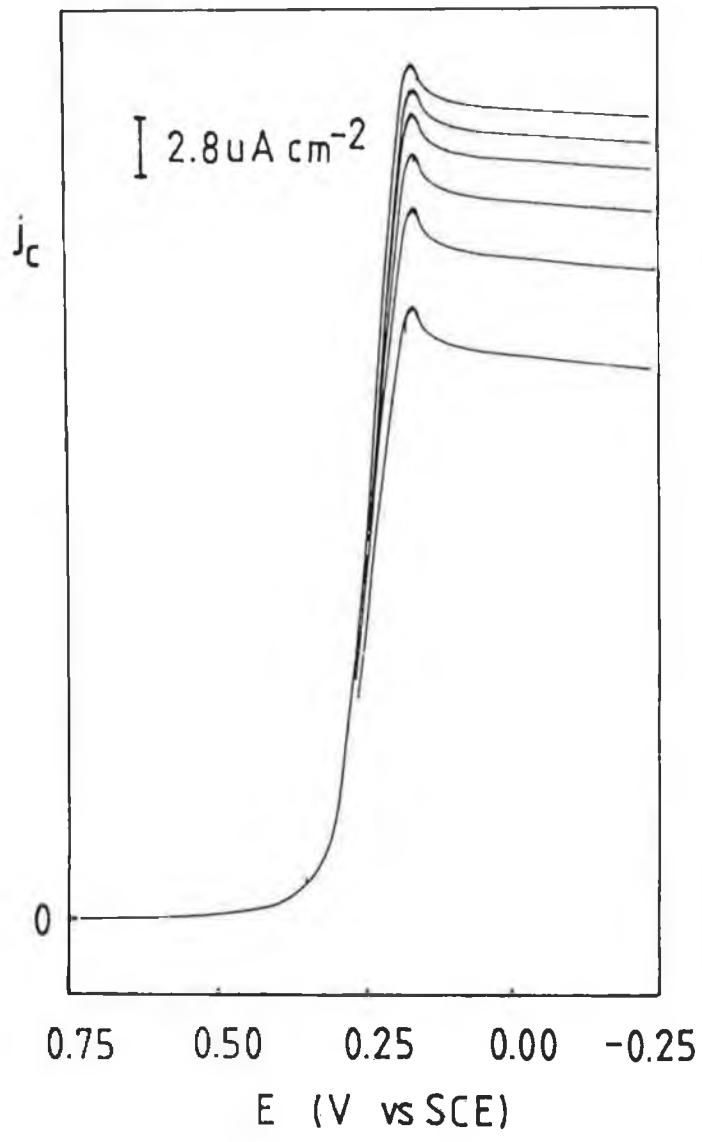

Figure 7.4.1 Reduction of a 0.2 mM solution of $[Fe(H_2O)_6]^{3+}$ in 0.1 M H_2SO_4 by $[Os(bipy)_2(PVP)_{10}Cl]Cl$. The rotation rates are, from bottom to top, 500, 1000, 1500, 2000, 2500 and 3000 rpm. Surface coverage 5 x 10^{-9} molcm^{-2}.

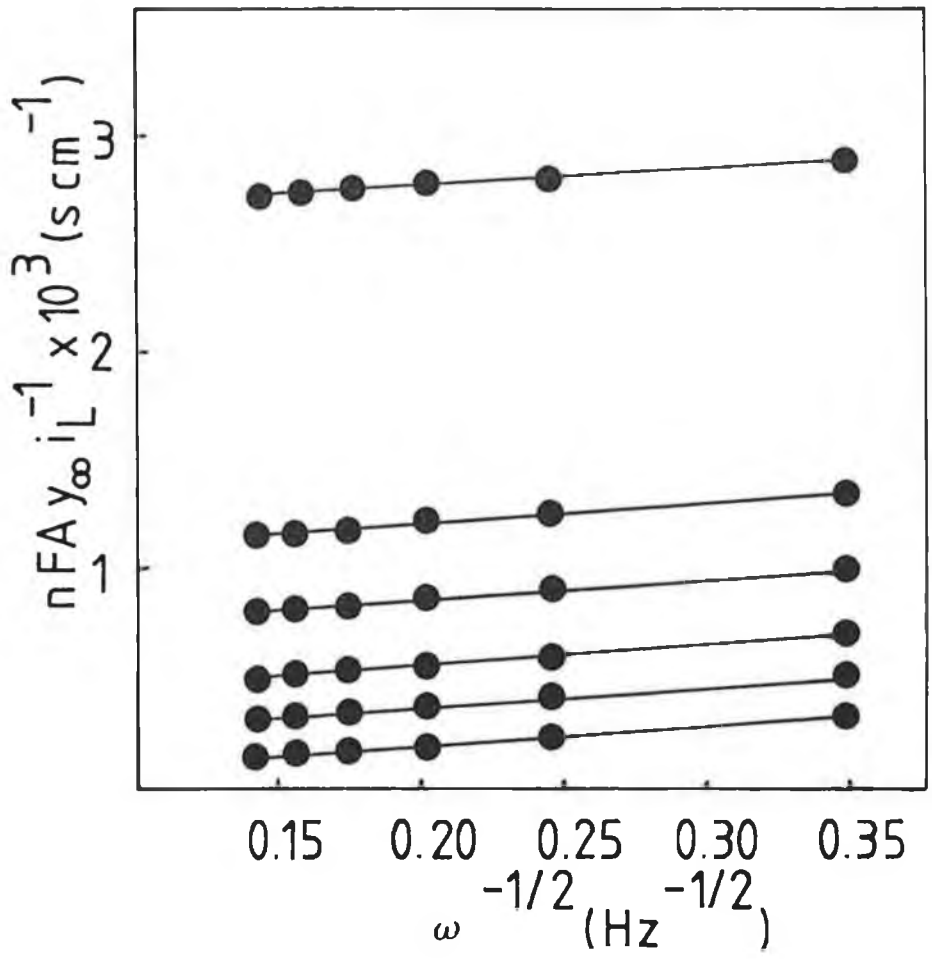

Figure 7.4.2 Typical Koutecky-Levich plots for the reduction of 0.2 mM $[Fe(H_2O)_6]^{3+}$ in 0.1 M H_2SO_4 at an $[Os(bipy)_2(PVP)_{10}Cl]Cl$ modified electrode. Surface coverages in mol cm^{-2} are, from top to bottom, 7.0 x 10^{-10}, 1.8 x 10^{-9}, 2.7 x 10^{-9}, 5.0 x 10^{-9}, 1.1 x 10^{-8} and bare platinum.

surface coverages examined and all give a slope of $9.4\pm0.8 \times 10^{-4}$ $cms^{-1/2}$. Since the limiting current is dependent on the rotation rate and the Koutecky-Levich plots are linear the St_e, LSt_e and LEk cases can be eliminated (see Figure 7.2.4). The $LRZt_et_y$ case is expected to have a slope which is smaller than that given by the Levich constant,

$$Lev=1.55D^{2/3}\upsilon^{-1/6} \qquad (25)$$

at a clean unmodified electrode. This has been evaluated as 1.01×10^{-3} $cms^{-1/2}$, Albery has examined this reaction and reports Lev as 1.04×10^{-3} $cms^{-1/2}$ [46]. The electroreduction of $[Fe(H_2O)_6]^{3+}$ at an electrode modified with polyhydroxyphenazine has been considered [47]. Using data reported in this paper a value of 1.14×10^{-3} $cms^{-1/2}$ for the Levich constant is obtained. Therefore, the slope of the $[Os(bipy)_2(PVP)_{10}Cl]Cl$ modified electrode is the same as that obtained at a bare electrode within experimental error. Given that the slopes of the Koutecky-Levich plots at bare and modified electrodes are the same the kinetic zone $LRZt_et_y$ can be eliminated. Thus having excluded the above cases, the modified electrode must lie within the Sk", LSk, Lk or LEt_y kinetic zones. These cases can be distinguished by examining the dependence of k'_{ME} on L. The modified electrode rate constant k'_{ME} can be evaluated from the intercept of the Koutecky-Levich plot as discussed earlier. The dependence of k'_{ME} on L is given in Table 7.4.1 for 0.8 and 0.2 mM $[Fe(H_2O)_6]^{3+}$. This shows that the modified electrode rate constant is first order with respect to the layer thickness. A similar behaviour is observed for the other concentrations examined.

Table 7.4.1 The dependence of k'_{ME} on the layer thickness L where the $[Fe(H_2O)_6]^{3+}$ concentration is 0.2 mM. Electrolyte 0.1 M H_2SO_4.

L (nm)[a]	$k'_{ME} \times 10^3$ (cms^{-1})
150	6.30
70	2.84
38	1.54
25	0.93

The dependence of k'_{ME} on layer thickness L where the $[Fe(H_2O)_6]^{3+}$ concentration is 0.8 mM. Electrolyte 0.1 M H_2SO_4.

L (nm)[a]	$k'_{ME} \times 10^3$ (cms^{-1})
230	2.52
70	0.78
45	0.48
15	0.16

[a] Layer thickness L calculated from surface coverage using a fixed site concentration of 0.7 M.

Since the dependence of k'_{ME} on L is first order the kinetic zone can be assigned via the flow chart to be Lk. In order to confirm this diagnosis the dependence of k'_{ME} on b_0, the concentration of mediator within the film, was investigated. k'_{ME} is anticipated to have a first order dependence on b_0 given that the kinetic zone is Lk.

In order to analyse the dependence on b_0 it is necessary to evaluate the concentration of Os(II) within the film as a function of electrode potential. Films of $[Os(bipy)_2(PVP)_{10}Cl]Cl$ show classical surface bound behaviour in 0.1 M H_2SO_4 at the sweep rates employed in the rotating disk voltammetry (chapter 3). This strongly suggests that the Nernst equation is valid. Controlled potential coulometry has also been used to further consider this behaviour. This procedure was implemented by incrementing the electrode potential negatively from 1.0 V, where the film is fully oxidised, to -0.4 V where the film is fully reduced. The potential increment was 50 mV and each potential was held for 5 minutes during which time the cathodic current was integrated, after this time the rate of charge accumulation was negligible. Extraneous background charging was corrected for by stepping the potential in a region where no redox reaction occurred and linearly extrapolating. The observed response is indeed Nernstian as shown for an $[Os(bipy)_2(PVP)_{10}Cl]Cl$ modified electrode in 0.1 M H_2SO_4 in Figure 7.4.3. The slope of this line is 58 ± 2mV per decade in close agreement with the theoretical slope of 59.6 mV/decade. This data can be used to calculate the fraction f of the film which is oxidised via the relation

$$\ln[f/(1-f)]=(F/RT)(E-E^0) \qquad (26)$$

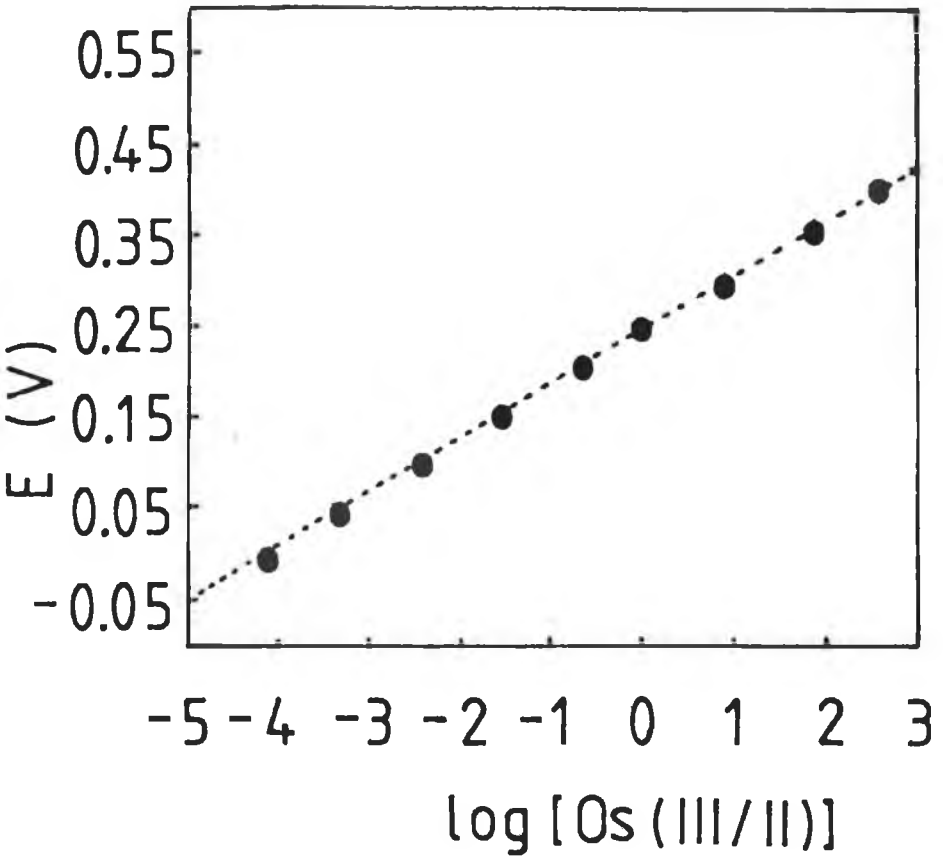

Figure 7.4.3 Nernst plot for an $[Os(bipy)_2(PVP)_{10}Cl]Cl$ modified electrode in 0.1 M H_2SO_4. Surface coverage 5 x 10^{-9} molcm^{-2}.

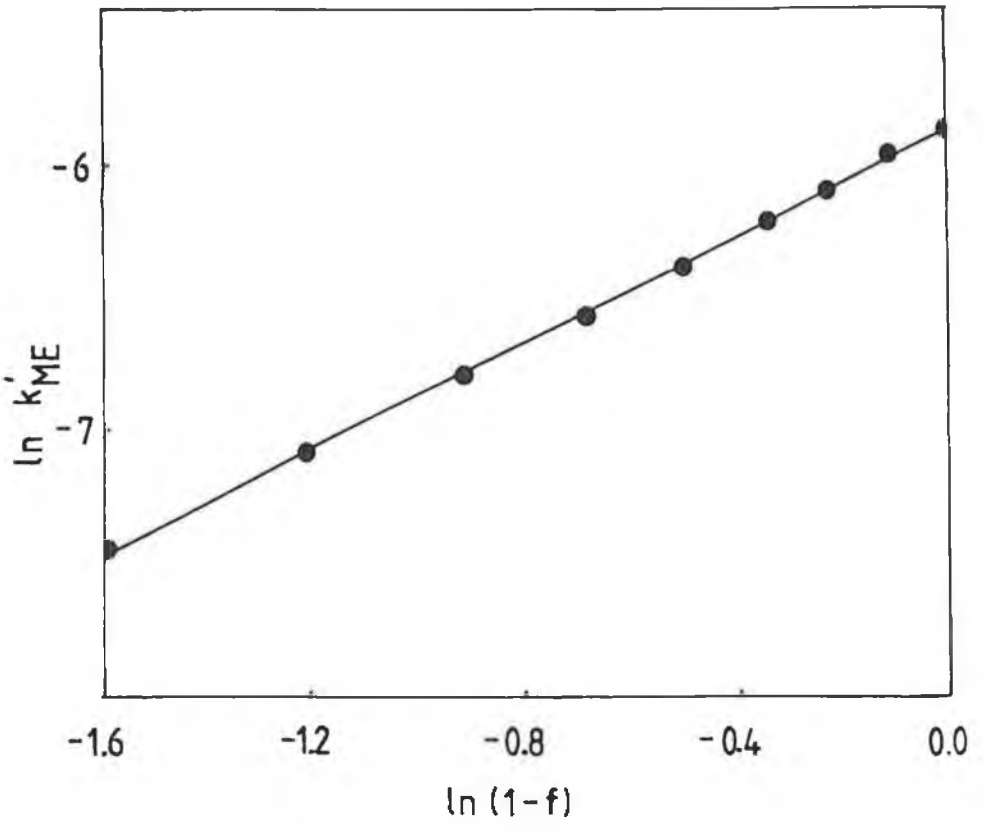

Figure 7.4.4 The effect of increasing the Os(III) concentration within the film on the modified electrode rate constant k'_{ME} for the reaction of 0.2 mM $[Fe(H_2O)_6]^{3+}$ in 0.1 M H_2SO_4. Surface coverage 5 x 10^{-9} molcm^{-2}.

and hence b_o can be evaluated. By analysing the rising portion of the rotating disk voltammogram k'_{ME} can be evaluated at various fractions of Os(III) reduction. Figure 7.4.4 shows the dependence of k'_{ME} obtained from Koutecky-Levich plots on (1-f). The plot is linear with a slope of 0.98±0.05. This agrees with the slope of 1 anticipated for an Lk case.

Having established that the mechanism is Lk, i.e the catalytic reaction occurs throughout the layer, the rate of reaction being limited by the catalytic reaction, k, between B and Y, k can be evaluated from equation 27

$$k'_{ME}=kKLb_o \qquad (27)$$

where K is the partition coefficient. The constant kK has been evaluated as $5.6x10^2M^{-1}s^{-1}$.

The kinetic zone diagram for this system is given in Figure 7.4.5. As discussed earlier for surface coverages between 1 x 10^{-8} and 7 x 10^{-10} molcm^{-2} the kinetic zone is of the Lk type. For these surface coverages the reaction is controlled by the polymer layer. For thick films Γ>1 x 10^{-7} molcm^{-2} the limiting current becomes independent of film thickness. This corresponds to total catalysis in that diffusion of $[Fe(H_2O)_6]^{3+}$ from solution to the electrode surface controls the process.

Section 7.5 Mediated Reduction of $[Fe(H_2O)_6]^{3+}$ by $[Os(bipy)_2(PVP)_{10}Cl]Cl$ in 1.0 M $HClO_4$.

The rate of charge transport through $[Os(bipy)_2(PVP)_{10}Cl]Cl$ films in contact with perchlorate containing solutions showed unusual behaviour, with much larger variations in D_{CT} as measured by potential step and sweep methods

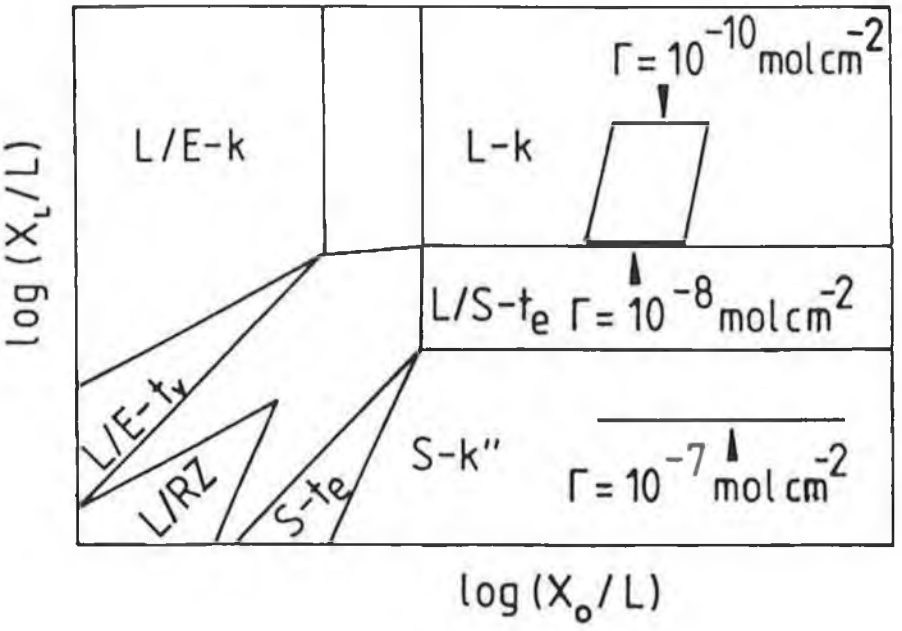

Figure 7.4.5 Kinetic zone showing the kinetic control of the mediating process for the reaction of Fe(III) and Os(II) immobilised within $[Os(bipy)_2(PVP)_{10}Cl]Cl$ as a function of surface coverage.

than was observed in other electrolytes (see Chapters 3 and 4). More significantly perhaps, the rate of charge transport as measured by linear sweep voltammetry decreased as the perchlorate concentration was increased. This was discussed in terms of a non-swollen, significantly dehydrated film which effectively excluded charge compensating counterions and restricted counterion and polymer chain motion within the film. These observations suggest that the presence of perchlorate salts might result in inhibited permeation of $[Fe(H_2O)_6]^{3+}$ resulting in a change of the kinetic zone assignment from the Lk case observed in sulphuric acid. A decrease in permeation would act to decrease X_L thus producing a kinetic zone of the surface type. To investigate these assumptions the mediation properties of $[Os(bipy)_2(PVP)_{10}Cl]Cl$ films in 1.0 M $HClO_4$ were investigated using $[Fe(H_2O)_6]^{3+}$ as substrate.

The examination of Koutecky-Levich plots, which corresponds to infinite rotation rate where negligible polarisation of the substrate occurs in the electrolyte phase, have again been used to identify the kinetic zone to which the system belongs. The limiting current like that observed in sulphuric acid is dependent on the rotation rate. The Koutecky-Levich plots are linear and have the same slope as that observed at a bare electrode. An example of this behaviour is shown in Figure 7.5.1. The dependence of k'_{ME} on L was first order in sulphuric acid, this dependence in perchloric acid is illustrated in Figure 7.5.2. This figure shows that k'_{ME} is independent of L. This independence suggests (Figure 7.2.4) that the kinetic zone is Sk" or LSk, both surface cases. To distinguish between these two situations requires, as before, an examination of the dependence of k'_{ME} on b_o. For the LSk case a reaction order of 1/2 is expected while for the Sk" case the reaction

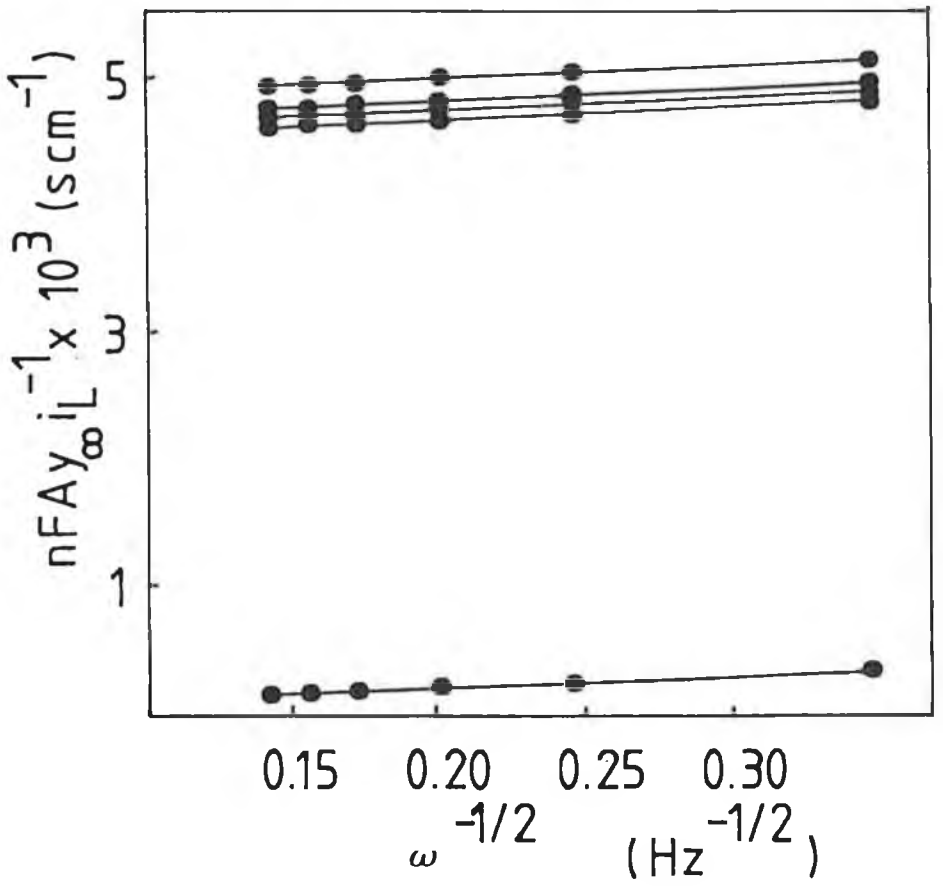

Figure 7.5.1 Typical Koutecky-Levich plots for the reduction of 0.2 mM $[Fe(H_2O)_6]^{3+}$ in 1.0 M $HClO_4$ at an $[Os(bipy)_2(PVP)_{10}Cl]Cl$ modified electrode. Surface coverages in molcm^{-2} are, from top to bottom, 7.0 x 10^{-10}, 1.8 x 10^{-9}, 2.7 x 10^{-9}, 5.0 x 10^{-9}, 1.1 x 10^{-8} and bare platinum.

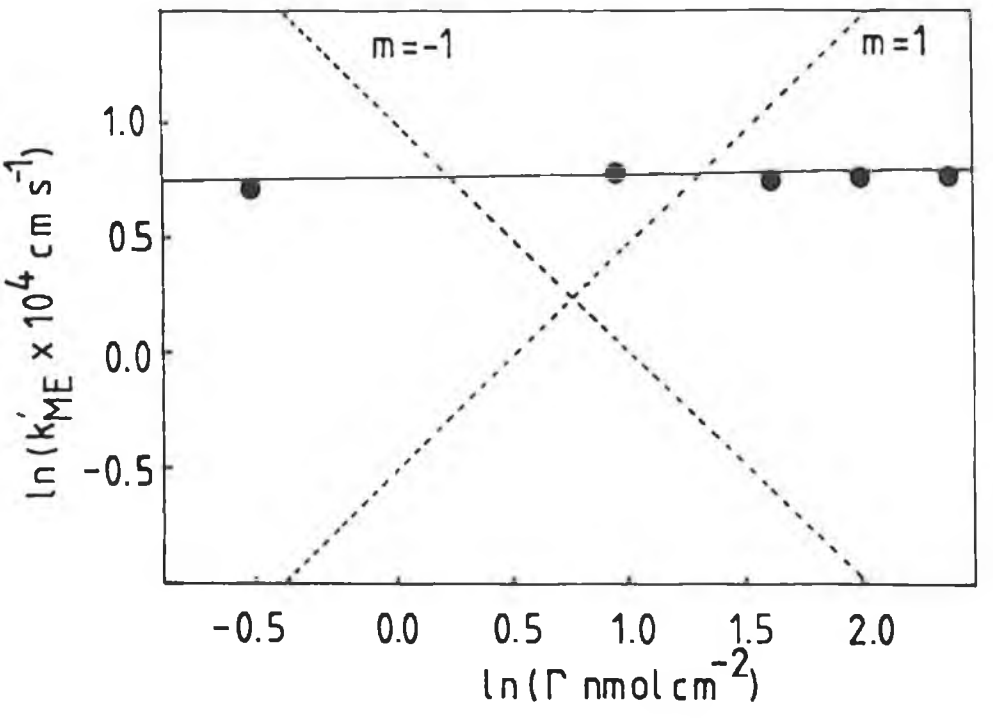

Figure 7.5.2 Plot showing the order of k'_{ME} for the reaction of a 0.2 mM $[Fe(H_2O)_6]^{3+}$ solution in 1.0 M $HClO_4$ with $[Os(bipy)_2(PVP)_{10}Cl]Cl$ with respect to the surface coverage Γ.

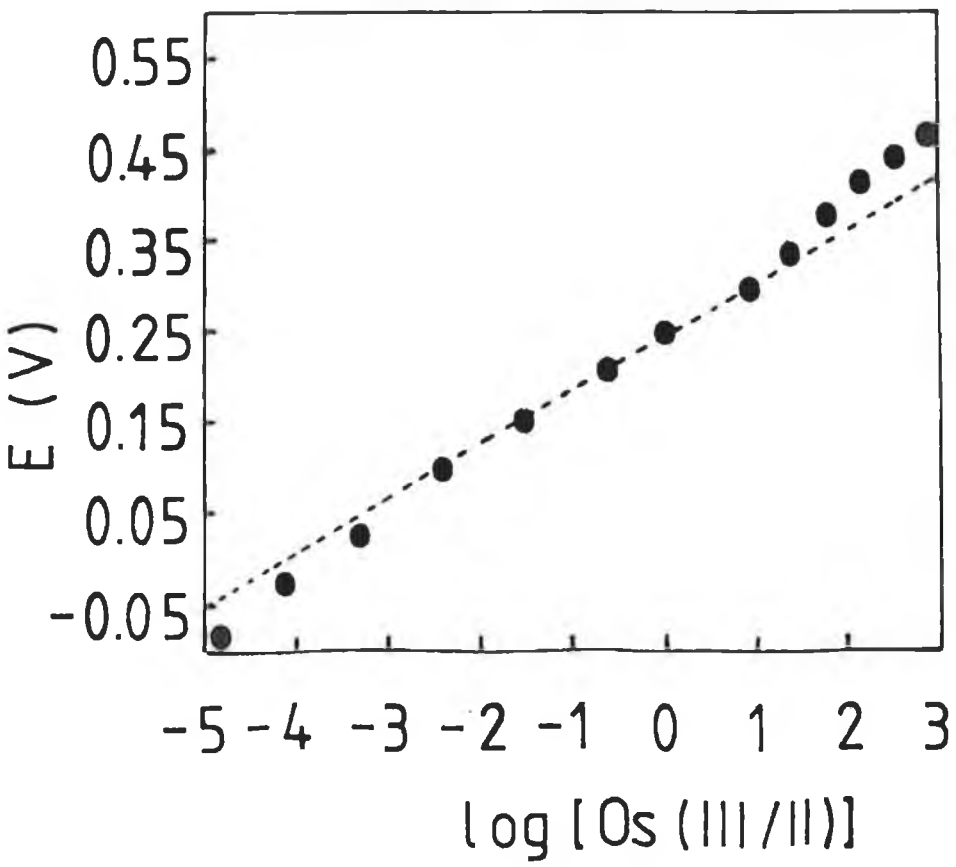

Figure 7.5.3 Nernst plot for an $[Os(bipy)_2(PVP)_{10}Cl]Cl$ modified electrode in 1.0 M $HClO_4$. Surface coverage 5 x 10^{-9} molcm^{-2}.

order should be unity. Controlled potential coulometry was used to examine the fraction converted as a function of the electrode potential and the results presented in Figure 7.5.3. The non-linearity of this plot suggests that the thermodynamics of the Os(III/II) reduction are more complex than those associated with a simple one electron transfer reaction. As a fully oxidised film undergoes reduction, the curve is approximately linear with a super Nernstian slope of 65-75 mV/decade. As the formal potential is approached the slope decreases and approaches a Nernstian value. After f = 0.5 the slope again increases and reaches a value of 80-100 mV/decade which is maintained until the oxidation is complete. The use of the term "slope" is used only as a convenience to identify those regions which are approximately linear. This data has been used to calculate the fraction converted and hence b_o.

By examining the rising portion of the rotating disk voltammograms in conjunction with this data the dependence of k'_{ME} on b_o can be evaluated. This behaviour is illustrated in Figure 7.5.4. The log-log plot is a reasonable straight line although some scatter exist in the data, the slope of the best fit line is 1.05 ± 0.2. It appears therefore that the reaction order with respect to b_o is unity. Thus the kinetic zone is of the Sk" type.

From Figure 7.5.4, where f = 0, corresponding to a fully reduced film, the modified electrode rate constant is $2.90\pm0.2 \times 10^{-4}$ cm^2s^{-1}. For the Sk" case k'_{ME} is equal to $k"b_o$, where k" is the second order rate constant for the reaction between the surface bound mediator and $[Fe(H_2O)_6]^{3+}$ in solution. Using a concentration of 0.7 M for the osmium concentration within the film this gives k" as 3.1×10^{-4} $mol^{-1}dm^3cms^{-1}$. The value of the homogeneous rate constant is similar to that obtained by Albery and Hillman (4×10^{-4} $mol^{-1}dm^3cms^{-1}$) for the

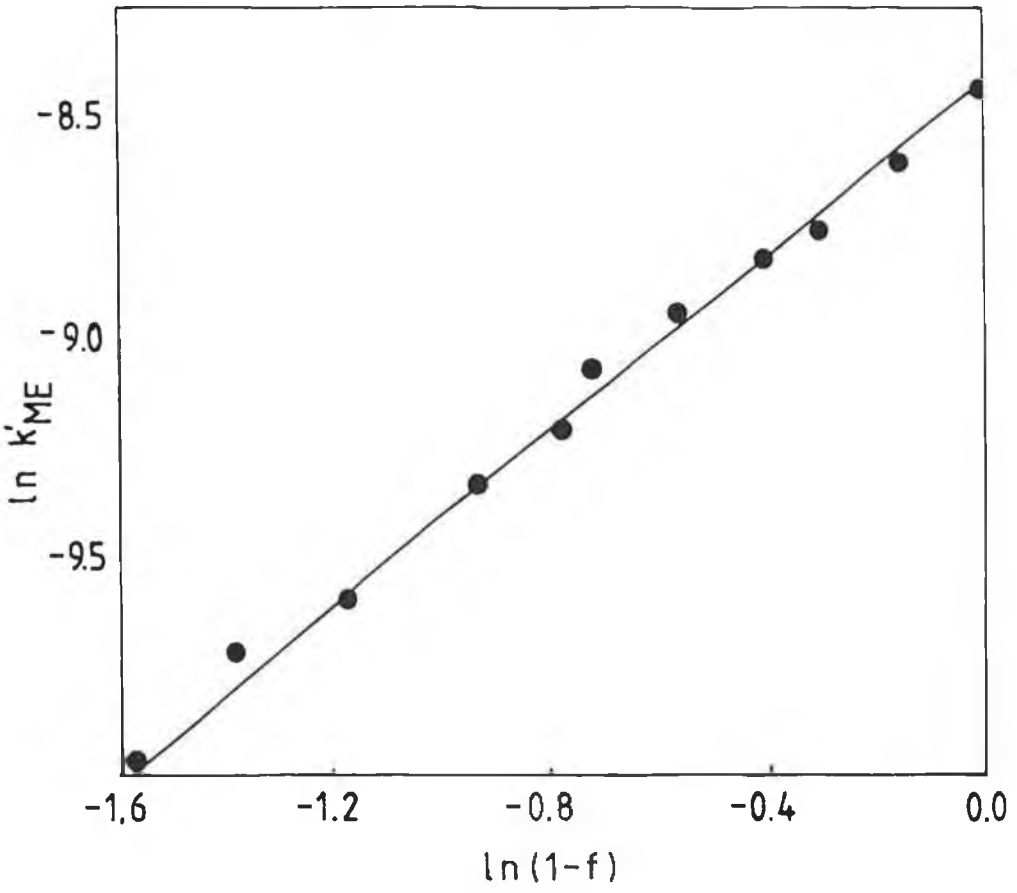

Figure 7.5.4 The effect of increasing the Os(III) concentration within the film on the modified electrode rate constant k'_{ME} for the reaction of 0.2 mM $[Fe(H_2O)_6]^{3+}$ in 1.0 M $HClO_4$. Surface coverage 5 x 10^{-9} molcm^{-2}.

reaction of $[Fe(H_2O)_6]^{3+}$ with a thionine modified electrode where a driving force of ~250 mV exists.

Section 7.6 Discussion of Mediation Processes for $[Os(bipy)_2(PVP)_{10}Cl]Cl$ films.

In sulphuric acid $[Os(bipy)_2(PVP)_{10}Cl]Cl$ films can catalyse the electroreduction of $[Fe(H_2O)_6]^{3+}$ efficiently giving rise to currents which are limited by substrate diffusion in solution for thick films. Catalysis occurs close to the formal potential which is approximately 200mV more negative than the Fe(III/II) formal potential. The fact that the immobilised films can act as three dimensional catalysts is significant. The results discussed previously in the charge transport section showed that in sulphuric acid charge transport was rapid ($D_{CT}=2.95 \times 10^{-9}$ cm^2s^{-1} when measured using potential step methods, and $D_{CT}=2.51 \times 10^{-10}$ cm^2s^{-1} when measured using linear sweep voltammetry) and that ion movement represents the rate limiting step. The protonated structure of the metallopolymer in this electrolyte appears sufficiently porous to permit considerable iron permeation despite the electrostatic repulsion which would be expected between protonated pyridine units and $[Fe(H_2O)_6]^{3+}$.

The fact that the kinetic zone, where perchloric acid is the supporting electrolyte is different to that observed in sulphuric acid and the observation that the reaction is a surface one correlates with the charge transport data presented previously in chapter 4. The rate of charge transport through these osmium containing films is of similar magnitude in both sulphuric and perchloric acid electrolytes when measured using potential step measurements. If this represents the true rate of charge transport through the film then it seems unlikely that electron transport through the film would be

sufficiently different between the two electrolyte systems to alter the kinetic zone from Lk to Sk". If charge transport through the outer portion is more accurately measured by linear sweep voltammetry then the reduced D_{CT} value would tend to push the system toward an LEk case. This leads to the conclusion that decreased $[Fe(H_2O)_6]^{3+}$ permeation leads to the surface case. This is consistent with the suggestion that the rate of charge transport as measured by linear sweep voltammetry decreases with increasing perchlorate concentration because of increasing film dehydration with consequent inhibited ion permeation. The fact that the kinetic zone is of the Sk" case means that the mediated reaction occurs between $[Fe(H_2O)_6]^{3+}$ still in solution and the film within a region of molecular dimensions.

Section 7.7 References.

1. S. Abe, T. Nonaka and T. Fuchigami, J. Am. Chem. Soc., 1983, 105, 3630
2. T. Komori and T. Nonaka, J. Am. Chem. Soc., 1984, 106, 2656
3. T. Komori and T. Nonaka, J. Am. Chem. Soc., 1983, 105, 5690
4. D. A. Buttry and F. C. Anson, J. Am. Chem. Soc., 1984, 106, 59
5. K. Okabayashi, O. Ikeda and H. Tamura, J. Chem. Soc. Chem Comm., 1983, 684
6. H. Behret, H. Binder, G. Sanstede and G. G. Scherer, J. Electroanal. Chem., 1981, 117, 29
7. P. Martigny and F. C. Anson, J. Electroanal. Chem., 1982, 139, 383
8. R. R. Durand, C. S. Bencosme, J. P. Collman and F. C. Anson, J. Am. Chem. Soc., 1983, 105, 2710
9. R. J. Forster and J. G. Vos in "Electrochemistry, Sensors and analysis", Ed. G. Sevhla, Elsevier, Amsterdam, in press
10. A. B. Bocarsly, S. A. Galvin and S. Sinha, J. Electrochem. Soc., 1980, 102, 3390
11. R. E. Malpas and B. Rushby, J. Electroanal. Chem., 1983, 157, 387
12. R. Noufi, D. Tench and L. F. Warren, J. Electrochem. Soc., 1980, 127, 2310
13. R. Noufi, A. J. Nozik, J. White and L. F. Warren, J. Electrochem. Soc., 1982, 129, 2261
14. K. Itaya, H. Akahoshi and S. Toshima, J. Electrochem. Soc., 1982, 129, 762
15. Y. Yoshino, K. Kaneto and Y. Inuishi, Jap. J. Appl. Phys., 1983, 22, L157
16. K. Kaneto, Y. Yoshino and Y. Inuishi, Jap. J. Appl. Phys., 1983, 22, L412
17. W. J. Albery and A. R. Hillman, R. S. C. Annual Report, 1981, 78, 377
18. F. C. Anson, J. M. Saveant and K. Shigehara, J. Phys. Chem., 1983, 87, 214
19. J. Leddy, A. J. Bard, J. T. Maloy and J. M. Saveant, J. Electroanal. Chem., 1985, 187, 205

20. R. D. Rocklin and R. W. Murray, J. Phys. Chem., 1981, 85, 2104

21. K. Shigehara, N. Oyama and F. C. Anson, J. Am. Chem. Soc., 1981, 103, 2552

22. D. A. Buttry and F. C. Anson, J. Electroanal. Chem., 1981, 130, 333

23. J. M. Saveant and K. B. Su, J. Electroanal. Chem., 1984, 171, 341

24. C. P. Andrieux, C. Blocman, J. M. Dumas-Bouchiat, F. M'Halla and J. M. Saveant, J. Electroanal. Chem., 1980, 113, 19

25. C. P. Andrieux and J. M. Saveant, J. Electroanal. Chem., 1978, 93, 163

26. C. P. Andrieux, J. M. Dumas-Bouchiat and J. M. Saveant, J. Electroanal. Chem., 1982, 131 1

27. C. P. Andrieux, J. M. Dumas-Bouchiat and J. M. Saveant, J. Electroanal. Chem., 1984, 169, 9

28. C. P. Andrieux and J. M. Saveant, J. Electroanal. Chem., 1984, 171, 65

29. C. P. Andrieux and J. M. Saveant, J. Electroanal. Chem., 1983, 142, 1

30. C. P. Andrieux and J. M. Saveant, J. Electroanal. Chem., 1982, 134, 163

31. W. J. Albery, A. W. Foulds, K. J. Hall and A. R. Hillman, J. Electrochem. Soc., 1980, 127, 654

32. W. J. Albery and A. R. Hillman, J. Electroanal. Chem., 1984, 170, 27

33. W. J. Albery, W. R. Bowen, F. S. Fisher, A. W. Foulds, K. J. Hall, A. R. Hillman, R. G. Edgell and A. F. Orchard, J. Electroanal. Chem., 1980, 107, 37

34. K. Aoki, K. Tokuda and H. Matsuda, J. Electroanal. Chem., 1986, 199, 69

35. M. Lovric, Electrochim. Acta., 1981, 26, 1639

36. F. C. Anson, J. Phys. Chem., 1980, 84, 3336

37. E. Laviron, J. Electroanal. Chem., 1982, 131, 61

38. X. Chen, P. He and L. R. Faulkner, J. Electroanal. Chem., 1987, 222, 223

39. E. T. Jones and L. R. Faulkner, J. Electroanal. Chem., 1987, 222, 201

40. C. P. Andrieux and J. M. Saveant, Ann. Phys. (Paris), 1986, 11, 3

41. V. G. Levich in "Physicochemical Hydrodynamics" Prentice-Hall, Englewood Cliffs, New York, 1962 68

42. T. Ikeda, C. R. Leidner and R. W. Murray, J. Electroanal. Chem., 1982, 138, 343

43. T. Ikeda, R. Schmehl, P. Denisevich, K. Willman and R. W. Murray, J. Am. Chem. Soc., 1982, 104, 2683

44. Y. Ohnuki, H. Matsuda, T. Ohsaka and N. Oyama, J. Electroanal. Chem., 1983 158, 55

45. F. C. Anson, J. M. Saveant and K. Shigehara, J. Electroanal. Chem., 1983, 145, 423

46. W. J. Albery, M. G. Boutelle and A. R. Hillman, J. Electroanal. Chem., 1985, 182, 99

47. C. P. Andrieux, O. Haas and J. M. Saveant, J. Am. Chem. Soc., 1986, 108, 8175

Chapter 8 Conclusions

Section 8.1 Conclusions

When deposited on electrode surfaces all of the metallopolymers described in this thesis show reversible, single electron redox reactions for surface bound species, where significant interaction between sites is absent. Ideal redox behaviour is observed in a wide variety of electrolytes, with the possible exception of those based on perchlorate ion. As well as this, the modified electrodes are stable toward thermal and photochemical ligand substitution reactions. Furthermore, the modified surface has a long lifetime even when exposed to 1.0 M acidic solutions. These are essential prerequisites for the examination of homogeneous and heterogeneous charge transfer reactions of materials of this type. This is because chemical reactions or loss of modifying material from the electrode, makes it impossible for parameters, such as the reaction entropy, where there is a small variation in the experimental observable to be accurately evaluated. The significant synthetic flexibility of these materials is evident since a wide variety of polymers based on the $[Os(bipy)_2]^{2+/3+}$ unit can be synthesised each with a different redox potential and charge transport property. The ability to control the redox potential is particularly useful in the design of modified electrodes for sensor application based on electrocatalysis.

In general both $D_{CT}(PS)$, $D_{CT}(CV)$ and k^0 are sensitive to the concentration of the supporting electrolyte, increasing with increasing concentration for all loading and electrolytes examined, with the exception of those based on perchlorate anion. The same rate of charge transport as measured by potential step and sweep measurements is only observed under certain circumstances, notably in sulphuric acid at high concentrations. Furthermore, the activation energies for the two techniques are frequently different. The

potential step measurements typically show low activation energies and negative entropy terms, suggesting that an ordering process, namely ion transport limits D_{CT}(PS). In contrast, the cyclic voltammetry experiments, particularly in high electrolyte/low redox site concentration combinations, show a lower rate of charge transport, higher activation energies and positive entropy terms. These observations suggest that a disordering process, segmental polymer chain motion limits D_{CT}(CV). The above arguments suggest that those species which attain equilibrium within the film during the charge transport process is time dependent. The results obtained from all of the polymer/active site loading/electrolyte combinations examined, suggest that at short times only those species of high mobility i.e. electrons and high mobility ions attain equilibrium due to kinetic barriers to mass transport processes. In the case of the longer timescale cyclic voltammetry experiments thermodynamic equilibrium is established. This involves an equilibrium of all mobile species including electrons, ions and polymer chains.

The rate determining step of the charge transport process is dependent on the experimental timescale, electrolyte type and concentration as well as, the redox site loading. However, for the present case the rate of charge transport at low electrolyte concentrations appears to be limited by ion movement within the films. Where the redox site loading is low, it appears that segmental polymer chain movement is required to bridge the intersite separation and allow electron transfer to occur. The rate determining step of electron self exchange is not observed. This appears to be related to the requirements for observing electron self exchange as the rate determining step. This will be favoured by a high concentration of oriented sites. However, a high metal content within the film results in poor swelling which is required for fast ion

transport. Thus at high redox site loadings the films become too compact for efficient ion transport and so an ion movement limitation is observed. Removal of the ion transport limitation by decreasing the active site loading invariably results in a more swollen film in which the intersite separation is larger and so polymer chain movement becomes the rate determining step. A possible solution to these problems is to have internal buffering of the system. In the materials discussed here, there are nitrogen moieties which can undergo protonation in acidic media. During the oxidation of the osmium centre, electroneutrality could be maintained by deprotonation of these nitrogens and expulsion of protons. The similarity of charge transport rates in both high and low pH electrolytes, notably in the poly(N-vinylimidazole) polymers suggests that such a process does not occur. The possibility of maintaining an excess of charge compensating counterion within the film to support the redox reaction requires further investigation.

The optimisation of electrode response for applications typically involves maximising the rate of charge transport through the film to the film/electrolyte interface. This ensures that the redox reaction occurring within the film does not constrain the electrode performance. In applications involving catalysis it means that the whole layer can be utilised, while in electrochromic applications it ensures a short response time. Traditional thinking on modified electrodes has sought to optimise charge transport rates by confining the highest possible concentrations of redox active material within the film. In the present case, the highest redox site loading explored was 1:5 osmium to monomer units. This situation means that the redox centres are at a concentration of approximately 1.2 M and that adjacent sites approximately touch. However, this situation typically failed to deliver the

optimum charge transport rate (the only exception being $[Os(bipy)_2(PVI)_5Cl]Cl$ in toluene-4-sulphonic acid). Despite this, it is to be remembered that these systems do frequently give the highest cyclic voltammetry peak currents and chronoamperometric responses, since even though the charge transport rate is not at a maximum the active site concentration is high thus giving a larger response. The films containing the maximum active site loading do not however, give the optimum response per unit cost.

The modified electrodes considered here frequently show Donnan exclusion behaviour. This acts to exclude charge compensating co-ions from the film where its concentration is below the fixed site concentration. This observation is important for applications of these materials, since where the total electrolyte concentration is low, the analyte may be excluded from the film resulting in a surface reaction and hence a small analytical response. At higher concentrations of electrolyte Donnan exclusion may break down, causing influx of the analyte thus utilising a greater proportion of the film, and hence resulting in an enhanced response. The Donnan exclusion behaviour is particularly interesting in perchlorate based media. The $[Os(bipy)_2(PVI)_{10}](Cl)_2$ films show a reverse Donnan behaviour in lithium perchlorate (Figure 6.3.5.1). For lithium perchlorate concentrations between 0.1 and 0.4 M $D_{CT}(PS)$ is large (4×10^{-9} cm^2s^{-1}) which decreases to 2×10^{-9} cm^2s^{-1} in 0.6 to 1.0 M electrolyte. This behaviour is thought to arise due to a breakdown of Donnan exclusion resulting in an ion influx. Perchlorate interacts with the film to give a dehydrated layer thus impeding ion transport and hence a reduced $D_{CT}(PS)$ is observed.

The rate of charge transport through the poly(4-vinylpyridine) and poly(N-vinylimidazole) metallopolymers have several features in common. For all electrolytes except those based on perchlorate D_{CT}(PS) and D_{CT}(CV) increase with increasing electrolyte concentration, similarly a maximum metal loading does not necessarily result in the optimum charge transport rate. In general the rate of charge transport through the poly(4-vinylpyridine) films is similar to those observed in the poly(N-vinylimidazole) polymers with the most rapid rate of charge transport being observed for intermediate loadings in high concentrations of sulphuric and p-toluene sulphonic acid.

It is interesting to note that the where the osmium centre is coordinated in a bis manner to the polymer backbone that a more porous material results. This is considered to arise because of the structural rigidity which this coordination mode imposes on the polymer. Unlike the mono-coordinated materials, this appears unable to adopt its lowest energy state, presumably an extended configuration to minimise electrostatic repulsion between the positively charged redox centres.

The rotating disk data presented in this work show that the choice of electrolyte for a given analytical application is important. Where it is desirable to avoid a reaction of the analyte at the underlying electrode surface an electrolyte, such as perchloric acid, which causes film compaction and results in a surface reaction may be desirable. In contrast, where the objective is to utilise as much as possible of the film a swelling electrolyte such as sulphuric acid should be used.

In final conclusion then, it is to be hoped that this work goes some way toward an understanding of charge transport from the underlying electrode into these films and within the layer. The results presented clearly show that

the charge transport behaviour of these materials cannot be clearly elucidated in a single electrolyte at a single redox loading.

Abbreviations

AES	Auger electron spectroscopy
bipy	2,2'-bipyridine
CPE	carbon paste electrode
GC	Glassy carbon
MeIm	methyl imidazole
NPV	Normal pulse voltammetry
pic	4-methyl pyridine
phen	phenanthroline
PLL	poly(L-Lysine)
Pol	polymer
p-TSA	p-toluene sulphonic acid
PVI	poly(N-vinylimidazole)
PVP	poly(4-vinylpyridine)
PVF	poly(vinylferrocene)
RDE	rotating disk electrode
SEM	scanning electron microscopy
TEAP	tetraethylammonium perchlorate
XPS	X-ray photoelectron spectroscopy

Roman Symbols

Symbol	Meaning	Dimension
A	area	cm^2
	absorbance	none
a_i	activity of ion i	M
C	concentration	M, mol cm^{-3}, mM
	capacitance	F
$C_j(x)$	concentration of species j at distance x	M, mol cm^{-3}
$C_j(x=0)$	concentration of species j at the electrode surface	M, mol cm^{-3}
$C_j(x,t)$	concentration of species j at distance x at time t	M, mol cm^{-3}
$C_j(0,t)$	concentration of species j at the electrode surface at time t	M, mol cm^{-3}
$C_j(y)$	concentration of species j at a distance y below an RDE	M, mol cm^{-3}
$C_j(y=0)$	concentration of species j at an RDE	M, mol cm^{-3}
$D_{CT}(CV)$	Rate of homogeneous charge transport measured by cyclic voltammetry	$cm^2\ s^{-1}$

$D_{CT}(PS)$	rate of homogeneous charge transport measured by potential step	$cm^2\ s^{-1}$
E	Potential of an electrode versus a reference	V
	emf of a reaction	V
ΔE	pulse height in differential pulse voltammetry	mV
E^o	standard potential of an electrode	V
	standard emf of a half reaction	V
ΔE^o	difference in standard potential for two couples	V, mV
E^o	formal potential of an electrode	V, mV
E_a	activation energy of a reaction	kJ/Mol
E_p	peak potential	V, mV
ΔE_p	$E_{pa}-E_{pc}$ in CV	V, mV
E_{pa}	anodic peak potential	V, mV
E_{pc}	cathodic peak potential	V, mV
$E_{1/2}$	half wave potential measured in voltammetry	V, mV
F	Faraday constant	C
G	Gibbs free energy	kJ
ΔG	Gibbs free energy change in a chemical process	kJ

ΔG^{o}	standard Gibbs free energy change in a chemical process	kJ
$\Delta G^{\neq}$	Standard Gibbs free energy of activation	kJ/Mol
H	enthalpy	kJ
ΔH^{o}	standard enthalpy change in a chemical reaction	kJ
$\Delta H^{\neq}$	standard enthalpy of activation	kJ/Mol
h	Planck's constant	J-sec
i	current	A, uA
i_a	anodic component current	A, uA
i_c	cathodic component current	A, uA
i_l	limiting current	A, uA
i_p	peak current	A, uA
i_{pa}	anodic peak current	A, uA
i_{pc}	cathodic peak current	A, uA
j	current density	A/cm^2, uA/cm^2
j_o	exchange current density	A/cm^2, uA/cm^2
k	rate constant for a homogeneous reaction	depends on order
k^o	standard (intrinsic) heterogeneous rate constant	cm/sec
k_b	heterogeneous rate constant for oxidation	cm/sec
k_f	heterogeneous rate constant for reduction	cm/sec

L	layer thickness of modifying film	cm
n	number of electrons per molecule oxidised or reduced	none
Ox	oxidised form of the standard system Ox + ne = Red	
Q	charge passed in electrolysis	C, uC
Red	reduced form of the standard system Ox + ne = Red	
R	gas constant	J Mol^{-1} K^{-1}
R_s	solution resistance	ohms
R_u	uncompensated resistance	ohms
ΔS	entropy change in a chemical process	kJ/K
ΔS°	standard entropy change in a chemical process	kJ/K
$\Delta S^{\neq}$	standard entropy of activation	kJ Mol^{-1} K^{-1}
T	absolute temperature	K
t	time	sec
ν	linear potential scan rate	mV/sec

Greek Symbols

α	transfer coefficient	none
θ_j	surface coverage of species j	mol cm^{-2}
δ	diffusion layer thickness	cm
τ	sampling time in sampled current voltammetry	sec
ω	angular frequency of rotation 2 x π rotation rate	sec^{-1}

Appendix A Acquisition and Analysis of Electrochemical Data Using Computer Based Systems

Introduction

In the course of this work the use of computer based methods for,

1) data capture and instrumental control,

2) data analysis and formatting,

3) data presentation and management,

was explored.

A1 Integrated Data Capture and Analysis

In this section an integrated approach in which the instrument is controlled by the host computer, and the data captured, analysed and presented without operator manipulation is illustrated for sampled current voltammetry. The use of a computer controlled potentiostat allows more complex wave forms, such as sampled current and square wave voltammetry to be implemented. This was achieved using a BBC microcomputer interfaced via an IEEE-488 interface to an E.G.& G. Model 273 potentiostat. For sampled current voltammetry a program has been written in BASIC to allow for data acquisition and analysis. This program features full front panel emulation allowing the operator to enter, via the computer the required experimental conditions such as potential limits, incremental potential step size and timescale. This information is then used to construct the required waveform which is then transferred via the IEEE-488 interface to the potentiostat. The waveform is then applied to the

electrochemical cell and the resulting data captured. This data is then transferred to the computer for analysis in the manner discussed in section 1.3.3. The resulting current-potential response is displayed on screen for operator evaluation. Further data processing such as smoothing and correction for capacitive currents is then possible. The rate of homogeneous charge transport and heterogeneous electron transfer are evaluated and presented on screen. A hardcopy output to an Epson Hi-80 plotter of the current-potential response and the calculated rate constants is also available. The computer program for this data control, capture, analysis and presentation is given in program listing 1.

Sampled Current Voltammetry

```
 10 P$=""
 20*KEY0 GOTO 3910
 30*KEY1 RUN
 40 DIM TIM(5)
 50 DIMHI$(300)
 60 YF=1
 70 CLS
 80 REM NORMAL PULSE WAVEFORM PROGRAMMER
 90 DIM OUTPUT$(300,0)
100 DIM BC$(10)
110 DIM BC(10)
120 DIM BACK$(300)
130LET PLACE = 0
140LET NERO = 0
150 LET ROGER = 1
160 LET NAP = 0
170 TIME = 0
180 DIM PULSEMAG$(200),Q$(200)
190 DIMA$(26)
200 MODE 128:CLS
210 PRINT
220 PRINT"FORMAL POTENTIAL IN MILLIVOLTS AS DETERMINED FROM CYCLIC "
230 INPUT"VOLTAMMETRY AT SLOW SWEEP RATES ";ER
240 PRINT
250 IF ER=0 THEN ER=400
260 INPUT"ENTER INTIAL POTENTIAL OF NORMAL PULSE PROGRAM ";INIT
270 IF INIT=0 THEN INIT=-400
280 PRINT
290 INPUT "FINAL POTENTIAL mV";FINAL
300 IF FINAL=0 THEN FINAL=1000
310 PULSES=1
320 RES$=""
330 PRINT
340 INPUT"ENTER FULL SCALE CURRENT IN MILLIAMPS ";POTFS
350 IF POTFS=0 THEN SOUND 1,-15,1000,10:CLS:GOTO 340
360 POTFS=POTFS*1E-3
370 PRINT
380 INPUT"TEMPERATURE IN DEGREES CENTIGRADE ";TEMP:TEMP=TEMP+273.1
390 IF TEMP =273.1 THEN TEMP=298.1
400 PRINT
410 GOSUB 550
420 IF ABS(VAL(OUTPUT$(1,0)))>1000 THEN SOUND 1,-15,1000,10:PRINT "CURRENT OVERLOAD, INCREASE CURRENT SETTING":END
430PRINT
440 PRINT
450 PLACE=0
460 ROGER=1
470PRINT
480 INPUT "NUMBER OF PULSES";PULSES
490 IF PULSES=0 THEN PULSES=1
500PRINT
```

```
 510  INPUT "OUTPUT TO DATA FILE Y/N";RES$
 520   IF RES$="N" OR RES$="" THEN 550
 530 PRINT
 540   INPUT "ENTER  FILENAME ";FILE$
 550     LET INCREM =(FINAL - INIT)/PULSES
 560 LET BASE$=STR$(INIT)
 570 FOR N=1 TO PULSES
 580LET PULSEMAG = INIT + N*INCREM
 590LET Z=4*INIT
 600LET LOO$ = STR$(-4*(INIT-PULSEMAG))
 610LET PULSEMAG$(N) = "ADD "+LOO$
 620  LET Q$(N)="LC 0 5 0 0 0 0 0"
 630LET SETE$="BIAS "+BASE$
 640 LET R$="LC 1999 1 0"
 650 NEXT N
 660 DATA "SIE 1","FP 0","LP 1999","MM 2","MR 2","TMB 100"
 670  DATA "DCV 0","SCV 2","PCV 2","CLR"
 680 DATA "PCV 0","CLR","NC","CELL 1","TC"
 690DATA "WCD","DC 0 1","DC 15 1","DC 25 1","DC 45 1","DC 105 1"
 700LET COM = 26
 710REM SETTING UP THE INTERFACE
 720 *IEEE
 730 cmd%=OPENIN("COMMAND")
 740 data%=OPENIN("DATA")
 750 PRINT#cmd%,"BBC DEVICE NO",7
 760 PRINT#cmd%,"CLEAR"
 770 PRINT#cmd%,"REMOTE ENABLE"
 780 PRINT#cmd%,"END OF STRING",CHR$(13)+CHR$(10)
 790 pot%=OPENIN("12")
 800 PRINT#cmd%,"LISTEN",pot%,"EXECUTE"
 810PRINT#data%,"DD 13 + 10"
 820  FOR M = 1 TO PULSES
 830 PRINT
 840 PRINT "PULSE ";M" NOW BEING APPLIED"
 850 PRINT
 860  GOSUB 1620
 870  RESTORE
 880  NEXT M
 890 PRINT
 900 SOUND 1,-15,1500,15
 910REM FINDS BACKGROUND CURRENT PER PULSE
 920 IF PULSES = 1 THEN GOTO 1190
 930 DIM I(5)
 940 EI=-400
 950 EF=0
 960 FIRST=ABS((INIT-EI)/INCREM*5 )
 970 LAST=ABS(INIT-EF)/INCREM*5
 980 FOR X= FIRST TO LAST  STEP 5
 990 BC(1)=BC(1)+VAL(OUTPUT$(1+X,0))
1000 BC(2)=BC(2)+VAL(OUTPUT$(2+X,0))
```

```
1010 BC(3)=BC(3)+VAL(OUTPUT$(3+X,0))
1020 BC(4)=BC(4)+VAL(OUTPUT$(4+X,0))
1030 NEXT X
1040 BC$(1)=STR$((BC(1))/((LAST-FIRST)/5))
1050 BC$(2)=STR$((BC(2))/((LAST-FIRST)/5))
1060 BC$(3)=STR$((BC(3))/((LAST-FIRST)/5))
1070 BC$(4)=STR$((BC(4))/((LAST-FIRST)/5))
1080 D=1
1090 TERM=PULSES%5
1100 FOR Y= 1 TO 4
1110 FOR X=0 TO TERM   STEP 5
1120 FACTOR=X/5%INCREM/(EF-EI)
1130 CORRECT=VAL(BC$(Y))%FACTOR
1140 BACK$(D+X)=LEFT$(STR$(VAL(OUTPUT$(D+X,0))-CORRECT),4)
1150 NEXT X
1160 D=D+1
1170 NEXT Y
1180 PRINT
1190 IF PULSES>1 THEN P$="]"
1200 IF P$="" THEN GOTO 1230
1210 IF P$<>"P" THEN GOTO 1440
1220 VDU 2
1230PRINT
1240PRINT "               SAMPLING TIME milli seconds    "
1250PRINT "VOLTS";" 0  ";"  1   ";"  2   ";"  4   ";"  10  "
1260FOR Y  = 0 TO PLACE-1
1270 IF NERO > 0 THEN 1350
1280 LET MOT$ = STR$(INCREM%ROGER + INIT)
1290 LET ROGER = ROGER + 1
1300 NERO = NERO + 1
1310  OUT=VAL(OUTPUT$(Y,0))/1024%POTFS
1320 OUT$=LEFT$(STR$(OUT),4)+RIGHT$(STR$(OUT),3)
1330 LET DUMP$ = MOT$ + "   " + OUT$
1340 GOTO 1380
1350 IF NERO = 1 THEN LET NAP = 9 ELSE NAP = NAP + 6
1360 DUMP$=LEFT$(STR$(VAL(OUTPUT$(Y,0))/1024%POTFS),4)+RIGHT$(STR$(VAL(OUTPUT$(Y,0))/1024%POTFS),3)
1370 LET NERO = NERO + 1
1380 PRINT TAB(NAP);DUMP$;
1390IF NERO < 5 THEN 1430
1400LET NERO = 0
1410 LET NAP = 0
1420PRINT
1430NEXT Y
1440 VDU 3
1450 IF RES$="Y" THEN 1460 ELSE 1610
1460 REM SENDS DATA TO DISK
1470 *DISK
1480 *CLOSE
1490 H=OPENOUT FILE$
1500 PRINT#H,STR$(PLACE)
```

```
1510 PRINT#H,STR$(INCREM)
1520 PRINT#H,STR$(INIT)
1530 PRINT#H,STR$(FINAL)
1540 PRINT#H,STR$(PULSES)
1550  FOR C = 0 TO PLACE-1
1560   PRINT #H,OUTPUT$(C,0)
1570  NEXT C
1580PRINT#H,"STOP"
1590 CLOSE#H
1600 '!EEE
1610 GOTO 2210
1620 FOR N=1 TO COM
1630 IF N=11 THEN A$(11)=PULSEMAG$(M):GOTO 1690
1640 IF N=12 THEN A$(12)=Q$(M):GOTO 1690
1650 IF N=13 THEN A$(13)=R$ :GOTO 1690
1660 IF N=17 THEN A$(17)=SETE$:GOTO 1690
1670 IF N=21 THEN A$(21)=SETE$:GOTO 1690
1680 READ A$(N)
1690 NEXT N
1700 TIME=0
1710REM MAIN LOOP OF STATIC INTERFACE
1720PRINT#cmd%,"UNLISTEN"
1730FOR N = 1 TO COM
1740REM GOES TO DEVICE DRIVER ROUTINE
1750 GOSUB 2040
1760  IF (ASC(serpoll$) AND 2)=2 THEN PRINT "ERROR"
1770  IF NO=0 THEN 1850
1780  FOR I = 0 TO NO
1790 GOTO 1810
1800PRINT OUTPUT$(PLACE,I);" ";
1810  NEXT I
1820 PLACE = PLACE + 1
1830 GOTO 1850
1840  PRINT
1850  NEXT N
1860  GOTO 2200
1870 REM SEND COMMAND TO 273
1880REM DO SERIAL POLL
1890GOSUB 2100
1900REM WAIT FOR PREVIOUS COMMAND TO BE DONE
1910IF (ASC(serpoll$) AND 1) THEN 1920 ELSE 1890
1920PRINT#cmd%,"LISTEN",pot%,"EXECUTE"
1930PRINT#data%,A$(N)
1940PRINT#cmd%,"UNLISTEN"
1950RETURN
1960REM GET RESPONSES
1970LET NO = 0
1980REM DO A SERIAL POLL
1990GOSUB 2100
2000IF (ASC(serpoll$) AND 128) = 128 THEN 2010  ELSE 2020
```

```
2010GOSUB 2140
2020IF (ASC(serpoll$) AND 1) = 1 THEN 2030 ELSE 1990
2030RETURN
2040REM DEVICE DRIVER
2050  REM   OUTPUT COMMAND TO DEVICE
2060GOSUB 1870
2070REM GET RESPONSES
2080   GOSUB 1960
2090   RETURN
2100REM SERIAL POLL
2110PRINT#cmd%,"SERIAL POLL",pot%,1
2120INPUT#cmd%,serpoll$
2130RETURN
2140REM RECEIVING OUTPUT FROM 273
2150PRINT#cmd%,"TALK",pot%
2160INPUT#data%,OUTPUT$(PLACE,NO)
2170PRINT#cmd%,"UNTALK"
2180NO = NO + 1
2190RETURN
2200 RETURN
2210 PRINT#cmd%,"GO TO LOCAL", pot%,"EXECUTE"
2220CLOSE#cmd%
2230CLOSE#data%
2240CLOSE#cmd%
2250 IF PULSES>1 THEN GOTO  2270
2260 RETURN
2270 DIM F$(5)
2280 PRINT
2290 INPUT"ENTER B FOR BACKGROUND CORRECTED VALUES ELSE RETURN ";BCORRECT$
2300 REM THIS PROGRAM OBTAINS THE STORED OUTPUT DATA FROM THE NORMAL PULSE EXPT
2310MODE 128
2320 NOOFSP=5
2330 VDU 28,0,5,60,0
2340 REM NORMAL PULSE WAVEFORM PROGRAMMER
2350 NERO=0
2360 ROGER=1
2370 NAP=0
2380TIME=0
2390 LET A = 0
2400*DISK
2410MOVE 0,0
2420 LET R = 0
2430 LET DUFF$="0"
2440 LET Y$="0"
2450FOR Z= 1 TO NOOFSP
2460MOVE 0,0
2470 DUFF$="0"
2480 Y$="0"
2490     FOR A = 0 TO 10
2500 LET D=10*A*NOOFSP
```

```
2510 IF D) PLACE-1 THEN 2660 ELSE R =R+1
2520    FOR X = 0 TO 9
2530  LET Y = Z + X*NOOFSP + 10*A*NOOFSP
2540   IF Y>PLACE-1 THEN 2640
2550   IF X = 0 THEN LET HI$(R) = "AM 0" + "," + DUFF$ + "," + Y$
2560 IF BCORRECT$="B" THEN B=VAL(BACK$(Y)):GOTO 2580
2570 B=VAL(OUTPUT$(Y,0))
2580  LET DUFF$=STR$(INCREM+INCREM*X+INCREM*10*A)
2590LET Y$=STR$(ABS(B*YF))
2600LET VOLT=INCREM+INCREM*X+INCREM*10*A
2610DRAW ( INIT+VOLT)/1.2,ABS(B*YF)
2620LABEL$="LA"+STR$(POTFS/YF*100)+"mA"
2630  LET HI$(R)=HI$(R) + "," + DUFF$ + "," + Y$
2640 NEXT X
2650 NEXT A
2660 NEXT Z
2670 PRINT
2680 INPUT "ENTER SCALE FACTOR ON CURRENT AXIS OR RETURN TO CONTINUE ";YF
2690PRINT
2700 IF YF=0 THEN YF=1
2710 IF YF>1 THEN CLS:GOTO 2300
2720
2730 INPUT"ENTER P FOR HARDCOPY TO PLOTTER, RETURN TO END ";PLT$
2740 IF PLT$="" THEN MODE128:GOTO 3010
2750 VDU 2
2760PRINT "MA 300,300"
2770 PRINT "DR"
2780 PRINT"AM 0,0,0,0,1000"
2790 PRINT "MA 0,0"
2800PRINT "AX 3,1400,7,1,-400,1000,50,0"
2810 PRINT"MA 0,0"
2820  FOR C = 1 TO R-1
2830 PRINT HI$(C)
2840  NEXT C
2850 PRINT "HO"
2860PRINT "MA -1500,0"
2870 PRINT "DR"
2880 PRINT "MA 400,-200"
2890 PRINT "CS3"
2900 PRINT "MA 800,-175"
2910 PRINT "SI 35,25"
2920 PRINT "LA  POTENTIAL mVolts "
2930 PRINT"AM 0,600,600,600,700"
2940 PRINT"MA 610,650"
2950 PRINT LABEL$
2960 PRINT "HO"
2970PRINT "MA -300,-300"
2980 PRINT "DR"
2990 VDU 3
3000 MODE 128
```

```
3010 TIM(4)=31.6227766
3020 TIM(3)=22.3606797B
3030 TIM(2)=15.8113883
3040 TIM(1)=10
3050 FOR I=4 TO 1 STEP -1
3060 XY=XY+(VAL(OUTPUT$(PLACE-I,0))/1024*POTFS)*TIM(I)
3070 TX=TX+TIM(I)
3080 TY=TY+(VAL(OUTPUT$(PLACE-1,0))/1024*POTFS)
3090 SX=SX+((TIM(I))^2)
3100 SY=SY+(VAL(OUTPUT$(PLACE-1,0))/1024*POTFS)^2
3110 NEXTI
3120 AX=TX/4
3130 AY=TY/4
3140 B=(XY-(4*AX*AY))/(SX-(4*(AX^2)))
3150 R=(XY-(4*AX*AY))/(((SX-(4*(AX^2)))*(SY-(4*(AY^2))))^0.5)
3160 C=AY-B*AX
3170 PRINT "REGRESSION LINE IS Y=";C"+";B"X"
3180PRINT
3190 PRINT
3200 PRINT "CORRELATION IS ";R
3210PRINT
3220 D=B/20949.2
3230 PRINT"D^1/2.C ";ABS(D)
3240 D2=(ABS(D)/0.7E-3)^2
3250D2$="LA D (0.7M) "+STR$(D2)
3260 DIFF$="LA D^1/2.C "+STR$(ABS(D))
3270 VDU2
3280 PRINT"DI 0,36"
3290 PRINT"MA 2000,100"
3300 PRINT DIFF$
3310 PRINTD2$
3320 PRINT"MA 2100,100"
3330 VDU3
3340 QQ=2100
3350 PRINT
3360 PRINT
3370 FOR J= 4 TO 1 STEP-1
3380 PRINT
3390 QQ=QQ+100
3400 PRINT
3410 X=0:Y=0:XY=0:TX=0:TY=0:SX=0:SY=0:N=0
3420 DL=25
3430 START=(INT((ER-INIT-DL)/INCREM))*5
3440  HL=300
3450 ND=(INT((ER-INIT+HL)/INCREM))*5
3460 X=(((START/5*INCREM)-400)/1000)
3470 FOR I= START-J TO ND STEP 5
3480 MTOP=ABS(VAL(OUTPUT$(I,0))/1024*POTFS)
3490 MBTM=ABS(VAL(OUTPUT$(PLACE-J,0))/1024*POTFS)
3500 M=MTOP/MBTM
```

```
3510 Z=(11610.709/TEMP)*(X-(ER/1000))
3520 TP=1.75*M^2*((1+EXP(-Z))^2)
3530 BTM=1-M*(1+EXP(-Z))
3540 IF BTM<0 THEN GOTO 3650
3550 Y=LN(M*((TP/BTM)^0.5))
3560 IF Y<-1THEN GOTO 3650
3570 IFY>1 THEN GOTO 3650
3580 N=N+1
3590 XY=XY+X*Y
3600 TX=TX+X
3610 TY=TY+Y
3620 SX=SX+(X^2)
3630 SY=SY+(Y^2)
3640 X=X+(INCREM/1000)
3650 NEXT I
3660 AX=TX/N
3670 AY=TY/N
3680 B=(XY-(N*AX*AY))/(SX-(N*(AX^2)))
3690 R=(XY-(N*AX*AY))/(((SX-(N*(AX^2)))*(SY-(N*(AY^2))))^0.5)
3700 C=AY-B*AX
3710 PRINT"REGRESSION LINE IS Y=";C"+";B"X"
3720 PRINT
3730 PRINT "CORRELATION IS ";R
3740 AA=B/(11610.709/TEMP)
3750 G=(ER/1000)-(-C/B)
3760 KEL=TIM(J)*3^0.5/4*EXP(AA*96485*G/8.31/298)
3770 K=KEL*ABS(D)
3780PRINT
3790 PRINT "ALPHA ";AA
3800 VDU2
3810 ALPHA$="LA ALPHA "+ STR$(AA)
3820 PRINT ALPHA$
3830 KINETIC$="LA KINETIC*CONC "+STR$(K)
3840 PRINT KINETIC$
3850 MV$="MA "+STR$(QQ)+",100"
3860 PRINTMV$
3870 VDU3
3880 PRINT
3890 PRINT"KINETIC * CONC ";K
3900 NEXT J
3910 VDU2
3920 PRINT"IN"
3930 VDU3
```

A2 Direct Data Analysis

A less complicated computer based system is to use the instrumental front panel to select the desired experimental conditions, and then to have direct data transfer to a computer for manipulation and analysis. Such a procedure was implemented for data capture from a Phillips 3311 digital storage oscilloscope used for short timescale potential step experiments. This was achieved via an IEEE-488 interface and BBC microcomputer. The data from the oscilloscope, resulting from the potential step experiment is transferred to the computer and displayed as a Cottrell plot. The results of several such experiments are obtained and signal averaged. Correction for background currents is achieved as desribed in section 3.3 and similarly averaged. The Faradaic current response is obtained by subtraction and then presented as a Cottrell plot. The operator then selects the region over which the homogeneous charge transport coefficient ($D_{CT}(PS)$) is calculated. This means that the region of analysis can be constrained to the semi-infinite diffusion regieme. Program listing 2 gives the BASIC program which implements this procedure.

Potential Step Chronoamperometry

```
 10DIM B(255)
 20DIM C(255)
 30DIMD(255)
 40XX$=""
 50DIMBC(255)
 60A=.3848
 70DIMB$(255)
 80DIMA$(268)
 90DIMCNT(255)
100DIM TIM(255)
110CLS
120PRINT:PRINT:PRINT:PRINT:PRINT
130PRINT"                          1. FOR NEW MEASUREMENT "
140PRINT:PRINT
150PRINT"                     2. RECONSTRUCT PREVIOUSLY SAVED TRACE"
160 PRINT:PRINT
170PRINT"                             3. SAVE DATA"
180 INPUTI$
190IFI$="1"THEN GOTO220
200IFI$="2"THEN GOTO1360
210IFI$="3"THEN GOTO1200
220 CLS
230 *IEEE
240cmd%=OPENIN("COMMAND")
250data%=OPENIN("DATA")
260PRINT#cmd%,"BBC DEVICE NO",7
270 PRINT #cmd%,"CLEAR"
280 PRINT #cmd%,"DEVICE CLEAR"
290PRINT#cmd%,"REMOTE ENABLE"
300 osc%=OPENIN("8")
310PRINT#cmd%,"SERIAL POLL",osc%,1
320INPUT#cmd%,statusmessage$
330 PRINT "RESULT OF SERIAL POLL ";ASC(statusmessage$)
340 PRINT
350 INPUT"ELECTRODE AREA IN CENTIMETRES SQUARED ";AREA
360 PRINT
370 INPUT"INPUT NUMBER OF REPEATED TRANSIENTS REQUIRED ";VV
380 PRINT
390 INPUT "RECORD FORWARD TRANSIENT AND PRESS RETURN TO CONTINUE ";ZZ$
400 PRINT
410PRINT#cmd%,"LISTEN",osc%,"EXECUTE"
420PRINT#data%,"SPR 32"
430PRINT#data%,"USP 47"
440PRINT#data%,"WTD 30"
450PRINT#data%,"REG 0/VER A/FCN ON/BGN 0/END 255/CNT 1/DAT ?"
460PRINT#cmd%,"UNLISTEN"
470PRINT"PLEASE WAIT WHILE DATA IS TRANSFERRED APPROX. DURATION 20 SECONDS"
480PRINT#cmd%,"TALK",osc%
490FOR I%=1TO255
500INPUT#data%,A$(I%)
```

```
510C(I%)=VAL(A$(I%))+C(I%)
520NEXT I%
530 PRINT#cmd%,"GO TO LOCAL",osc%,"EXECUTE"
540 J=J+1:IF J <VV  THEN INPUT"RECORD NEXT TRANSIENT PRESS RETURN ";J$ :GOTO 410
550PRINT#cmd%,"REMOTE ENABLE"
560FORI=1TO255
570A$(I)=STR$(C(I)/VV)
580 NEXT I
590PRINT#cmd%,"UNTALK"
600PRINT#cmd%,"UNLISTEN"
610 PRINT#cmd%,"GO TO LOCAL",osc%,"EXECUTE"
620CC=0
630AVI=0
640FORA=1TO30
650IFABS(VAL(A$(A))-VAL(A$(2)))<10 THENAVI=AVI+VAL(A$(A))
660IFABS(VAL(A$(A))-VAL(A$(2)))<10 THEN CC=CC+1
670NEXTA
680AVI=AVI/CC
690PRINT
700INPUT"VERTICAL SCALE IN VOLTS PER FIVE DIVISIONS ";SCV:
710PRINT
720 INPUT"POTENTIOSTAT FULL SCALE IN MILLIAMPS ";POTFS:POTFS=POTFS/1000
730FORI=2TO255
740CNT(I)=((VAL(A$(I))-AVI)/25.5*SCV*POTFS/5)
750NEXTI
760 PRINT
770 GOSUB1910
780IF CC< CBC THEN CC=CBC
790REM:TIMES CORRESPONDING TO CURRENTS
800PRINT
810INPUT"TIME IN MILLISECONDS PER DIVISION ";TDIV:TDIV=TDIV/1000
820FORI=1TO255
830TIM(I)=((I-CC-2)/255*10*TDIV)
840NEXTI
850 PRINT
860INPUT"STARTING POINT OF ANALYSIS ";Z
870PRINT
880INPUT"END POINT OF ANALYSIS MAX 255 ";F
890 IF F>255 THEN F=255
900IN=CC+Z+3
910 XY=0:TX=0:TY=0:SX=0:SY=0:AX=0:AY=0:N=0
920N=F-IN+1
930 IF XX$="C"THEN GOTO 980
940 FOR I=CC+3 TO 255
950 TIM(I)=1/(TIM(I)^0.5)
960CNT(I)=CNT(I)-(BC(I)*4)
970 NEXTI
980 FOR  J = IN TO F
990XY=XY+CNT(J)*TIM(J)
1000TX=TX+(TIM(J))
```

```
1010TY=TY+(CNT(J))
1020SX=SX+((TIM(J))^2)
1030SY=SY+((CNT(J))^2)
1040AX=TX/N
1050AY=TY/N
1060NEXTJ
1070B=(XY-(N*AX*AY))/(SX-(N*(AX^2)))
1080R=(XY-(N*AX*AY))/(((SX-(N*(AX^2)))*(SY-(N*(AY^2))))^0.5)
1090C=AY-B*AX
1100CLS
1110PRINT"REGRESSION LINE IS Y=";C"+";B"X"
1120PRINT
1130PRINT"CORRELATION IS ";R
1140 D=((B/(96485*AREA*0.75E-3))*1.77)^2
1150PRINT
1160PRINT"DIFFUSION COEFFECIENT ";D
1170VDU3
1180GOSUB 2310
1190PRINT
1200*DISC
1210INPUT"FILENAME ",F$
1220PRINT
1230INPUT"TITLE OR OTHER RELEVANT COMMENTS ";T$
1240PRINT
1250PRINT
1260INPUT"TITLE OR OTHER RELEVANT COMMENTS FOR BACKGROUND CORRECTION";TB$
1270  X=OPENOUT F$
1280PRINT#X,T$
1290PRINT#X,TB$
1300FORI=1TO 255
1310PRINT#X,A$(I),B$(I)
1320NEXTI
1330*CLOSE
1340END
1350PRINT
1360REM TRACE RECONSTRUCTION NB NO BACKGROUND CORRECTION
1370*DISC
1380INPUT"GIVE FILENAME ",F$
1390X=OPENIN F$
1400INPUT#X,TB$
1410INPUT#X,T$
1420PRINT
1430PRINTTB$
1440PRINT
1450FORI=1TO255
1460INPUT#X,A$(I),B$(I)
1470NEXTI
1480 *CLOSE
1490*IEEE
1500cmd%=OPENIN("COMMAND")
```

```
1510data%=OPENIN("DATA")
1520PRINT#cmd%,"BBC DEVICE NO",7
1530PRINT#cmd%,"CLEAR"
1540PRINT#cmd%,"REMOTE ENABLE"
1550 osc%=OPENIN("8")
1560PRINT#cmd%,"LISTEN",osc%,"EXECUTE"
1570PRINT#data%,"SPR 32"
1580PRINT#data%,"USP 47"
1590PRINT#data%,"REG 1/VER A/FCN ON/BGN 0/END 255/CNT 1"
1600PRINT#data%,"DAT 128"
1610FOR I=1TO255
1620PRINT#data%,STR$(VAL(A$(I)))
1630NEXT I
1640PRINT#cmd%,"UNLISTEN"
1650 PRINT#cmd%,"GO TO LOCAL",osc%,"EXECUTE"
1660*DISC
1670 INPUT"PRESS ANY KEY FOR ASSOCIATED BACKGROUND TRANSIENT RECONSTRUTION ";HH$
1680 X=OPENIN F$
1690PRINT
1700PRINTT$
1710CLOSE#X
1720*IEEE
1730cmd%=OPENIN("COMMAND")
1740data%=OPENIN("DATA")
1750PRINT#cmd%,"BBC DEVICE NO",7
1760PRINT#cmd%,"CLEAR"
1770PRINT#cmd%,"REMOTE ENABLE"
1780 osc%=OPENIN("8")
1790PRINT#cmd%,"LISTEN",osc%,"EXECUTE"
1800PRINT#data%,"SPR 32"
1810PRINT#data%,"USP 47"
1820PRINT#data%,"REG 1/VER A/FCN ON/BGN 0/END 255/CNT 1"
1830PRINT#data%,"DAT 128"
1840FOR I=1TO255
1850PRINT#data%,STR$(VAL(B$(I)))
1860NEXT I
1870PRINT#cmd%,"UNLISTEN"
1880 PRINT#cmd%,"GO TO LOCAL",osc%,"EXECUTE"
1890END
1900REM BACKGROUND CORRECTION
1910INPUT"INPUT NUMBER OF REPEATED BACKGROUND TRANSIENTS REQUIRED ";VV
1920PRINT
1930 INPUT "RECORD BACKGROUND TRANSIENT AND PRESS RETURN TO CONTINUE ";C$
1940PRINT
1950J=0
1960PRINT#cmd%,"LISTEN",osc%,"EXECUTE"
1970PRINT#data%,"SPR 32"
1980PRINT#data%,"USP 47"
1990PRINT#data%,"WTD 30"
2000PRINT#data%,"REG 0/VER A/FCN ON/BGN 0/END 255/CNT 1/DAT ?"
```

```
2010PRINT#cmd%,"UNLISTEN"
2020PRINT"PLEASE WAIT WHILE DATA IS TRANSFERRED APPROX. DURATION 20 SECONDS"
2030PRINT#cmd%,"TALK",osc%
2040FOR I%=1TO255
2050INPUT#data%,B$(I%)
2060D(I%)=VAL(B$(I%))+D(I%)
2070NEXT I%
2080 PRINT#cmd%,"GO TO LOCAL",osc%,"EXECUTE"
2090J=J+1:IF J<VV THEN INPUT"RECORD NEXT TRANSIENT PRESS RETURN ";V$  :GOTO 1960
2100PRINT
2110PRINT#cmd%,"REMOTE ENABLE"
2120FOR I=1TO255
2130B$(I)=STR$(D(I)/VV)
2140NEXTI
2150PRINT#cmd%,"UNTALK"
2160PRINT#cmd%,"UNLISTEN"
2170 PRINT#cmd%,"GO TO LOCAL",osc%,"EXECUTE"
2180AVI=0
2190FORA=1TO30
2200IFABS(VAL(B$(A))-VAL(B$(2)))<10 THENAVI=AVI+VAL(B$(A))
2210IFABS(VAL(B$(A))-VAL(B$(2)))<10 THEN CBC=CBC+1
2220NEXTA
2230AVI=AVI/CBC
2240INPUT"VERTICAL SCALE IN VOLTS PER DIVISION ";SCV:
2250PRINT
2260 INPUT"POTENTIOSTAT FULL SCALE IN MILLIAMPS ";POTFS:POTFS=POTFS/1000
2270FORI=2TO255
2280BC(I)=((VAL(B$(I))-AVI)/25.5*SCV*POTFS/5)
2290NEXTI
2300RETURN
2310XF=1100/TIM(IN)
2320YF=900/ CNT(IN)
2330MOVE50,50
2340DRAW1279,50
2350MOVE50,50
2360DRAW50,1023
2370FORI=50TO1023STEPYF
2380PLOT69,49,I:PLOT69,48,I:NEXTI
2390FORI=50 TO 1279STEPXF:PLOT69,I,47:PLOT69,I,46:NEXTI
2400FORI=IN TO F
2410X=TIM(I)*XF
2420Y=CNT(I)*YF
2430PLOT69,X+50,Y+50
2440NEXTI
2450PRINT
2460 INPUT"PRESS C TO ALTER ANALYSIS BOUNDARIES ";XX$
2470IFXX$="C" THEN PRINT:GOTO 860
2480 GOTO110
2490FORI=1TO255:PRINTI;"   ";TIM(I);"   ";CNT(I);"   ";BC(I)
2500NEXTI
```

A3 2 Analysis of Electrochemical Data.

In order to evaluate rate constants such as the rate of homogeneous charge transport from electrochemical data within the framework of the theoretical models discussed in Section 1.3 several BASIC programs have been written. This software does not interact directly with the experiments but is postrun on an IBM compatible computer. All programs in this section were written using GW-BASIC.

Program 1 calculates $D_{CT}(CV)$ from the cyclic voltammetry peak current, redox site concentration and surface coverage with a finite diffusion space from the model of Aoki et al. discussed in section 1.3.1. This is achieved using an iterative procedure based on the bisection method. Iteration is continued until the error on the predicted peak current is less than 1%. As well as calculating $D_{CT}(CV)$ the parameter W describing the ratio of the thickness of the diffusion space to the film thickness is also calculated and assigned to either of the two limiting cases i.e a surface or semi-infinite diffusion space.

Program 1 Linear Sweep Voltammetry With Finite Diffusion Space.

```
10    REM PROGRAM TO CALCULATE DIFFUSION COEFFICIENTS FROM CYCLIC
      VOLTAMMETRIC DATA FOR A REVERSIBLE REACTION USING THE AOKI A
20    CLS
30    INPUT"SURFACE COVERAGE IN MOLES PER CENTIMETRE SQUARED ";SC
40    IF SC=0 THEN CLS:BEEP :GOTO 30
50    PRINT
60    INPUT"CONCENTRATION OF ELECTROACTIVE SPECIES IN MOLES
      PER CENTIMETRE CUBED ";CONC
70    IF CONC=0 THEN CLS:BEEP:GOTO 60
80    PRINT
```

```
250     TY=TY+Y
260     SX=SX+(X^2)
270     SY=SY+(Y^2)
280     PRINT
290     GOTO 100
300     AX=TX/NN
310     AY=TY/NN
320     B=(XY-(NN*AX*AY))/(SX-(NN*(AX^2)))
330     R=(XY-(NN*AX*AY))/(((SX-(NN*(AX^2)))*(SY-(NN*(AY^2))))^.5)
340     C=AY-B*AX
350     D.5C=B/269000!/A
360     D=(D.5C/CONC)^2
370     PRINT:PRINT
380     PRINT "DIFFUSION COEFFICIENT BASED ON LINE SLOPE IS ";D;"CM^2 S^-1"
390     PRINT
400     IF C <0 THEN PRINT"REGRESSION LINE IS Y=";B;"X";C
410     IF C >0 THEN PRINT "REGRESSION LINE IS  Y=";B;"X+";C
420     PRINT
430     PRINT"CORRELATION COEFFICIENT IS ";R
```

The evaluation of thermodynamic parameters from the temperature dependence of both the cyclic voltammetry and potential step measurements formed a central part of this work. The following program uses previously obtained data for the dependence of the cyclic voltammetry peak current on temperature to calculate thermodynamic parameters. Initially the charge transport rate is calculated at each temperature, depending on the accuracy with which the peak current is reproduced the operator decides whether to accept or reject the data point. The effect of increased temperature on the ratio of the diffusion layer thickness to film thickness is explored via the parameter W. The Arrhenius plot is displayed on screen, with an option for

hardcopy output, points can be deleted as required. Least squares linear regression is then applied to calculate the activation energy and enthalpy terms. Using the value of the intersite separation entered by the operator and the Eyring equation the entropy is calculated. Finally the enthalpy term is calculated.

Program 3 Evaluation of Thermodynamic Parameters for Homogeneous Charge Transport Using Cyclic Voltammetry With Finite Diffusion Space.

```
10    REM PROGRAM TO CALCULATE ACTIVATION ENERGIES, ENTROPIES, ENT
      GIBBS FREE ENERGIES
20    SCREEN 2
30    YMIN=1E+08:XMIN=1E+08
40    YMAX=-1E+08:XMAX=0
50    KEY 1,"LIST "+ CHR$(13)
60    KEY 3, "GOTO 640" + CHR$(13)
70    CLS
80    INPUT"PRESS P FOR RESULTS TO PRINTER ";PRN$
90    PRINT
100   IF PRN$="P" OR PRN$="p" THEN INPUT "PLEASE INPUT ELECTROLYTE
      USED ";T$:PRINT
110   INPUT "SEPARATION OF ELECTROACTIVE CENTRES IN ANGSTROMS ";SEP
120   IF SEPN=0 THEN BEEP:CLS:GOTO 110
130   SEPN=SEPN*1E-10
140   PRINT
150   INPUT"CONCENTRATION OF ELECTROACTIVE SPECIES IN MOLES
      PER CENTIMETRE CUBED ";CONC
160   CONC=CONC*.001
170   IF CONC=0 THEN CLS:BEEP:GOTO 150
180   PRINT
190   DIM X(100),Y(100)
200   NN=0
```

```
210    INPUT"SURFACE COVERAGE IN MOLES PER CENTIMETRE SQUARED ";SC
220    IF SC=0 THEN BEEP :CLS :GOTO 210
230    PRINT
240    INPUT "ELECTRODE AREA IN CENTIMETRES SQUARED ";A
250    IF A=0 THEN A=.3848
260    PRINT
270    INPUT "NUMBER OF ELECTRONS TRANSFERRED ";N
280    IF N=0 THEN N=1
290    F=96485!:R=8.310001
300    PRINT
310    INPUT"TEMPERATURE IN DEGREES CENTIGRADE ";T
320    IF T=0 THEN BEEP:CLS: GOTO 310
330    T=T+273.1
340    PRINT
350    V=.1
360    INPUT"PEAK CURRENT IN MICROAMPS ";IP:IP=IP*.000001
370    IF IP = 0 THEN BEEP: CLS:GOTO 360
380    PRINT
390    K1=.001
400    K2=4000
410    PRINT
420    CLS
430    DEF FNTH(X)=(.5*(EXP(X)-EXP(-X)))/(.5*(EXP(X)+EXP(-X)))
440    W=N*F*V*K1/R/T
450    C=.56*(W^.5)+(.05*W)
460    IF C>5 THEN E1=.446*N*F*A*SC/K1*(W^.5)-IP:GOTO 480
470    E1=.446*N*F*A*SC/K1*(W^.5)*FNTH(C)-IP
480    W=N*F*V*K2/R/T
490    C=.56*(W^.5)+(.05*W)
500    IF C>5 THEN E2=.446*N*F*A*SC/K2*(W^.5)-IP:GOTO 520
510    E2=.446*N*F*A*SC/K2*(W^.5)*FNTH(C)-IP
520    K3=(K1+K2)/2
530    PRINT K1,K2,K3
540    IF E2>0 THEN PRINT "PROBLEM IN LIMITS !!!!!!!!":END
550    W=N*F*V*K3/R/T
```

```
560    C=.56*(W^.5)+(.05*W)
570    IF C>5 THEN E3=(.446*N*F*A*SC*(W^.5)/K3)-IP:GOTO 590
580    E3=.446*N*F*A*SC/K3*(W^.5)*FNTH(C)-IP
590    IF E3<=0 THEN K2=K3 600 IF E3>0 THEN K1=K3:
610    IF ABS(K1-K2)<.0001 THEN GOTO 630
620    GOTO 440
630    PRINT:PRINT "THICKNESS^2/DIFFUSION COEFFICIENT IS ";K1
640    LET LT=SC/CONC
650    PRINT
660    D =(LT^2)/K1
670    W=N*F/R/T*V*K1
680    IPE=.446*N*F*A*SC/K1*(W^.5)
690    IF IPE <IP*.999 OR IPE>IP*1.001 THEN BEEP
700    PRINT "PREDICTED PEAK CURRENT FROM THIS VALUE OF
       THICKNESS SQUARED / DIFFUSION COEFFICIENT IS ";IPE
710    LC=N^2*F^2*V*SC/4/R/T
720    PRINT
730    PRINT "LANGMUIR CURRENT IS ";LC
740    IF IPE > LC THEN BEEP:BEEP
750    PRINT
760    PRINT "ESTIMATED DIFFUSION COEFFICIENT IS ";D" CM^2/S"
770    PRINT
780    PRINT "LOG DIFFUSION COEFFICIENCT ";LOG(D)
790    PRINT
800    PRINT "1/T ";1/T
810    PRINT
820    PRINT "LAYER THICKNESS ";LT/100;" METRES"
830    PRINT
840    IF W>6.9 THEN PRINT "THIS VALUE OF W (";W") IMPLIES A
       DIFFUSIONAL BEHAVIOUR"
850    IF W<1.3 THEN PRINT "THIS VALUE OF W(";W") IMPLIES A SURFACE WAVE"
860    PRINT
870    INPUT "PRESS RETURN TO ACCEPT THIS ENTRY OR N TO REJECT ";N$
880    IF N$="" THEN NN=NN+1:X(NN)=1/T: Y(NN)=LOG(D)
```

```
890   IF N$="" AND NN=1  AND PRN$="P" THEN LPRINT:LPRINT:LPRINT:
      LPRINT:LPRINT:LPRINT "TEMP 'K   1/T   Ip   Dct   Ln DcT"
900   IF N$="" AND PRN$="P" THEN LPRINT T"    ";1/T"     ";IP"
      ";D"     ";LOG(D)
910   PRINT
920   INPUT "INPUT E TO END, RETURN TO INPUT ANOTHER SWEEP RATE
      UNDER SAME CONDITIONS ";CC$
930   IF CC$="E" OR CC$="e" THEN GOTO 950
940   CLS :GOTO 310
950   FOR J=1 TO NN
960   IF X(J)>XMAX THEN XMAX=X(J)
970   IF Y(J)<YMIN THEN YMIN=Y(J)
980   IF Y(J)>YMAX THEN YMAX=Y(J)
990   IF X(J)<XMIN THEN XMIN=X(J)
1000  XY=XY+(X(J)*Y(J))
1010  TX=TX+X(J)
1020  TY=TY+Y(J)
1030  SX=SX+((X(J)^2))
1040  SY=SY+((Y(J)^2))
1050  NEXT J
1060  AX=TX/NN
1070  AY=TY/NN
1080  B=(XY-(NN*AX*AY))/(SX-(NN*(AX^2)))
1090  R=(XY-(NN*AX*AY))/(((SX-(NN*(AX^2)))*(SY-(NN*(AY^2))))^.5)
1100  C=AY-B*AX
1110  IF PRN$="P" THEN LPRINT
1120  PRINT
1130  GOSUB 1430
1140  IF PRN$="P" THEN LPRINT:LPRINT
1150  IF B>0 THEN PRINT "REGRESSION LINE IS Y=";C"+";B"X"
1160  IF B>0 AND PRN$="P" THEN LPRINT "REGRESSION LINE IS Y=";C"+";B"X"
1170  IF B<0 THEN PRINT "REGRESSION LINE IS Y=";C;B"X"
1180  IF B<0 AND PRN$="P" THEN LPRINT "REGRESSION LINE IS Y=";C;B"X"
1190  PRINT
1200  IF PRN$="P" THEN LPRINT
```

```
1210    PRINT "CORRELATION COEFFICIENT IS ";R
1220    IF PRN$="P" THEN LPRINT "CORRELATION COEFFICIENT IS ";R
1230    PRINT
1240    IF PRN$="P" THEN LPRINT:LPRINT
1250    ACT=-B*8.310001/1000
1260    IF PRN$="P" THEN LPRINT "ELECTROLYTE USED IS ";T$
1270    IF PRN$="P" THEN LPRINT
1280    PRINT "ACTIVATION ENERGY IS ";ACT" kJ/Mol"
1290    IF PRN$="P" THEN LPRINT "ACTIVATION ENERGY IS ";ACT" kJ/Mol"
1300    PRINT:IF PRN$="P" THEN LPRINT
1310    DCTO=EXP(C)
1320    ENT1=(DCTO/2.718/1.38E-23/298*6.6E-34/10000)^.5
1330    ENT2=(ENT1/SEPN)^2
1340    ENT=((LOG(ENT2)))*8.310001
1350    PRINT "ENTROPY IS ";ENT"J/Mol":IF PRN$="P" THEN LPRINT
      "ENTROPY IS ";ENT" J/Mol"
1360    PRINT:IF PRN$="P" THEN LPRINT
1370    PRINT "ENTHALPY IS ";ACT-2.47"kJ/Mol":IF PRN$="P" THEN LPRINT
     "ENTHALPY IS ";ACT-2.47"kJ/Mol"
1380    PRINT:IF PRN$="P" THEN LPRINT
1390    FE=ACT-2.47-(298*ENT/1000)
1400    PRINT "FREE ENERGY IS ";FE"kJ/Mol":IF PRN$="P" THEN LPRINT
     "FREE ENERGY IS ";FE"kJ/Mol"
1410    PRINT:IF PRN$="P" THEN LPRINT
1420    END
1430    REM graphics routine
1440    CLS
1450    XFAC=600/(XMAX-XMIN)
1460    YFAC=200/(YMAX+ABS(YMIN))
1470    XL=0:YL=0
1480    FOR J=1 TO NN
1490    X=(X(J)-XMIN)*XFAC:Y=200-(Y(J)+ABS(YMIN))*YFAC
1500    PSET (X,Y)
1510    LINE (XL,YL)-(X,Y)
1520    XL=X:YL=Y
```

```
1530    CIRCLE (X,Y),5
1540    NEXT J
1550    INPUT "PRESS RETURN TO CONTINUE ";XX$
1560    RETURN
```

Using cyclic voltammetry data obtained under semi-infinite diffusion conditions thermodynamic parameters can be similarly evaluated using the temperature dependence of D_{CT} obtained via the Randle-Sevcik equation.

Program 4 Evaluation of Thermodynamic Parameters for Homogeneous Charge Transport Using Cyclic Voltammetry with Semi-infinite Diffusion Space

```
10      REM PROGRAM TO CALCULATE ACTIVATION ENERGIES, ENTROPIES, ENT
        AND GIBBS FREE ENERGIES
20      SCREEN 2
30      YMIN=1E+08:XMIN=1E+08
40      YMAX=-1E+08:XMAX=0
50      KEY 1,"LIST "+ CHR$(13)
60      KEY 3, "GOTO 770" + CHR$(13)
70      CLS
80      INPUT "PLEASE INPUT ELECTROLYTE USED ";TITLE$
90      PRINT
100     INPUT"ENTER P FOR RESULTS TO PRINTER ";P$
110     PRINT
120     INPUT"SEPARATION OF REDOX CENTRES IN ANGSTROMS ";SEPN
130     SEPN=SEPN*1E-10
140     IF SEPN=0 THEN BEEP:CLS: GOTO 120
150     PRINT
160     INPUT "OSMIUM CONCENTRATION IN MOLES PER CM^3 ";CONC
170     IF CONC=0 THEN CLS:BEEP:GOTO 160
180     CONC=CONC*.001
190     PRINT
```

```
200     INPUT "ELECTRODE AREA IN CM^2 DEFAULT 0.3848 ";A
210     IF A=0 THEN A=.3848
220     PRINT
230     DIM X(100),Y(100)
240     NN=0
250     IF N=0 THEN N=1
260     F=96485!:R=8.310001
270     INPUT"TEMPERATURE IN DEGREES CENTIGRADE ";T$
280     IF T$="/" THEN GOTO 410
290     T=VAL(T$)
300     IF T=0 THEN BEEP:CLS: GOTO 270
310     T=T+273.1
320     PRINT
330     INPUT "PEAK CURRENT OBTAINED AT 100 mV/S IN MICROAMPS ";IP
340     IP=IP*.000001
350     D=(IP/4640000!/A/.3162/CONC*(T^.5))^2
360     NN=NN+1:X(NN)=1/T: Y(NN)=LOG(D)
370     IF NN=1 AND P$="P" THEN LPRINT:LPRINT:LPRINT:LPRINT:LPRINT:
        LPRINT "TEMP 'K        1/T          Dct              Ln DcT"
380     IF N$="" AND P$="P" THEN LPRINT:LPRINT T"    ";1/T"     ";D"
          ";LOG(D)
390     PRINT
400     CLS :GOTO 270
410     FOR J=1 TO NN
420     IF X(J)>XMAX THEN XMAX=X(J)
430     IF Y(J)<YMIN THEN YMIN=Y(J)
440     IF Y(J)>YMAX THEN YMAX=Y(J)
450     IF X(J)<XMIN THEN XMIN=X(J)
460     XY=XY+(X(J)*Y(J))
470     TX=TX+X(J)
480     TY=TY+Y(J)
490     SX=SX+((X(J)^2))
500     SY=SY+((Y(J)^2))
510     NEXT
520     AX=TX/NN
```

```
530     AY=TY/NN
540     B=(XY-(NN*AX*AY))/(SX-(NN*(AX^2)))
550     R=(XY-(NN*AX*AY))/(((SX-(NN*(AX^2)))*(SY-(NN*(AY^2))))^.5)
560     C=AY-B*AX
570     IF P$="P" THEN LPRINT
580     PRINT
590     GOSUB 900
600     IF P$="P" THEN LPRINT:LPRINT
610     IF B>0 THEN PRINT "REGRESSION LINE IS Y=";C"+";B"X"
620     IF B>0 AND P$="P" THEN LPRINT "REGRESSION LINE IS Y=";C"+";B"X"
630     IF B<0 THEN PRINT "REGRESSION LINE IS Y=";C;B"X"
640     IF B<0 AND P$="P" THEN LPRINT "REGRESSION LINE IS Y=";C;B"X"
650     PRINT
660     IF P$="P" THEN LPRINT
670     PRINT "CORRELATION COEFFICIENT IS ";R
680     IF P$="P" THEN LPRINT "CORRELATION COEFFICIENT IS ";R
690     PRINT
700     IF P$="P" THEN LPRINT:LPRINT
710     ACT=-B*8.310001/1000
720     IF P$="P" THEN LPRINT "ELECTROLYTE USED IS ";TITLE$
730     IF P$="P" THEN LPRINT
740     PRINT "ACTIVATION ENERGY IS ";ACT" kJ/Mol"
750     IF P$="P" THEN LPRINT "ACTIVATION ENERGY IS ";ACT" kJ/Mol"
760     PRINT:IF P$="P" THEN LPRINT
770     DCTO=EXP(C)
780     ENT1=(DCTO/2.718/1.38E-23/298*6.626E-34/10000)^.5
790     ENT2=(ENT1/SEPN)^2
800     ENT=((LOG(ENT2)))*8.310001
810     PRINT "ENTROPY IS ";ENT"J/Mol":IF P$="P" THEN LPRINT
      "ENTROPY IS ";ENT" J/Mol"
820     PRINT:IF P$="P" THEN LPRINT
830     PRINT "ENTHALPY IS ";ACT-2.47"kJ/Mol":IF P$="P" THEN LPRINT
      "ENTHALPY IS ";ACT-2.47"kJ/Mol"
840     PRINT:IF P$="P" THEN LPRINT
850     FE=ACT-2.47-(298*ENT/1000)
```

```
860     PRINT "FREE ENERGY IS ";FE"kJ/Mol":IF P$="P" THEN LPRINT
        "FREE ENERGY IS ";FE"kJ/Mol"
870     PRINT:IF P$="P" THEN LPRINT
880     PRINT
890     END
900     REM graphics routine follows
910     CLS
920     XFAC=600/(XMAX-XMIN)
930     YFAC=200/(YMAX+ABS(YMIN))
940     XL=0:YL=0
950     FOR J=1 TO NN
960     X=(X(J)-XMIN)*XFAC:Y=200-(Y(J)+ABS(YMIN))*YFAC
970     PSET (X,Y)
980     LINE (XL,YL)-(X,Y)
990     XL=X:YL=Y
1000    CIRCLE (X,Y),5
1010    NEXT
1020    INPUT "PRESS RETURN TO CONTINUE ";XX$
1030    RETURN
```

A BASIC program to calculate the thermodynamic parameters from the temperature dependence of D_{CT} calculated from potential step has also been developed.

Program 5 Evaluation of Thermodynamic Parameters for Homogeneous charge Transport Using Potential Step Data with Semi-infinite Diffusion Space.

```
10      REM PROGRAM TO CALCULATE ACTIVATION ENERGIES, ENTROPIES,
        ENTHALPY AND GIBBS FREE ENERGIES
20      SCREEN 2
30      YMIN=1E+08:XMIN=1E+08
40      YMAX=-1E+08:XMAX=0
```

```
50      KEY 1,"LIST "+ CHR$(13)
60      KEY 3, "GOTO 770" + CHR$(13)
70      CLS
80      INPUT "PLEASE INPUT ELECTROLYTE USED ";TITLE$
90      PRINT
100     INPUT"ENTER P FOR RESULTS TO PRINTER ";P$
110     PRINT
120     INPUT"SEPARATION OF REDOX CENTRES IN ANGSTROMS ";SEPN
130     SEPN=SEPN*1E-10
140     IF SEPN=0 THEN BEEP:CLS: GOTO 120
150     PRINT
160     DIM X(100),Y(100)
170     NN=0
180     IF N=0 THEN N=1
190     F=96485!:R=8.310001
200     INPUT "POWER OF DIFFUSION COEFFICIENT DEFAULT 1E-9 ";MAN
210     IF MAN=0 THEN MAN=1E-09
220     PRINT
230     INPUT"TEMPERATURE IN DEGREES CENTIGRADE ";T$
240     IF T$="/" THEN GOTO 360
250     T=VAL(T$)
260     IF T=0 THEN BEEP:CLS: GOTO 230
270     T=T+273.1
280     PRINT
290     INPUT "DIFFUSION COEFFICIENT OBTAINED USING CHRONAMPEROMETR
300     D=D*MAN
310     NN=NN+1:X(NN)=1/T: Y(NN)=LOG(D)
320     IF NN=1 AND P$="P" THEN LPRINT:LPRINT:LPRINT:LPRINT:LPRINT:
        LPRINT "TEMP 'K        1/T          Dct              Ln DcT"
330     IF N$="" AND P$="P" THEN LPRINT:LPRINT T"    ";1/T"     ";D"
          ";LOG(D)
340     PRINT
350     CLS :GOTO 230
360     FOR J=1 TO NN
370     IF X(J)>XMAX THEN XMAX=X(J)
```

```
380   IF Y(J)<YMIN THEN YMIN=Y(J)
390   IF Y(J)>YMAX THEN YMAX=Y(J)
400   IF X(J)<XMIN THEN XMIN=X(J)
410   XY=XY+(X(J)*Y(J))
420   TX=TX+X(J)
430   TY=TY+Y(J)
440   SX=SX+((X(J)^2))
450   SY=SY+((Y(J)^2))
460   NEXT
470   AX=TX/NN
480   AY=TY/NN
490   B=(XY-(NN*AX*AY))/(SX-(NN*(AX^2)))
500   R=(XY-(NN*AX*AY))/(((SX-(NN*(AX^2)))*(SY-(NN*(AY^2))))^.5)
510   C=AY-B*AX
520   IF P$="P" THEN LPRINT
530   PRINT
540   GOSUB 960
550   IF P$="P" THEN LPRINT:LPRINT
560   IF B>0 THEN PRINT "REGRESSION LINE IS Y=";C"+";B"X"
570   IF B>0 AND P$="P" THEN LPRINT "REGRESSION LINE IS Y=";C"+";B"X"
580   IF B<0 THEN PRINT "REGRESSION LINE IS Y=";C;B"X"
590   IF B<0 AND P$="P" THEN LPRINT "REGRESSION LINE IS Y=";C;B"X"
600   PRINT
610   IF P$="P" THEN LPRINT
620   PRINT "CORRELATION COEFFICIENT IS ";R
630   IF P$="P" THEN LPRINT "CORRELATION COEFFICIENT IS ";R
640   PRINT
650   IF P$="P" THEN LPRINT:LPRINT
660   ACT=-B*8.310001/1000
670   IF P$="P" THEN LPRINT "ELECTROLYTE USED IS ";TITLE$
680   IF P$="P" THEN LPRINT
690   PRINT "ACTIVATION ENERGY IS ";ACT" kJ/Mol"
700   IF P$="P" THEN LPRINT "ACTIVATION ENERGY IS ";ACT" kJ/Mol"
710   PRINT:IF P$="P" THEN LPRINT
720   DCTO=EXP(C)
```

```
730     ENT1=(DCTO/2.718/1.38E-23/298*6.626E-34/10000)^.5
740     ENT2=(ENT1/SEPN)^2
750     ENT=((LOG(ENT2)))*8.310001
760     PRINT "ENTROPY IS ";ENT"J/Mol":IF P$="P" THEN LPRINT
      "ENTROPY IS ";ENT" J/Mol"
770     PRINT:IF P$="P" THEN LPRINT
780     PRINT "ENTHALPY IS ";ACT-2.47"kJ/Mol":IF P$="P" THEN LPRINT
      "ENTHALPY IS ";ACT-2.47"kJ/Mol"
790     PRINT:IF P$="P" THEN LPRINT
800     FE=ACT-2.47-(298*ENT/1000)
810     PRINT "FREE ENERGY IS ";FE"kJ/Mol":IF P$="P" THEN LPRINT
      "FREE ENERGY IS ";FE"kJ/Mol"
820     PRINT:IF P$="P" THEN LPRINT
830     PRINT
840     END
850     CLS
860     XFAC=600/(XMAX-XMIN)
870     YFAC=200/(YMAX+ABS(YMIN))
880     XL=0:YL=0
890     FOR J=1 TO NN
900     X=(X(J)-XMIN)*XFAC:Y=200-(Y(J)+ABS(YMIN))*YFAC
910     PSET (X,Y)
920     LINE (XL,YL)-(X,Y)
930     XL=X:YL=Y
940     CIRCLE (X,Y),5
950     NEXT
960     REM
970     RETURN
```

The ability to diagnose the presence of interactions between redox centres immobilised within a polymeric film can aid the interpretation of processes such as non-Nernstian thermodynamics. For all of the metallopolymers examined here a Nernstian response was observed in all electrolytes at a sufficiently low sweep rate with the exception of those based on perchlorate

anion. Interactions between sites may be an explanation of these observations. In the following program the magnitude of the interaction between sites can be determined from the peak width at half height of the slow sweep rate cyclic voltammetry response.

Program 6 Evaluation of Interaction Parameters From Peak Width of Surface Wave Cyclic Voltammograms.

```
10    KEY 3, "GOTO 370" + CHR$(13)
20    REM interaction parameters from peak widths
30    REM THIS PROGRAM IS QUITE INACCURATE AROUND ZERO INTERACTIO
40    CLS
50    INPUT "PEAK WIDTH IN MILLIVOLTS ";PW
60    PRINT
70    INPUT "SURFACE CONCENTRATION IN MOLED PER CENTIMETRE SQUARE
80    PRINT
90    IF SC=0 THEN SC=1E-08
100   INPUT "TEMPERATURE IN DEGREES CENTIGRADE ";T:T=T+273.1
110   IF T=273.1 THEN T=298.1
120   PRINT
130   INPUT "NUMBER OF ELECTRONS PASSED ";N
140   IF N=0 THEN N=1
150   PRINT
160   IF PW=90 AND N=1 THEN CLS:PRINT"INTERACTION PARAMETER IS ZERO !!
170   IF PW=45 AND N=2 THEN CLS:PRINT"INTERACTION PARAMETER IS ZERO !!
180   CLS
190   PW=PW/1000*N*96484.6/(8.31441*T)
200   T1=-2
210   T2=2
220   F1=.5+.5*((1-(4/(8-2*T1)))^.5)
230   Y1=(LOG(F1/(1-F1))-(T1*(2*F1-1)))
240   Y1=Y1*2
```

```
250     F2=.5+.5*(1-(4/(8-2*T2)))^.5
260     Y2=(LOG(F2/(1-F2))-T2*(2*F2-1))
270     Y2=Y2*2
280     T3=(T1+T2)/2
290     F3=.5+.5*(1-(4/(8-2*T3)))^.5
300     Y3=(LOG(F3/(1-F3))-T3*(2*F3-1))
310     Y3=Y3*2
320     PRINT Y1,Y2,Y3,PW
330     IF ABS(Y3-PW)<.0000005 THEN GOTO 360
340     IF Y3<PW THEN T2=T3:GOTO 220
350     IF Y3>PW THEN T1=T3:GOTO 220
360     R=T1/SC
370     CLS
380     BEEP
390     PRINT "SURFACE CONCENTRATION * R =";T1
400     PRINT
410     PRINT"INTERACTION PARAMETER, R=";R
```

Computer analysis of experimental results has also been exploited in this work in the field of electrocatalysis to investigate the linearity of i_l vs $w^{-1/2}$ and to calculate a modified electrode rate constant.

Program 7 Evaluation of a Modified Electrode Rate Constant (k_{ME}) From the Dependence of i_L with Rotation Rate.

```
10      REM THIS PROGRAM USES ROTATING DISK DATA TO CALCULATE A
        MODIFIED ELECTRODE RATE CONSTANT ACCORDING TO THE ALBERY-HI
20      REM
30      SCREEN 2
40      YMIN=1E+08:XMIN=1E+08
50      YMAX=-1E+08:XMAX=0
```

```
60      KEY 1,"LIST "+ CHR$(13)
70      KEY 3, "GOTO 770" + CHR$(13)
80      CLS
90      INPUT"ENTER P FOR RESULTS TO PRINTER ";P$
100     PRINT
110     INPUT "ELECTRODE AREA DEFAULT 0.0706 ";AREA
120     IF AREA=0 THEN AREA=.0706
130     PRINT
140     DIM X(100),Y(100)
150     NN=0
160     IF N=0 THEN N=1
170     INPUT "ROTATION RATE IN R.P.M.";ROT$
180     IF ROT$="/" THEN GOTO 310
190     ROT=VAL(ROT$)
200     IF ROT =0 THEN BEEP:CLS:GOTO 170
210     ROT=ROT/60
220     T=ROT
230     PRINT
240     INPUT "LIMITING CURRENT IN MICROAMPS ";D
250     IF D=0 THEN BEEP:CLS:GOTO 240
260     D=D*.000001
270     NN=NN+1:X(NN)=1/(T^.5): Y(NN)=1/D
280     REM NN=NN+1:X(NN)=(D^-2): Y(NN)=((D^-2)*(T^-.5))
290     PRINT
300     GOTO 170
310     FOR J=1 TO NN
320     IF X(J)>XMAX THEN XMAX=X(J)
330     IF Y(J)<YMIN THEN YMIN=Y(J)
340     IF Y(J)>YMAX THEN YMAX=Y(J)
350     IF X(J)<XMIN THEN XMIN=X(J)
360     XY=XY+(X(J)*Y(J))
370     TX=TX+X(J)
380     TY=TY+Y(J)
390     SX=SX+((X(J)^2))
400     SY=SY+((Y(J)^2))
```

```
410    NEXT
420    AX=TX/NN
430    AY=TY/NN
440    B=(XY-(NN*AX*AY))/(SX-(NN*(AX^2)))
450    R=(XY-(NN*AX*AY))/(((SX-(NN*(AX^2)))*(SY-(NN*(AY^2))))^.5)
460    C=AY-B*AX
470    IF P$="P" THEN LPRINT
480    PRINT
490    GOSUB 720
500    IF P$="P" THEN LPRINT:LPRINT
510    IF B>0 THEN PRINT "REGRESSION LINE IS Y=";C"+";B"X"
520    IF B>0 AND P$="P" THEN LPRINT "REGRESSION LINE IS Y=";C"+";B"X"
530    IF B<0 THEN PRINT "REGRESSION LINE IS Y=";C;B"X"
540    IF B<0 AND P$="P" THEN LPRINT "REGRESSION LINE IS Y=";C;B"X"
550    PRINT
560    IF P$="P" THEN LPRINT
570    PRINT "CORRELATION COEFFICIENT IS ";R
580    IF P$="P" THEN LPRINT "CORRELATION COEFFICIENT IS ";R
590    PRINT
600    PRINT
610    LEV=.001
620    CCALC =1/(LEV*B*AREA*96485!)
630    PRINT"CONCENTRATION REQUIRED TO GIVE LEVICH
     SLOPE IS ";CCALC
640    PRINT
650    INPUT"REQUIRED CONCENTRATION ";CONC
660    IF CONC=0 THEN CONC=CCALC
670    PRINT
680    PRINT"LEVICH SLOPE GIVEN CONC =";CONC"MOLS/L IS
     "1/(B*96485!*CONC*AREA)
690    PRINT
700    PRINT"k ME IS ";1/(C*AREA*96485!*CONC)
710    END
720    REM graphics routine follows
730    CLS
```

```
740     XFAC=600/(XMAX-XMIN)
750     YFAC=200/(YMAX-(YMIN)):
760     XL=0:YL=0
770     FOR J=1 TO NN
780     X=(X(J)-XMIN)*XFAC:Y=200-(Y(J)-(YMIN))*YFAC
790     PSET (X,Y)
800     IF J<> 1 THEN LINE (XL,YL)-(X,Y)
810     XL=X:YL=Y
820     CIRCLE (X,Y),5
830     NEXT
840     INPUT "PRESS RETURN TO CONTINUE ";XX$
850     RETURN
```

The application of computers in the manner described here is likely to become increasingly widespread in the near future. The limitations in processing power, memory and graphics of machines such as the BBC microcomputer, used for potentiostat programming and data manipulation, have now been removed with recent widespread introduction of machines based on the Intel 80386 and Motorola 68020 chips. The application of computers in the manner described in section 1 involving data acquisition, formatting, analysis, storage and presentation is becoming increasingly widespread. Computer based methods have the advantage of flexibility and the ability to exploit new theoretical models without waiting for a dedicated instrument. A more significant development is that more time can be devoted to actual research rather than "number crunching". The integrated approach described in section 1 is the preferred route, since all aspects of the experiment can be computer controlled. This can include optimisation of experimental conditions, data acquisition, capture, analysis and presentation. Data obtained in this manner is also readily portable and can be used directly in statistical analysis packages as well as word processing environments.

Appendix B Publications

1. The Effect of Supporting Electrolyte and Temperature on the Rate of Charge Propogation Through Thin Films of $[Os(bipy)_2PVP_{10}Cl]Cl$ Coated on Stationary Electrodes.

   Robert J. Forster, Andrew J. Kelly, Johannes G. Vos and M. E. G. Lyons. J. Electroanal. Chem, 1989, 270, 365.

2. Synthesis, Characterisation, Reactivity and X-Ray Structure of cis-Carbonylchlorobis[1-methyl-3-(pyridin-2-yl)-1,2,4-triazole-N^4N']ruthenium Hexafluorophosphate.

   Robert J. Forster, Aidan Boyle, Johannes G. Vos, Ronald Hage, Anouk H. J. Dijkhuis, Rudolf A. G. de Graaff, Jaap G. Haasnoot, Rob Prins and Jan Reedijk. J. Chem. Soc., Dalton Trans., 1990, 121.

3. Electrodeposition of Silver onto $[Os(bipy)_2PVP_{10}Cl]Cl$ Modified Electrodes.

   Renyi Wang, Robert J. Forster, Alan Clarke and Johannes G. Vos. Electrochim. Acta. 1990, 35, 985

4. Synthesis, Characterisation and Properties of a Series of Osmium and Ruthenium Containing Metallopolymers.

   Robert J. Forster and Johannes G. Vos. Macromolecules in press.

5. Theory and Analytical Applications of Modified Electrodes.

Robert J. Forster and Johannes G. Vos in "Electrochemistry, sensors and Analysis", Anal. Chem. Symposia, Elsevier, in press.

6. Charge Transport Properties of Poly(N-vinylimidazole) Polymers Containing $[Os(N_6)]^{2+/3+}$ Moities.

Robert J. Forster and Johannes G. Vos, J. Inorganic and Organometallic Polymers. in press.

7. Factors Affecting the Nature of the Charge Transport Processes in $[Os(bipy)_2(PVP)_nCl]Cl$ Redox Polymer Modified Electrodes.

Robert J. Forster, Michael E. G. Lyons and Johannes G. Vos, J. Phys. Chem. Submitted for publication.

8. Thermodynamics and Kinetics of Heterogeneous Electron Transfer at Glassy Carbon/Osmium Containing Metallopolymer Interfaces.

Robert J. Forster, Michael E. G. Lyons and Johannes G. Vos, J. Phys. Chem. Submitted for publication.

9. Determination of in-situ Solvent Transport by Isotopic Substitution in an Osmium Polymer Film Using a Quartz Crystal Microbalance.

Andrew J. Kelly, Takeo Ohsaka, Noboru Oyama, Robert J. Forster and Johannes G. Vos, J. Electroanal. Chem. submitted for publication.

Poster and Oral Presentations.

1. Charge Transport Through Thin Films of Osmium Containing Polymers.

   Robert J. Forster and Johannes G. Vos., Poster Presentation at Charge Tansfer in Polymeric Systems, The Royal Society of Chemistry, Faraday Division, General Discussion No. 88.

2. Charge Propagation Through Osmium Containing Poly(N-vinylimidazole) Films on Electrode Surfaces.

   Robert J. Forster and Johannes G. Vos. Oral presentation at 177th Electrochemical Society Meeting, Montreal, Canada. May 1990

J. Electroanal. Chem., 270 (1989) 365–379
Elsevier Sequoia S.A., Lausanne – Printed in The Netherlands

The effect of supporting electrolyte and temperature on the rate of charge propagation through thin films of $[Os(bipy)_2PVP_{10}Cl]Cl$ coated on stationary electrodes

Robert J. Forster, Andrew J. Kelly and Johannes G. Vos *

School of Chemical Sciences, Dublin City University, Dublin 9 (Ireland)

Michael E.G. Lyons

Physical Chemistry Laboratory, University of Dublin, Trinity College, Dublin 2 (Ireland)

(Received 21 March 1989; in revised form 2 May 1989)

ABSTRACT

The rate of charge transport through $[Os(bipy)_2(PVP)_{10}Cl]Cl$ films has been investigated using chronoamperometry, chronocoulometry and cyclic voltammetry (bipy = 2,2'-bipyridyl; PVP = poly-4-vinylpyridine). The apparent charge transport diffusion parameter $D_{CT}^{1/2}c$ for the Os(II/III) oxidation, is measured as a function of electrolyte and temperature. The values obtained by these techniques, for $D_{CT}^{1/2}c$ and for the activation energy are discussed in relation to the rate determining step in the charge transport process. The implication of these observations in relation to sensor application is considered.

INTRODUCTION

Considerable effort has been made in the field of redox polymer modified electrodes because of their potential applications in electrocatalysis [1–3], photoelectrochemistry [4,5] and macromolecular electronics [6]. Their applicability in many of these areas will be determined by the rates of charge propagation through the redox polymer films. This rate of charge propagation will be controlled by one of three processes: (i) The intrinsic barrier to self exchange for electron hopping between polymer bound redox centres. (ii) Counterion movement into/out of the film as oxidation or reduction occurs. (iii) Physical displacement of the polymeric chains to which the redox centre is bound in order to allow their mean separation to become sufficiently small for electron exchange.

* To whom correspondence should be addressed.

0022-0728/89/$03.50

The evaluation of charge transport rates in modified electrodes using chronocoulometry (CC) and chronoamperometry (CA) has received much attention [7]. In recent times the question of migration effects has been addressed for the case of mobile redox ions incorporated into polymeric matrices [8] and more recently for fixed site systems such as the one examined in this contribution [9]. These theoretical models indicate that, where significant migration is present, potential step methods are limited for the evaluation of charge transport rates and may lead to serious overestimation of charge percolation rates.

The use of steady methods rather than transient methods to consider charge transport dynamics through metallopolymers has also received attention of late [10,11]. These methods can avoid problems with migration effects and thus reveal more interesting and subtle aspects of electron transfer dynamics [12,13].

In this contribution, the charge transport process for the Os(II/III) oxidation has been investigated for glassy carbon electrodes modified with poly-4-vinylpyridine (PVP) bound $Os(bipy)_2Cl_2$ groupings (bipy = 2,2′-bipyridyl). In this study both potential step techniques [7] and cyclic voltammetry (CV) [14,15] have been utilised. It was hoped that by using these two techniques, the charge transport process throughout the whole layer, rather than just close to the electrode/film interface, could be studied. It is recognised that measurements at longer times including cyclic voltammetry are limited due to the expected inhomogeneity of the polymer layer [16]. However the observed trends should remain valid; in particular the activation energies obtained will be useful to distinguish between the different limiting processes.

EXPERIMENTAL

Materials

Glassy carbon electrodes of either 3 or 7 mm diameter mounted in teflon shrouds were used throughout the experiments and were prepared by mechanical polishing using 0.5 μm alumina slurry on a felt bed followed by thorough washing with water and methanol. Poly-4-vinylpyridine (PVP) was prepared from freshly distilled 4-vinylpyridine by bulk polymerisation under nitrogen at 70–75 °C using 2,2′-azo-isobutyronitrile and purified by repeated precipitation in diethyl ether from methanol. The molar mass, as determined by viscometry in absolute ethanol, was found to be 4.3×10^5 g. $Os(bipy)_2Cl_2$ was prepared by standard laboratory procedures [17]. The modifying metallopolymer was prepared as reported for the corresponding ruthenium containing polymer by refluxing $Os(bipy)_2Cl_2$ with a 10-fold excess of PVP in ethanol [18].

Apparatus and procedures

Electrochemical measurements were performed using an EG&G PAR 175 universal programmer and 363 potentiostat and coulometric measurements were obtained from a 379 digital coulometer. Where necessary, *IR* compensation was achieved via positive feedback circuitry. Electrochemical cells were of conventional

design and were thermostatted to $\pm 1°C$. Transient current/charge measurements were made over the time range 0 to 20 ms by means of a Philips 3311 digital storage oscilloscope interfaced to a BBC microcomputer for data interrogation and allowing signal averaged results to be obtained. For both the redox active potential step and for background correction, typically 5 signals were averaged. This regime typically gave a response which obeyed the Cottrell equation. For the perchlorate based electrolytes however significant migration effects were observed which resulted in non zero intercepts on the current axis. The data was analysed by taking the linear portion of the Cottrell plot without forcing the data through the origin. Adherent electrode coatings were obtained by evaporation of a few microlitres of a 1% solution of the metallopolymer in ethanol on the electrode surface in a solvent saturated chamber followed by air drying. All potentials are referenced with respect to the potassium chloride saturated calomel electrodes (SCE) without regard for liquid junction potentials.

Surface coverages were estimated by graphical integration of the background corrected slow sweep rate cyclic voltammograms (1 mV/s), and were typically $2-4 \times 10^{-8}$ mol cm^{-2}. Layer thickness was estimated from the density of the dry complex (1.2 g/cm^3) as measured by flotation; this gave a concentration for redox centres within the film of 0.7 *M* and this values was used for calculating D_{CT} in Tables 1–3.

The results for $D_{CT}^{1/2}c$ and D_{CT} presented in this work are all obtained from different electrode coatings. This avoids possible problems from " memory effects" where the rate of charge transport through a film would be dependent on the electrolytes to which it had previously been exposed.

The values for the activation parameters are reproducible to $\pm 2\%$ on a single coating and to $\pm 10\%$ between coatings. Some hysteresis is observed between those values obtained when the temperature is increased and when it is decreased, approximately $\pm 10\%$.

RESULTS

General layer properties

When deposited from ethanolic solutions onto glassy carbon electrodes, the metallopolymer shows the expected single electron redox behaviour in all electrolytes examined (see Fig. 1). The Os(II/III) redox couple is observed at about 250 mV vs. SCE, depending on the electrolyte, and is photochemically and thermally stable. The formal peak potential observed in CH_3CN + 0.1 *M* TEAP of 335 mV vs. SCE is similar to that observed for the analogous mononuclear model compound $[Os(bipy)_2(pic)Cl]^+$ ($E_{1/2}$ = 345 mV; pic = 4-methylpyridine) and is consistent with data observed for other osmium compounds [19]. The electrochemical data together with electronic spectra, synthetic conditions and elemental analysis are consistent with the molecular formula $[Os(bipy)_2PVP_{10}Cl]Cl$. A detailed discussion of the synthesis and spectroscopic properties of these and other osmium containing polymers will be published elsewhere [20].

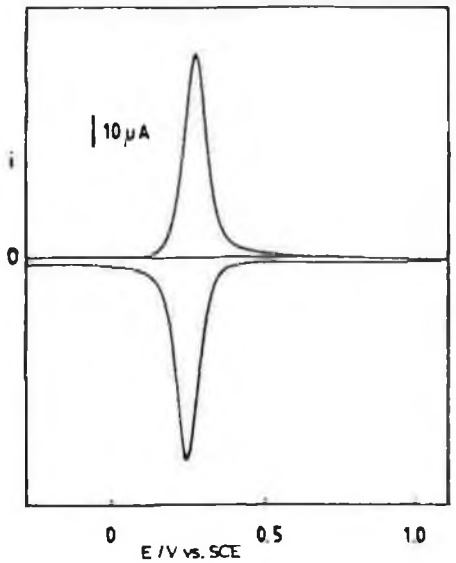

Fig. 1. Cyclic voltammogram of $[Os(bipy)_2PVP_{10}Cl]Cl$ on a glassy carbon electrode. Scan rate 10 mV s^{-1}. 0.1 *M* H_2SO_4 as background electrolyte.

Electrolyte dependence of charge transport

Potential step chronoamperometry and chronocoulometry were employed to estimate the charge transport rates for the Os(II/III) oxidation as apparent diffusion parameters $D_{CT}^{1/2}c$ and D_{CT}. As the results obtained using the two potential step techniques were the same within experimental error, only those obtained by chronoamperometry will be discussed further. In general, linear Cottrell plots were obtained from times up to about 10–20 ms.

In the cyclic voltammetry (CV) experiments, sweep rates between 100 and 500 mV/s were utilised giving linear i_p versus v plots. This permits the use of the Randles–Sevčik analysis (eqn. 1) for the evaluation of D_{CT} [21].

$$i_p = 0.4463(nF)^{3/2} A D_{CT}^{1/2} c v^{1/2} / (RT)^{1/2} \quad (1)$$

where n is the number of electrons passed, F the Faraday constant, A the geometric electrode area, D_{CT} the apparent charge transport diffusion coefficient, c the concentration of redox active sites within the film, v the sweep rate, R the gas constant, T the absolute temperature.

The theoretical model proposed by Aoki et al. [15] (eqn. 2) which combines both surface and semi-infinite diffusional behaviour, has also been applied for this purpose. The peak current is given by:

$$i_p = 0.446nFA\{D_{CT}c/L\}W^{1/2} \tanh Y \quad (2)$$

TABLE 1

The effect of concentration of chloride based supporting electrolytes on charge transport parameters of $[Os(bipy)_2PVP_{10}Cl]Cl$ modified electrodes

Conc. /M	$10^9 D_{CT}^{1/2}c$/ mol cm^{-2} s$^{-1/2}$ [a]	$10^{11} D_{CT}$/ cm^2 s^{-1} [a,c]	$10^8 D_{CT}^{1/2}c$/ mol cm^{-2} s$^{-1/2}$ [b]	$10^9 D_{CT}$/ cm^2 s^{-1} [b,c]	$E^{\circ\prime}$/V
HCl electrolyte					
0.1	0.76 (0.02)	0.12	3.1 (0.20)	1.96	0.215
0.2	1.20 (0.03)	0.29	3.9 (0.32)	3.10	0.205
0.3	1.86 (0.10)	0.71	4.1 (0.28)	3.43	0.215
0.4	2.33 (0.12)	1.11	4.1 (0.21)	3.43	0.190
0.6	4.40 (0.15)	3.95	4.4 (0.38)	3.95	0.200
0.8	4.89 (0.18)	4.88	6.8 (0.70)	9.44	0.168
1.0	5.81 (0.10)	6.88	9.2 (1.00)	17.27	0.160
2.0	5.85 (0.08)	6.98	9.6 (0.84)	18.81	0.160
NaCl electrolyte					
0.1	1.15 (0.017)	0.27	1.78 (0.07)	0.65	0.275
0.2	1.33 (0.007)	0.36	2.30 (0.08)	1.08	0.265
0.4	2.03 (0.066)	0.84	2.83 (0.11)	1.63	0.270
0.5	2.14 (0.031)	0.93	3.04 (0.21)	1.89	0.200
0.6	2.37 (0.011)	1.15	3.26 (0.10)	2.17	0.210
0.8	2.39 (0.010)	1.17	3.26 (0.15)	2.17	0.240
1.0	2.41 (0.005)	1.19	5.31 (0.21)	5.75	0.230

[a] Evaluated from cyclic voltammetry using the anodic peak current and the Randles–Sevčik equation.
[b] Evaluated from chronoamperometry using the Cottrell equation.
[c] D_{CT} calculated using $c = 0.7$ *M* (see text).

where

$$W = nFL^2v/D_{CT}RT \tag{3}$$

$$Y = 0.56W^{1/2} + 0.05W \tag{4}$$

L is the layer thickness, and all other symbols are as in eqn. (1).

Chloride based electrolytes

The concentration dependence of D_{CT} as measured from CA in HCl using the Cottrell equation at short times is illustrated in Table 1 and Figure 2. The results obtained show clearly a strong dependence of the charge transport rates depending on the ion concentration of the contacting electrolyte solution. The concentration dependence of $D_{CT}^{1/2}c$ and D_{CT} in the same electrolytes was also calculated using the anodic peak currents from cyclic voltammograms over the sweep range 100–500 mV/s, using both the Randles–Sevčik and the Aoki approach (see Fig. 3). This figure shows that both the Randles–Sevčik and Aoki approach give essentially the same results. The same behaviour was observed in all other electrolytes. Therefore only the results as obtained from the Randles–Sevčik approach are included in the tables. The most striking results obtained from the measurements is the difference in

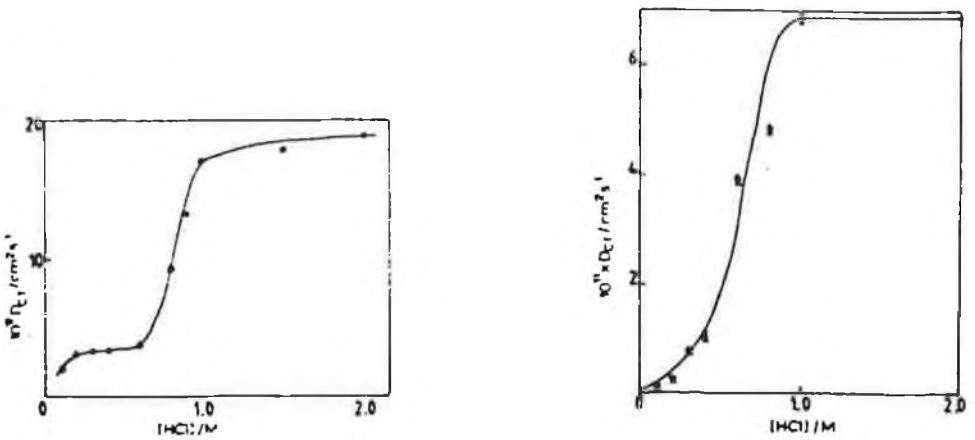

Fig. 2 The effect of HCl concentration on the rate of charge transport, measured as D_{CT} through films of $[Os(bipy)_2PVP_{10}Cl]Cl$ as determined from chronoamperometry.

Fig. 3. The effect of HCl concentration on the rate of charge transport, measured as D_{CT} through films of $[Os(bipy)_2PVP_{10}Cl]Cl$ as measured by cyclic voltammetry using the Randles-Sevčik (●) and Aoki (×) equation.

the transport parameters, which are typically found to be an order of magnitude smaller in the potential sweep experiments. D_{CT} was also determined for a range of chloride concentrations at near neutral pH in NaCl solutions. In Table 1 it can be seen that at high pH, the diffusion parameters are generally lower compared to those at low pH but that a similar type of behaviour is obtained in both electrolytes.

Perchlorate based electrolytes

The perchlorate anion has a similar hydrated molar volume to that of chloride (96.9 vs. 93.6 $cm^3\ mol^{-1}$ [22]. It is expected, therefore, that if ion transport alone limits D_{CT}, a similar result will be observed [23]. However, the insolubility of the perchlorate salt of the metallopolymer can also be expected to influence the morphology of the immobilised film and hence ion permeation rates.

The effect of perchloric acid concentration on the magnitude of the charge transport diffusion parameter evaluated from potential step experiments at short times is shown in Fig. 4 and Table 2. The effect of raising the perchloric acid concentration from 0.1 to 1 *M* on the charge transport rate is not as significant as that found in HCl.

The effect of concentration of perchloric acid on the diffusion parameter as evaluated from CV data is shown in Fig. 5. The CV results show a *decrease* in D_{CT} with an *increasing* concentration of supporting electrolyte.

The behaviour in perchlorate solutions around pH 7 was examined using aqueous $LiClO_4$ (Table 2). The trend of decreasing diffusion parameter as evaluated from CV data with increasing electrolyte concentration was again observed.

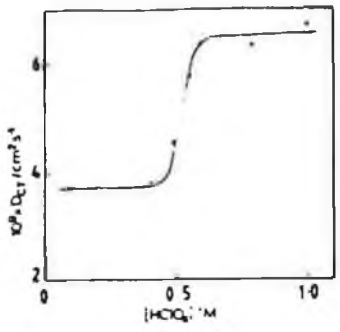

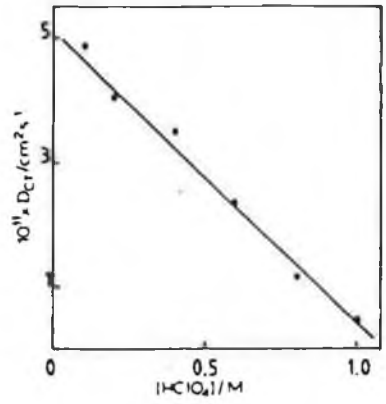

Fig. 4. The effect of $HClO_4$ concentration on the rate of charge transport, measured as D_{CT} through films of $[Os(bipy)_2PVP_{10}Cl]Cl$ as determined from chronoamperometry.

Fig. 5. The effect of $HClO_4$ concentration on the rate of charge transport, measured as D_{CT} through films of $[Os(bipy)_2PVP_{10}Cl]Cl$ as determined from cyclic voltammetry using the Randles–Sevčik equation.

Toluene-4-sulphonic acid

Toluene-4-sulphonic acid was investigated because of the large molar volume of this electrolyte [22]. Because of this larger volume one would expect a significantly reduced diffusion parameter if counter ion transport alone is rate determining.

TABLE 2

The effect of concentration of perchlorate based supporting electrolytes on charge transport parameters of $[Os(bipy)_2PVP_{10}Cl]Cl$ modified electrodes

Conc. /M	$10^9 D_{CT}^{\frac{1}{2}}c$ / mol cm^{-2} s$^{-\frac{1}{2}}$ [a]	$10^{11} D_{CT}$ / cm^2 s^{-1} [b,c]	$10^8 D_{CT}^{\frac{1}{2}}c$ / mol cm^{-2} s$^{-\frac{1}{2}}$ [b]	$10^9 D_{CT}$ / cm^2 s^{-1} [b,c]	$E^{\circ\prime}$/V
$HClO_4$					
0.1	4.89 (0.21)	4.88	4.25 (0.31)	3.69	0.215
0.2	4.45 (0.07)	4.04	4.30 (0.32)	3.77	0.220
0.4	4.15 (0.07)	3.51	4.12 (0.28)	3.69	0.215
0.6	3.40 (0.17)	2.36	5.58 (0.46)	6.35	0.170
0.8	2.39 (0.15)	1.17	5.58 (0.41)	6.35	0.142
1.0	1.50 (0.02)	0.46	5.74 (0.55)	6.72	0.125
$LiClO_4$					
0.1	2.59 (0.07)	1.37	2.63 (0.11)	1.41	0.255
0.2	2.53 (0.05)	1.31	2.53 (0.09)	1.31	0.235
0.4	2.01 (0.03)	0.82	2.53 (0.10)	1.31	0.245
0.6	1.72 (0.04)	0.60	3.24 (0.20)	2.14	0.230
0.1	2.56 (0.07)	1.34	2.69 (0.12)	1.48	0.255

[a] Evaluated from cyclic voltammetry using the anodic peak current and the Randles–Sevčik equation.
[b] Evaluated from chronoamperometry using the Cottrell equation.
[c] D_{CT} calculated using $c = 0.7$ *M* (see text).

TABLE 3

The effect of concentration of sulphate based and toluene sulphonic acid supporting electrolytes on charge transport parameters of $[Os(bipy)_2PVP_{10}Cl]Cl$ modified electrodes

Conc. /M	$10^6 D_{CT}^{1/2} c$ / mol cm^{-2} s$^{-1/2}$ [a]	$10^{11} D_{CT}$ / cm^2 s^{-1} [b,c]	$10^8 D_{CT}^{1/2} c$ / mol cm^{-3} s$^{-1/2}$ [b]	$10^9 D_{CT}$ / cm^2 s^{-1} [b,c]	$E^{\circ\prime}$/V
H_2SO_4					
0.1	11.1 (2.25)	25.14	3.8 (0.13)	2.95	0.260
0.2	17.3 (5.01)	61.08	4.3 (0.28)	3.77	0.248
0.3	20.7 (7.05)	87.45	4.6 (0.37)	4.32	0.250
0.4	25.0 (5.80)	127.55	5.6 (0.47)	6.40	0.250
0.6	27.0 (4.00)	148.78	6.6 (0.74)	8.89	0.250
1.0	28.6 (8.10)	166.93	6.7 (0.76)	9.16	0.250
K_2SO_4					
0.2	3.64 (0.16)	2.70	1.46 (0.03)	0.44	0.210
0.4	5.04 (0.26)	5.18	1.56 (0.04)	0.49	0.195
0.6	7.50 (0.90)	11.48	3.47 (0.11)	2.46	0.200
0.8	9.31 (0.96)	17.69	4.12 (0.30)	3.46	0.135
1.0	11.4 (0.11)	26.52	4.16 (0.31)	3.53	0.160
Toluene-4-sulphonic acid					
0.1	6.36 (0.80)	8.25	2.00 (0.08)	0.82	0.290
0.2	7.89 (0.90)	12.70	2.31 (0.11)	1.09	0.255
0.4	9.40 (0.60)	18.03	4.10 (0.25)	3.43	0.250
0.6	10.5 (1.00)	22.50	4.25 (0.37)	3.69	0.265
0.8	11.3 (0.80)	26.06	4.25 (0.43)	3.69	0.265
1.0	13.2 (1.12)	35.56	4.24 (0.29)	3.67	0.240

[a] Evaluated from cyclic voltammetry using the cathodic peak current and the Randles–Sevčik equation.
[b] Evaluated from chronoamperometry using the Cottrell equation.
[c] D_{CT} calculated using $c = 0.7$ *M* (see text).

Table 3 shows that indeed for the diffusion parameters obtained from potential step measurements a small decrease is obtained, but the values obtained from CV are among the highest obtained for the modified electrodes studied here.

Sulphate based electrolytes

The charge transport diffusion parameters for varying concentrations of H_2SO_4 and K_2SO_4, evaluated by potential step and sweep techniques are outlined in Table 3. The values obtained indicate an increase of charge transport rates with increasing electrolyte concentration. What is significant is that the values obtained from both techniques are more closely related to one another. In the case of 1.0 *M* HCl, D_{CT} as measured from CA was approximately 250 times larger than the CV value, while in 1.0 *M* H_2SO_4, this factor is just 6. The D_{CT} values obtained from CV are the highest obtained for the system studied. The rates of charge transport in K_2SO_4 are slower, and show greater variation between the potential step and sweep experiments.

Temperature effects

Given the problems of specifying the rate determining steps in the charge transport process it is expected that the evaluation of activation parameters for the charge transfer process will be fruitful in the specification of the nature of the rate determining step [24]. Therefore the temperature dependence of D_{CT} as measured by CA and CV of [Os(bipy)$_2$PVP$_{10}$Cl]Cl modified electrodes over the range 276–309 K in 0.1 and 1 *M* solutions of the above electrolytes has been investigated. The Arrhenius equation

$$D_{CT} = D_{CT}^{\circ}\, e^{-E_a/RT}$$

has been used to calculate activation energies and the Eyring equation

$$D_{CT}^{\circ} = e\delta^2(k_B T/h)\exp(\Delta S^{*}/R)$$

to calculate entropies. In this equation, δ denotes the mean separation of osmium centres (~ 50 nm), e is the base of the natural log, k_B is the Boltzmann constant and h is the Planck constant. The activation parameters as obtained from CV are listed in Table 4. This table shows clearly a substantial variation in activation parameters, not only between the different electrolytes, but also with varying concentration. Where the activation parameters in chloride electrolytes appear to be relatively insensitive to concentration, for sulphate based electrolytes the activation energy varies from 10.5 kJ mol^{-1} in 0.1 *M* to 115 kJ mol^{-1} for 1 *M* H_2SO_4. The experimental data with regard to the determination of the activation energy using cyclic voltammetry over the sweep range 100–500 mV/s in 0.1 *M* H_2SO_4 has been presented in Fig. 6. The Cottrell plots are presented in Fig. 7. In perchloric acid a

TABLE 4

Activation parameters for charge transport through [Os(bipy)$_2$PVP$_{10}$Cl]Cl films as obtained by cyclic voltammetry

Electrolyte	E_a (= $\Delta H^{*} + RT$)/ kJ mol^{-1}	ΔS^{*}/ J mol^{-1} K^{-1}	ΔG^{*}/ kJ mol^{-1}
0.1 *M* $LiClO_4$	117	212.7	51.2
1.0 *M* $LiClO_4$	36	−64	51.3
0.1 *M* $HClO_4$, $T > 285$ K	224	248	147.6
0.1 *M* $HClO_4$, $T < 285$ K	35	−106	64
1.0 *M* $HClO_4$	92	105.5	51
0.1 *M* H_2SO_4	10.5	−115	43
1.0 *M* H_2SO_4	115	220	47
0.1 *M* K_2SO_4	16	−100	43
1.0 *M* K_2SO_4	122	241.5	48
0.1 *M* toluene-4-sulphonic acid	15	−142	54.8
1.0 *M* toluene-4-sulphonic acid	40	−32	47
0.1 *M* NaCl	17	−116.8	49.5
1.0 *M* NaCl	16	−122.5	50
0.1 *M* HCl	18	−118.6	51
1.0 *M* HCl	16	−109.7	47

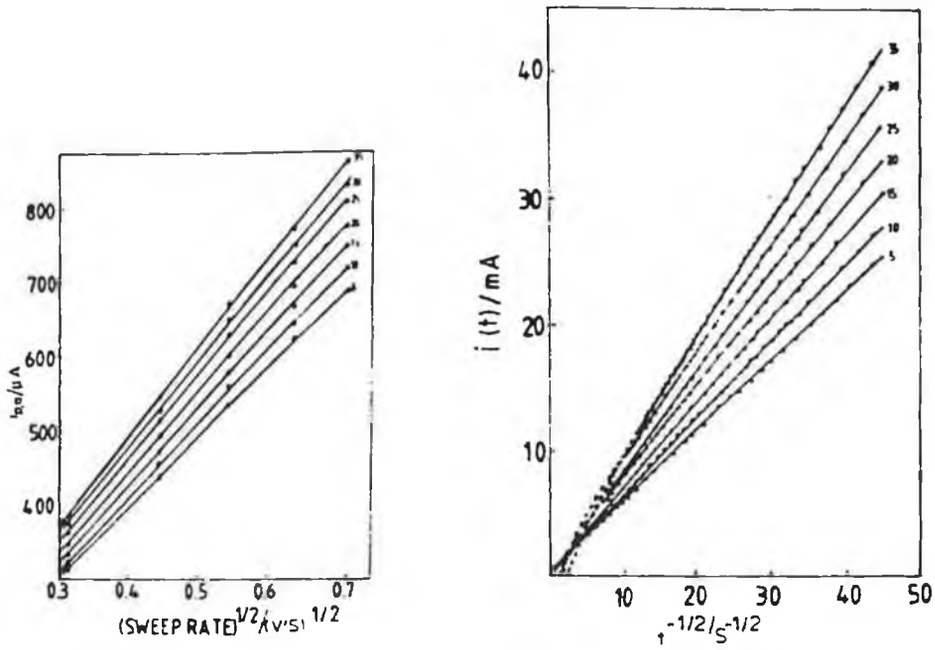

Fig. 6. The effect of temperature on the sweep rate dependence of $i_{p,a}$ as determined by Randles–Sevčik analysis. 0.1 *M* H_2SO_4 as background electrolyte. The temperature in degrees centigrade of the containing electrolyte is indicated on each line.

Fig. 7. The effect of temperature on the chronoamperometric response presented as Cottrell plots for $[Os(bipy)_2PVP_{10}Cl]Cl$ modified electrodes in 0.1 *M* H_2SO_4. The temperature in degrees centigrade is indicated on each line.

TABLE 5

Activation parameters for charge transport through $[Os(bipy)_2PVP_{10}Cl]Cl$ films as obtained by chronoamperometry

Electrolyte	E_a ($= \Delta H^* + RT$) kJ mol^{-1}	ΔS^* / J mol^{-1} K^{-1}	ΔG^* / kJ mol^{-1}
0.1 *M* $LiClO_4$	15	−104.6	44
1.0 *M* $LiClO_4$, $T > 285$ K	16	−92	41
1.0 *M* $LiClO_4$, $T < 285$ K	2	−141	41
0.1 *M* $HClO_4$	14.5	−102.5	42.7
1.0 *M* $HClO_4$, $T > 285$ K	134	250	56.5
1.0 *M* $HClO_4$, $T < 285$ K	51	−38	60
0.1 *M* H_2SO_4	24	−72	42.7
1.0 *M* H_2SO_4	6	−116.7	38.3
0.1 *M* K_2SO_4	23	−79	44.5
0.6 *M* K_2SO_4	45	27.5	34.5
0.1 *M* toluene-4-sulphonic acid	74	116	37
1.0 *M* toluene-4-sulphonic acid	46	96	41.5
0.1 *M* NaCl	22	−75	42
1.0 *M* NaCl	13	−108	42
0.1 *M* HCl	27	−62	42.7
1.0 *M* HCl	9	−104	37.5

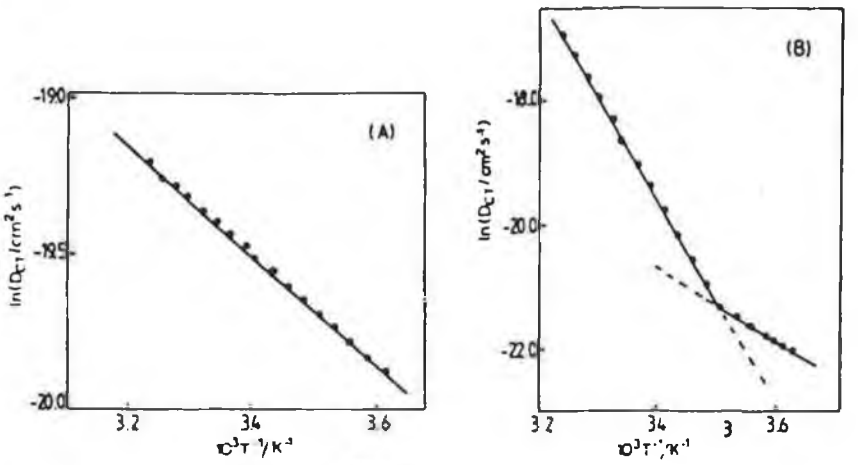

Fig. 8. Temperature dependence of D_{CT} as measured from chronoamperometry. (A) background electrolyte 0.1 *M* $HClO_4$, (B) background electrolyte 1 *M* $HClO_4$.

different situation is seen again, where at 0.1 *M*, two distinct linear regions are observed in the Arrhenius plot, leading to an activation energy of 224 kJ mol^{-1} at high temperatures and a value of 35 kJ mol^{-1} below 285 K. However, at 1 *M* $HClO_4$ a linear Arrhenius plot is obtained with an activation energy of 92 kJ mol^{-1}.

The temperature dependence of the CA response was also investigated and the results are given in Table 5. The activation parameter results obtained for CA are quite different from those given in Table 4. For non-perchlorate based electrolytes, a decrease in activation has been obtained (with the exception of K_2SO_4) with increasing electrolyte concentration. In perchloric acid based electrolyte two distinct activation energies have been obtained at high electrolyte concentration (see Fig. 8).

The entropy values obtained by CV or CA are related to the activation energies in that for those situations where a high activation energy is observed large positive entropies are obtained. If the activation energy is low then negative entropy terms are found.

DISCUSSION

The experimental variable which has been evaluated in these studies is $D_{CT}^{1/2}c$. It is apparent therefore that changes in $D_{CT}^{1/2}c$ may reflect a variation in the charge transport rate or the fixed site concentration within the film.

Firstly the sulphate, chloride and toluene sulphonic acid based electrolytes will be considered. It is thought likely that the observed increase in $D_{CT}^{1/2}c$ with increasing electrolyte concentration reflects, at least in part, an increased charge transport rate. This is likely since in acidic electrolytes, the effect of increased supporting electrolyte concentration is expected to be to reduce the fixed site concentration within the film as a result of the protonation of the unbound pyridine

units within the film (pK_a of PVP ≅ 3.3 [25]). With increased protonation film expansion is likely due to electrostatic repulsion. It seems unlikely therefore that $D_{CT}^{1/2}c$ increases because of an increase in concentration of the fixed site within the film.

In neutral pH electrolytes, a similar increase in $D_{CT}^{1/2}c$ is observed (see Tables 1–3). This could result from a more compact film at higher electrolyte concentration or an increased charge transport rate. It has been suggested [26] that, at low supporting electrolyte concentrations, the ability of the contacting solution to reduce the electrostatic repulsions of the charged fixed site is limited. Thus the redox sites adopt an extended configuration so as to minimise these coulombic repulsions. As supporting electrolyte concentration is increased the contacting solution can act to shield the redox centres and so a more compact structure is possible.

An increase in the concentration of the charge compensating counterion in the supporting electrolyte need not necessarily result in a greater ion availability within the film. It is known [27] that, for polyelectrolyte films, ions can be excluded at concentrations of supporting electrolyte below the fixed site concentration by the film's associated Donnan potential. Such an effect appears to be reflected for some electrolytes examined here. In HCl, when D_{CT} is measured using CV, a rapid increase is observed in going from 0.4 and 0.6 *M* electrolyte solutions (see Fig. 3). For the CA results a similar increase is observed, but now on going from 0.6 to 0.8 *M* electrolyte solutions (see Fig. 2). This suggests that the fixed site concentration for that part of the film where the potential step experiment is performed is higher than that in the remainder of the film. This would suggest that the region of the film contacting the electrolyte directly is more swollen that that portion adjacent to the underlying glassy carbon. A breakdown of the Donnan exclusion effect also appears to be reflected in the formal potentials which in certain cases show sharp decreases between 0.4 and 0.8 *M* (see Table 1), possibly reflecting increased ion permeation.

D_{CT} values as obtained by CV and CA both show a dependence on the concentration of supporting electrolyte; however their magnitudes differ greatly between the two techniques (Table 1). This may arise since, in the CA experiment, ion motion will be "short range" while for CV it will by necessity be of a "long range" type due to the extent of the redox reaction. Alternatively there may be regions of distinct morphology within the film. It has been reported [28] that PVP films contain a smooth base layer and a more irregular outer region. It is in this amorphous portion that part of the redox reaction will occur in the CV measurement of D_{CT}.

The temperature dependence results give support to the view of ion transport limitations at low electrolyte concentrations. For the electrolytes examined (except for those based on ClO_4^-), the activation energies of between 10 and 27 kJ mol^{-1} obtained at 0.1 *M* electrolyte are consistent with ion transport within an analogous film [29]. The activation energies measured for the ion transport process are dependent on the techniques employed, but are consistent for all the electrolytes examined. The CV value (10–18 kJ mol^{-1}, Table 4) is thought to be associated with

long range ion movement through the structurally more porous outer region of the film which makes ion transport more facile, while the CA value (Table 5) of approximately 20–25 kJ mol^{-1} represents ion movement through the more compact, smooth underlying base coat of the immobilised film. An interesting observation is that for the CV experiments in H_2SO_4, where charge transport was most rapid presumably due to film solubilisation and hence efficient ion transport, the CV activation energy is low with a value of 10.5 kJ mol^{-1}, indicating facile ion movement. The CA value is, however, similar to that seen in the other electrolytes, possible indicating that even H_2SO_4 is unable to alter the base layer morphology significantly. Charge transport in 0.1 *M* toluene-4-sulphonic acid does not appear to be related to ion transport in the CA case. The activation energy obtained of 74 kJ mol^{-1} is higher than those seen earlier and has a positive entropy term. It would appear that in this case, charge transport is associated with segmental motions of the polymer chains to allow transport of this large ion. The positive entropy term indicates the disorder which segmental motion induces within the film.

Activation parameters obtained at 1.0 *M* electrolyte suggest that only for certain systems has the ion movement limitation been eliminated. For the CV experiments, H_2SO_4, K_2SO_4 and toluene sulphonic acid show increased activation energies and positive entropies in contrast to the low concentration electrolytes. This suggests that the limiting charge transport process has changed from ion movement to polymer chain motions [29]. The combined results can be rationalised as follows; due to the redox site separation (~ 50 nm) the overall rate limiting step for charge transport is the rate of redox site juxtaposition as dictated by polymer chain movement. Only when electrolyte concentrations are increased can ion transport become sufficiently facile e.g. in H_2SO_4 to allow charge percolation to proceed at a rate dictated by the rate of redox site juxtaposition. This is observed only for swelling electrolyte solutions such as sulphuric acid which make at least the outer portion of the film sufficiently porous to ensure rapid ion movement. For the CA experiment the activation energy generally decreases at 1.0 *M* electrolyte (6–13 kJ mol^{-1}; Table 5) except for K_2SO_4. The different behaviour in K_2SO_4 may be related to crystallisation of the salt within the film when high concentrations are present during redox. The reduced activation energy remains associated with an ordering process (the entropy term remaining negative) except for toluene-4-sulphonic acid. The toluene-4-sulphonic acid value continues to be connected to the segmental chain motion required for ion influx. These lower activation energies observed in H_2SO_4, HCl and NaCl may be associated with the intrinsic barrier to electron self exchange or more likely an effect of polymer swelling with temperature.

Perchlorate based electrolytes

The concentration dependence results suggest that as the perchlorate concentration is increased, ion transport becomes increasingly hindered due to increasing contraction of the film as a consequence of the film's insolubility. Alternatively it is possibly based on ion pair associations within the film. Ion pair associations within the polyelectrolyte [30] can act as crosslinks thus increasing matrix rigidity and

opposing the ion movement into the film required for electroneutrality. The short range nature of the ion movement proposed for potential step experiments could explain the increased $D_{CT}^{1/2}c$ when the electrolyte concentration is increased because the ion shortage seen for CV is not expected to be so pronounced with CA.

The activation energies obtained in 0.1 M ClO_4^- electrolytes are significantly different for the potential step and sweep experiments. For CV, large activation energies are obtained, which is consistent with the model discussed above. In 0.1 M $HClO_4$ the CV response shows a behaviour previously seen in ruthenium containing co-polymers [31] i.e. a distinct activation energy at high and low temperatures. The activation energy obtained at high temperature (224 kJ mol^{-1}) may be indicative of segmental chain motion where chain motion is restricted due to considerable film compaction. The low temperature value of 35 kJ mol^{-1} correlated with that observed for an analogous ruthenium polymer (40 kJ mol^{-1}) [29] and is consistent with ion motion inside a compact matrix. At high $HClO_4$ concentrations, a single E_a is obtained using CV. The value of 92 kJ mol^{-1} is associated with increasing disorder within the film (the entropy being positive +105 J mol^{-1} K^{-1}) and probably represents polymer strand motion. It seems that the matrix has become so compact or crosslinked that only by polymer chain motion can ions move into the film.

CONCLUDING REMARKS

The establishment of a link between D_{CT} and a physical process within the polymer film is of great importance, not only fundamentally, but also for the successful application of modified electrodes. The results suggest that the ultimate rate limiting step for charge transport is segmental polymer chain motion required to bridge the distance ($\sim$ 50 nm) between redox centres. However, the charge transport process will reflect this latter process only at high concentrations of background electrolyte (typically > 1 M). At low supporting electrolyte concentrations the effect of either Donnan exclusion and/or insufficient ion concentration means that ion transport limitations control the process.

ACKNOWLEDGEMENTS

The support of EOLAS is gratefully acknowledged. We thank Dr. J.C. Cassidy for his critical review of this manuscript.

REFERENCES

1 A.R. Guadalupe, D.A. Usifer, K.T. Potts, A.E. Mogstad and H.D. Abruna, J. Am. Chem. Soc., 110 (1988) 3462.
2 C.P. Andrieux, O. Haas and J.M. Savéant, J. Am. Chem. Soc., 108 (1986) 8175.
3 W.J. Albery and A.R. Hillman, J. Electroanal. Chem., 170 (1984) 27.
4 D.A. Buttry and F.C. Anson, J. Am. Chem. Soc., 104 (1982) 4824.
5 I. Rubinstein and A.J. Bard, J. Am. Chem. Soc., 103 (1981) 5007.

6 C.E.D. Chidsey and R.W. Murray, Science, 231 (1986) 25.
7 N. Oyama, T. Ohsaka, T. Ushirogouchi, S. Sanpei and S. Nakamura, Bull. Chem. Soc. Jpn., 61 (1988) 3103.
8 R. Lange and K. Doblhofer, J. Electroanal. Chem., 237 (1987) 13.
9 C.P. Andrieux and J.M. Savéant, J. Phys. Chem., 92 (1988) 6761.
10 J.C. Jernigan and R.W. Murray, J. Am. Chem. Soc., 109 (1987) 1738.
11 B.A. White and R.W. Murray, J. Am. Chem. Soc., 109 (1987) 2576.
12 C.E.D. Chidsey and R.W. Murray, J. Phys. Chem., 90 (1986) 1479.
13 P.G. Pickup, W. Kutner, C.R. Leidner and R.W. Murray, J. Am. Chem. Soc., 106 (1984) 1991.
14 K.M. O'Connell, E. Waldner, L. Roullier and E. Laviron, J. Electroanal. Chem., 162 (1984) 77.
15 K. Aoki, K. Tokuda and H. Matsuda, J. Electroanal. Chem., 146 (1983) 417.
16 D.E. Bartak, B. Kazee, K. Shimazu and T. Kuwana, Anal. Chem., 58 (1986) 2756.
17 D.A. Buckingham, F.P. Dwyer, H.A. Goodwin and A.M. Sargeson, Aust. J. Chem., 17 (1964) 325.
18 J.M. Clear, J.M. Kelly, C.M. O'Connell and J.G. Vos, J. Chem. Res. (M), (1981) 3037.
19 E.M. Kober, J.V. Caspar, B.P. Sullivan and T.J. Meyer, Inorg. Chem., 27 (1988) 4587.
20 R. Forster and J.G. Vos, in preparation.
21 A. Ševčik, Collect. Czech. Chem. Commun., 44 (1948) 327.
22 Y. Marcus, Ion Solvation, Wiley-Interscience, New York, 1985.
23 W.J. Albery, M.G. Boutelle, P.J. Colby and A.R. Hillman, J. Electroanal. Chem., 133 (1982) 135.
24 J.Q. Chambers and G. Inzelt, Anal. Chem., 57 (1985) 1117.
25 P. Ferruti and R. Barbucci, Adv. Polym. Sci., 58 (1984) 55.
26 G. Inzelt Electrochim. Acta, 34 (1989) 83.
27 H. Braun, W. Storck and K. Doblhofer, J. Electrochem. Soc., 130 (1983) 807.
28 K. Aoki, K. Tokuda and H. Matsuda, J. Electroanal. Chem., 176 (1984) 139.
29 C.P. Andrieux in M.R. Smyth and J.G. Vos (Eds.), Electrochemistry, Sensors and Analysis, Analytical Symposia Series, Vol. 25, Elsevier, Amsterdam, 1986, 235.
30 A. Eisenberg, Macromolecules, 3 (1970) 147.
31 M.E.G. Lyons, H.G. Fay, J.G. Vos and A.J. Kelly, J. Electroanal. Chem., 250 (1988) 207.

ELECTRODEPOSITION OF SILVER ONTO ELECTRODES COATED WITH $[Os(bipy)_2(PVP)_{10}Cl]Cl$

R. WANG, R. J. FORSTER, A. CLARKE, and J. G. VOS

School of Chemical Sciences, Dublin City University, Dublin 9, Ireland

(*Received* 30 *May* 1989; *in revised form* 7 *August* 1989)

Abstract—Silver has been deposited electrochemically onto glassy carbon electrodes modified with the redox polymer $[Os(bipy)_2(PVP)_{10}Cl]Cl$, where bipy = 2,2'-bipyridyl and PVP = poly-4-vinylpyridine. The electrodeposition process has been studied using cyclic voltammetry. For electrodes coated with the analogous ruthenium containing polymer $[Ru(bipy)_2(PVP)_{10}Cl]Cl$ no electrodeposition was observed. These results suggest a mediated electrodeposition in the case of the osmium polymer. Chronocoulometry experiments show that the charge transport behaviour of the osmium coatings does not change upon deposition of silver.

Key words: silver, electrodeposition, osmium, poly-4-vinylpyridine, redox polymer.

INTRODUCTION

In recent years it has been recognised that modified electrodes can be further modified by introducing metal particles into the polymer matrix[1–9]. A number of investigations have focused on the electrodeposition of metals onto conducting polymers. Kao and Kuwana[1] found that Pt particles dispersed into poly (vinylacetic acid) electrocatalyse hydrogen evolution and oxygen reduction. More recenty, Kuwana *et al.* reported that Pt electrodeposited into polyaniline films catalyses the reduction of hydrogen and the oxidation of methanol[2]. The electrodeposition of palladium particles within poly(thiophene) modified electrodes and their electrocatalytic activity for the reduction of oxygen was investigated by Yassar *et al.*[4].

Less attention has been paid to metal electrodeposition onto redox polymers. However, the first example of metal deposition onto polymer coatings was reported by Wrighton's group using a redox polymer[6, 7]. In this investigation Pt(IV) and Pd(II) complexes were introduced into surface bound *N*,*N*'-dialkyl-4,4'-bipyridinium layers and then reduced to Pt(0) and Pd(0) by electrochemical or photochemical techniques. It was demonstrated that the efficiency of hydrogen evolution at a semiconductor photocathode was improved by this modification. Wrighton and coworkers also reported catalytic generation of hydrogen by deposited Rh and Pd in a cobaltacenium redox polymer on a semiconductor electrode[8]. The electrodeposition of metal particles in the redox polymer poly-$[Ru(bipy)_2(4\text{-vinylpyridine})_2]^{2+}$ has been reported by Pickup *et al.*[9].

The modification of redox polymer modified electrodes with metal particles is interesting, not only because of the aforementioned catalytic activity, but also because of other potential applications. For instance, copper deposition was used to study the microstructure of Nafion films containing conducting crystals[10]. Also, "sandwich" modified electrodes, *ie* polymer coated electrodes coated with a metal layer, have been proposed for the study of charge transport processes in redox polymers[11] whereas the application of such assemblies in electronic devices has also been proposed[12].

In this paper, we report the electrodeposition of silver onto a glassy carbon electrode coated with the redox polymer $[Os(bipy)_2PVP_{10}Cl]Cl$ (Fig. 1). To obtain information about how the electrodeposition is initiated, experiments were also carried out with the corresponding ruthenium polymer.

EXPERIMENTAL

Materials

$[Os(bipy)_2PVP_{10}Cl]Cl$ and $[Ru(bipy)_2PVP_{10}Cl]Cl$ were prepared as described elsewhere[13, 14]. All the reagents were of AR grade and used without further purification.

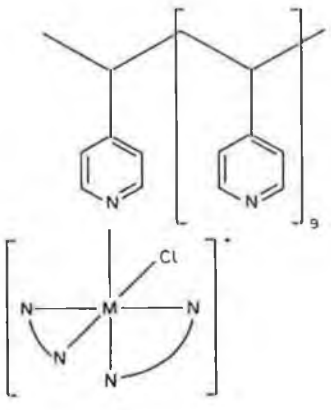

Fig. 1. Molecular structure of redox polymers $[M(bipy)_2PVP_{10}Cl]Cl$, M = Os(II), Ru(II), N–N = 2,2'-bipyridyl (bipy).

Apparatus and methods

Cyclic voltammetry was conducted using an EDT ECP133 potentiostat and galvanostat. Chronocoulometry was carried out using an EG&G PAR 175 universal programmer and 363 potentiostat, combined with a 397 digital coulometer. A Philips 3311 digital storage oscilloscope interfaced to a BBC microcomputer was used for transient data acquisition and analysis. Transient coulometric measurements were made in the 20 ms range while the potential was stepped from −0.2 to 0.8 V. By microcomputer typically three signals were averaged and background signals were subtracted. The surface coverage of the electrode surfaces was estimated from cyclic voltammograms obtained at a scan rate of 1 mV s^{-1}. As the actual swelling of the polymer in the different electrolytes is not known, it is not possible to obtain an accurate measure for the layer thickness. An estimate can be made from the density of the dry polymer (1.2 g cm^{-3}), if swelling is ignored a typical surface coverage of 1.5×10^{-8} mol cm^{-2}, has a calculated thickness of about 200 nm. The electrochemical cell used was a conventional three electrode cell. All the electrochemical potentials are referenced to *sce*. In cyclic voltammetry experiments, agar–KNO_3 salt bridges were used for separating the working solution and reference electrode. Pt foil with an area of *ca* 1.6 cm^2 was used as auxiliary electrode. Working electrodes were Teflon shrouded glassy carbon disc electrodes with a diammeter of 0.7 cm. The supporting electrolyte used for electrodeposition was 0.1 M H_2SO_4. Silver was electrodeposited using the perchlorate salt. All the experiments were performed in 20 ±2°C. Experiments on $[Ru(bipy)_2PVP_{10}Cl]Cl$ coated electrodes were conducted in the dark to avoid photochemically induced ligand exchange reactions [15, 16].

RESULTS AND DISCUSSION

Earlier experiments with the osmium containing polymer have shown the material to be very stable in a range of electrolytes. The redox potential of the Os(II/III) redox couple of interest in these studies is around +200 mV *vs sce*, depending on the electrolyte used[17]. When a $[Os(bipy)_2PVP_{10}Cl]Cl$ coated electrode in 0.1 M H_2SO_4 containing 1 mM $AgClO_4$ was held at +0.22 V for a few minutes or cycled between +0.7 and −0.2 V *vs sce*, the formation of a clear silver coating could be observed. Under these experimental conditions the redox potential of the polymer coating is +200 mV *vs sce*. This suggests that at the deposition potential used, mediation of the reduction of Ag^+ by the surface bound redox couple, as in reactions (1) and (2), is thermodynamically possible:

$$Ag^+ + Os^{2+} \rightarrow Ag^0 + Os^{3+}, \quad (1)$$

$$Os^{3+} + e^- \rightarrow Os^{2+}. \quad (2)$$

However, it is also possible that Ag^+ ions permeate from solution through the polymer and are then electrodeposited directly onto the glassy carbon surface. Further deposition on this directly deposited silver can then also result in the formation of a silver coating throughout the film. To obtain information about the nature of the electrodeposition process cyclic voltammetry was employed. On bare glassy carbon, the electrodeposition starts at about +160 mV (Fig. 2a). In the first scan, a slight hysteresis is seen, indicating the overpotential for electrodeposition of silver onto glassy carbon. This overpotential is eliminated as soon as nucleation has started (Fig. 2b). During the positive scan, a very sharp anodic wave reflects the stripping of silver from the electrode surface. In the second scan, the electrodeposition starts at a more positive potential relative to the first scan. A permanent silver coating on glassy carbon cannot be obtained using cyclic voltammetry as the deposit is stripped off during the positive scan.

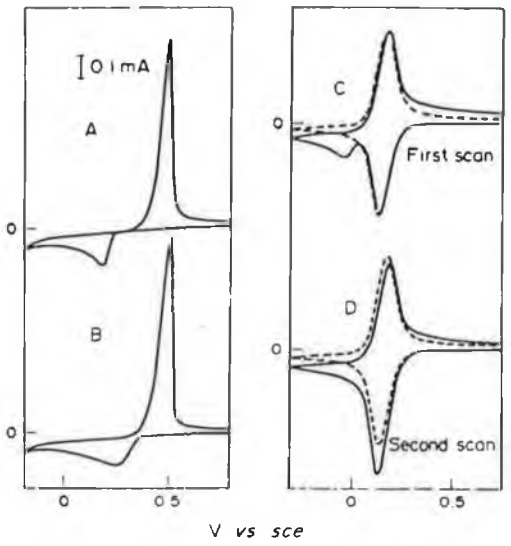

Fig. 2. Cyclic voltammograms of bare glassy carbon electrode (A, B) and $[Os(bipy)_2PVP_{10}Cl]Cl$ coated electrode (C, D) in 0.1 M H_2SO_4 + 1 mM $AgClO_4$(--- in 0.1 M H_2SO_4), scan rate 100 mV s^{-1}, surface coverage = 2.2×10^{-8} mol cm^{-2}. the current scale is the same in 2A–2D.

A $[Os(bipy)_2PVP_{10}Cl]Cl$ polymer coated electrode was first cycled in background electrolyte until the cyclic voltammogram became stable. Then the electrode was transferred to a Ag^+-containing solution and cyclic voltammograms were recorded (Fig. 2). During the first scan of the polymer coated electrode, in addition to the polymer reduction wave, a small cathodic wave appears at a potential of about +100 mV *vs sce* (Fig. 2c). During the positive scan, instead of very sharp anodic wave observed in the bare glassy carbon electrode experiment, only a small shoulder on the polymer oxidation wave is present. From the second scan on, the wave at +100 mV no longer appears, but the reductive wave of the polymer is enhanced and a small cathodic plateau current is observed. (Fig. 2d) at the same time the anodic plateau becomes lower. At slower scan rates, two slightly separated reduction peaks are seen and an anodic stripping wave is observed at + 400 mV (Fig. 3). If the scanning potential is limited to more positive potentials, where the small wave in the first scan was not reached, the reduction wave of the polymer still increases gradually and stabilises after a few minutes, indicating that also under these conditions deposition

of silver is taking place. The effect of the silver ion concentration, scanning limits and of the film thickness is shown in Fig. 4. This figure shows that at higher substrate concentration and for thin films the cathodic plateau is increased, but that there is also evidence for anodic stripping, as evidenced by a wave at +400 mV *vs sce* (compare Figs 4a and 4b). Figure 4c shows that by scanning to less negative potentials the direct deposition can be reduced considerably, so that no stripping wave is observed.

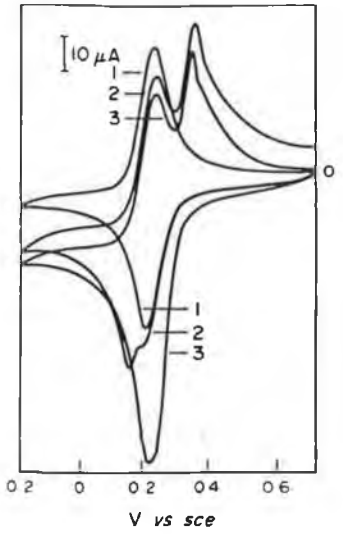

Fig. 3. Cyclic voltammetry of $[Os(bipy)_2PVP_{10}Cl]Cl$ coated electrode in 0.1 M H_2SO_4 (1) and in 0.1 M H_2SO_4 containing 1 mM $AgClO_4$, 2 and 3 are respectively the first and second scan in the silver containing solution; scan rate 5 mV s^{-1}, surface coverage 2.7×10^{-8} mol cm^{-2}

The results obtained so far clearly indicate the large influence of the polymer coating on, especially, the stripping process. It appears that the electrodeposition is, at least in part, mediated by the polymer coating and not just arising from a direct deposition of silver on the underlaying electrode surface. To further investigate the relative importance of direct and mediated electrodeposition, the analogous redox polymer $[Ru(bipy)_2PVP_{10}Cl]Cl$ was investigated. The ruthenium containing polymer is expected to have a very similar structure as the osmium containing polymer. However, the ruthenium polymer is thermodynamically unable to mediate the reduction of Ag^+ as its formal potential is more positive (about 640 mV *vs sce*) than that of the $Ag^{+/0}$ couple (590 mV *vs sce*). Therefore only electrodeposition directly on the underlaying glassy carbon surface is possible for an electrode coated with this polymer. Electrodes coated with the ruthenium containing polymer were scanned over the same potential range as used for the above described experiments with the osmium coatings. In contrast with the results obtained for the osmium coatings (Fig. 2) no reduction wave was observed at +100 mV and no differences between the first and subsequent scans was observed (Fig. 5). In the positive scan, a very small stripping wave was observed at about +400 mV indicating some electrodeposition onto the glassy carbon. It is important to note here that contrary to what is observed for the osmium polymer, the stripping process can be mediated by the polymer coating. However, when the scanning range was extended past the ruthenium redox couple, only a very small increase of the ruthenium oxidation wave, that could be interpreted as a stripping of silver, was observed (Fig. 5).

So the results obtained for the ruthenium polymer support the suggestion made before that the electrodeposition is mediated by the osmium polymer and that the osmium centres are involved in the electrodeposition process. As is also observed for the

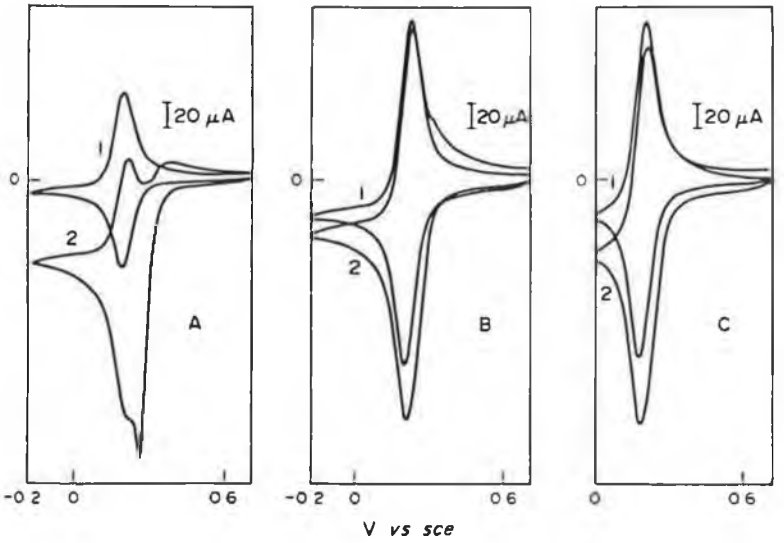

Fig. 4. Cyclic voltammetry of $[Os(bipy)_2PVP_{10}Cl]Cl$ coated electrodes in 0.1 M H_2SO_4 without (1) and with (2) $AgClO_4$, scan rate: 10 mV s^{-1}, Ag(I) concentration; (A) 3 mM and (B, C) 2 mM, surface coverage $= 1.5 \times 10^{-8}$ mol cm^{-2} for (A) and 7×10^{-8} mol cm^{-2} for (B, C); negative scan limit −200 mV *vs sce* for A and B, 0.00 mV *vs sce* for C.

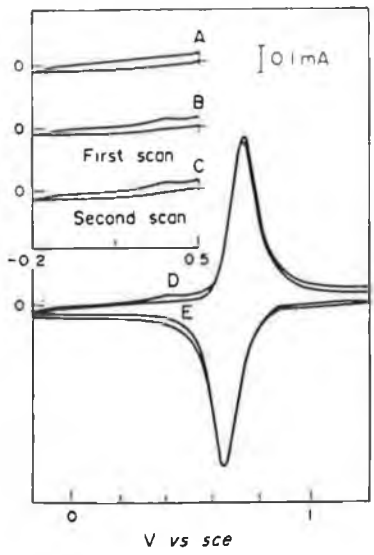

Fig. 5. Cyclic voltammetry of a $[Ru(bipy)_2(PVP)_{10}Cl]Cl$ coated electrode in 0.1 M H_2SO_4 (A, E) and in 0.1 M H_2SO_4 + 1 mM $AgClO_4$ (B, C, D,) scan rate 100 mV s^{-1}, Surface coverage 1.5×10^{-8} mol cm^{-2}.

bare electrode, the mediation of the Ag(I) reduction by Os(II) is initially slow, but as soon as any nucleation occurs the subsequent deposition becomes easier. The location of this nucleation process is at this stage unclear. That direct deposition on the glassy carbon surface occurs can be seen clearly from the stripping current observed at about +400 mV *vs sce*. The magnitude of the direct deposition can be controlled by adjusting variables such as substrate concentration, layer thickness and scanning range (Fig. 4). Deposition might occur either at the underlying glassy carbon surface or in the polymer layer. However the results obtained from the ruthenium polymer suggest that even if initially direct deposition on the electrode occurs, the presence of osmium centres is needed to propagate the process through the whole layer. As stripping of the silver deposit by the osmium polymer is thermodynamically not possible, any stripping current observed must come from silver deposited directly onto the glassy carbon.

Potential-step chronocoulometry were carried out for the Os(II/III) oxidation wave using glassy carbon electrodes with a surface coverage of $2 \pm 1 \times 10^{-8}$ mol cm^{-2}. From an Anson type analysis[18] of the transient data, apparent diffusion coefficients of $6.0 \pm 1 \times 10^{-9}$ $cm^2 s^{-1}$ for the coating containing metal particles and $5.6 \pm 1 \times 10^{-9}$ $cm^2 s^{-1}$ for the polymer coating before deposition were estimated. This clearly shows that the overall charge transport properties of the layer have not been effected by the presence of the silver particles.

CONCLUSION

This study shows that it is possible to introduce metal particles into the osmium containing redox polymer *via* mediation at quite positive potentials. As anodic stripping of the silver from the polymer layer is thermodynamically unfavourable, the metal deposits can be maintained on the polymer. In this manner metal deposits with specific catalytic properties can be obtained without destroying the redox activity of the polymer itself.

Acknowledgements—The financial assistance of EOLAS for this project is gratefully acknowledged. The authors thank Johnson Matthey for a generous loan of ruthenium trichloride.

REFERENCES

1. W-H Kao and T. Kuwana, *J. Am. chem. Soc.* **106**, 473 (1984).
2. K. M. Kost, D. E. Bartak, B. Kazee and T. Kuwana, *Anal. Chem.* **60**, 2379 (1988).
3. M. D. Imisides and G. G. Wallace, *J. electroanal. Chem.* **246**, 181 (1988).
4. A. Yassar, J. Roncali and F. Garnier, *J. electroanal. Chem.* **255**, 53 (1988).
5. G. K. Chandler and D. Pletcher, *J. appl. Electrochem.* **16**, 62 (1986).
6. R. N. Dominey, N. S. Lewis, J. A. Bruce, D. C. Bookbinder, and M. S. Wrighton, *J. Am. chem. Soc.* **104**, 467 (1982).
7. J. A. Bruce, T. Murahashi and M. S. Wrighton, *J. phys. Chem.* **86**, 1552 (1982).
8. R. A. Simon, T. E. Mallouk, K. A. Daube and M. S. Wrighton, *Inorg. Chem.* **24**, 3119 (1985).
9. P. G. Pickup, K. N. Kuo and R. W. Murray, *J. electrochem. Soc.* **130**, 2205 (1983).
10. T. P. Henning, H. S. White and A. J. Bard, *J. Am. chem. Soc.* **104**, 5862 (1982).
11. P. G. Pickup and R. W. Murray, *J. Am. chem. Soc.* **105**, 4510 (1983).
12. P. G. Pickup and R. W. Murray, *J. electrochem. Soc.* **131**, 833 (1984).
13. J. M. Clear, J. M. Kelly, C. M. O'Connell and J. G. Vos, *J. Chem. Res.* (M) 3037, (1981).
14. R. J. Forster and J. G. Vos, to be published.
15. O. Haas, M. Kriens and J. G. Vos, *J. Am. chem. Soc.* **103**, 1318, (1981).
16. O. Haas, J. G. Vos and H. R. Zumbrunnen, *Electrochim. Acta* **30**, 1551 (1985).
17. R. J. Forster, A. J. Kelly, J. G. Vos and M. E. G. Lyons, *J. electroanal. Chem.* **270**, 365 (1989).
18. F. C. Anson, T. Ohsaka, and J. M. Saveant, *J. Am. chem. Soc.* **105**, 4883 (1983).

Determination of in-situ Solvent Transport by Isotopic Substitution in an Osmium Polymer Film Using a Quartz Crystal Microbalance.

Andrew J.Kelly, Takeo Ohsaka and Noboru Oyama*

Department of Applied Chemistry for Resources, Tokyo University of Agriculture and Technology, Koganei, Tokyo 184, Japan

Robert J.Forster and Johannes G.Vos

School of Chemistry, Dublin City University, Dublin 7, Ireland

*Author to whom correspondence should be addressd.

INTRODUCTION

The object of this preliminary note is to present measurements of the mass transport process in thin films of $[Os(bpy)_2PVP_{10}Cl]Cl$ during redox of the $Os^{2+/3+}$ couple (bpy=2,2'-bipyridyl; PVP=poly-4-vinylpyridine). Specifically we demonstrate that the mass transport process shows considerable variation with supporting electrolyte and solvent and quantitative information on solvent transport is able to be obtained using the quartz crystal microbalance(QCM) in solution[1,2]. Solvent transport during redox of thin films has been shown to be important in their electrochemical behaviour[3] The ability of substrates to move freely into polymer films is an important property in the use of modified electrodes as electrocatalysts which is dependent on the degree of swelling of the polymer film[4].

We have previously examined the charge propagation in thin films of this osmium polymer complex[5] and of the ruthenium analogue[6]. The diffusion coefficient for apparent charge transport, D_{app}, is dependent on the supporting electrolyte anion. It has recently been shown that an osmium polymer film of this type is capable of the oxidation of the glucose oxidase enzyme[7].

Qualitative evidence, obtained with the QCM, for solvent transport during electroneutrality requiring ion transport in thin films has been shown in the case of poly(vinylferrocene)[8,9], polyaniline[10,11] and nitrated poly(styrene)[12]. The use of deuterated solvent allowed the unambiguous quantitation of solvent transport in the nickel analogue of Prussian Blue to be clarified[13]. In this report we have used this approach to elucidate quantitative information on the reversible mass transport processes occuring during the redox reaction of thin films of this osmium polymer complex.

EXPERIMENTAL

5 MHz AT cut quartz crystals of 13 mm diameter (Toyo Kurafuto) were coated on both faces with Au (ca.300nm) using a Cr adhesion layer (2nm) by vacuum deposition. An asymmetric keyhole electrode arrangement was used in which the piezoelectrically active area (0.28cm^2) was smaller than the area of the working electrode face (0.64cm^2). This arrangement has a mass sensitivity of $5.65 \times 10^7 Hz cm^2 g^{-1}$[14].

Thin films (0.1-0.5μm) of the Osmium polymer complex were deposited by evaporation from ethanol over the whole electrode face until visibly smooth. The polymer films were allowed to dry for 1 week under ambient conditions before attachment of the crystal to the side arm of an electrochemical cell using silicone rubber. The geometric area of the film exposed to solution, not covered with silicone was determined accurately for each case but was typically 0.5cm^2.

The resonant frequency was determined with the crystal as the active element of an oscillation circuit using a Hewlet Packard 5334B universal counter. Electrochemical measurements were conducted with the working electrode at ground in an operational amplifier based potentiostat/galvanostat(Polarization Unit PS-06, Toho Technical Research). A Pt wire was used as the counter electrode in a frit separated compartment and as reference electrode, a saturated sodium chloride calomel electrode(SSCE) was used in aqueous electrolytes while a Ag wire pseudoreference was used in acetonitrile solutions.

Acetonitrile (reagent grade) was purified by distillation under reduced pressure after drying over moleculer sieve for 2 days. Doubly distilled deionized water and Dueterium oxide (99.8%, Merck) were used for preparation of aqueous electrolytes. Tetraethylammonium para toluene sulphonate (TEApTS), tetrabutylammonium perchlorate(TBAP), sodium p-toluene sulphonate(NapTS) and sodium perchlorate($NaClO_4$) were guaranteed reagent grade(>99%) and used as received.

RESULTS and DISCUSSION

The typical steady state QCM response and cyclic voltammetric response for the Osmium polymer complex in 0.1M TBAP and in 0.1M TEApTS acetonitrile solutions are shown in figure 1a and 1b respectively. The frequency decreases during oxidation of the

Os $^{2+/3+}$ couple which indicates that the mass of the film increases. A comparison of the steady state charge passed with the steady state frequency change allows the molar mass equivalent(Meq) to be determined, this corresponds to qualitative identification of the mass transporting species. The Meq was found to be 129g/mol for 0.1M TBAP and 192g/mol for 0.1M TEApTS. The Meq determined remained constant(±5%) with sweep rate in the range 1-100mV/s indicating the absence of any kinetic effects[14]. The molecular masses of the anions are 99g/mol, ClO_4 and 171g/mol, pTS and the behaviour here is consistent with the permselective movement of anion into the polymer film in order to maintain electronuetrality. There may be a small amount of solvent ingress during oxidation. The good agreement between Meq and the molecular mass shows that the film behaves as a rigid layer describable by the Sauerbrey equation[14]. The half mass change and half charge potentials coincided to within 5mV up to 20mV/s at a minimum frequency sampling time of 0.4s which shows that the mass transport process and electron transfer process occur simultaneously.

The behaviour in aqueous electrolyte solutions is shown in figure 2. The frequency response for 0.1M $NaClO_4$ is again typical of permselective anion mass transport, Meq 94g/mol, with little or no cation or solvent movement. However the frequency behaviour in 0.1M NapTS is quite different, the frequency change is still consistent with the mass increase of the film during oxidation but the Meq determined is 602g/mol. This remains constant with sweep rate in the range (5-100mV/s) and there is still good agreement of the half mass change and half charge change potentials indicating a simultaneous process. A possible reason for this disparity is that there is movement of water into the film during oxidation. We have investigated this by replacing H_2O with deuterium oxide, D_2O. The average Meq determined was 651g/mol(±5%) and the effect of isotopic substitution on Meq (after substracting the molecular mass of the pTS anion) was an 11% increase for D_2O as shown in Table 1. A similar film with a surface coverage of 21μg/cm^2 i.e. three times lower had a substitution increase of 13%. It is clear that the excess mass in Meq for 0.1M NapTS as suporting electrolyte is consistent with the increase in the molecular mass of water due to deuteration of 11%. The good agreement here may indicate that the rigid layer

approximation is still valid which would indicate that 24 molecules of water accompany anion movement into or out of the film during oxidation or reduction. This would indicate a considerable change in the solution properties of the film between the initial Os^{2+} state and the oxidized Os^{3+} state. At the slowest sweep rate used, 1mV/s this corresponds to a 13% swelling due to water uptake. The diffusion coefficient, D_{app}, for the oxidation and reduction processes were found to be 1.6×10^{-12} cm^2/s and 3.8×10^{-12} cm^2/s respectively, determined by potential-step chronocoulometry, which was constant for both H_2O and D_2O as solvents.

It must also be noted that a change in the surface morphology, the polymer film becomes more uneven between the oxidized and reduced states, should also lead to a similar solvent dependence as more solvent molecules would become trapped in the polymer solution interface region[16]. If this can occur then the magnitude of the frequency change may also be dependent on the replacement of H_2O by D_2O and as such the increase in viscosity and density would correspond to a 16 % increase in frequency[17]. A morphology change is considered to be unlikely as no similar effect was observed in acetonitrile.

The effect of compressional stress is mitigated against by using a piezoelectrically active area which is smaller than the electrochemically active area(asymmetric electrode arrangement) as only the radial distribution of mass sensitivity is stress dependent and not the integral of the mass sensitivity which remains constant[18]. It is concluded therefore that compressional stress is not a contributing factor. The movement of water during electroosmosis cannot be considered to be contributing to this behaviour as it would have the opposite effect, water movement out of the film during oxidation. The difference in mass transport in aqueous systems between $NaClO_4$ and NapTS is not unusual as the perchlorate salt of the polymer is highly insoluble and swelling effects are the normal situation for other anions.

A discussion of the in situ mass transport behaviour of various electrolyte counter ions and solvent will be presented in a complete publication which is in preparation.

ACKNOWLEDGEMENT

This research work was partially supported by a Grant-in-Aid for Scientific Research from the Ministry of Education, Science and Culture, Japan(No.01470064), and A.J.Kelly acknowledges the receipt of a scholarship from the Ministry of Education, Science and Culture, Japan.

REFERENCES

1) J.H.Kaufman, K.K.Kanazawa and G.B.Street, Phys. Rev. Lett., 53, 2461(1984).

2) S.Bruckenstein and M.Shay, Electrochim. Acta., 30, 1295(1985).

3) R.W.Murray in A.J.Bard(Ed.), Electroanalytical Chemistry, Marcel Dekker, New York, 13, 191(1984).

4) N.Oyama and F.C.Anson, J. Electrochem. Soc., 129, 640(1980).

5) R.J.Foster, A.J.Kelly, J.G.Vos and M.E.G.Lyons, J. Electroanal. Chem., 270, 365 (1989).

6) M.E.G.Lyons, H.Fay, J.G.Vos and A.J.Kelly, J. Electroanal. Chem., 250,207(1989).

7) B.A.Gregg and A.Heller, Anal. Chem., 62, 258(1990).

8) P.T.Varineau and D.A.Buttry, J. Phys. Chem., 91,1292(1987).

9) A.R.Millman, D.C.Loveday and S.Bruckenstein, J. Electroanal. Chem., 274, 157 (1989).

10) D.Orata and D.A.Buttry, J. Am. Chem. Soc., 109, 3574 (1987).

11) H.Daifuku, T,Kawagoe, N.Yamamoto, T.Ohsaka and N.Oyama, J. Electroanal. Chem., 274,313(1989).

12) R.Borjas and D.A.Buttry, J. Electroanal. Chem.,280, 73 (1990).

13) S.J.Lasky and D.A.Buttry, J. Am.Chem. Soc.,110, 6285 (1988).

14) G.Sauerbrey, Z.Phys., 155, 206 (1959).

15) S.Bruckenstein, C.P.Wilde, M.Shay, A.R.Hillman and D.C.Loveday, J. Electroanal. Chem., 258,457(1989).

16) R.Schumacher, J.G.Gordon and O.Melroy, J. Electroanal. Chem., 216,127(1987).

17) K.K.Kanzawa and J.G.Gordon, Anal. Chim. Acta., 175,99(1985).

18) D.M.Ullevig, J.E.Evans and M.G.Albrecht, Anal. Chem., 54,2341(1982).

Table 1 Frequency and charge changes evaluated from steady state cyclic voltammograms in 0.1 M NapTS with (a) H_2O and (b) D_2O as solvent. Surface coverage of polymer film : 67μg/cm².

(a) H_2O

Sweep rate	ΔF^a	ΔQ^b	M_{eq}
mV/s	Hz	mC	g/mol
1	658	1.05	488
5	586	0.78	580
10	487	0.61	620
20	355	0.44	628
35	263	0.32	635
50	218	0.31	543
100	154	0.20	606

(b) D_2O

1	694	0.99	546
5	540	0.62	632
10	417	0.48	678
20	286	0.33	664
35	214	0.24	686
50	187	0.23	586
100	124	0.15	658

a. Change in frequency at steady state from maximum to minimum.

b. Change in charge, average of anodic and cathodic charges.

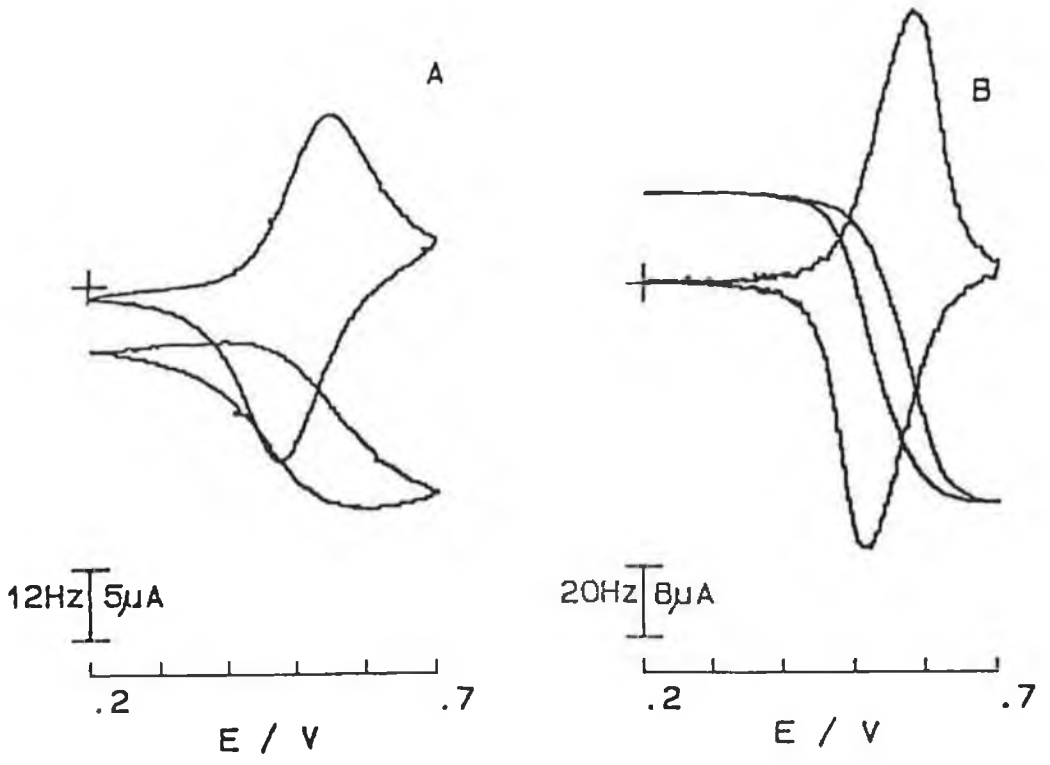

Figure 1

Frequency and current response of steady state cyclic voltammogram at 10mV/s in acetonitrile for (a)0.1M TBAP, surface coverage=13μg/cm^2 and (b)0.1M TEApTS, surface coverage=21μg/cm^2. Potentials quarted versus Ag wire reference.

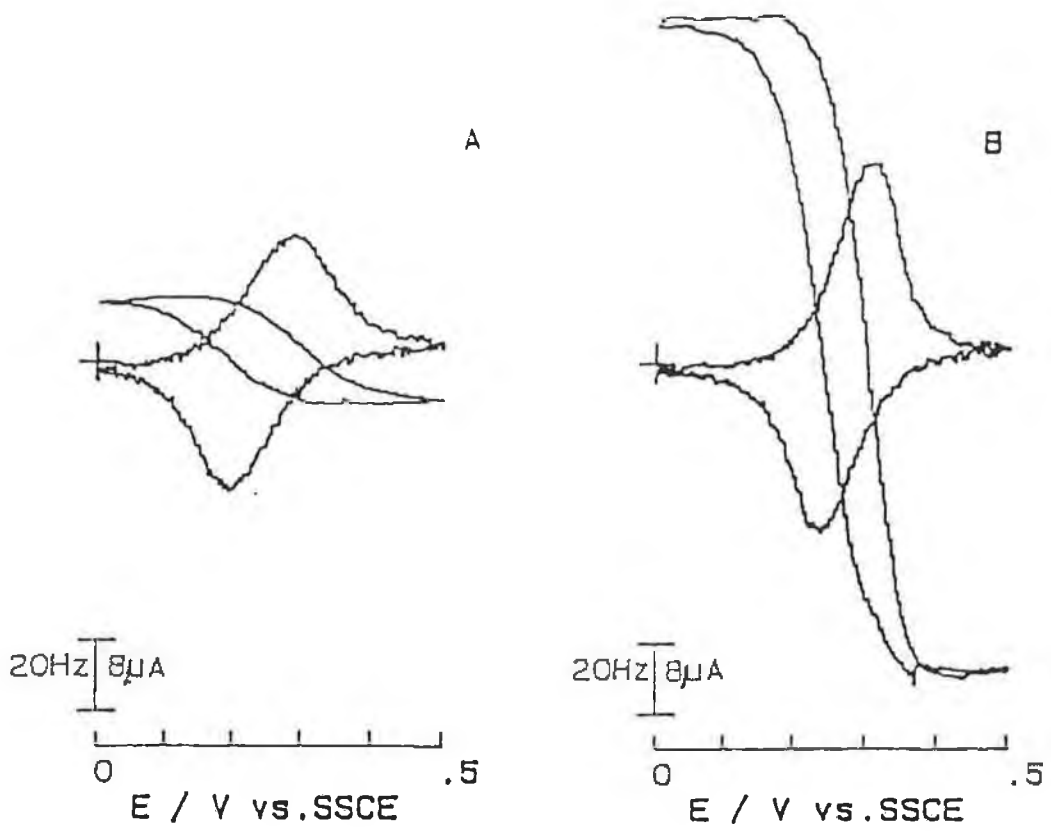

Figure 2

Frequency and current response of steady state cyclic voltammogram at 10mV/s in water, (a)0.1M $NaClO_4$ and (b)0.1M NapTS for a film of surface coverage $=21\mu g/cm^2$.

Synthesis, Characterisation, Reactivity, and *X*-Ray Structure of *cis*-Carbonylchlorobis[1-methyl-3-(pyridin-2-yl)-1,2,4-triazole-N^4N']ruthenium Hexafluorophosphate†

Robert J. Forster, Aidan Boyle, and Johannes G. Vos*
School of Chemical Sciences, Dublin City University, Dublin 9, Ireland
Ronald Hage, Anouk H. J. Dijkhuis, Rudolf A. G. de Graaff, Jaap G. Haasnoot, Rob Prins, and Jan Reedijk
Department of Chemistry, Gorlaeus Laboratories, Leiden University, 2300 RA Leiden, The Netherlands

The compound $[Ru(L–L')_2(CO)Cl]PF_6$ [L–L' = 1-methyl-3-(pyridin-2-yl)-1,2,4-triazole] has been obtained in high yield from ruthenium trichloride and the pyridyltriazole ligand in dimethylformamide, as a mixture of co-ordination isomers. One of these isomers was obtained using crystallisation techniques and crystallises in the monoclinic space group $P2_1/n$ with unit-cell parameters a = 11.085(1), b = 13.120(2), c = 16.108(2) Å, β = 97.17(1)°, and Z = 4. The metal cation has a *cis* geometry for CO and Cl, and the triazole ring is bound to the ruthenium centre *via* its N^4 nitrogen atom. The CO and Cl groups are *trans* to the triazole rings of the pyridyltriazole ligand. The average ruthenium nitrogen distance is 2.09 Å. From this compound the species $[Ru(L–L')(CO)L]^+$ have been obtained, where L = NCS^- or H^-. All the compounds have been characterised by spectroscopic, electrochemical, and high-performance liquid chromatographic methods. The results, and in particular the high yield in which the title compound is obtained, strongly suggest that the pyridyltriazole ligand is a weaker π acceptor than 2,2'-bipyridyl.

There is at present much interest in the chemistry of ruthenium polypyridyl compounds because of their possible application as photochemical or electrochemical catalysts.[1–3] Recently a series of ruthenium polypyridyl carbonyl compounds have been reported[4–7] with the overall formula of $[Ru(bipy)_2(CO)L]^{n+}$ (n = 1 or 2, bipy = 2,2'-bipyridyl, L = a series of monodentate ligands including CO), showing some very unusual and interesting properties. The electronic properties of these compounds are quite different from those normally expected for ruthenium polypyridyl complexes, also photochemical lability of the carbonyl ligand has been observed. The use of the compound $[Ru(bipy)_2(CO)Cl]^+$ as a catalyst in the water-gas shift reaction has been reported.[8,9] This compound and also the osmium carbonyl hydride compound have been proposed as catalysts for the electrochemical reduction of CO_2.[10] Detailed investigations, including hydride-transfer studies, have also been carried out on $[Ru(bipy)_2(CO)H]PF_6$,[11,12] a possible intermediate in the earlier mentioned ruthenium-catalysed water-gas shift reaction.

We have started a systematic investigation[13] of the physical properties of ruthenium compounds with asymmetric ligands of the type L–L', where L–L' is a series of pyridyl-1,2,4-triazoles. In this contribution we report the synthesis, characterisation, and reactivity of the compound $[Ru(L–L')_2(CO)Cl]PF_6$, where the ligand L–L' is 1-methyl-3-(pyridin-2-yl)-1,2,4-triazole and the molecular structure of one of its isomers. It was anticipated that with this study information would be obtained about the electronic properties of the ligand. The properties of the compounds obtained are compared with those observed for the corresponding 2,2'-bipyridyl carbonyl compounds.

Results and Discussion

Preparation of $[Ru(L–L')_2(CO)Cl]PF_6$.—The compound is obtained by reaction of ruthenium trichloride trihydrate with 2 equivalents of the ligand in refluxing dimethylformamide (dmf) [reaction (1)]. The formation of such carbonyl compounds, is

$$RuCl_3 + 2L–L' \xrightarrow{dmf} [Ru(L–L')_2(CO)Cl]^+ \quad (1)$$

most likely the result of a decarbonylation of the solvent, dmf.[4–7] The ligand was added in small portions, so as to avoid the formation of $[Ru(L–L')_3]^{2+}$. The corresponding bipy compound has been prepared in the same manner.[4] However, in that case the yield obtained is only about 40%, while with our pyridyltriazole ligand a yield of close to 100% is obtained. N.m.r. spectra of the products obtained (see below) clearly show the presence of different co-ordination isomers. The first fraction to crystallise out was used for the *X*-ray analysis. As this fraction contained however only about 15% of the overall yield there is no guarantee that only one isomer is obtained. For the bipy compound the main product is $[Ru(bipy)_2Cl_2]$, however no evidence for the formation of such a compound was obtained with the pyridyltriazole ligand. This suggests that

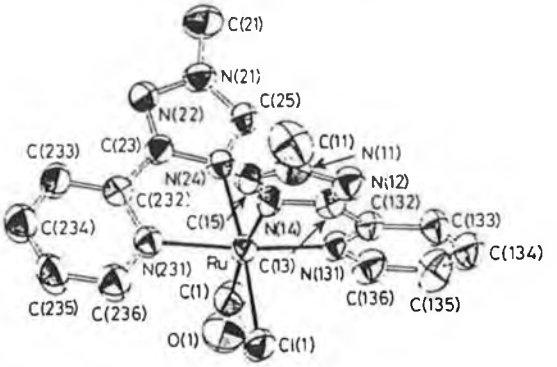

Figure 1. ORTEP drawing of *cis*-$[Ru(L–L')_2(CO)Cl]PF_6$, showing the atom labelling system

† *Supplementary data available*: see Instructions for Authors, *J. Chem. Soc., Dalton Trans.*, 1990, Issue 1, pp. xix–xxii.

Table 1. Fractional atomic co-ordinates ($\times 10^5$ for Ru; $\times 10^4$ for C, Cl, F, O, N, and P) of $[Ru(L\text{-}L')_2(CO)Cl]PF_6$

Atom	*X*/*a*	*Y*/*b*	*Z*/*c*	Atom	*X*/*a*	*Y*/*b*	*Z*/*c*
Ru	23 480(4)	4 705(4)	14 941(2)	N(22)	5 049(4)	2 395(4)	878(3)
Cl	783(1)	−776(1)	1 242(1)	C(23)	4 188(5)	1 696(4)	835(3)
C(1)	3 380(5)	−567(5)	1 887(4)	N(24)	3 669(4)	1 597(3)	1 551(3)
O	3 936(5)	−1 240(4)	2 137(3)	C(25)	4 238(5)	2 265(5)	2 066(3)
N(11)	−578(5)	2 475(4)	716(3)	N(231)	2 863(4)	416(4)	281(3)
C(11)	−1 480(8)	3 062(6)	201(5)	C(232)	3 743(5)	1 067(4)	115(3)
N(12)	−694(4)	2 278(4)	1 552(3)	C(233)	4 151(5)	1 116(5)	−648(4)
C(13)	280(5)	1 729(4)	1 779(3)	C(234)	3 638(6)	486(6)	−1 282(4)
N(14)	995(4)	1 573(4)	1 162(3)	C(235)	2 753(6)	−144(6)	−1 122(4)
C(15)	431(5)	2 050(4)	507(4)	C(236)	2 386(6)	−178(5)	−350(4)
N(131)	1 697(4)	723(3)	2 634(3)	P	6 529(2)	1 026(2)	3 789(1)
C(132)	669(5)	1 295(4)	2 596(3)	F(1)	6 201(4)	738(4)	4 680(3)
C(133)	58(6)	1 440(5)	3 268(4)	F(2)	5 628(5)	1 934(4)	3 769(3)
C(134)	499(7)	977(6)	4 020(4)	F(3)	6 854(5)	1 331(4)	2 915(3)
C(135)	1 520(6)	420(6)	4 063(4)	F(4)	7 482(5)	174(4)	3 836(3)
C(136)	2 103(6)	312(5)	3 379(4)	F(5)	7 510(5)	1 733(5)	4 225(4)
N(21)	5 073(4)	2 748(4)	1 678(3)	F(6)	5 556(6)	355(6)	3 352(4)
C(21)	5 974(6)	3 497(5)	2 019(4)				

Table 2. Selected bond lengths (Å) and angles (°) of $[Ru(L\text{-}L')_2(CO)Cl]PF_6$ with estimated standard deviations (e.s.d.s) in parentheses

Ru–N(14)	2.104(5)	C(13)–N(14)	1.362(6)	C(135)–C(136)	1.352(9)	N(21)–N(22)	1.367(6)
Ru–N(131)	2.082(4)	N(14)–C(15)	1.317(6)	C(233)–C(234)	1.380(8)	N(22)–C(23)	1.318(6)
Ru–N(24)	2.074(4)	C(15)–N(11)	1.329(7)	C(234)–C(235)	1.333(9)	C(23)–N(24)	1.357(6)
Ru–N(231)	2.104(4)	C(13)–C(132)	1.450(7)	C(235)–C(236)	1.357(8)	N(24)–C(25)	1.313(6)
Ru–C(1)	1.839(7)	N(131)–C(132)	1.359(7)	N(231)–C(236)	1.336(7)	C(25)–N(21)	1.338(7)
Ru–Cl	2.382(2)	C(132)–C(133)	1.360(7)	C(1)–O	1.123(7)	C(23)–C(232)	1.458(7)
C(11)–N(11)	1.440(8)	C(133)–C(134)	1.388(9)	C(136)–N(131)	1.342(7)	N(231)–C(232)	1.348(7)
N(11)–N(12)	1.394(6)	C(134)–C(135)	1.341(9)	C(21)–N(21)	1.458(7)	C(232)–C(233)	1.363(7)
N(12)–C(13)	1.312(7)						
Cl–Ru–N(14)	87.0(1)	Ru–N(14)–C(15)	141.5(4)	N(131)–C(132)–C(133)	122.7(5)	N(24)–C(23)–C(232)	118.9(5)
Cl–Ru–N(131)	86.2(1)	Ru–N(14)–C(13)	112.3(4)	C(13)–C(132)–C(133)	123.1(6)	N(22)–C(23)–C(232)	127.3(5)
Cl–Ru–N(24)	172.6(1)	C(15)–N(14)–C(13)	104.6(5)	C(132)–C(133)–C(134)	118.5(6)	N(24)–C(25)–N(21)	109.1(5)
Cl–Ru–N(231)	95.4(1)	C(15)–N(11)–N(12)	110.5(5)	C(135)–C(134)–C(133)	119.1(6)	Ru–N(231)–C(232)	116.7(4)
Cl–Ru–C(1)	87.6(2)	C(15)–N(11)–C(11)	128.6(6)	C(136)–C(135)–C(134)	120.1(6)	Ru–N(231)–C(236)	126.7(4)
N(14)–Ru–N(131)	78.5(2)	N(12)–N(11)–C(11)	120.9(6)	N(131)–C(136)–C(135)	123.0(6)	C(232)–N(231)–C(236)	116.5(5)
N(14)–Ru–N(24)	89.9(2)	N(11)–N(12)–C(13)	101.5(5)	Ru–N(24)–C(25)	141.7(4)	N(231)–C(232)–C(23)	112.5(5)
N(14)–Ru–N(231)	93.1(2)	N(14)–C(13)–N(12)	114.4(5)	Ru–N(24)–C(23)	113.8(4)	N(231)–C(232)–C(233)	122.5(5)
N(14)–Ru–C(1)	171.7(2)	N(14)–C(15)–N(11)	109.1(5)	C(25)–N(24)–C(23)	104.5(5)	C(23)–C(232)–C(233)	125.0(5)
N(131)–Ru–N(24)	99.7(2)	N(14)–C(13)–C(132)	118.0(5)	C(25)–N(21)–N(22)	110.2(5)	C(232)–C(233)–C(234)	119.1(6)
N(131)–Ru–N(231)	171.3(2)	N(12)–C(13)–C(132)	127.6(5)	C(25)–N(21)–C(21)	128.6(5)	C(233)–C(234)–C(235)	118.3(6)
N(131)–Ru–C(1)	94.8(2)	Ru–N(131)–C(132)	115.4(3)	N(22)–N(21)–C(21)	121.0(5)	C(234)–C(235)–C(236)	120.6(6)
N(24)–Ru–N(231)	78.1(2)	Ru–N(131)–C(136)	127.6(4)	N(21)–N(22)–C(23)	102.3(4)	N(231)–C(236)–C(235)	122.9(6)
N(24)–Ru–C(1)	96.2(2)	C(132)–N(131)–C(136)	116.6(5)	N(24)–C(23)–N(22)	113.8(5)	Ru–C(1)–O	174.9(6)
N(231)–Ru–C(1)	93.7(2)	N(131)–C(132)–C(13)	114.2(5)				

the pyridyltriazole ligands are less strong π acceptors, as weak π acceptors are expected to stabilise the chlorocarbonyl compound with respect to the dichloride because of a decreased competition for electron density with the carbonyl ligand.[4]

The compound $[Ru(L\text{-}L')(CO)_2Cl_2]$ was obtained as reported before for the corresponding bipy compound in high yield, by treating L–L′ with a CO-containing methanol–water solution of $RuCl_3$.[4b]

X-Ray Structure of cis-$[Ru(L\text{-}L')_2(CO)Cl]PF_6$.—Fractional co-ordinates are given in Table 1, relevant bond distances and angles in Table 2. An ORTEP projection of the $[Ru(L\text{-}L')_2(CO)Cl]^+$ cation is shown in Figure 1 together with the atom labelling system used. The unit-cell packing of the $[Ru(L\text{-}L')_2(CO)Cl]PF_6$ ion pairs is shown in Figure 2

The co-ordination geometry around the central metal ion is slightly distorted octahedral, with the L–L′ ligands co-ordinated in a *cis* fashion in such a way that the triazole groups are mutually *cis* and the pyridines mutually *trans*. The largest distortion is the small value of the angle between the ruthenium ion and two co-ordinating nitrogen atoms [*e.g.* N(14)–Ru–N(131) 78.5, N(24)–Ru–N(231) 78.1°]. These angles, which are significantly smaller than 90°, appear to be imposed on the

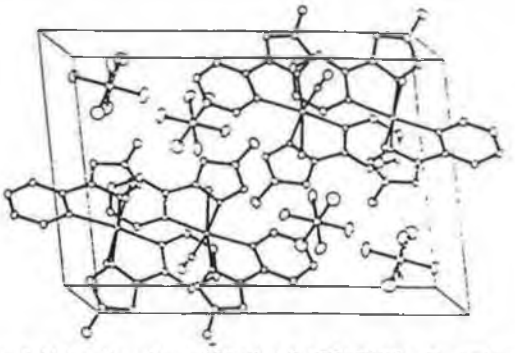

Figure 2. Unit-cell packing of $[Ru(L\text{-}L')_2(CO)Cl]PF_6$. The hydrogen atoms are omitted for clarity

structure by the rigidity of the pyridyltriazole ligands. The small bite angle has been observed before in compounds containing ligands with comparable geometries[14] and is similar to that found for bipy.[15,16] The ligands are bound to the metal ion *via* the pyridine nitrogen and the N^4 atom of the triazole ring. Co-ordination through this nitrogen atom of the triazole ring leads to less steric hindrance than that through the N^2 atom. The pyridine groups are *trans* to each other with the carbonyl and chloride ligands *trans* to triazole ring, probably because in this manner the possibilities for metal-to-ligand back bonding are optimised. The Ru–N distances of between 2.104 and 2.074 Å are as expected for divalent ruthenium compounds. The *trans* effect observed for the CO and Cl ligands is, however, much smaller than that observed in $[Ru(bipy)_2(CO)Cl]^+$, where a difference of 0.11 Å for the Ru–N distances *trans* to these ligands was observed (2.06 *vs.* 2.17 Å).[4a] This is possibly related to the fact that the triazole ring is not expected to be involved in the π-back bonding system. The Ru–C bond is 1.84 Å with the C–O distance of 1.12 Å and a Ru–C–O angle of 175°. These values and also the other metal–ligand distances are very similar to those in the corresponding bipy compound.[4a]

Reactivity.—Attempts were made to prepare a series of compounds with the general formula $[Ru(L\text{–}L')_2(CO)L]^{n+}$ by refluxing $[Ru(L\text{–}L')_2(CO)Cl]^+$ in the presence of an excess of ligand [reaction (2)]. As attempts to isolate the different isomers of the chloro carbonyl compound failed, the reactivity studies were carried out with samples containing a mixture of co-ordination isomers. Reaction (2) was found to be efficient for the

$$[Ru(L\text{–}L')_2(CO)Cl]^+ + L \longrightarrow [Ru(L\text{–}L')_2(CO)L]^{n+} + Cl \quad (2)$$

preparation of the bipy analogues and a range of compounds with L = pyridine, acetonitrile, NCS^-, *etc.* has been reported.[4d] For the chlorocarbonyl compound reported here reaction (2) was extremely slow and it appeared to be very difficult to replace the chloride ligand with neutral ligands. The chloride ligand is not exchanged at all upon refluxing in organic solvents for up to 3 d. The addition of water to the reaction mixture does lead to a slow release of the anion. Numerous attempts were made to prepare $[Ru(L\text{–}L')_2(CO)(H_2O)]^{2+}$, from refluxing acetone–water mixtures, also in the presence of acids, base, or $AgNO_3$. However, no pure products were obtained in this manner. The best results were obtained by the acid decomposition of the hydride compound. The results given below for the aqua and CH_3CN compounds are obtained from samples prepared in this manner.

As the variations in electronic spectra, obtained as a result of the ligand-exchange process, are very small u.v.–visible spectroscopy could not be used to monitor these reactions. The reactions were therefore followed by high-performance liquid chromatography (h.p.l.c.). In experiments where we tried to prepare compounds with a 2+ charge, compounds with ligands such as H_2O and CH_3CN, recombination of the displaced chloride ligand with the 2+ species formed occurred upon injection of a sample of the reaction mixture into the, mainly organic, mobile phase.

The exchange of the chloride ion with other anions is more efficient. The NCS^- compound could be prepared, but this is also not very stable. The compound $[Ru(L\text{–}L')_2(CO)H]ClO_4$ was prepared at room temperature [reaction (3)].[4c] It is

$$[Ru(L\text{–}L')_2(CO)Cl]^+ + NaBH_4 \xrightarrow{CH_3OH} [Ru(L\text{–}L')_2(CO)H]^+ \quad (3)$$

however, not very stable. Addition of NH_4PF_6 and also excess of the borohydride decomposed the compound, but the hydride could be isolated as the perchlorate salt using $NaClO_4$. A similar behaviour was observed before for $Ru(bipy)_2$ hydrides containing phosphine ligands and can be attributed to the acidity of the NH_4^+ group.[4c] The stability of the chlorocarbonyl compound is further emphasised by the experiments carried out with $[Ru(L\text{–}L')(CO)_2Cl_2]$. When we attempted to prepare $[Ru(L\text{–}L')_2(CO)_2]^{2+}$ by treating $[Ru(L\text{–}L')(CO)_2Cl_2]$ with 1 equivalent of the chelating ligand the major product obtained was the chlorocarbonyl compound, with only a relatively small amount of a dicarbonyl species identified by i.r. spectroscopy and h.p.l.c.

As expected the carbonyl ligands are photochemically labile.[4d] The chlorocarbonyl compound was photolysed in acetonitrile using u.v. irradiation. Both h.p.l.c. and u.v.–visible spectroscopy show the formation of one product, with a $\lambda_{max.}$ in the visible of 420 nm for short irradiation times. Upon prolonged irradiation a small amount of a second product is formed with an absorption maximum at about 385 nm. The products obtained were not isolated, but from spectroscopic and h.p.l.c. data it is concluded that the initial product is most likely $[Ru(L\text{–}L')_2(CH_3CN)Cl]^+$. A similar product was obtained for the corresponding bipy compound.[4d] while the second product most likely is $[Ru(L\text{–}L')_2(CH_3CN)_2]^{2+}$.

Purification of the compounds prepared by column chromatography using neutral alumina was not possible as they did adhere to the top of the column. The purity of the compounds was therefore checked by h.p.l.c. using a method described in the Experimental section. The retention times observed are given in Table 3. It proved very difficult to obtain samples having satisfactory elemental analyses. Satisfactory spectroscopic and electrochemical data could be obtained for the compounds with L = H_2O, CH_3CN, Cl^-, NCS^-, or H^-. The purity of these compounds was better than 95% as judged by h.p.l.c. Satisfactory elemental analyses could only be obtained for the Cl^-, NCS^-, and H^- compounds. Most likely slow decomposition of the compounds is taking place.

N.M.R. Spectroscopy.—N.m.r. spectroscopy was used to establish the co-ordination sphere around the ruthenium ion. This technique is particularly suited to identify isomers, especially because of the presence of a methyl group in the pyridyltriazole ligand.[13] All compounds prepared show a series of resonances in the δ 7.5—10.0 range which can be attributed to the pyridyltriazole ligands. Around δ 4.0, signals due to the methyl groups in the complex are observed. The proton spectrum of the sample used for the *X*-ray analysis is given in Figure 3. Assignments were made by comparison with spectra obtained for the free ligand and for similar compounds reported in the literature.[13] For this compound, two further signals, attributed to methyl resonances, are observed at δ 4.01 and 3.97. The presence of these two methyl resonances and also the presence of two resonances for the triazole H^5 proton are in agreement with the crystal structure obtained. The n.m.r. spectrum shows clearly that both pyridyltriazole ligands are inequivalent. This is confirmed by the ^{13}C n.m.r. spectrum of this sample (see Experimental section).

An ^1H n.m.r. spectrum of other samples of the chlorocarbonyl compound appeared to be far more complicated. Depending on the particular sample, between 6 and 10 signals were obtained in the δ 4—5 region that can be attributed to the triazole methyl group. This strongly suggests the presence of more than one isomer. Because of the asymmetry of the ligand six geometrical isomers can be obtained for the *cis* compound. On the basis of molecular models all isomers are expected to be of the *cis* configuration. As a result of the complexity of the situation no analysis of the spectra obtained was carried out to identify these isomers. There are however two distinctly different sets of

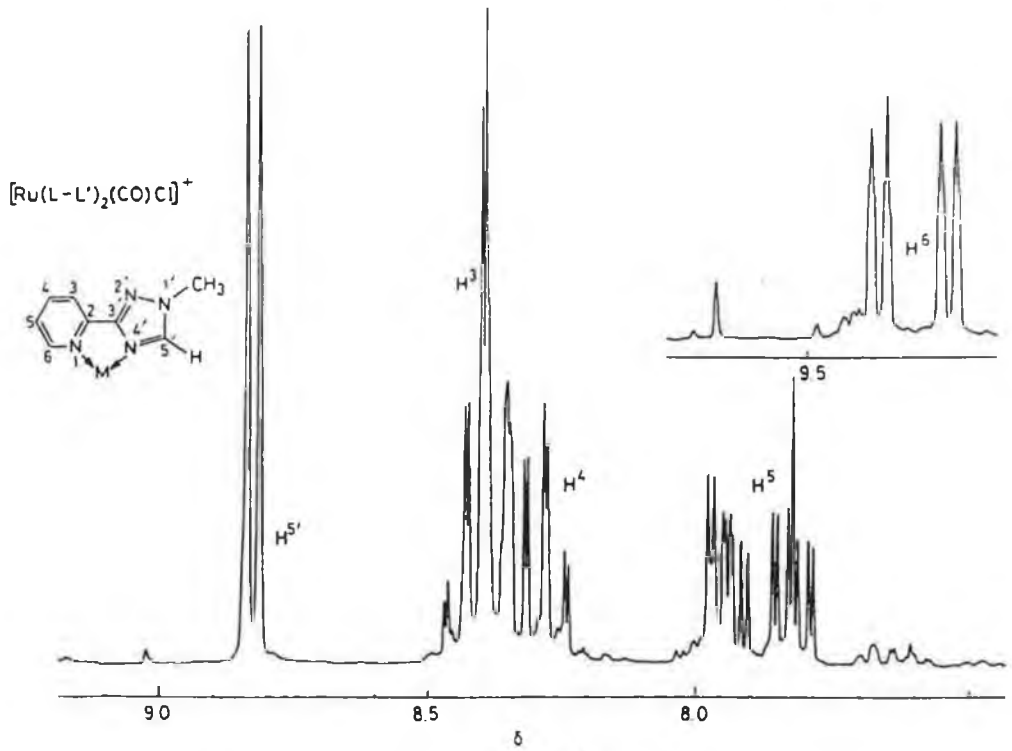

Figure 3. 200-MHz Proton n.m.r. spectrum of the *X*-ray sample of $[Ru(L–L')_2(CO)Cl]PF_6$, together with the assignment of the different resonances. Solvent $(CD_3)_2SO$–$(CD_3)_2CO$ (4:1)

Table 3. Spectroscopic, electrochemical, and h.p.l.c. data for $[Ru(L–L')_2(CO)L]^{n+}$ and some related compounds

Compound	ν(CO)/ cm^{-1}	$Ru^{2+/3+}$ ligand-based reductions/ V *vs.* s.c.e.		H.p.l.c. retention time/min
$[Ru(L–L')_2(CO)Cl]^+$	1 967	1.58	−1.56 *	2.67
$[Ru(L–L')_2(CO)(NCS)]^+$	1 983	1.47 *	−1.57 *	2.30
$[Ru(L–L')_2(CO)H]^+$	1 916	1.15 *	−1.83 *	2.04
$[Ru(L–L')_2(CO)(H_2O)]^{2+}$	1 981		−1.56 *	8.20
$[Ru(L–L')_2(CO)(CH_3CN)]^{2+}$	2 008		−1.47 *	8.12
$[Ru(L–L')(CO)_2Cl_2]$	2 067, 1 988			2.00
$[Ru(bipy)_2(CO)Cl]^+$	1 970	1.50	−1.34 −1.56	
$[Ru(bipy)_2(CO)(NCS)]^+$	1 982	1.47 *	−1.25 −1.46	
$[Ru(bipy)_2(CO)H]^+$	1 912	1.03 *	−1.55 −1.75	
$[Ru(bipy)_2(CO)(H_2O)]^{2+}$	1 995			
$[Ru(bipy)_2(CO)(CH_3CN)]^{2+}$	2 015		−1.18 −1.38	
$[Ru(bipy)(CO)_2Cl_2]$	1 997, 2 055			

Data on bipy compounds from ref. 4*d*.
* Irreversible redox process.

methyl resonances, one set at about δ 4.0 and another at about 4.3 with a ratio of about 1:1. The presence of a set of resonances at about δ 4.3 suggests strongly that the triazole N^2 atom is also able to co-ordinate to the central metal ion.[13] This is contrary to the results obtained for compounds of the type $[Ru(bipy)_2(L–L')]^{2+}$, where for the ligand reported here only co-ordination *via* N^4 was observed.[13b] The different behaviour found here is possibly explained by the extra space present round the metal ion because of the absence of the bipy ligands.

The spectrum obtained for the hydride compound contains resonances at δ −12.51, −12.66, −13.46, and −13.57 that can be attributed to the hydride ion,[4e] also suggesting the presence of several isomers in this compound. Carbon-13 n.m.r. spectra were obtained for $[Ru(L–L')_2(CO)Cl]PF_6$ and $[Ru(L–L')(CO)_2Cl_2]$ (see Experimental section). For the first compound, using the *X*-ray analysis fraction, two sets of resonances were observed indicating the presence of two different pyridyltriazole ligands. The ^{13}C n.m.r. spectrum obtained for $[Ru(L–L')(CO)_2Cl_2]$ shows one set of resonances, indicating the presence of only one isomer. This is further confirmed by the proton n.m.r. spectrum of this compound (see Experimental section). For the dicarbonyl compound two resonances are obtained for the CO ligands at δ 206.5 and 196.2 p.p.m. For the chlorocarbonyl compound one signal is found at 206.8 p.p.m.

Infrared Spectroscopy.—The carbonyl stretching frequencies of the compounds together with those observed for a number of analogous bipy compounds are given in Table 3. The i.r. spectra did not give any indication for the presence of more than one isomer. Within the series of pyridyltriazole compounds the frequency of the carbonyl vibration varies with the nature of the sixth ligand as expected.[4] The small differences observed between the series and those found for the corresponding bipy compounds is surprising in view of the differences in π-acceptor properties of the pyridyltriazole and bipy ligands. The presence of the chloride ligand in $[Ru(L–L')_2(CO)Cl]PF_6$ is confirmed by a M–Cl stretching vibration at 330 cm^{-1}, absent for all other monocarbonyl compounds obtained. For $[Ru(L–L')(CO)_2Cl_2]$ a single M–Cl stretching vibration is found at 330 cm^{-1}. For the hydride no metal–hydrogen stretching vibration could be observed. This band is however expected to be hidden under the strong CO stretching vibration.[4] The presence of the NCS^-

group was confirmed by medium-strong bands at 2 110 and 2 057 cm^{-1}. The presence of the two bands is again indicative of the fact that more than one isomer is formed.

Electronic Spectra.—The u.v.–visible absorption spectra are dominated by the strong $\pi \longrightarrow \pi^*$ L–L′ based transitions at about 240 and 270 nm. As for the analogous bipy compounds, $d_\pi \longrightarrow \pi^*$ transitions are expected in the u.v. region and are hidden by the strong ligand-based transitions. The high energy of these transitions is explained by the strong back donation to the carbonyl ligand.[4] Only the hydride compound shows a well defined transition in the visible region (400 nm), in agreement with the strong donor properties of the hydride ion.[4c,7]

Electrochemistry.—The data obtained are given in Table 3. No reversible ligand-based reductions were found. Of the ruthenium-based oxidations only the chlorocarbonyl compound shows a reversible $Ru^{2+/3+}$ redox couple. For the compounds with a 2+ charge no metal-based oxidation was observed; as for the bipy compounds such an oxidation is expected at potentials around 2 V *vs.* saturated calomel electrode (s.c.e.), outside the range of the solvent used. The $Ru^{2+/3+}$ redox potentials obtained for the L–L′ compounds are very similar to those obtained for their bipy analogues and show the expected variation.[4d]

Conclusions

The fact that in the reaction between $RuCl_3$ and 1-methyl-3-(pyridin-2-yl)-1,2,4-triazole the chlorocarbonyl complex is obtained as the only product can be considered to be strong evidence for the reduced π-acceptor properties of this ligand with respect to bipy. Also the reduced stability of the hydride points to reduced π-acceptor properties for the pyridyl triazole ligand. It is therefore somewhat surprising that the physical properties of the compounds, such as metal-to-ligand distances, ν(CO) frequencies, and redox potentials, are so similar to those obtained for the corresponding bipy compounds. An exception has to be made however for the reactivity. Whereas the synthesis of compounds of the type $[Ru(bipy)_2(CO)L]^{n+}$ from the parent compound $[Ru(bipy)_2(CO)Cl]^+$ is easy, the synthesis of the corresponding L–L′ compounds is much more difficult especially when the sixth ligand is neutral. As the NCS^- and H^- compounds are formed more easily, the stability of the parent chloro compound is probably based on kinetic rather than thermodynamic reasons.

Another point worth mentioning is the presence of many co-ordination isomers. Although this would be expected on the basis of the asymmetry of the pyridyltriazole ligands, the n.m.r. evidence that the N^2 atom is able to bind to the ruthenium ion is somewhat unexpected considering the presence of the methyl group on the neighbouring nitrogen atom. Certainly this co-ordination mode is not found in the $Ru(bipy)_2$ complex of 1-methyl-3-(pyridin-2-yl)-1,2,4-triazole.[13b]

Experimental

X-Ray Crystallography.—A yellow bar-shaped crystal with approximate dimensions of 0.4 × 0.2 × 0.3 mm was used. The density of the crystals was determined using the flotation method.

Crystal data. $C_{17}H_{16}ClF_6N_8OPRu$, M = 629.86, monoclinic, space group $P2_1/n$, a = 11.085(1), b = 13.120(2), c = 16.108(2) Å, β = 97.17(1)°, U = 2 324.2(2) $Å^3$, D_m = 1.81(1) Mg m^{-3}, Z = 4, D_c = 1.80 Mg m^{-3}, $F(000)$ = 1 243.56, μ(Mo-K_α) = 9.2 cm^{-1}, λ(Mo-K_α) = 0.710 730 Å.

Data collection and processing. An Enraf-Nonius CAD4 diffractometer with graphite-monochromated Mo-K_α radiation was employed. Intensities of 5 304 independent reflections were measured at room temperature ($2.0 < \theta < 27.0$). Lattice parameters were determined by measuring 25 reflections with θ from 9.5 to 14.0°. No absorption correction was applied. The range of h, k, and l used was $-14 \leqslant h \leqslant 14$, $0 \leqslant k \leqslant 16$, and $0 \leqslant l \leqslant 20$. The intensity standards used were the reflections (6 1 1), (1 6 0), and (−1 0 11). The intensity variation throughout the experiment was 5%.

Solution and refinement of the structure. Atomic scattering factors for neutral atoms with corrections for anomalous dispersion were taken from ref. 17. Patterson techniques and the program AUTOFOUR [18] were used to find the positions of the heavy atoms. All subsequent least-square refinements and Fourier synthesis were based on the 2 501 significant reflections [$I > 2\sigma(I)$] only. All but one of the hydrogen atoms were located in successive difference Fourier maps. The position of the last hydrogen atom, H(236), was calculated geometrically before least-squares refinement. In this refinement all hydrogen atoms were given the thermal parameter of the carbon atom to which they are bound and were kept at a given distance from this carbon atom.

In the final difference Fourier synthesis, having a minimum value of −0.32 e $Å^{-3}$ and a maximum value of +0.82 e $Å^{-3}$, there were still three small but significant peaks. These were located near the ruthenium atom. Disorder of the fluorine atoms can be deduced from the high anisotropy in the thermal parameters. A model was applied consistently of two $[PF_6]^-$ units with identical phosphorus positions and different positions for the fluorine atoms.

Additional material available from the Cambridge Crystallographic Data Centre comprises H-atom co-ordinates, thermal parameters and remaining bond lengths and angles.

The conventional final residual was $R = \Sigma|\Delta F|/\Sigma F_o = 0.037$ for the 2 501 reflections used in the refinement, $R' = [\Sigma w(\Delta F)^2/\Sigma w(F_o)^2]^{\frac{1}{2}} = 0.044$.

Physical Measurements.—High performance liquid chromatography was carried out using a Waters 990 photodiode array h.p.l.c. system in conjunction with a NEC APC III computer, a Waters pump model 6000 A, a 20-μl injector loop, and a μ Partisil SCX radial PAK cartridge; the detection wavelength was 280 nm. The chromatography was carried out using acetonitrile–water (80:20) containing 0.08 mol dm^{-3} $LiClO_4$ as a mobile phase. The flow rate was 3.0 cm^3 min^{-1}.

U.v.–visible spectra were recorded on a Shimadzu UV 240 spectrophotometer, i.r. spectra on a Perkin-Elmer 599 spectrophotometer as KBr disks. Proton n.m.r. spectra were obtained on a JEOL JNX-FX 200 spectrometer, ^{13}C n.m.r. spectra on a JEOL 50.1-MHz spectrometer, using $SiMe_4$ as an internal standard. Electrochemical measurements were carried out using an E.G. and G. PAR model 174A polaragraphic analyser, a PAR 175 universal programmer and a platinum working electrode. The samples were measured in spectroscopic grade MeCN dried over molecular sieves using 0.1 mol dm^{-3} NEt_4ClO_4 as supporting electrolyte. The scan rate used was 100 mV s^{-1}. A KCl-saturated electrode was used as the reference electrode.

Materials.—The ligand 1-methyl-3-(pyridin-2-yl)-1,2,4-triazole was prepared as described before.[13,19] The compound $RuCl_3 \cdot 3H_2O$ was obtained from Johnson Matthey. All other materials used for the syntheses were of reagent grade used without further purification.

Preparation of Compounds.—$[Ru(L–L')_2(CO)Cl]PF_6$. The salt $RuCl_3 \cdot 3H_2O$ (2.10 g, 8 mmol) was refluxed in dmf (60 cm^3) for 1 h. Then 2 equivalents of L–L′ were added in five portions at

5-min interval. The resulting mixture was heated at reflux for another 6 h. The product was precipitated by the addition of an excess of aqueous NH_4PF_6, recrystallised from an acetone-toluene mixture, and dried *in vacuo* at room temperature. Yield 2.1 g (85%) (Found: C, 32.1; H, 2.5; Cl, 6.0; N, 17.9. C_{1}-$H_{16}ClF_6N_8OPRu$ requires C, 32.4; H, 2.6; Cl, 5.6; N, 17.8%). ^{13}C N.m.r. $[(CD_3)_2SO]$: δ 38.0, 37.7 (Me), 122.5, 122.6 (C^3), 127.2, 127.6 (C^5), 139.3, 140.4 (C^4), 145.7, 147.6, 148.7 ($C^{5'}$, C^2), 153.2, 156.7 (C^6), 160.0, 161.2 ($C^{3'}$), and 206.8 p.p.m. (CO).

$[Ru(L–L')_2(CO)(NCS)]PF_6$-$0.5H_2O$. This compound was prepared as the analogous bipy complex.[4d] Yield 75% (Found: C, 32.2; H, 2.4; N, 19.3. $C_{18}H_{17}F_6N_9O_{3.5}PRuS$ requires C, 32.6; H, 2.6; N, 19.0%).

$[Ru(L–L')_2(CO)H]ClO_4$·H_2O. This compound was prepared as the corresponding bipy complex.[4c] It was precipitated however by addition of $NaClO_4$ as the perchlorate compound as addition of NH_4PF_6 resulted in decomposition of the hydride. Yield 90% (Found: C, 35.6; H, 2.8; N, 19.5. $C_{17}H_{19}ClN_8O_4Ru$ requires C, 35.9; H, 3.3; N, 19.7%).

$[Ru(L–L')(CO)_2Cl_2]$. This was prepared like the corresponding ruthenium bipy analogue.[4b] Yield 86% (Found: C, 31.0; H, 1.9; Cl, 18.6; N, 14.8. $C_{10}H_8Cl_2N_4O_2Ru$ requires C, 31.0; H, 2.1; Cl, 18.3; N, 14.4%). N.m.r. $[(CD_3)_2SO]$: ^1H, δ 9.81 (1 H, s, $H^{5'}$), 9.16 (1 H, q, H^6), 8.32 (2 H, m, H^3, H^4), 7.85 (1 H, m, H^5), and 4.16 (3 H, s, Me); ^{13}C δ 37.9 (Me), 122.5 (C^3), 128.0 (C^5), 141.0 (C^4), 146.1 (C^2), 147.2 ($C^{5'}$), 153.3 (C^6), 160.4 ($C^{3'}$), 196.2 (CO), and 206.5 p.p.m. (CO).

Attempted Preparations.—*$[Ru(L–L')_2(CO)(H_2O)][PF_6]_2$ by acid hydrolysis of the hydride.* The hydride compound (0.16 g) was dissolved in acetone (20 cm^3) and then water (30 cm^3) was added. Concentrated H_2SO_4 (0.5 cm^3) was added but subsequent addition of NH_4PF_6 did yield pure material (h.p.l.c.).

$[Ru(L–L')_2(CO)(CH_3CN)][PF_6]_2$. For this compound the same approach was used. Acetonitrile was however used to dissolve the hydride compound. The product obtained was h.p.l.c. pure but, as for the aquo compound, did not yield a satisfactory elemental analysis.

Acknowledgements

We gratefully acknowledge the assistance of S. Gorter in collecting the crystal data. We thank Johnson Matthey for a generous loan of ruthenium trichloride. This project was partly sponsored by EOLAS, the Irish Science and Technology Agency.

References

1 E. A. Seddon and K. R. Seddon, 'The Chemistry of Ruthenium,' Elsevier, Amsterdam, 1984.
2 K. Kalyanasundaram, *Coord. Chem. Rev.*, 1982, **46**, 159.
3 T. J. Meyer, *Prog. Inorg. Chem.*, 1983, **30**, 389.
4 (*a*) J. M. Clear, J. M. Kelly, C. M. O'Connell, J. G. Vos, C. J. Cardin, S. R. Costa, and A. J. Edwards, *J. Chem. Soc., Chem. Commun.*, 1980, 750; (*b*) J. M. Kelly, C. M. O'Connell, and J. G. Vos, *Inorg. Chim. Acta*, 1982, **64**, L75; (*c*) J. M. Kelly and J. G. Vos, *Angew. Chem., Int. Ed. Engl.*, 1982, **21**, 628; (*d*) J. M. Kelly, C. M. O'Connell, and J. G. Vos, *J. Chem. Soc., Dalton Trans.*, 1986, 253; (*e*) J. M. Kelly and J. G. Vos, *ibid.*, p. 1045.
5 D. J. Cole-Hamilton, *J. Chem. Soc., Chem. Commun.*, 1980, 1213; D. Choudhury, R. F. Jones, G. Smyth, and D. J. Cole-Hamilton, *J. Chem. Soc., Dalton Trans.*, 1982, 1143.
6 D. St. C. Black, G. B. Deacon, and N. C. Thomas, *Transition Met. Chem. (Weinheim, Ger.)*, 1980, **5**, 317; *Aust. J. Chem.*, 1982, **35**, 2445; *Polyhedron*, 1983, **2**, 409.
7 J. V. Caspar, B. P. Sullivan, and T. J. Meyer, *Organometallics*, 1983, **2**, 55; B. P. Sullivan, J. V. Caspar, S. R. Johnson, and T. J. Meyer, *ibid.*, 1984, **3**, 1241.
8 D. Choudhury and D. J. Cole-Hamilton, *J. Chem. Soc., Dalton Trans.*, 1982, 1885.
9 K. Tanaka, M. Morimoto, and T. Tanaka, *Chem. Lett.*, 1983, 901.
10 H. Ishida, K. Tanaka, and T. Tanaka, *Organometallics*, 1987, **6**, 181; M. R. M. Bruce, E. Megehee, B. P. Sullivan, H. Thorp, T. R. O'Toole, A. Downard, and T. J. Meyer, *ibid.*, **7**, 238.
11 J. G. Haasnoot, W. Hinrichs, O. Weir, and J. G. Vos, *Inorg. Chem.*, 1986, **25**, 4140.
12 S. M. Geraty, P. Harkin, and J. G. Vos, *Inorg. Chim. Acta*, 1987, **131**, 217.
13 (*a*) R. Hage, J. G. Haasnoot, J. Reedijk, and J. G. Vos, *Inorg. Chim. Acta*, 1986, **118**, 73; (*b*) R. Hage, R. Prins, J. G. Haasnoot, J. Reedijk, and J. G. Vos, *J. Chem. Soc., Dalton Trans.*, 1987, 1389; (*c*) R. Hage, A. H. J. Dijkhuis, J. G. Haasnoot, R. Prins, J. Reedijk, B. E. Buchanan, and J. G. Vos, *Inorg. Chem.*, 1988, **27**, 2185; (*d*) P. J. Steel, F. Lahousse, D. Lerner, and C. Marzin, *ibid.*, 1983, **22**, 1488.
14 F. S. Key, R. A. G. de Graaff, J. G. Haasnoot, and J. Reedijk, *J. Chem. Soc., Dalton Trans.*, 1984, 2093.
15 R. Hage, J. P. Turkenburg, R. A. G. de Graaff, J. G. Haasnoot, J. Reedijk, and J. G. Vos, *Acta Crystallogr., Sect. C*, 1989, **45**, 381.
16 D. P. Rillema, D. S. Jones, and H. Levy, *J. Chem. Soc., Chem. Commun.*, 1979, 849.
17 'International Tables for *X*-Ray Crystallography,' Kynoch Press, Birmingham, 1974.
18 A. J. Kinneging and R. A. G. de Graaff, *J. Appl. Crystallogr.*, 1984, **17**, 364.
19 S. Kubota, M. Uda, and T. Nakagawa, *J. Heterocycl. Chem.*, 1975, **12**, 855.

Received 21*st September* 1988; *Paper* 8/036821